

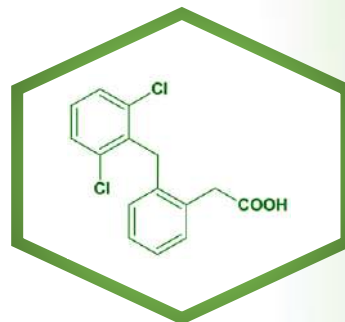
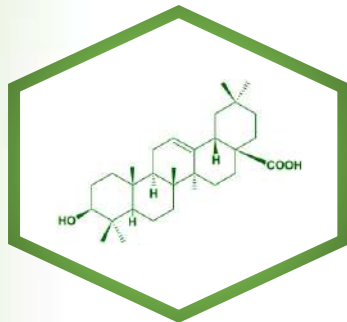


UNIVERSIDAD DE GRANADA

Programa de Doctorado en Bioquímica y Biología Molecular

TESIS DOCTORAL

CARACTERIZACIÓN DE LA CAPACIDAD ANTICANCERÍGENA Y ANTIINFLAMATORIA DEL OADP, DERIVADO AMINOPEGILADO SEMISINTÉTICO DEL ÁCIDO OLEANÓLICO Y APROXIMACIÓN A ESTAS ACTIVIDADES EN N-DERIVADOS DEL DICLOFENACO



Doctoranda

FATIN JANNUS

Directores de Tesis

Dr. FERNANDO JESÚS REYES ZURITA

Dra. MARTA FILOMENA MEDINA O'DONNELL

Granada, Octubre 2022



UNIVERSIDAD DE GRANADA

FACULTAD DE CIENCIAS

DEPARTAMENTO DE BIOQUÍMICA Y BIOLOGÍA MOLECULAR I

PROGRAMA DE DOCTORADO EN BIOQUÍMICA Y BIOLOGIA MOLECULAR
(B16.56.1)

TESIS DOCTORAL

**CARACTERIZACIÓN DE LA CAPACIDAD ANTICANCERÍGENA Y
ANTIINFLAMATORIA DEL OADP, DERIVADO
AMINOPEGILADO SEMISINTETICO DEL ÁCIDO OLEANÓLICO Y
APROXIMACIÓN A ESTAS ACTIVIDADES EN N-DERIVADOS
DEL DICLOFENACO**

FATIN JANNUS

Granada, 2022



CARACTERIZACIÓN DE LA CAPACIDAD ANTICANCERÍGENA Y ANTIINFLAMATORIA DEL OADP, DERIVADO AMINOPEGILADO SEMISINTETICO DEL ÁCIDO OLEANÓLICO Y APROXIMACIÓN A ESTAS ACTIVIDADES EN N-DERIVADOS DEL DICLOFENACO

Memoria presentada por la licenciada en Biología
Fatin Jannus para optar al grado de Doctor
por la Universidad de Granada

Fatin Jannus

Los directores de la Tesis Doctoral

Dr. Fernando Jesús Reyes Zurita
Profesor Titular de Universidad en Bioquímica y
Biología Molecular. Universidad de Granada.

Dra. Marta Filomena Medina O'Donnell
Profesora Contratada en Química Orgánica.
Universidad de Granada.

Editor: Universidad de Granada. Tesis Doctorales
Autor: Fatin Jannus
ISBN: 978-84-1117-593-7
URI: <https://hdl.handle.net/10481/77985>

Esta tesis doctoral ha sido realizada gracias a la colaboración de nuestro grupo de investigación, “Drogas, Tóxicos Ambientales y Metabolismo Celular” con el grupo de investigación “Biotecnología y Química de Productos Naturales” financiada por los proyectos concedidos por la Consejería de Economía, Conocimiento, Empresas y Universidad, Junta de Andalucía: B1-BIO-281-UGR18 y B1-FQM-217-UGR18. Proyectos de desarrollo tecnológico (prototipos y pruebas de concepto), Universidad de Granada, P30-3.

¡Lee! Que tu Señor es el más Generoso.

El que enseñó con el lápiz.

Enseñó al humano lo que no sabía.

(Traducción de las Aleyas 3-5 del Corán Surah

Al-Alaq)

Dedicada

A la memoria de mis abuelos.

A mis padres y a mis hermanas,

por apoyarme todos estos años.



AGRADECIMIENTOS



AGRADECIMIENTOS

Te agradezco Señor por haberme creado y por haberme traído a este mundo para aprender tus leyes. Gracias por iluminar mi corazón para encontrar la verdad. Gracias por lo no visto y lo visto. Gracias por el pasado y por el presente. Gracias por todo.

Me gustaría expresar mi más profundo y sincero agradecimiento a todas las instituciones y personas que han contribuido para la realización de esta tesis doctoral. En especial a la Facultad de Ciencias, a la Escuela Internacional de Posgrado, de la Universidad de Granada e a todos vosotros por ayudarme de forma directa o indirecta mediante esta etapa de mi vida. He sido muy afortunada de conocerlos a todos.

En primer lugar, quiero dar mis más sinceros agradecimientos a la inestimable dirección y disponibilidad de mis directores al doctor Fernando Jesús Reyes Zurita y la doctora Marta Filomena Medina O'Donnell mediante la realización de esta tesis doctoral. Gracias Fernando por darme la oportunidad de formar parte de tu grupo de investigación que me permitió formarme en un área investigación que siempre me fascino, por depositar en mí toda tu confianza y sobre todo por ser un ejemplo a seguir. Gracias Marta por introducirme en el mundo de química orgánica y sobre todo por tus valiosos consejos.

En segundo lugar, agradezco enormemente a mi familia mis padres, mis hermanas, y mis sobrinos. Gracias, por vuestro amor, confianza y apoyo incondicionado. Gracias, padres por vuestro apoyo emocional y económico para alcanzar todas mis metas. Y especialmente por enseñarme madre que con la paciencia y el trabajo continuo se logra lo imposible. Y especialmente por enseñarme padre de nunca renunciar mis sueños. Gracias queridos padres por todo lo que habéis sembrado en mí, valores, buenos hábitos, autodisciplina, tenacidad, perseverancia y por todo lo que me habéis dado a lo largo de mi vida viviendo a vuestro lado en Marruecos y lejos de vosotros en España. Me siento muy orgullosa de ser vuestra hija. Gracias a vosotros estoy donde estoy hoy.

En tercer lugar, expreso mi más sincero agradecimiento al director del grupo de investigación al Catedrático Dr. José Antonio Lupiáñez Cara. Gracias José Antonio por tu inestimable confianza y continuo apoyo. Además, agradezco a los miembros del grupo a las doctoras Eva, Amalía y Leticia. Gracias por vuestros ánimos. Gracias Eva por tu inestimable ayuda y consejos.

Agradezco a los miembros del Grupo de Investigación "Biotecnología y Química de Productos Naturales" al Catedrático Andrés Parra, al Dr. Francisco Rivas y al Dr. Antonio Martínez, del departamento de química orgánica de la Facultad de Ciencias por su colaboración con nuestro grupo de investigación que dio lugar a la primera parte de los resultados presentados en esta tesis doctoral.

Asimismo, agradezco a los miembros del Grupo de Investigación "Biotecnología de Hongos y Síntesis de Moléculas Bioactivas" al Dr. José Quílez del Moral y el doctorando Alberto Galisteo del departamento de química orgánica y a los doctores Amalia García García, Sara Rojas, Antonio Rodríguez Diéguez del departamento de Química Inorgánica ambos de la Facultad de Ciencias por su colaboración con nuestro grupo de investigación que dio lugar a la segunda parte de los resultados presentados en esta tesis doctoral.

Expreso mi más sincero agradecimiento a la directora del departamento de Bioquímica y Biología Molecular I la Catedrática Dra. Mari Paz Carrasco Jiménez por ser mi tutora en esta tesis doctoral. Gracias Mari Paz por tu inestimable disponibilidad y dirección mediante mi formación predoctoral.

Asimismo, agradezco a todo el comité de dirección de la Escuela de Doctorado de Ciencias de la Salud de la universidad de Granada y en especial al Coordinador del Programa de Doctorado en Bioquímica y Biología Molecular al Dr. Jesús Torres de Pinedo y a la excoordinadora la Dra. Esperanza Ortega Sánchez por sus inestimables labores con las que han contribuido a mi formación.

Quisiera expresar, así mismo mi más sincero agradecimiento al Dr. Hilario Ramírez Rodríguez, por iniciarme en el mundo de la investigación y el razonamiento científico mediante el uso de la Bioinformática. Gracias Hilario por tu inestimable ayuda, continuo apoyo, confianza, por darme la oportunidad de adquirir conocimientos y habilidades que han sido primordiales en mi formación como investigadora y por ser un ejemplo a seguir.

Además, quiero expresar mi agradecimiento al departamento de Biología Celular de la Facultad de Ciencias especialmente a las doctoras Verónica Elisabeth Neubrand y María del Rosario Sepúlveda Justo por realizar los ensayos histológicos de las muestras biológicas.

Quiero dar las gracias al personal del Centro de Instrumentación Científica de la Universidad de Granada. Especialmente al Dr. Jaime Lazuen Alcón, por la realización de la técnica de citometría de flujo, a la Dra. Hoda Khaldy Belkadi, por la realización de la técnica de ELISA, al Dr. Ali Haïdour por la realización de espectros de RMN y al Centro de Investigación Biomédica por facilitar la experimentación animal.

Agradezco a todo el personal de la Escuela Internacional de Posgrado por estar siempre dispuestos a aclarar cualquier duda y especialmente al jefe de Servicio al Dr. José balderas Cejudo por su inestimable ayuda.

Quiero agradecer a los doctores y al personal del departamento de Bioquímica y Biología Molecular I de la facultad de Ciencias de la Universidad de Granada. A María José, A Milagros, A José Manuel, A Víctor, A Juan Antonio, A Miguel, A Pedro Real, A Marichu, A Susana, A Ana, A Signe, A Carmen, A Sonia, A Alberto, A Nerea, A Patricia, A María, A Enrique, A Rosa y A Maite, por vuestras interesantes

conversaciones y palabras de apoyo. Y especialmente A María José y A Milagros por vuestra colaboración en los estudios realizados in vivo de esta tesis doctoral, A María por tu amistad, A Alberto, A Sonia, A Enrique y A Rosa por vuestra inestimable ayuda.

Asímismo, agradezco a mis compañeros del laboratorio A Luis, A Isabel, A Houssam, A Oscar, A Paloma, A Blanca, A Celia y A Alberto. Gracias por formar parte de nuestro grupo de investigación. Y especialmente agradezco A Luis y A Houssam por su colaboración en algunos estudios realizados en esta tesis doctoral.

Quisiera expresar, así mismo, mi agradecimiento al Dr. Rachid Chahboun Karimi y a la Dra. Houda Zentar. Gracias por vuestros consejos y por estar siempre dispuestos a ayudarme en lo que sea.

Expreso mis más sinceros agradecimientos al amigo de mi padre A José Manuel y a su familia. Gracias por vuestra amistad y hospitalidad. Y especialmente agradezco a su hija Susana. Gracias Susana por tu inestimable ayuda y apoyo.

Igualmente, expreso mis más sinceros agradecimientos al amigo de mi padre Francisco y a su familia. Gracias por vuestra amistad y hospitalidad. Y especialmente te agradezco Francisco por tu inestimable ayuda para arreglar ciertos trámites.

Quiero agradecer a todas mis amigas que han estado a mi lado apoyándome, ayudando y confiando en mí. A Hakima, A Hanane, A Chadia, A Alicia y A Houda. Gracias por vuestra amistad y por todos los buenos momentos compartidos juntas.

Expreso mi agradecimiento a mis vecinos, A Angela, A Juan y A su hija María Ángel, de estar a mi lado todas las veces que los necesite. Gracias por vuestra amistad y hospitalidad.

Asímismo, quiero dar las gracias a mis cuñados que me han ayudado y apoyado a lo largo de estos años. Gracias por considerarme como vuestra hermana. Y sin olvidarme de la inestimable ayuda de mi tío Mohamed. Gracias, tío por ayudarme varias veces incondicionalmente.

Además, agradezco a Aicha y sus hijos especialmente a Sofia y Daniel. Gracias por vuestra amistad, hospitalidad, ayuda y apoyo.

Por último, pero no menos importante, agradezco a todas mis compañeras del piso y especialmente A Fátima, A Samar, A Nur, A Duaae, A Hayar, A Safa y A Ferdaws. Gracias por la agradable convivencia a lo largo de estos años.

ABREVIATURAS

3-A,28-MOA	3-acetoxy, 28-methylester oleanolic acid
3-AOA	3-acetoxyoleanolic acid
AH-Me	Achyranthoside H
AIF	Apoptosis inductor factor
AP-1	Activator proteins 1
Apaf-1	Apoptosis protease-activating factor 1
Akt	Protein Kinase B (PKB)
B5G9	Piperazine derivative of 23-hydroxy betulinic acid (23-HBA)
Bad	Bcl-2 associated death protein
Bak	Bcl-2 antagonist/killer protein
Bax	Bcl-2 associated x protein
BA	Betulinic acid
Bcl-2	B cell lymphoma- 2 protein
Bcl-xL	B cell lymphoma protein XL
BH3	Bcl homology domain 3
Bid	BH-3 interacting DD protein
Bim	Bcl-2 interacting protein
Bmf	Bcl2 modifying factor
BD	Binding domain
CARD	Caspase recruitment domains
CCl2	C-C Motif Chemokine Ligand 2
CD95/Fas	FS7 (foreskin cell strain) associated sAg,
CDDO	2-cyano-3,12-dioxooleana-1,9(11)-dien-28-oic acid
CDDO-Im	CDDO imidazole
CDDO-Me	CDDO-methyl ester
c-myc	v-myc: avian myelocytomatosis viral oncogene
COX	Cyclooxygenase
Con A	Concanavalin A
CD14	Cluster of differentiation 14
CD95/Fas	FS7 (foreskin cell strain) associated sAg
CDKI	Cyclin-dependent kinase inhibitor
CRD	Cysteine rich domain
CXCL8	C-X-C Motif Chemokine Ligand 8
DAMP	Damage-associated molecular patterns
DD	Death domain
DED	Death effector domain
DCF	Diclofenac
DHR	Dihydrorhodamine
DISC	Death inducing signaling complex
DMAPP	Dimethylallyl pyrophosphate
DMEM	Dulbecco's modified Eagle's medium
DR	Death receptor
ENDO G	Endonucleasa G

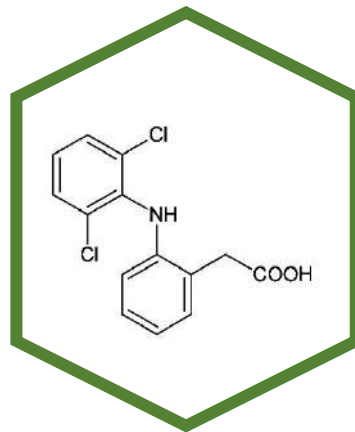
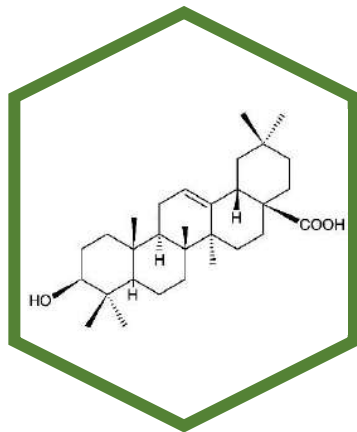
E2F	E2 Factor
FADD	Fas-Associated protein with death domain
FBS	Fetal bovine serum
FDA	Food and Drug Administration
FLIP	C-FLICE inhibitory protein
FPP	Farnesyl pyrophosphate
HCC	Hepatocellular carcinoma
HMG-CoA	Hydroxymethylglutaryl CoA
GADD45 α	Growth arrest and DNA damage-45 alpha
5-HETE	Hydroxyicosatetraenoic acid
HpETE	5-hydroxyperoxyeicosatetraenoic acid
IAP	Inhibit of apoptosis protein
IFN	Interferon
IKK	IkappaB kinase
IL	Interleukin
I κ B α	Nuclear factor of kappa light polypeptide gene enhancer in B- cells inhibitor alpha
iNOS	Inducible nitric oxide synthase
IPP	Isopentenyl pyrophosphate
Keap1	Kelch like ECH associated protein 1
JNK	C-Jun N-terminal kinase
LBP	Lipopolysaccharide Binding Protein
LOXs	Lipoxygenases
LT	Leukotrienes
LPS	Lipopolysaccharide
LX	Lipoxins
MAPK	Mitogen-activated protein kinases
MA	Maslinic Acid
MTT	1-(4,5-Dimethylthiazol-2-yl)-3,5-diphenylformazan, Thiazolyl blue formazan
MVA-5PP	Mevalonic acid 5-pyrophosphate
MMP	Mitochondrial membrane potential
MOMP	Mitochondrial outer membrane permeabilization
MyD88	Myeloid differentiation primary response gene 88
NADPH	Nicotinamide adenine dinucleotide phosphate
NF- κ B	Factor Nuclear Kappa
Nrf2	Nuclear factor erythroid 2-related factor 2
NO	Nitric Oxid
NQO1	NAD(P)H Quinone oxidoreductase 1
NSAIDs	Nonsteroidal anti-inflammatory drugs
OA	Oleanolic Acid
OADP	N-(3-(2-((3-aminopropoxy)methoxy)ethoxy)propyl)-3 β -hydroxyolean-12-en-28-amide
OSC	Oxidosqualene cyclases
p21	activating factor-1/cyclin-dependent kinase inhibitory protein-1 of 21 KDa
p38	mitogen-activated protein kinase of 38 KDa
p44/42	mitogen-activated protein kinases of 42 and 44 KDa
p53	Tumor suppressor protein of 53 KDa

PAMP	Pathogen-associated molecular pattern
PARP	Poly(ADP-ribose) polymerase
PBS	Phosphate-buffered saline
PDK	Phosphoinositide-dependent protein kinase
PEG	Polyethylene Glycol
PGs	Prostaglandins
PI3K	Phosphatidylinositol 3-kinase
PI	Propidium iodide
PLA ₂	Phospholipases A ₂
PMN	Polymorphonuclear
PTEN	Phosphatase and tensin homolog
ROS	Reactive oxygen species
SAPK	Stress-activated protein kinases
SOD-1	Superoxide dismutase 1
TLR	Toll receptor
TLR4	Toll-like receptor 4
TNF	Tumor necrosis factor
TNFR	Tumor necrosis factor receptor
TPA	12-O-tetradecanoylphorbol-13-acetate
TRADD	TNFR1-associated death domain
TRAF	Tumor necrosis factor receptor-associated factor
TRAIL	TNF-related apoptosis-inducing ligand
TSLP	Thymic stromal lymphopietin
TXA ₂	Thromboxane
UA	Ursolic Acid
WHO	World Health Organization

ÍNDICE

1. RESUMEN	3
2. INTRODUCCION	7
2.1. PLANTAS NATURALES: FUENTE DE NUEVOS FÁRMACOS.....	8
2.2. TRITERPENOS PENTACÍCLICOS: GENERALIDADES.....	11
1.1.1. <i>Ácido oleanólico</i>	13
2.2.1. <i>Actividad anticancerígena de los triterpenos pentacíclicos</i>	14
2.2.2. <i>Actividad antiinflamatoria de los triterpenos pentacíclicos</i>	16
2.3. DICLOFENACO: GENERALIDADES.....	18
2.3.1. <i>Mecanismo anticancerígeno del diclofenaco y de sus derivados</i>	19
2.3.2. <i>Mecanismo antiinflamatorio del diclofenaco y de sus derivados</i>	21
2.4. MECANISMOS DE ACTIVACIÓN DE LA MUERTE CELULAR PROGRAMADA	22
2.4.1. <i>Caspasas en apoptosis</i>	23
2.4.2. <i>Vía extrínseca de inducción de apoptosis</i>	24
2.4.3. <i>Vía intrínseca de inducción de apoptosis</i>	24
2.4.4. <i>El ciclo celular</i>	27
2.5. LA INFLAMACIÓN.....	28
2.5.1. <i>Modelos de inflamación</i>	30
2.5.2. <i>Citoquinas y moléculas mediadoras de inflamación</i>	32
2.5.2.1 Citoquinas Proinflamatorias	32
2.5.2.2 Mediadores lipídicos.....	33
2.5.2.3 Factor de transcripción NF-κB.....	34
2.5.2.4 MAP quinasas (MAPKs).....	35
2.5.2.5 Óxido nítrico (NO).....	35
3. OBJETIVOS	39
3.1. OBJETIVOS ESPECÍFICOS	39
4. PUBLICACIONES	41
4.1. PUBLICACIÓN 1.....	43
4.2. PUBLICACIÓN 2.....	45
4.3. PUBLICACIÓN 3.....	47
5. DISCUSIÓN	51
6. CONCLUSIONES	57
7. BIBLIOGRAFÍA	61
8. OTRAS COLABORACIONES	69

RESUMEN



1. RESUMEN

En los últimos años, ha existido un gran interés científico en el estudio de las propiedades terapéuticas de compuestos orgánicos naturales destacando actividades biológicas tan importantes como sus efectos antiinflamatorio y anticancerígeno. Dentro de este abanico de compuestos orgánicos encontramos los compuestos de origen natural como son los terpenos, metabolitos secundarios que se encuentran presentes en el reino vegetal. Dentro de los terpenos destacamos a los triterpenos que se caracterizan por presentar 30 átomos de carbono constituyendo uno de los grupos con mayor cantidad de compuestos bioactivos. Por otro lado, encontramos otro tipo de compuestos orgánicos como son los antiinflamatorios no esteroideos destacando el diclofenaco que se encuadra dentro de los compuestos fenólicos (derivado del ácido fenilacético) con propiedades antiinflamatorias.

En base a esto, esta tesis doctoral se divide en dos partes, la primera corresponde a la extracción, purificación del ácido oleanólico (OA), síntesis del derivado aminoPEGilado de ácido oleanólico (OADP) y la caracterización de las actividades anticancerígenas y antiinflamatorias de este derivado, determinando sus mecanismos moleculares de acción. La segunda parte, corresponde a un estudio preliminar de las actividades anticancerígenas y antiinflamatorias de diferentes amino-derivados del diclofenaco.

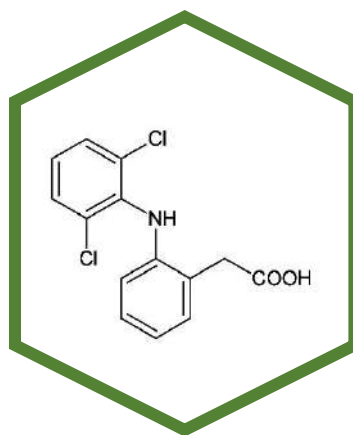
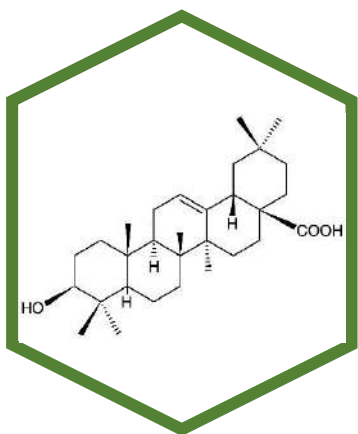
En la primera parte de la presente tesis doctoral, se procedió a la extracción y purificación del triterpeno pentacíclico, ácido oleanólico, a partir de los desechos de la molturación de la aceituna y posterior derivatización, se obtuvo como resultado el derivado aminoPEGilado N-(3-(2-((3-aminopropoxi) methoxi) ethoxi) propil)-3b-hidroxiolean-12-en-28-amida (OADP). A continuación, se realizaron ensayos bioquímicos para determinar el efecto anticancerígeno *in vitro* de este compuesto, tras cuantificar su efecto citotóxico en líneas cancerígenas de adenocarcinoma de colon humano (HT29), melanoma de piel (B16-F10) y hepatocarcinoma humana (HepG2), se mostró, que el OADP es significativamente más citotóxico en la línea tumoral HepG2 con un valor de $IC_{50} = 0.14 \mu\text{g/ml}$ y menos citotóxico en comparación en la línea celular no tumoral hepática humana (WRL68). De modo, que mediante el análisis de citometría de flujo se reveló el efecto apoptótico de OADP con porcentajes de apoptosis entorno al 74% - 95%, provocando la detención del ciclo celular en la fase G0/G1 e induciendo la pérdida del potencial de membrana mitocondrial (MMP). Además, mediante ensayos de Western blot tras 72 h de tratamiento con el OADP se observó un incremento de expresión de las caspasas iniciadoras, caspasa-8 y caspasa-9, así como de la caspasa efectora, caspasa-3, de la proteína pro-apoptótica mitocondrial Bak, de la proteína supresora tumoral p53 y de la proteína p21, proteína p53 dependiente, acompañados con una baja regulación de proteína mitocondrial anti-apoptótica Bcl-2. De modo, que concluimos que el OADP es capaz de activar ambas vías apoptóticas, la extrínseca e intrínseca. Activado probablemente en primer lugar la ruta extrínseca de inducción de apoptosis y de manera secundaria la ruta intrínseca probablemente para reforzar la señal apoptótica inicial.

A continuación, se evaluó el efecto antiinflamatorio *in vitro* e *in vivo* del OADP. De modo, que para determinar el potencial antiinflamatorio del OADP *in vitro*, se estableció la citotoxicidad de OADP en la línea celular de macrófagos/monocitos de ratón RAW 264.7 mediante el ensayo de MTT. A continuación, se indujo el proceso de inflamación mediante lipopolisacárido bacteriano (LPS) en células RAW 264.7, determinando los niveles de producción de óxido nítrico (NO) utilizando concentraciones subcitotóxicas de OADP, alcanzando el 75% de inhibición tras 72h de tratamiento. Además, el análisis del ciclo celular mostró, que OADP induce la reversión de la detención en la fase G0/G1 del ciclo en células RAW 264.7 estimuladas con LPS.

Mediante el ensayo de western blot, se evaluaron las proteínas implicadas en el proceso antiinflamatorio, en macrófagos murinos RAW 264.7 estimulados con LPS. Encontrando, que el tratamiento con OADP tras 72h, inhibió la expresión de las citoquinas proinflamatorias TNF- α e IL-1 β . A su vez, se inhibió la expresión de las principales proteínas mediadoras Cox-2, iNOS y de la proteína señalizadora p-IkBa. Asimismo, se determinó el efecto antiinflamatorio del OADP *in vivo*, mediante el modelo de inflamación aguda por edema inducido sobre oreja de ratón. Para lo cual, la inflamación fue inducida por TPA (12-O-tetradecanoilforbol-13-acetato). Los resultados obtenidos ponen de manifiesto que el tratamiento con OADP indujo una mayor supresión del edema en grupos tratados en comparación con el grupo control y disminuyó el grosor de la oreja un 14% más que el diclofenaco. Además, se analizaron los niveles de concentración de la IL-6 como marcador de inflamación, sobre los diferentes grupos de animales mediante la técnica Elisa encontrando, que, en las orejas derechas de los animales control, mostraron la evidente inducción de la expresión de IL-6 en respuesta al tratamiento con TPA. Mientras el tratamiento con el diclofenaco y OADP disminuyó efectivamente la producción de la IL-6 con un porcentaje de 60% mayor en el caso del OADP que en el caso del diclofenaco. Además, mediante los cortes histológicos de ambas orejas control y tratados se observó el descenso en los niveles de edema y de infiltración de leucocitos polimorfonucleares, principalmente neutrófilos.

En la segunda parte de la tesis doctoral, se estudió la capacidad anticancerígena y antiinflamatoria de varios compuestos amino derivados del diclofenaco, fármaco antiinflamatorio no esteroideo. En primer lugar, se estableció si estos compuestos también eran capaces de producir un efecto anticancerígeno. Se determinó el efecto citotóxico de los mismos sobre diferentes líneas tumorales, de hepatoma (HepG2), carcinoma de colon (HT29) y melanoma (B16-F10). A partir de los resultados obtenidos se seleccionó la línea tumoral HepG2 para profundizar sobre la actividad pro-apoptótica de los dos compuestos con menor IC₅₀, mediante ensayos por citometría de flujo. Se determinó la extensión de los fenómenos apoptóticos desencadenados tras 72 h de incubación en estas células con los compuestos mencionados. A continuación, se analizó el efecto de estos compuestos sobre el ciclo celular con ioduro de propidio (PI) observándose una parada del ciclo celular en la fase G0/G1 o en fase S dependiendo del compuesto. Finalmente, se analizó el potencial de membrana mitocondrial por tinción con dihidrorodamina 123 (DHR). Con respecto al efecto antiinflamatorio de estos compuestos, se determinó, la citotoxicidad de los mismos sobre la línea celular de macrófagos / monocitos de ratón RAW 264.7 mediante el ensayo de MTT. A continuación, se midió sus potenciales antiinflamatorios, a las concentraciones sub-citotóxicas ($\frac{1}{4}$ IC₅₀, $\frac{1}{2}$ IC₅₀ y $\frac{3}{4}$ IC₅₀) y a diferentes tiempos (24, 48 y 72 horas), mediante la determinación de los niveles de óxido nítrico usando la reacción de Griess, sobre células RAW264.7 activadas con LPS. Los resultados mostraron que casi todos los compuestos derivados del diclofenaco presentaron un importante efecto antiinflamatorio mucho más acentuado que el propio diclofenaco.

INTRODUCCIÓN



2. INTRODUCCION

Las plantas están unidas a la historia de la humanidad ya que han sido enormemente útiles para su supervivencia. Por un lado, aportan el oxígeno necesario para su respiración y, por otro lado, son fuente de nutrientes, vitaminas y minerales [1]. Pero el mayor descubrimiento en el uso de las plantas por parte del hombre ha sido el tratamiento de enfermedades y manejo del dolor [2].

Las plantas son capaces de biosintetizar diferentes tipos de compuestos:

- Metabolitos primarios que son los compuestos involucrados en las funciones primarias de la planta y son indispensables para el desarrollo fisiológico de la misma (aminoácidos, carbohidratos, lípidos, ácidos nucleicos) (**Figura 1**) [1].
- Metabolitos secundarios que son los compuestos químicos que no intervienen en las funciones esenciales de la planta, pero desempeñan un papel importante en su defensa frente a otros organismos (depredadores y patógenos) y su relación con el entorno [3].

Los productos naturales usados para fines medicinales son en su mayoría metabolitos secundarios y se clasifican principalmente en tres grandes grupos: alcaloides, compuestos fenólicos y terpenoides (terpenos) (**Figura 1**) [3].

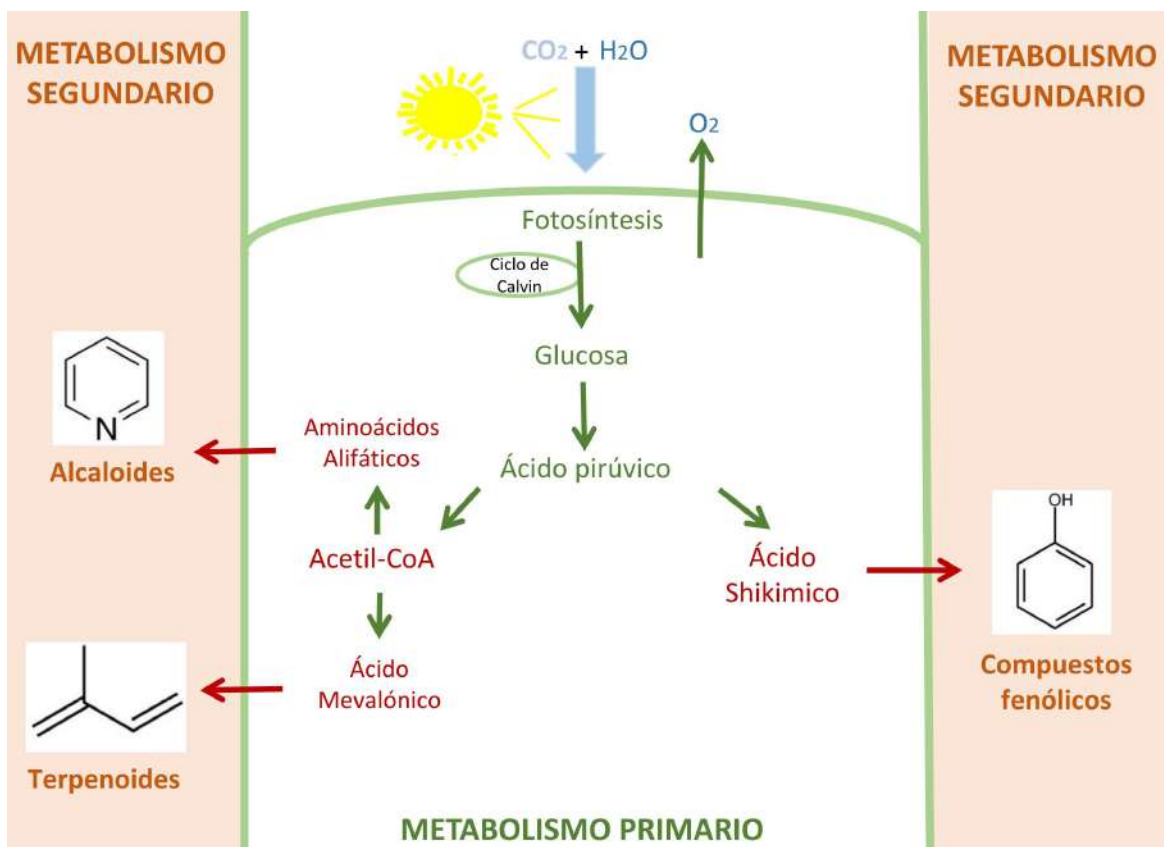


Figura 1: Representación esquemática de los principales metabolitos primarios y metabolitos secundarios de las plantas.

En 1815 Seydler definió la Farmacognosia, como la ciencia que se dedica al estudio de las materias primas de origen natural que el farmacéutico o la industria farmacéutica emplean para la elaboración de los medicamentos [4]. Más adelante esta definición ha ido adquiriendo una relevancia muy importante dentro del entorno farmacéutico y social. Las plantas medicinales han participado significativamente en la medicina moderna al proporcionar un número relevante de fármacos extremadamente útiles. De modo que el conocimiento de las plantas medicinales se sistematizó gradualmente hasta ocupar un lugar relevante en las farmacopeas [5].

Actualmente, la Sociedad Americana de farmacognosia incluye en su definición el estudio de las propiedades físicas, químicas, bioquímicas y biológicas de los productos naturales, así como la búsqueda de nuevos medicamentos de fuentes naturales. Esta definición aclara la relación entre la química orgánica, la médica y biológica para el estudio y búsqueda de productos naturales con fines terapéuticos [6].

Uno de los principales objetivos en el desarrollo de nuevos fármacos es conseguir compuestos de alta bioactividad, que ejerzan su efecto terapéutico a dosis bajas y que presenten muy baja toxicidad. Como consecuencia, se emplea una estrategia que consiste en modificar químicamente compuestos naturales o sintéticos, de bioactividad reconocida, introduciendo, nuevos grupos funcionales, dando como resultado, derivados semisintéticos con bioactividades extremadamente potenciadas con respecto a sus precursores naturales o sintéticos [7], [8].

En base a esto, nuestro grupo de investigación, “Drogas, Tóxicos Ambientales y Metabolismo Celular” ha venido desarrollando hasta ahora diversas investigaciones vinculadas al estudio de las actividades biológicas de los triterpenos extraídos de los desechos de molturación de la aceituna del orujo de la especie *Olea europaea L.* específicamente el ácido maslínico y el ácido oleanólico y sus derivados [8], colaborando con el grupo de investigación “Biotecnología y Química de Productos Naturales”. En este marco, la investigación planteada consiste en la extracción, aislamiento, purificación y síntesis de compuestos bioactivos y su estudio biológico sobre diferentes modelos (*in vitro e in vivo*), con el objetivo de descubrir nuevos agentes terapéuticos antiinflamatorios y/o anticancerígenos. Por consiguiente, esta colaboración entre ambos grupos de investigación pretende seguir con estos mismos objetivos, donde se enmarca esta tesis doctoral.

Asimismo, nuestro grupo de investigación estudio las actividades anticancerígenas y antiinflamatorias de N-derivados del diclofenaco colaborando con el grupo de investigación “Biotecnología de Hongos y Síntesis de Moléculas Bioactivas”. En consecuencia, los resultados obtenidos conforman la segunda parte de esta tesis doctoral.

2.1. Plantas naturales: Fuente de nuevos fármacos

Desde la antigüedad los productos naturales han sido un sistema tradicional del tratamiento de enfermedades en todo el mundo y han constituido uno de los pilares esenciales en el desarrollo histórico y cultural. El uso de estas moléculas bioactivas como medicamentos supera los miles de años atrás [2]. Según la Unión Internacional de la Conservación de la Naturaleza, hay entre 50.000 y 80.000 especies de plantas para el uso medicinal [9]. De modo, que las plantas han proporcionado los compuestos farmacológicamente activos de muchos medicamentos de gran éxito, derivados directa o indirectamente de las plantas [10].

Por lo tanto, se pone de manifiesto la importancia de las plantas medicinales el creciente número de trabajos publicados a lo largo de las últimas décadas. Se observa un continuo aumento de publicaciones desde 1960 a 2001, con más de 1300 estudios publicados, así como la tendencia en gran aumento hasta 2011, alcanzando más de 6200 publicaciones. Finalmente, el número de publicaciones se estabiliza aproximadamente en 5000 por año (**Figura 2**) [11].

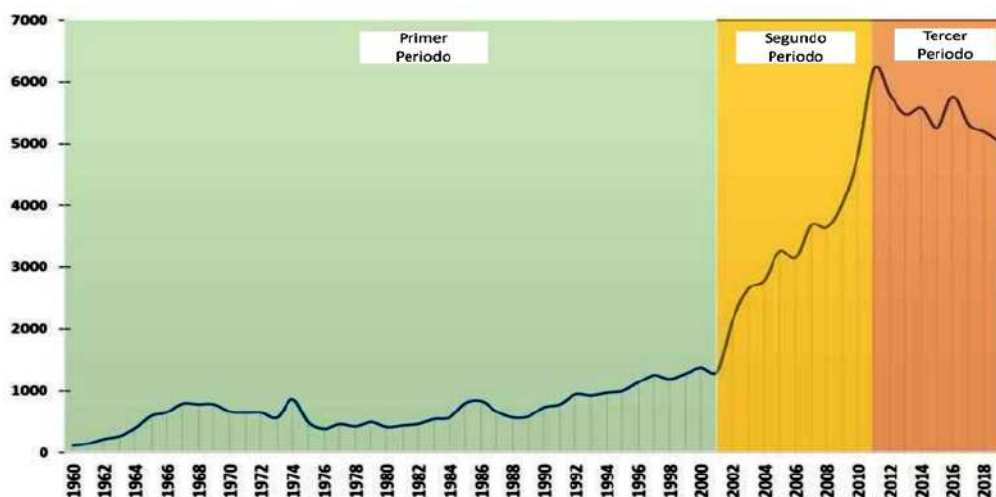


Figura 2: Evolución temporal mundial de las publicaciones en plantas medicinales [11].

Asimismo, se ha probado que los productos naturales han ejercido un papel esencial en el desarrollo de medicamentos modernos, especialmente para agentes antibacterianos y antitumorales (**Figura 3**) [12]. Por ejemplo, de los 162 fármacos antibacterianos aprobados por la FDA (Agencia del Departamento de Salud y Servicios Humanos de los EE. UU.), a lo largo de los últimos años, 78 de ellos son fármacos de origen natural mientras los fármacos sintéticos representan solo 36 de los aprobados (**Figura 3, A**). Asimismo, de los 259 fármacos anticancerígenos aprobados por la FDA desde 1946 hasta 2019, aproximadamente 101 de ellos son de origen natural, siendo solo 53 son fármacos sintéticos aprobados (**Figura 3, B**) [12].

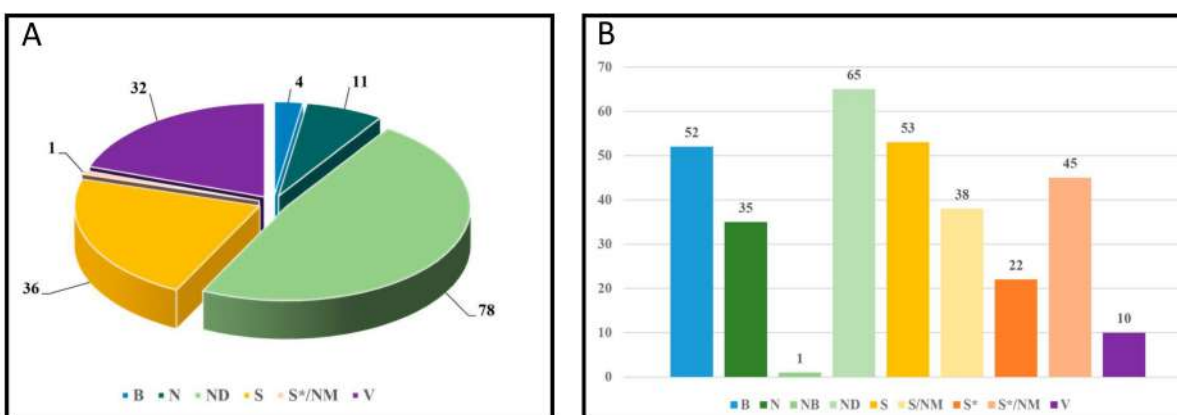


Figure 3: Porcentaje de fármacos aprobados por la FDA. A: antibacterianos y B: anticancerígenos dependiendo de su origen. "B": macromolécula biológica; "N": producto natural inalterado; "NB": medicamento botánico (mezcla definida); "ND": derivado de productos naturales; "S": Fármacos sintéticos; "S*": Fármaco sintético (NP farmacóforo); "V": vacuna; "/NM": análogo del producto natural (Figura adaptada de [12]).

Alcaloides, fenoles y terpenos son los principales metabolitos secundarios usados en el tratamiento de enfermedades. Dentro del grupo de alcaloides encontramos varios fármacos como la morfina y el cannabidiol. La morfina, fármaco analgésico, es el primer producto natural puro comercializado para su uso terapéutico extraído de la especie *Papaver Somniferum* [13]. En cuanto al cannabidiol, *Cannabis sativa*, presenta un potente efecto anticancerígeno (**Figura 4**) [14].

En el grupo de los fenoles encontramos otros fármacos como salicina y silibina, aislados de *Salix alba* y *Silybum marianum*, que actúan como un agente antiinflamatorio y frente a enfermedades hepáticas respectivamente (**Figura 4**) [15], [16]. Por último, encontramos los fármacos del grupo de los terpenos. La forskolina y el paclitaxel, son dos fármacos diterpénicos. El primero, extraído de la especie *Plectranthus barbatus*, trata las enfermedades cardíacas y respiratorias [17] y el segundo, extraído de la especie *Taxus brevifolia*, se utiliza en el tratamiento de varios tipos de cáncer principalmente en cáncer de pulmón, de ovario y de mama [18]. Hay que destacar el derivado de ácido oleanólico, bardoxolona metilada que ha sido evaluada en ensayos clínicos, fase 1 para tumores sólidos avanzados y linfoma en 47 pacientes [19] (**Figura 4**). El ácido oleanólico se puede extraer de varias plantas vegetales pero su principal fuente es la especie *Olea europea*.

Los productos naturales descubiertos hasta el día de hoy han desempeñado un papel crucial en la mejora de la salud y cada vez más, está creciendo el interés de los investigadores en descubrir nuevos productos de origen natural frente a dianas terapéuticas de diferentes enfermedades [20]. En este sentido, nuestro principal objetivo consistirá en evaluar los efectos anticancerígeno y antiinflamatorio del OADP, derivado del OA, extraído del orujo de oliva para nuestro estudio.

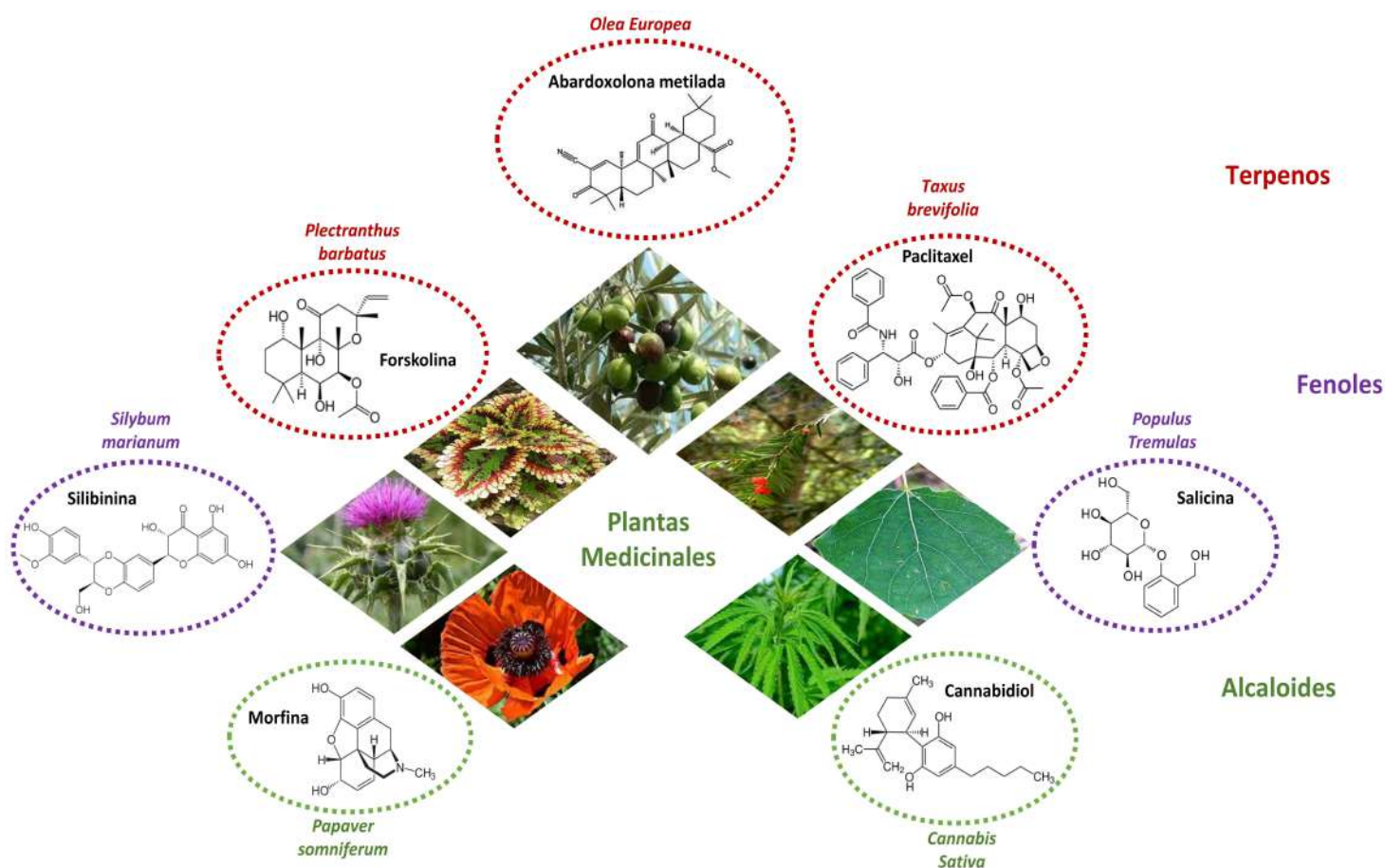


Figura 4. Estructuras químicas de algunos fármacos de origen natural y sus plantas de origen.

2.2. Triterpenos pentacíclicos: Generalidades

Uno de los principales metabolitos secundarios con interés terapéutico son los terpenos, ampliamente distribuidos en la naturaleza, se encuentran principalmente en las plantas. Es un grupo diverso de productos naturales que se clasifica según el número de unidades de isopreno y el número de carbonos que presentan en su estructura: monoterpenos (dos unidades de isopreno con 10 carbonos), sesquiterpenos (tres unidades de isopreno con 15 carbonos), diterpenos (cuatro unidades de isopreno con 20 carbonos), sesterterpenos (cinco unidades de isopreno con 25 carbonos), triterpenos (seis unidades de isopreno con 30 carbonos) y tetraterpenos (ocho unidades de isopreno con 40 carbonos) [21].

Los triterpenos están muy distribuidos, especialmente en hojas, corteza, frutos y semillas de plantas [22]. Se consideran uno de los grupos más grandes y diversos de productos naturales, se conocen más de 100 variaciones esqueléticas con aproximadamente 20.000 triterpenos diferentes. Su biosíntesis transcurre a través de la ruta del mevalonato en el citosol de las plantas. Esta vía de biosíntesis consiste en la condensación de dos unidades de acetil CoA para formar acetoacetil CoA, que tras la incorporación de una tercera molécula y sufrir una reacción de hidrólisis, da lugar al compuesto 3-hidroxi-3-metilglutaril-CoA (HMG-CoA) que sufre una reacción de reducción con NADPH produciendo el ácido mevalónico. Este ácido sufre una fosforilación y descarboxilación formándose pirofosfato de isopentenilo (IPP). Este IPP mediante una isomerasa sufre una isomerización a pirofosfato de dimetilalilo (DMAPP). El DMAPP posee un buen grupo saliente, el pirofosfato, formándose un carbocatión que actuará de electrófilo. Por otro lado, IPP actúa como nucleófilo. La combinación de una unidad de DMAPP y otra de IPP dan lugar a pirofosfato de geranilino (GPP) precursor de los monoterpenos (C₁₀).

El GPP reacciona con otra unidad de IPP dando lugar al pirofosfato de farnesilo (FPP) que es el precursor de los sesquiterpenos (C₁₅). La adición de una nueva unidad de IPP forma el pirofosfato de geranilgeranilino (GGPP), precursor de los diterpenos (C₂₀). Posteriormente el acoplamiento cabeza-cabeza de dos unidades de FPP conlleva la formación del escualeno, precursor de los triterpenos [21]. El escualeno sufre una reacción de oxidación, catalizado por una enzima escualeno epoxidasa [23], a partir del cual se formarán los diferentes triterpenos según tipo de plegamiento y tipo de enzimas que participen. Los esqueletos de tipo ursano (ácido ursólico), tipo oleanano (ácido oleanólico y maslínico) y lupano (ácido betulínico) son los más importantes desde el punto de vista biológico (**Figuras 5A, 5B**).

Estos esqueletos están ampliamente distribuidos en las plantas y principalmente en la especie *Olea europea L.* donde se han encontrado en todos sus órganos y específicamente en sus brotes florales y en su fruta madura. El grupo oleanano constituye el 98-99% del total de triterpenos siguiéndole los esqueletos de ursano y lupano. Asimismo, se ha demostrado que estos triterpenos están presentes en el aceite de oliva virgen y en el de orujo de *Olea europaea L.* Sus concentraciones en aceite de oliva virgen dependen de la calidad del aceite de oliva y de la variedad de aceituna [24], [25].

En este trabajo nos vamos a centrar en los triterpenos pentacíclicos de la especie de *Olea europea L.* obtenidos a partir de los residuos de la molturación de la aceituna en el proceso de la obtención del aceite. Este subproducto de oliva contiene altas concentraciones de ácidos oleanólico y maslínico [25]. El grupo de investigación "Biotransformación y Química de Productos Naturales" ha desarrollado varias patentes, nacional (P96061652) e internacional (W098/04331) para la extracción de estos ácidos. Este grupo lleva muchos años trabajando en el aislamiento y purificación de estos ácidos, con el objetivo de derivatizar dichos triterpenos obteniendo una gran biblioteca de nuevos productos mejorando sus propiedades biológicas [26].

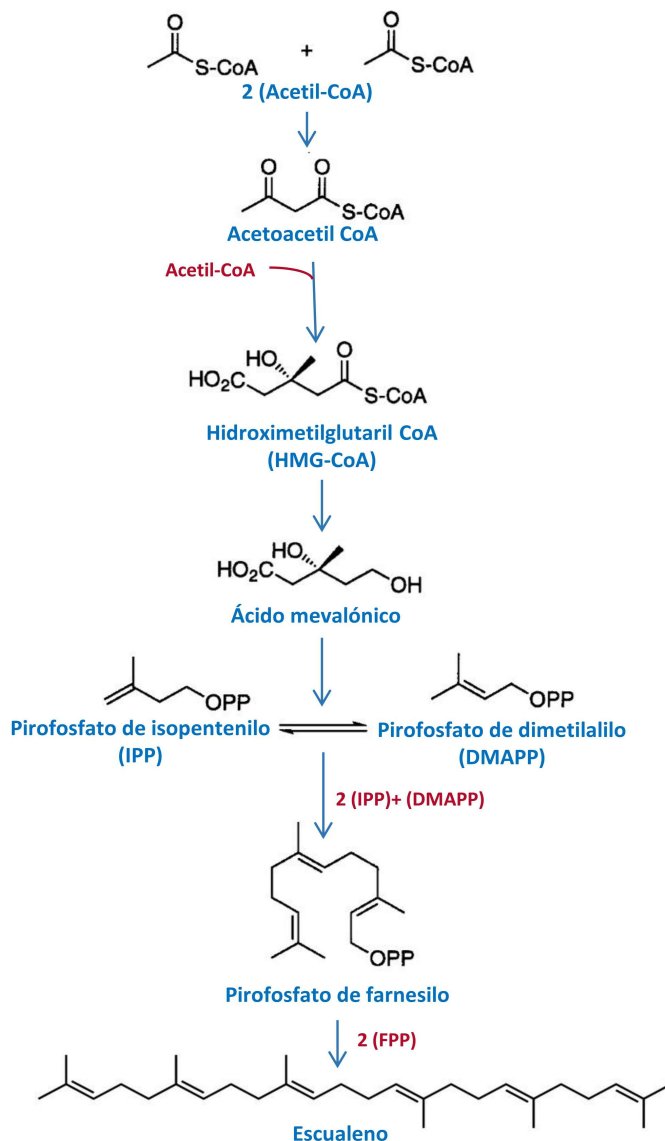


Figura 5A. Biosíntesis del escualeno

Hay un creciente interés con respecto al potencial biofarmacéutico de los triterpenos extraídos del orujo de olivo llevando a determinar sus mecanismos de acción [27], [28]. De hecho, en esta última década, diferentes trabajos han demostrado diversas bioactividades de los triterpenos pentacíclicos entre las que se incluyen, actividades anticancerígenas, antiinflamatorias, antivirales, antidiabéticas, antimicrobianas, hepatoprotectoras cardioprotectoras entre otras. Siendo los efectos antitumorales y antiinflamatorios de los triterpenos pentacíclicos los que han recibido la mayor atención [29].

Para la obtención del OA, se utilizó la extracción soxhlet con acetato de etilo, obteniendo un extracto enriquecido con ácido oleanólico y otros triterpenos como el ácido maslínico. A continuación, se procedió a purificar dicho extracto mediante cromatografía en columna flash empleando como disolventes una mezcla de diclorometano y acetona de polaridades crecientes, obteniendo ácido oleanólico puro. Los ácidos oleanólico y maslínico, se purificaron y aislaron por separado, posteriormente, se procedió a derivatizar el ácido oleanólico mediante reacción de PEGilación, por unión covalente de 4,7,10-trioxatridecano-1,13-diamina (PEG de tipo amino) sobre el grupo carboxilo de C-28. Como resultado se obtuvo un derivado aminoPEGilado de ácido oleanólico, N-(3-(2-((3-aminopropoxi) methoxi) ethoxi) propil)-3b-hidroxiolean-12-en-28-amida (OADP). Este método de extracción fue usado en esta tesis para extraer y obtener ácido oleanólico puro para su posterior uso en la síntesis del derivado OADP.

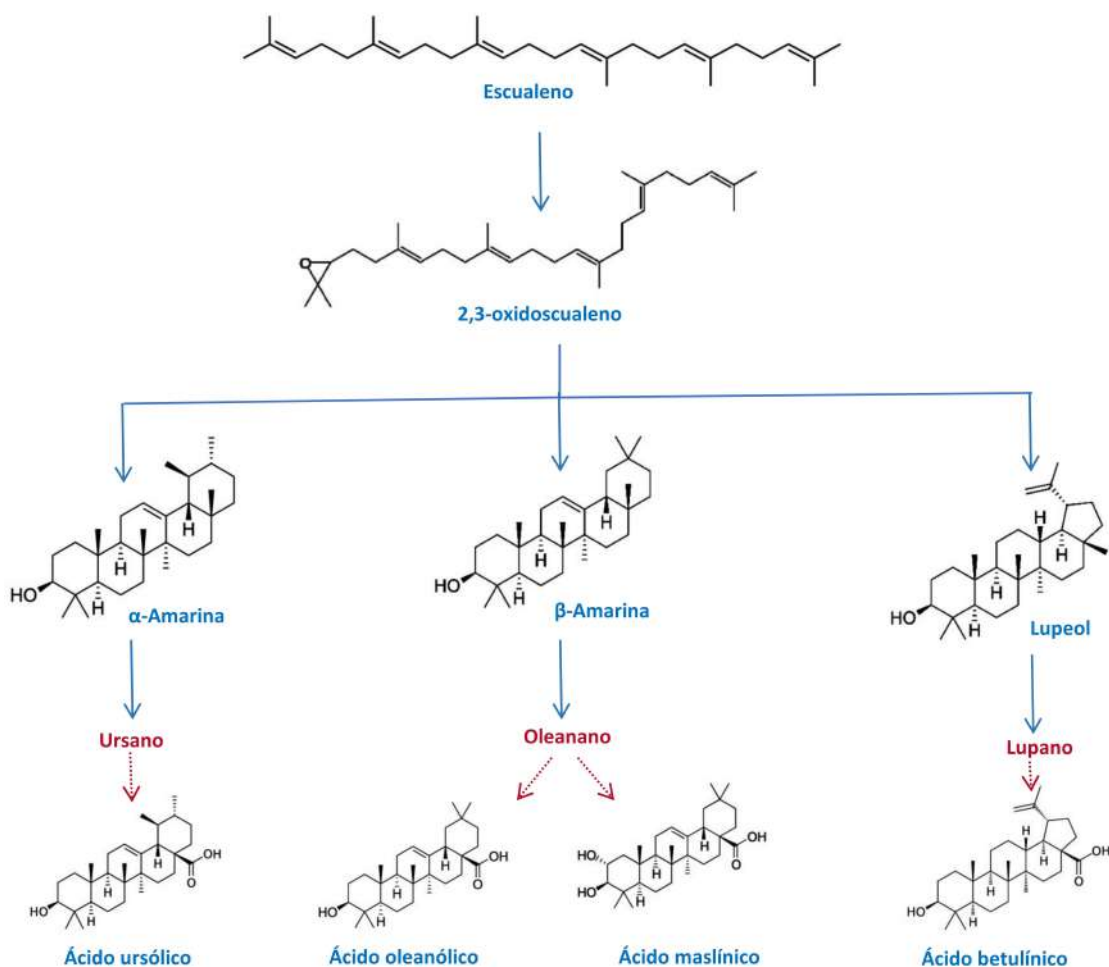


Figura 5B. Biosíntesis de los triterpenos.

1.1.1. Ácido oleanólico

A continuación, nos vamos a centrar principalmente en los triterpenos pentacíclicos presentes en *Olea Europea L.* y más específicamente en el ácido oleanólico, objeto de nuestro estudio. El Ácido oleanólico se ha aislado en más de 2000 especies de plantas, la mayoría de ellas son plantas comestibles y medicinales. Es muy abundante en la planta de olivo (*Olea europea*) y en las hojas de la especie calluna vulgaris. La planta de olivo es la principal fuente comercial para el compuesto y de donde proviene su nombre [25], [30].

El ácido oleanólico $C_{30}H_{48}O_3$ (OA, ácido 3β-hidroxiolean-12-en-28-oico), es un triterpeno pentacíclico bioactivo e hidrofóbico perteneciente a la familia de oleananos, constituido por cinco anillos de seis elementos, con un grupo hidroxilo en el carbono C-3, dos grupos metilo en C-4 y C-20 y un grupo metilo en C-8, C-10 y C-14. Además, posee un grupo carboxilo ubicado en la posición C-17 y un doble enlace entre C-12 y C-13. Además, la estereoquímica del grupo -OH en la posición C-3 tiene implicaciones fisiológicas importantes. En este sentido, los isómeros 3α-OH menos comunes tienen diferentes actividades biológicas que no comparten los isómeros 3β-OH más comunes. Estas propiedades estéricas del metilo exocíclico y otros grupos en los triterpenos naturales son determinantes esenciales en su actividad y seguridad en contextos farmacológicos, convirtiéndose en objetivos de modificación para la derivatización de este compuesto [31], [32] (**Figura 6**).

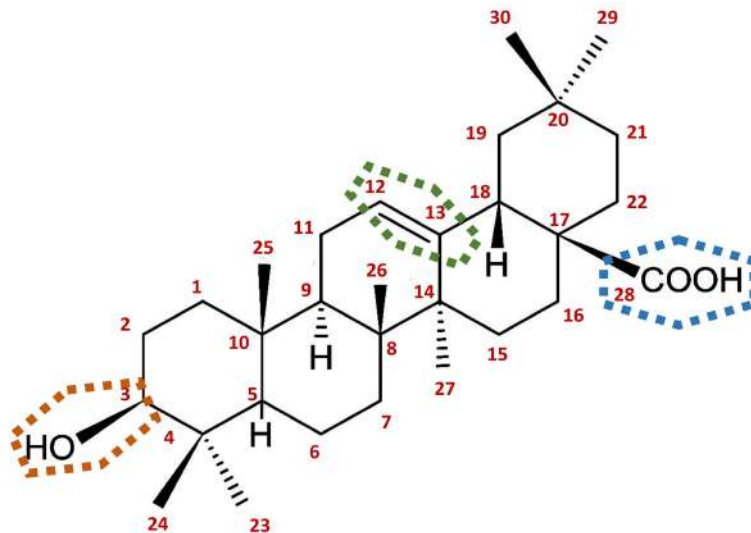


Figura 6. Estructura química del ácido oleanólico destacando sus sitios activos.

El OA se produce en las hojas, granos y frutos del olivo como cristales casi puros que protegen de los ataques de hongos y funciona como un compuesto de defensa frente a los herbívoros o patógenos. Este existe en la naturaleza como un ácido libre, pero también se presenta como aglicona de saponinas, triterpeno unido a una o más unidades de azúcar formando glucósidos. Como se ha mencionado, el OA se puede obtener fácilmente con alto rendimiento a partir de residuos sólidos de molturación de aceituna, ya que se encuentra en altas cantidades de forma libre en la cera epicuticular de su fruto (aceituna). Varios trabajos han demostrado las importantes actividades farmacológicas del OA y de sus derivados *in vitro* e *in vivo* como potente agente antiinflamatorio y antitumoral, así como inductor de apoptosis en varias células cancerosas [33].

2.2.1. Actividad anticancerígena de los triterpenos pentacíclicos

En este apartado nos vamos a concentrar principalmente en la actividad anticancerígena de los triterpenos pentacíclicos enfocándonos más concretamente en OA y sus derivados. En esta última década, varios trabajos han demostrado los efectos anticancerígenos y antitumorales de los triterpenos pentacíclicos [34], [35]. El OA es conocido por sus efectos anticancerígenos y antitumorales en varios tipos de cánceres y en diferentes modelos *in vitro* e *in vivo*. El OA inhibió el crecimiento de tumores trasplantados en ratones y la proliferación de células de hepatoma (HepG2), mediante la detención del ciclo celular, regulación de la proteína tumoral p53 e inducción de la activación de la vía apoptótica mitocondrial [36]. Se ha demostrado que OA disminuyó la proliferación de células cancerosas de mama [37]. Además el OA indujo apoptosis mediante la vía mitocondrial e inhibió la expresión de XIAP en células de hepatocarcinoma HuH7 [38] (**Figura 7**).

Sin embargo, el OA muestra una baja solubilidad en agua y por tanto una baja biodisponibilidad, impidiendo que sus actividades biológicas se expresan efectivamente. Por ello, varios trabajos han mejorado su biodisponibilidad al incluirle ciertas modificaciones. Estas modificaciones han tenido en cuenta los tres sitios activos del OA que son: el hidroxilo C-3, el doble enlace entre C-12 y C-13 y el ácido carboxílico de C-28. Lo que dio lugar a varios derivados con importantes actividades antitumorales. Uno de ellos el profármaco de O²-(2,4-dinitrofenil) diazeniodiolato, mostró una potente actividad antiproliferativa *in vitro* e *in vivo*, induciendo apoptosis en las células HepG2, provocando una parada del ciclo celular en la fase G2/M, activando tanto la vía mitocondrial como la vía MAPK, mejorando la producción intracelular de ROS [31] (**Figura 7**).

Asimismo, se usa la PEGilación para mejorar la biodisponibilidad de los fármacos. Se trata de la unión covalente de polietilenglicol (PEG) a una molécula determinada que puede ser una proteína, un péptido, un oligonucleótido, un fragmento de anticuerpo, una pequeña molécula orgánica o un fármaco potenciando su efecto terapéutico [7]. El PEG es un polímero soluble en agua y biocompatible que se utiliza para la administración de fármacos y está aprobado por la FDA. Por lo tanto, la técnica de la PEGilación se considera una de las técnicas más innovadoras y fiables para el desarrollo de medicamentos anticancerígenos [39]. De modo que nuestros resultados presentados en la publicación 1, han sido prometedores al unir el polietilenglicol (PEG) al ácido oleanólico en C-28. El OADP ha sido 718 veces más efectivo que su precursor, el OA en la línea tumoral de hepatoma humano HepG2.

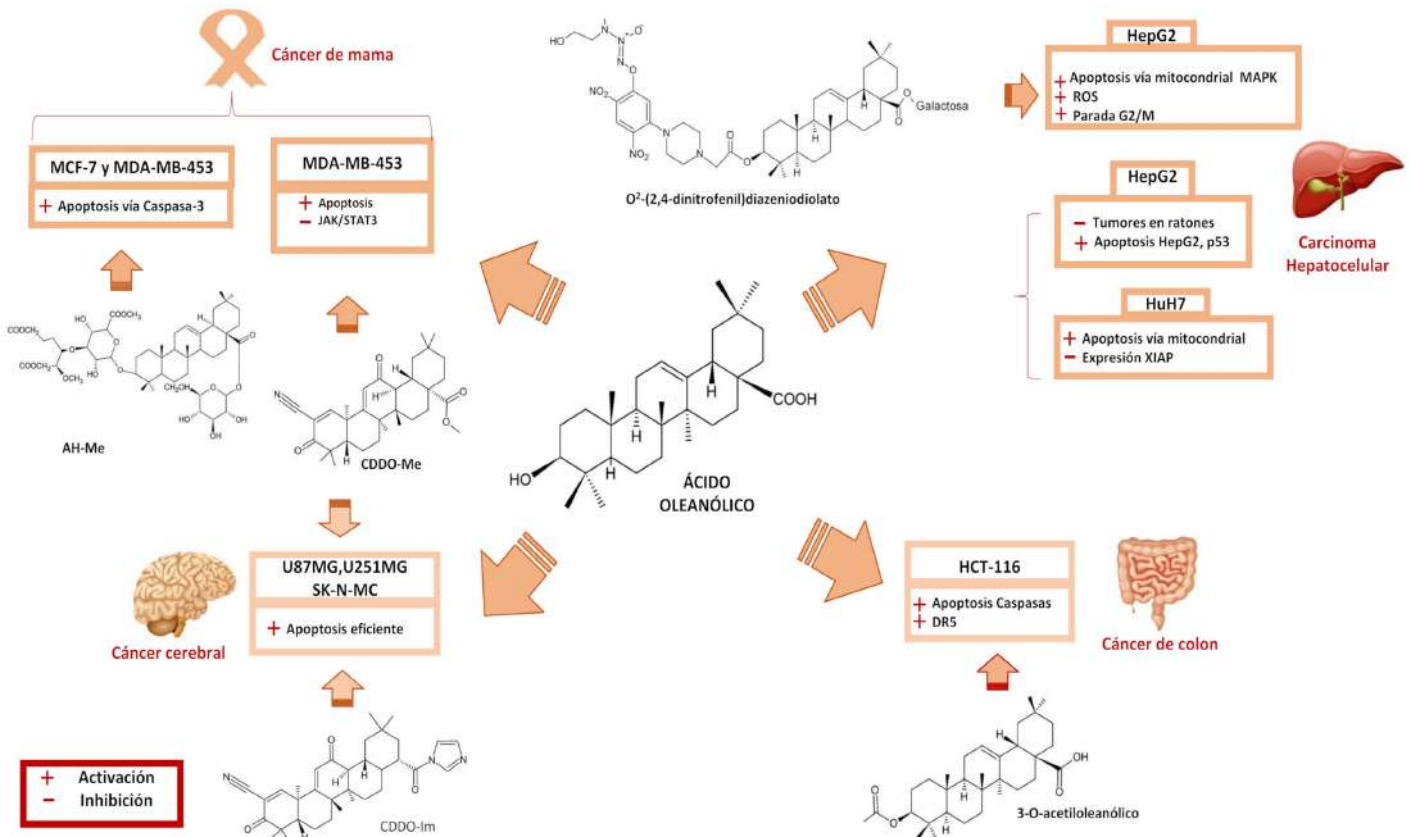


Figura 7. Mecanismos anticancerígenos encontrados en el ácido oleanólico y de sus derivados.

En cuanto a su derivado sintético, el éster metílico *Achyranthoside H* (AH-Me) mostró una citotoxicidad significativa en las líneas celulares del cáncer de mama humano MCF-7 y MDA-MB-453 y produciendo apoptosis mediada por la caspasa-3 [40]. El derivado del OA, CDDO-Me inhibió la vía JAK/STAT3 en células de cáncer de mama MDA-MB-468 [41]. En caso de tumores cerebrales primarios que responden débilmente a los agentes quimioterapéuticos, los derivados del OA, CDDO (*1-[2-cyano-3,12-dioxoleana-1,9(11)-dien-28-oyl]*), CDDO-Me (*CDDO* metil éster en C-28) y CDDO-Im (*CDDO*-Imidazol) inhibieron el crecimiento de células de glioblastoma (U87MG, U251MG) y células de neuroblastoma (SK-N-MC). De modo que el CDDO-Me y CDDO-Im mostraron actividad anticancerígena eficiente, e indujeron apoptosis en estas líneas celulares [42]. Otro trabajo mostró que el derivado ácido 3-O-acetiloleanólico, indujo apoptosis en células HCT-116 activando la cascada de señalización de caspasas extrínseca y produciendo el incremento de expresión del receptor de muerte 5 (DR5) [32] (**Figura 7**).

Otros oleananos como el ácido maslínico (MA) también han mostrado actividades anticancerígenas y pro-apoptóticas. En cuanto a la actividad anticancerígena *in vitro* del MA, nuestro grupo de investigación demostró sus propiedades anticancerígenas en la línea de cáncer de colon Caco-2, mediante la inducción de apoptosis extrínseca, regulada por la activación de las caspasas -8 y -3, aumentando los niveles de t-Bid [27]. Asimismo, demostró que el tratamiento de las células HT29 con MA produjo la activación de la vía apoptótica mitocondrial mediante la inhibición de la expresión de la proteína Bcl-2, activando la expresión de Bax, induciendo una alteración mitocondrial, estimulando la liberación del citocromo-c al citosol y finalmente activando las caspasas -9 y -3 [43].

El ácido betulínico (BA) y sus derivados, han mostrado efectos anticancerígenos en varias líneas tumorales. Por ejemplo, B5G9 derivado piperazidínico de BA, alcanzó un 80% en la tasa de inhibición del crecimiento tumoral en las células HepG2, produjo la pérdida del potencial de membrana mitocondrial e indujo la activación de caspasa-9 y caspasa-3, dando lugar a la escisión de poli-ADP-ribosa polimerasa [44]. Con respecto a la actividad anticancerígena del ácido ursólico (UA), ha sido también demostrado en varios tipos de cánceres. Sin embargo, el UA tiene una baja solubilidad en agua. Lo que ha llevado a realizar algunas modificaciones en su estructura para mejorar su biodisponibilidad. Obteniendo derivados, con una destacada actividad anti-HCC (anti-hepatocelular carcinoma) con valores de IC_{50} de $1.26 \pm 0.17 \mu M$ e inferiores a $1 \mu M$ [45].

2.2.2. Actividad antiinflamatoria de los triterpenos pentacíclicos

En este apartado nos vamos a centrar principalmente en la actividad antiinflamatoria de los principales triterpenos pentacíclicos del olivo, enfocándonos más en OA y sus derivados. Numerosos trabajos han mostrado que los procesos inflamatorios inducen varias enfermedades incluso el cáncer [46]. Por lo tanto, hay varios trabajos que han demostrado el efecto antiinflamatorio de OA y de sus derivados. Se observó que OA inhibe la colitis inducida por dextrano sulfato de sodio (*DSS*, *dextran sulfate sodium*), por inhibición de los linfocitos T efectoros (Th17), de la expresión de la interleuquina 1 (IL-1), NF- κ B, MAP quinasas, y del factor de transcripción ROR γ t (*RAR-related orphan receptor gamma*), activación de la expresión de FOXP3 (gen marcador de células T reguladoras), interleuquina 10 (IL-10) y mieloperoxidasa (enzima oxidorreductasa) en el colon, demostrándose que OA podría prevenir la inflamación aguda de colon o colitis [47] (**Figura 8**).

En cuanto a sus derivados, en la evaluación el efecto antiinflamatorio del derivado OADP, objeto de estudio en esta tesis, hemos obtenidos resultados muy interesantes presentados en la publicación 2, en la cual se muestra los efectos de este compuesto en modelos de inflamación *in vitro* e *in vivo*. En el primer modelo se usó las células de macrófagos/monocitos de ratón RAW 264.7 estimulados con LPS, el tratamiento con OADP a 72 h, inhibió la producción de óxido nítrico un 75%. Asimismo, en el modelo de inflamación aguda por edema inducido sobre oreja de ratón, el tratamiento con el OADP redujo eficazmente la producción de interleuquina 6 (IL-6) alcanzando un porcentaje de inhibición del 60%, superior que en el caso del tratamiento con el diclofenaco.

Asimismo, en trabajos publicados por otros autores, el derivado de OA, CDDO-Me, mostró un efecto antiinflamatorio, mediante la reducción de los niveles de infiltración de macrófagos en tejido, de los marcadores de proliferación COX-2, Ki67 y de los marcadores pro-inflamatorios IL-6, NF- κ B y el factor de necrosis tumoral (TNF- α), mientras que mostró un aumento en la expresión de CD206 (receptor de manosa de los macrófagos) e interleuquina 10 (IL-10) en el caso de inflamación crónica en el colon de roedores [48]. Del mismo modo, el derivado sintético de OA, CDDO-Im inhibió la expresión de IL-6 e IL-17,

aliviando de este modo la colitis inducida por DSS en ratones. Por lo tanto, se demostró que OA y sus derivados tienen un potente efecto antiinflamatorio en las enfermedades inflamatorias intestinales [49]. En modelos de inflamación en ratas Wistar macho, los derivados acetilados y metilados (3-A,28-MOA) y (3AOA) de AO, exhibieron mejores propiedades antiinflamatorias *in vitro* e *in vivo*, en comparación con el OA [50] (**Figura 8**).

En cuanto al efecto antiinflamatorio del ácido maslínico (MA) se demostró en células RAW264.7 estimuladas con lipopolisacárido que redujo la producción de NO y la expresión de iNOS en células RAW264.7. El MA inhibió la liberación de IL-6 y promovió la liberación de IL-10, inhibiendo significativamente la producción de ROS (especies Reactivas de oxígeno), la translocación de NF-κB, la liberación de Nrf2 (factor de transcripción que regula la transcripción de enzimas detoxificantes y antioxidantes), al mismo tiempo, inhibió la separación de Keap1 y Nrf2 en esta línea. Además, MA activó la expresión de p-JNK1/2, p-ERK1/2 y p-p38MAPK [51].

El efecto antiinflamatorio del ácido betulínico (BA), ha sido probado en varios trabajos. Este ácido exhibió una potente actividad antiinflamatoria en un modelo de shock endotóxico en ratón protegiendo a los animales de una dosis letal de lipopolisacárido (LPS), así como también, inhibió significativamente la liberación del factor de necrosis tumoral TNF-α inducida por LPS y aumentó el nivel de interleuquina IL-10 en el suero. Experimentos *in vitro* mostraron también que el tratamiento con ácido betulínico inhibe la producción de TNF-α y NO en macrófagos activados por LPS, mejorando la producción de IL-1 [52].

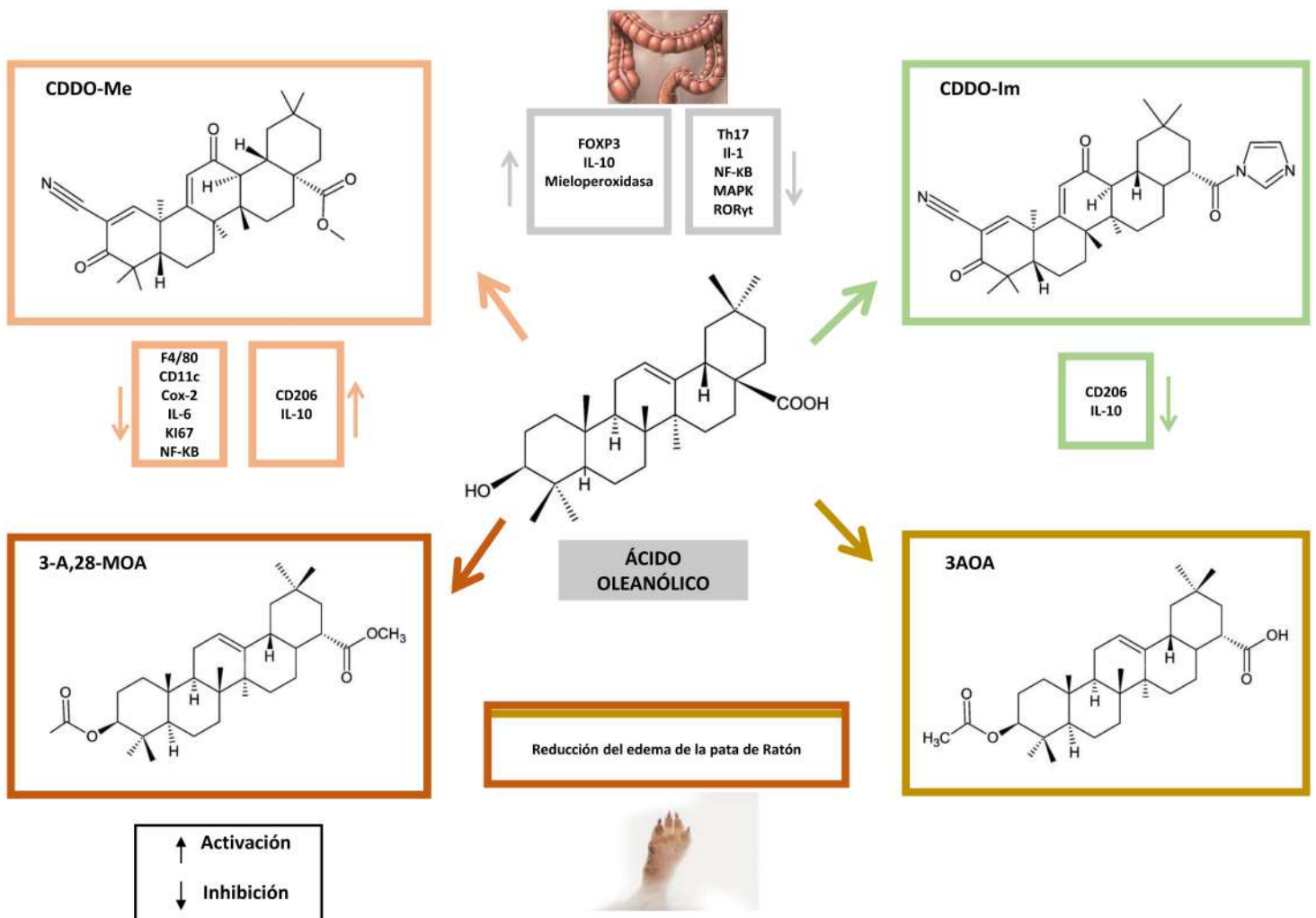


Figura 8. Actividades antiinflamatorias de ácido oleanólico y sus derivados.

La capacidad antiinflamatoria del ácido ursólico fue mostrada mediante la disminución de la producción de TNF- α en células RAW 267.4 y en células epiteliales alveolares (A549) infectadas con *Mycobacterium tuberculosis* y en esplenocitos de rata estimulados con Concanavalin A (Con A). Este ácido inhibió significativamente los niveles de expresión de citoquinas proinflamatorias (IL-1 β , IL-6, TNF- α) así como también inhibió COX-2 (ciclooxigenasa-2) e iNOS (óxido nítrico sintasa inducible) en las células estimuladas y disminuyó la liberación de NO [53].

2.3. Diclofenaco: Generalidades

La historia de los medicamentos antiinflamatorios no esteroideos NSAIDs, se remonta a Hipócrates, considerado como el padre de la medicina occidental, prescribía la corteza de sauce para varias afecciones. Sin embargo, no fue hasta el siglo XIX cuando se consiguió aislar y purificar los principios activos de las plantas, destacando la corteza del sauce donde encontraron la salicina. Este hecho permitió entre otros el desarrollo de la Química Orgánica. Finalmente, se consiguió aislar y acetilar el ácido acetyl salicílico, principal antiinflamatorio no esteroideo [54]. A partir de ese momento, comenzó la búsqueda y la síntesis de medicamentos antiinflamatorios no esteroideos siendo estos compuestos los más prescritos para tratar enfermedades inflamatorias. Los más conocidos son la aspirina, paracetamol, indometacina, diclofenaco e ibuprofeno [55].

El diclofenaco (DCF), es uno de los fármacos más comunes para tratar la inflamación aguda y el dolor [56]. Es un derivado del ácido fenilacético, fitohormona de tipo auxina identificada en plantas, hongos y bacterias. El diclofenaco presenta una alta actividad antiinflamatoria y destaca por su tolerabilidad. Reúne las propiedades de otros antiinflamatorios no esteroideos como la fenilbutazona, el ácido mefenámico y la indometacina, todos estos compuestos son ácidos débiles con constante de acidez de entre 4-5, presentan un grado de lipofilidad y coeficientes de partición similares, por tanto sus comportamientos farmacocinéticos, absorción, capacidad de unión a proteínas plasmáticas, receptores y grados de excreción son similares [57]. El diclofenaco, presenta una constante de acidez de 4.0 y coeficiente de partición de 13.4. En cuanto a su estructura, observamos que deriva del ácido fenilacético al que se le incorpora un fenilo formado por dos átomos de cloro en posición orto, que causan un máximo torsión de este anillo. Destacamos en su estructura el grupo carboxilo (R_2) y el grupo amino (R_1) como zonas diana para formar posibles derivados del diclofenaco (**Figura 9**). La primera preparación del diclofenaco como compuesto activo fue aprobada por la FDA (Administración de Alimentos y Medicamentos de Estados Unidos) en 1988, como Voltaren, siendo el principio activo la sal sódica de este compuesto [58].

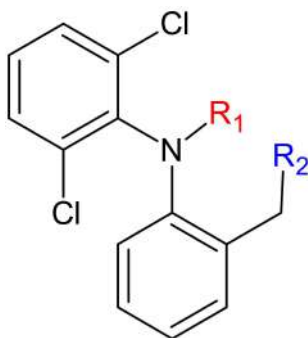


Figura 9. Estructura química del DCF destacando la posición amina secundaria y los radicales modificados R_1 y R_2 para obtener los N-derivados del DCF.

2.3.1. Mecanismo anticancerígeno del diclofenaco y de sus derivados

Varios estudios epidemiológicos han demostrado que el uso regular de medicamentos antiinflamatorios no esteroideos (NSAIDs) puede asociarse con un menor riesgo frente a varios tipos de cánceres como el cerebral, entre otros [59]. Además, experimentos *in vitro* e *in vivo* demostraron que los NSAIDs disminuyen la iniciación tumoral y la progresión en diferentes tipos de cánceres [60]. Varios estudios han demostrado el potente efecto anticancerígeno del DCF en varias líneas cancerígenas y en varios modelos *in vitro* e *in vivo*, mostrando un efecto citotóxico, antiproliferativo y proapoptótico en las líneas cancerígenas (HeLa, HT-29, MCF-7) [61]. Además, se demostró que el DCF detiene el ciclo celular en distintas líneas cancerígenas de adenocarcinoma de ovario (HEY, OVCAR5 y UCI-101) dando lugar a la detención del ciclo en las fases G2/M y S [62].

En lo que concierne al mecanismo molecular anticancerígeno del diclofenaco, se demostró que el diclofenaco induce apoptosis en línea celular tumoral HepG2 (hepatocarcinoma humana), mediante la inducción de la activación de la quinasa N-terminal c-Jun (JNK). Además, el diclofenaco inhibe la activación del factor nuclear κ B (NF- κ B) inducida por el factor de necrosis tumoral α (TNF- α) y provoca la apoptosis sinérgica de los hepatocitos [63]. Asimismo, en varias líneas celulares cancerígenas, LMA (leucemia mieloide), THP-1 (monocitos de un paciente con leucemia) y HL-60 (mieloblastoma humano), el DCF indujo apoptosis, induciendo la activación transcripcional de la proteína de arresto del crecimiento, inducible por daños en el ADN (GADD45 α), mediante la vía MAPK/JNK. Además, los miembros de la familia del factor de transcripción AP-1, c-Jun, JunB y Fra-2 se activaron transcripcionalmente en células de LMA [64]. El tratamiento de las células de cáncer de colon (HCT116) con DCF desencadenó la inhibición de la ruta de supervivencia celular PTEN/PDK/Akt. Induciendo la inhibición de la ruta de supervivencia celular PI3K/Akt y activando MAP quinasas como p44/42, y p38 y la ruta SAPK/JNK (MAP quinasas activadas por estrés que modulan procesos apoptóticos) [65].

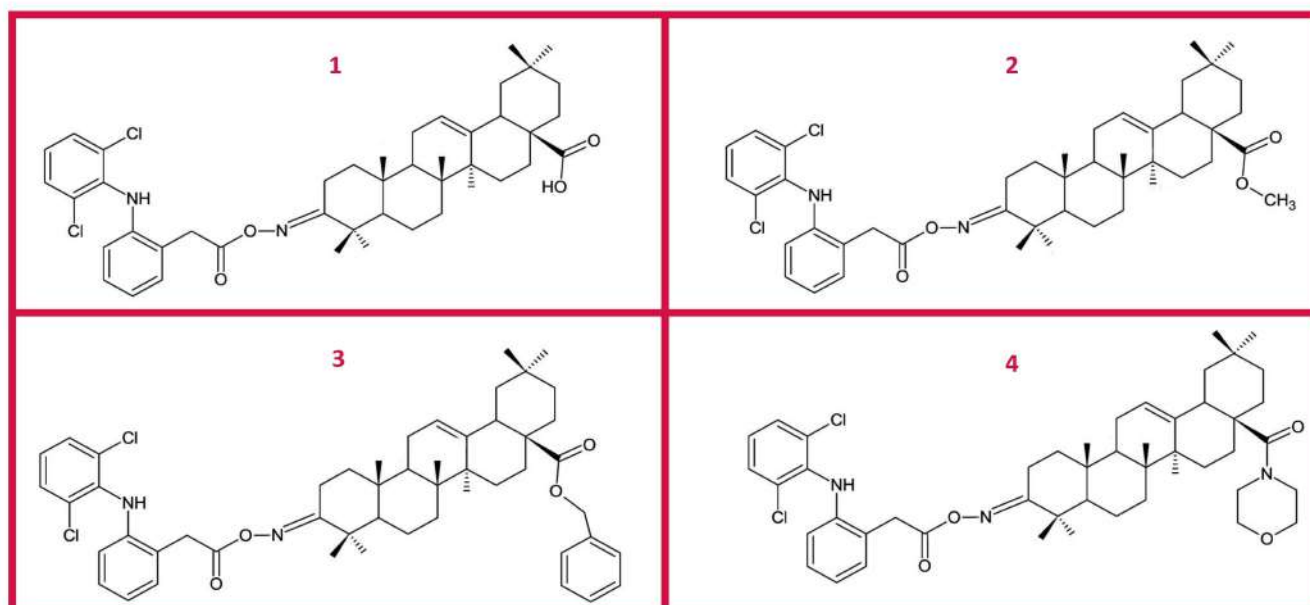


Figura 10. Estructura química de algunos de los conjugados del DCF con actividad antiinflamatoria y anticancerígena; (1) ácido 3-diclofenacoxiiminooleano 12 en 28 oico; (2) éster metílico del ácido 3-diclofenacoxiiminooleano 12 en 28 oico; (3) éster bencílico del ácido 3-diclofenacoxiiminooleano 12 en 28 oico; (4) Morfolida del ácido diclofenacoxiiminooleano 12 en 28 oico.

El tratamiento de células tumorales HepG2 con conjugados de oximas del ácido oleanólico con diclofenaco, mostraron un potente efecto antiinflamatorio y anticancerígeno. Estos conjugados (**Figura 10**) indujeron un efecto proapoptótico mediante la activación de Bax (regulador de apoptosis) y Caspasa-3. Además, inhibieron la activación del factor de transcripción Nrf2 (*Nuclear factor erythroid related 2*, proteína que regula la expresión de enzimas detoxificantes y antioxidantes), la expresión del superóxido dismutasa 1, SOD-1 y de la quinona oxidorreductasa 1 (NQO1). Asimismo, aumentaron la producción de ROS y p-ERK y redujeron el volumen tumoral de xenoinjertos en ratones. Los mejores resultados fueron obtenidos por los compuestos 3,4 (**Figura 10**) con un porcentaje de apoptosis aproximadamente el 67 % y 77%, respectivamente [66].

En la presente tesis doctoral se ha estudiado el efecto anticancerígeno de 8 nuevos N-derivados del DCF, que incluyen modificaciones en los radicales R₁ y/o R₂ (**Figura 9**), evaluando sus actividades anticancerígenas y antiinflamatorias, presentando estos resultados en la publicación 3, obtenidos como fruto de la colaboración con el grupo de investigación “Biotecnología de Hongos y Síntesis de Moléculas Bioactivas”. Nuestros resultados muestran que efectivamente las modificaciones realizadas en la posición amina secundaria del DCF dio lugar a 8 derivados 2, 4, 6, 8c, 9c y 10a-c (**Figura 11**), presentando la mayoría de estos una IC₅₀ menor que el DCF en las tres líneas cancerígenas ensayadas HT29, HepG2 y B16-F10. Dos de estos derivados 4 y 8c fueron seleccionados mostrando en las líneas tumorales HT29 y HepG2 porcentajes de apoptosis entre un 30 a un 60%, arresto del ciclo celular, sin cambios en el potencial de la membrana mitocondrial, indicando la posible activación de la ruta extrínseca de inducción de apoptosis.

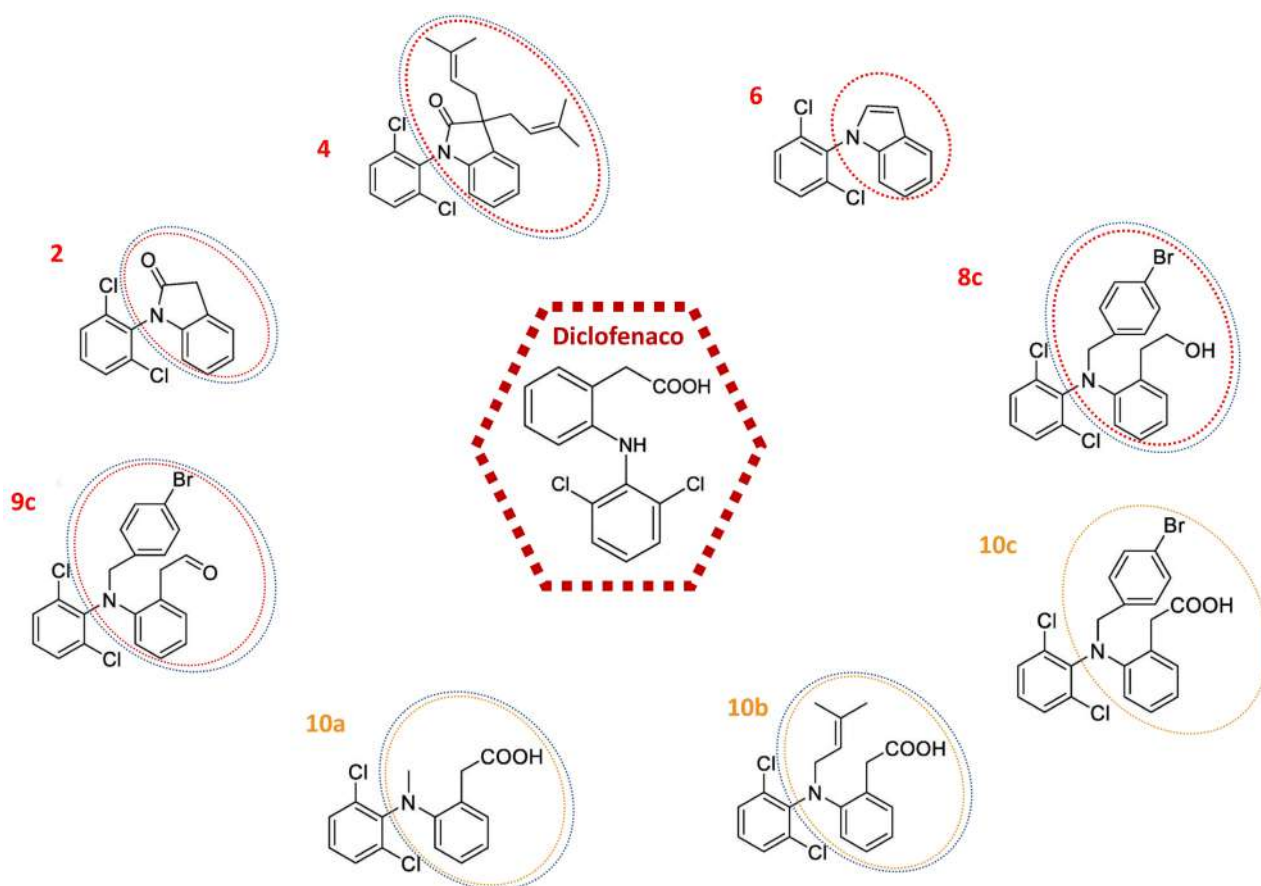


Figura 11. Estructura química del DCF y de sus N-derivados destacando los radicales R₁ y R₂ modificados en la posición amina secundaria. El círculo rojo señala los radicales modificados con mejor actividad anticancerígena, el círculo naranja los radicales modificados con menor actividad anticancerígena y el círculo azul los radicales modificados con mejor actividad antiinflamatoria.

2.3.2. Mecanismo antiinflamatorio del diclofenaco y de sus derivados

La actividad farmacológica de los NSAIDs está relacionada con la supresión de la biosíntesis de prostaglandinas a partir del ácido araquidónico mediante la inhibición de las enzimas ciclooxigenasas (COX-1 y COX-2) [67]. Asimismo, se ha demostrado que el DCF ejerce un efecto antiinflamatorio mediante la vía del receptor transmembrana TLR4 (*Toll-like receptor 4*) en el hígado, tras realizar ejercicio intenso, disminuyendo la producción de citoquinas proinflamatorias y del factor de diferenciación miloide 88, MyD88, (*myeloid differentiation primary response gene 88*) en hígado [68].

El diclofenaco se encuentra entre los NSAIDs más utilizados en todo el mundo [7]. Sin embargo, los NSAIDs representan diversos efectos secundarios que incluyen riesgos gastrointestinales, renales y cardiovasculares [69]. Para potenciar su efecto terapéutico, se han sintetizado varios derivados del diclofenaco que son ampliamente utilizados en comparación con otros medicamentos antiinflamatorios debido a su eficacia, principalmente por la potente inhibición de la prostaglandina sintasa o ciclo oxigenasa inducible, COX-2, con una mayor eficacia que COX-1, constitutiva [58]. Así mismo presenta menos efectos secundarios al modificar el grupo ácido carboxílico del DCF (**Figura 9**, R₂) [70], [71].

Estudios recientes, ponen de manifiesto que derivados del diclofenaco como el derivado 1 (**Figura 12A**), mostró efectos antiinflamatorios *in vivo*, a una dosis de 10 mg/kg en modelo de edema inducido por carragenina en extremidad rata. Disminuyendo de un 33,8% a un 74,4% la formación de edema tras 2 y 4 horas de tratamiento, mediante la inhibición efectiva de la enzima COX-2, acompañada de un menor grado de potencial ulcerogénico en comparación con otros NSAIDs [70]. Varios derivados del diclofenaco con sustituyentes de oxadiazol mostraron un importante efecto antiinflamatorio mediante la eliminación de especies reactivas de oxígeno (ROS) intracelular en neutrófilos, y la inhibición de producción del óxido nítrico (NO) en macrófagos J774.2. Este compuesto (**Figura 12B**), mostró la mayor inhibición de ROS intracelular y de óxido nítrico con valores de IC₅₀_{ROS}=1,7 ± 0,4 µg/mL e IC₅₀_{NO}=7,13 ± 1,0 µg/mL, respectivamente, mostrando una mayor actividad antiinflamatoria que el diclofenaco [72]. También, en modelo de edema inducido por carragenina en extremidad de rata, varios derivados del diclofenaco mostraron claros efectos antiinflamatorios encontrando, que los compuestos 1 y 2 (**Figura 12C**) actúan sobre la respuesta tardía de la inflamación. Siendo el compuesto 2 el que presentó la mayor actividad antiinflamatoria con respecto al diclofenaco alcanzando una inhibición en el modelo de inflamación en extremidad de rata del 61,32% [73]. El efecto antiinflamatorio de varios derivados del diclofenaco con sustituyentes bioactivos (**Figura 12D**), como triazol (1) y oxadiazol (2) mostraron una potente actividad antiinflamatoria en este modelo de edema inducido tras 2 y 4h de tratamiento con una inhibición del edema del 64,10% y 76,92% para el compuesto 1 y con una inhibición del 57,69% y 74,36% para el compuesto 2, respectivamente. Este efecto se relaciona con la presencia de grupos éster y carboxílicos en la cadena lateral de los compuestos de anillos de triazol (1) y oxadiazol (2) [67].

Asimismo, otros autores, para mejorar la solubilidad del diclofenaco en agua y potenciar su actividad antiinflamatoria, sintetizaron dos estructuras anfipáticas mediante la doble esterificación de dos moléculas de diclofenaco con tres polietilenglicoles-PEG- diferentes (trietilenglicol, PEG 400 y PEG 600) (**Figura 12E**). De modo, que los derivados obtenidos el Dic-PEG400-Dic (1), Dic-PEG600-Dic (2) produjeron una inhibición en la expresión de TNF-α de hasta un 87,4% y un 84% respectivamente tras 48h de tratamiento. La inhibición producida por el DFC fue de solo un 42,3%, mejorando claramente así su actividad antiinflamatoria [7]. Asimismo, evaluaron el efecto antiinflamatorio del conjugado oxima del ácido oleanólico con diclofenaco (4) (**Figura 10**) en células de cáncer de páncreas humano (PSN-1). El tratamiento de las células PSN-1 mostró una reducción en la activación y expresión de NF-κB, del ARNm de RelA (p65) miembro de la familia de NF-κB, y la transcripción de COX-2 acompañada con un aumento de la translocación de Nrf2 [74].

En la presente tesis doctoral se han evaluado las actividades antiinflamatorias de 8 los N-derivados del DCF mostrados anteriormente (**Figura 11**) presentando los resultados en la publicación 3, donde se ha demostrado que los derivados 2, 4, 8c, 9c, 10a-c inhibieron la producción de óxido nítrico entre un porcentaje de 25-75% en células murinas de macrófagos-monocitos RAW 264.7 activadas con LPS. De modo, que mediante los ensayos realizados ponen de manifiesto que efectivamente los cambios estructurales en la posición amina secundaria de los radicales R_1 y/o R_2 mejoró la actividad antiinflamatoria de estos derivados con respecto al diclofenaco.

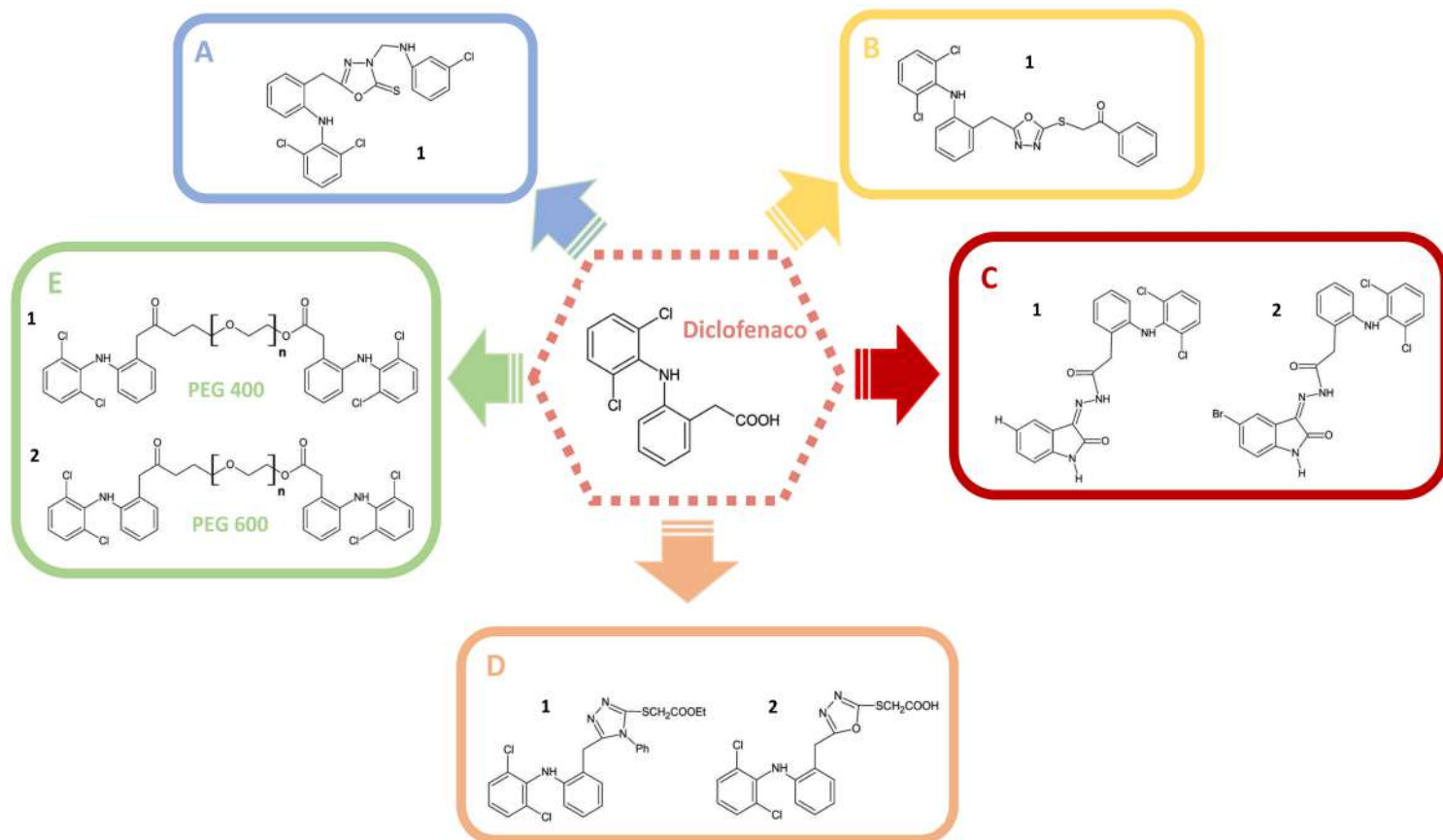


Figura 12. Estructura química del DCF y de algunos de sus derivados con actividad antiinflamatoria

2.4. Mecanismos de activación de la muerte celular programada

Todos los organismos pluricelulares mantienen el equilibrio entre la proliferación y la muerte de las células que los componen. Este equilibrio se conserva desde el embrión hasta el organismo adulto. De modo, que millones de células se mueren constantemente sin afectar al buen funcionamiento del organismo. Una de las formas de muerte celular es el mecanismo de apoptosis o muerte celular programada, siendo una de las formas de muerte celular más estudiada y ampliamente caracterizada por considerarse crucial en el mantenimiento y la regulación de la homeostasis en los organismos pluricelulares. En el mecanismo de apoptosis las células se autodestruyen sin inducir ninguna reacción inflamatoria ni producir cicatrices en los tejidos. Además, se conoce como una muerte natural, por la cual se deshace de las células dañadas o infectadas, protegiendo de esta forma de varias enfermedades. También es un mecanismo importante por el cual, el sistema inmune elimina las células, infectadas por patógenos o con mutaciones cancerígenas sin alterar la función normal de los tejidos circundantes [75].

2.4.1. Caspasas en apoptosis

Las vías apoptóticas están constituidas por una importante actividad proteolítica llevada a cabo por las caspasas. Esta familia es un grupo de cisteín proteasas, sintetizadas mediante zimógenos, inducidas por proteólisis. En los mamíferos se distinguen distintas caspasas: las iniciadoras (caspasa-2,-8,-9,-10) y las efectoras (caspasa-3,-6,-7). Las caspasas iniciadoras están formadas por 3 dominios esenciales, un dominio N-terminal de longitud variable (prodominio), una parte catalítica formada por una subunidad de mayor (p20) y una subunidad menor (p10). Asimismo, las caspasas son inactivas y se activan por la ruptura proteolítica de sus secuencias de aminoácidos diana, formadas por residuos de aspártico, que se sitúan entre el prodominio y la subunidad mayor, y entre la subunidad mayor y la menor (**Figura 13**). La caspasa-9, su secuencia diana de activación está entre la subunidad grande y la pequeña. Tan pronto que se activan, las caspasas forman heterotetrámeros [76].

Las caspasas efectoras (como la caspasa-3, -6 y -7 en ratones y humanos) son los mediadores de la destrucción celular a través de la proteólisis de los dominios celulares. Las formas monoméricas inactivas de estas caspasas hacen que formen dímeros activos e inicien cascadas de muerte celular. Las caspasas iniciadoras (como la caspasa-2, -8, -9 y -10) tienen un prodominio de mayor longitud para integrar las señales apoptóticas internas o externas y activar a las caspasas efectoras (**Figura 13**). Estas caspasas efectoras se sitúan esencialmente en el citoplasma, constituyendo dímeros inactivos. Requieren el corte en un bucle determinado permitiendo al centro activo obtener la conformación precisa para activarse. Su activación induce la degradación celular, mediante la actividad de cisteinil-proteasa sobre varios sustratos citoplasmáticos, que suponen proteínas esenciales para la viabilidad celular, inhibidores de apoptosis y reguladores del ciclo celular. La apoptosis se puede iniciar a través de dos vías, la vía extrínseca o de receptor de muerte, inducida por estímulos externos y la vía intrínseca o mitocondrial, inducida por estímulos internos. Ambas vías utilizan las caspasas como sus efectores de muerte orquestando las etapas finales de apoptosis [76].

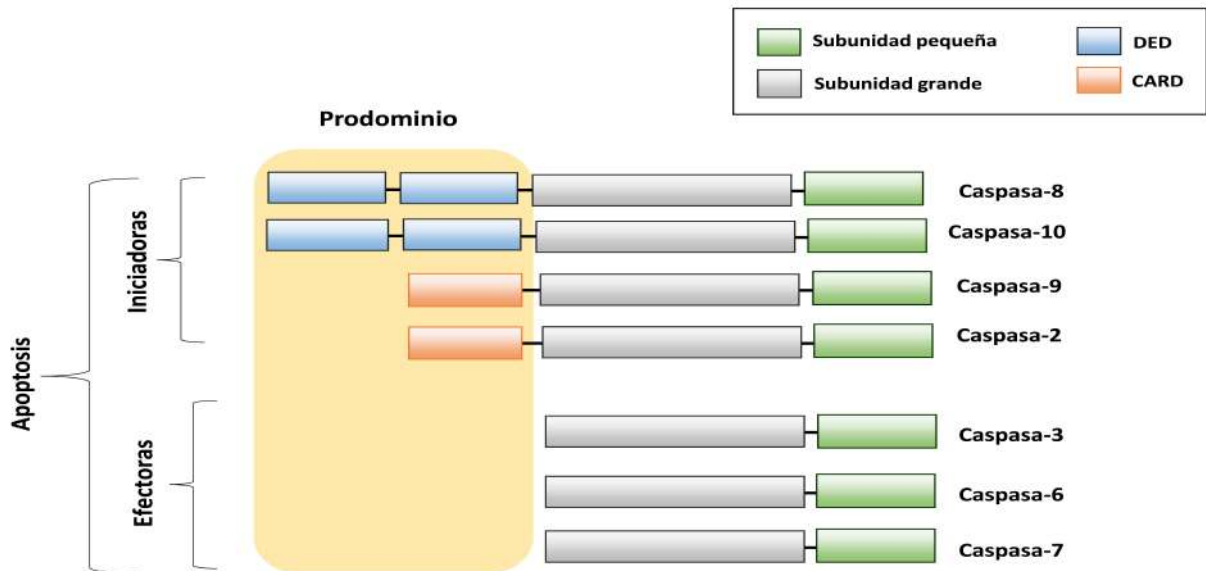


Figura 13: Estructura y organización de los dominios de las caspasas apoptóticas. Las caspasas iniciadoras tienen prodominios largos, CARD o DED, mientras que las caspasas efectoras tienen prodominios cortos. Ambas están formadas por una subunidad mayor y menor (Figura adaptada de [76]).

2.4.2. Vía extrínseca de inducción de apoptosis

Señales extracelulares de estrés mediadas por receptores de membrana plasmática pueden inducir apoptosis mediante la activación de la vía extrínseca (**Figura 14**). Esencialmente estos receptores de muerte que son un subconjunto de la superfamilia de receptores del factor de necrosis tumoral entre los que se incluyen a CD95 o FASR, DR4, DR5 y TNFR, cuando se unen con sus respectivos ligandos: CD95L también conocido como ligando FAS para CD95, TRAIL para DR4 y DR5 y TNF para TNFR, reclutan la proteína adaptadora FADD (*Fas-Associated protein with Death Domain*) o TRADD (*TNFR1-associated death domain protein*), activando finalmente a las procaspasas iniciadoras -8 o -10 [77].

Una vez que FADD se combina con el receptor de muerte o en el caso de TNFR después de que se recluten, tanto FADD como la segunda proteína adaptadora (TRADD), los monómeros inactivos de caspasa-8 se reclutan y se dimerizan en homodímeros activos de caspasa-8. El conjunto de activación formada por la combinación del receptor de la muerte (DD), la proteína adaptadora (Fas) y la caspasa-8 se conoce como el complejo de inducción de muerte celular (DISC). Una vez formado, el homodímero de caspasa-8 se escinde, liberándose del DISC y así activar a las caspasas-3 y -7 para promover la apoptosis [77]. En resumen, los complejos proteicos obtenidos ayudan a la dimerización de las procaspasas, estabilizando el dímero, proporcionando la proximidad espacial precisa para que se activen recíprocamente. Después, escinden de las moléculas adaptadoras, deshaciendo de la unión con sus prodominios para soltar las formas activas de caspasa-8 o -10 que activan a las caspasas efectoras -3, -6 y -7 para comenzar la proteólisis celular [77].

2.4.3. Vía intrínseca de inducción de apoptosis

La vía intrínseca de inducción de apoptosis se activa a través de una variedad de señales intracelulares que van desde el daño del ADN hasta el estrés oncogénico. La muerte celular intrínseca está asociada con la permeabilización de la membrana externa de la mitocondria (MOMP) que está regulada principalmente por la familia de proteínas Bcl-2 (*B-cell lymphoma 2*). El proceso comienza con la activación por señales intracelulares de las proteínas de la familia Bcl-2 pro-apoptóticas, como Bax y Bak presentes en el citosol, perdiéndose el equilibrio entre las proteínas de la familia Bcl-2 proapoptótica y antiapoptóticas como Bcl-2 o Bcl-XL, formando poros en la membrana externa mitocondrial, perdiéndose el equilibrio electroquímico, interrumpiendo la integridad de la membrana y liberando factores mitocondriales como el citocromo c o Apaf1 (*Apoptosis protease-activating factor-1*). Una vez liberados estos factores, el citocromo c se une a Apaf1 para promover la formación del complejo multimérico, apoptosoma, responsable finalmente de la activación de la caspasa iniciadora -9 [78].

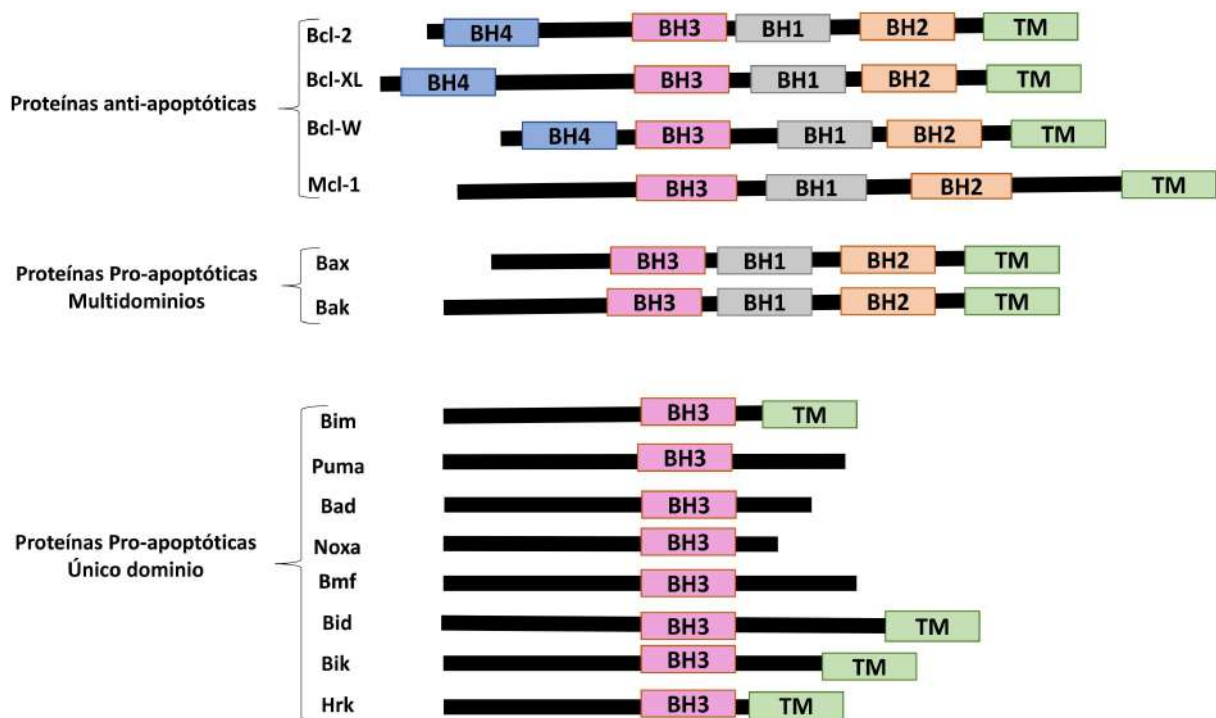


Figura 14: Las proteínas de la familia Bcl-2 comparten cuatro dominios conocidos como dominios de homología Bcl-2 (BH) indicados en segmentos coloreados. Las proteínas anti-apoptóticas tienen los cuatro dominios. Mientras las proteínas pro-apoptóticas multidomínios no tienen el dominio BH4. Sin embargo, las proteínas pro-apoptóticas único dominio carecen de todo menos de un dominio BH3. TM, dominio transmembrana. (Figura adaptada de [79]).

La familia de Bcl-2 se distingue por cuatro dominios con una homología estructural conservada BH1, BH2, BH3 y BH4 necesarios para que estas proteínas de la familia de Bcl-2 interactúen entre sí. Esta familia se divide en tres grupos: proteínas anti-apoptóticas, proteínas pro-apoptóticas y proteínas de dominio único BH3 (**Figura 14**). Estas últimas, envían señales de muerte a la mitocondria. Las proteínas pro-apoptóticas único dominio (por ejemplo, Bid, Bim, Puma y Noxa) contienen uno de los cuatro dominios de homología Bcl-2, y algunos de estos pueden activar directamente las proteínas formadoras de poros, Bax y Bak. Las proteínas anti-apoptóticas (Bcl-2, Bcl-XL, A1 y Mcl-1) se unen y antagonizan a las proteínas de único dominio, así como actúan directamente para inhibir Bax activo y Bak [77], [79]. Bad y Noxa reprimen la acción de proteínas anti-apoptóticas como Bcl-2 o Bcl-XL. Bim, Bid y Puma inducen la activación de las proteínas pro-apoptóticas como Bax/Bak. Bim, proteína con un único dominio BH3, es una potente activadora del proceso apoptosis. Bim, inhibe a Bcl-XL y Mcl-1, permitiendo la liberación de Bak y de citocromo c [77], [78]. Además, la activación de la vía intrínseca mitocondrial de inducción de apoptosis puede ser causada por la escisión proteolítica de la proteína Bid, que tiene una forma bioactiva truncada (tBid). Bid es activada proteolíticamente por la caspasa 8, activando la vía apoptótica intrínseca, reforzando la señal apoptótica extrínseca inicial (**Figura 15**) [77], [79].

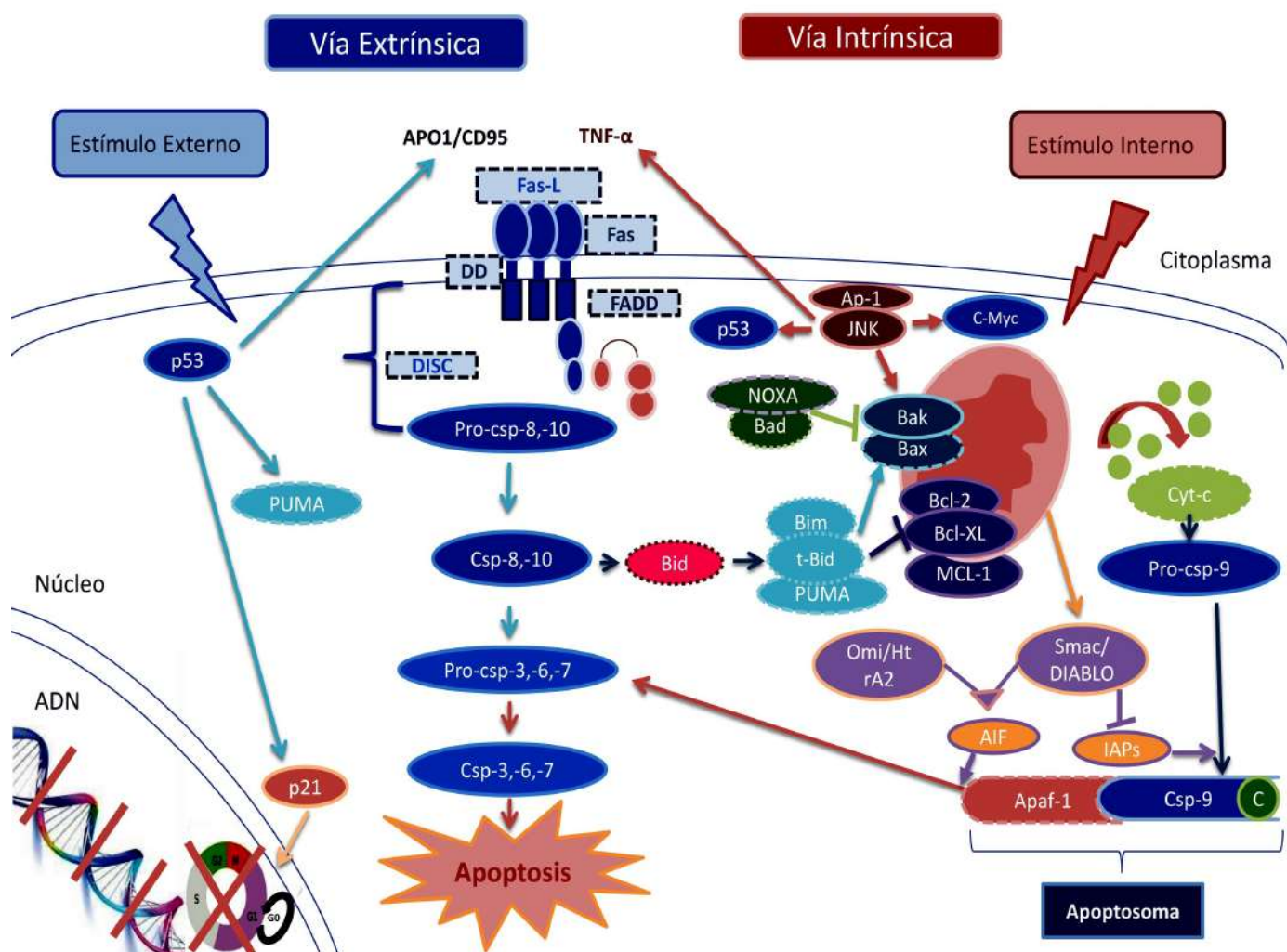


Figura 15: Representación esquemática del mecanismo molecular apoptótico extrínseco e intrínseco.

Algunas de estas proteínas son activadas mediante el daño del ADN, como por ejemplo Puma, Noxa y Bid, que están bajo el control transcripcional del supresor tumoral p53. p53 aumenta la expresión de varios genes que poseen elementos sensibles a p53 presentes en sus promotores, como las proteínas proapoptóticas BH3 Puma, Noxa y Bid. Como resultado, las células en las que se estabiliza p53 se sensibilizan para la activación de la ruta de muerte celular mitocondrial. Además, p53 puede afectar directamente la integridad mitocondrial sin necesidad de activación génica. De hecho, se ha documentado que p53 puede unirse a Bcl-2 y Bcl-X_L en las mitocondrias, promoviendo así la desestabilización mitocondrial [77], [79]. Puma, juega un papel importante en la apoptosis, su sobreexpresión *in vitro* está acompañada por una mayor expresión de Bax, cambio conformacional de Bax, translocación a la mitocondria, liberación de citocromo c y reducción del potencial de membrana mitocondrial. Se ha demostrado que Noxa puede localizarse en las mitocondrias e interactuar con los miembros de la familia Bcl-2 antiapoptóticos, lo que resulta en la activación de la caspasa-9. Dado que tanto Puma como Noxa son inducidos por p53, podrían mediar en la apoptosis provocada por el daño genotóxico o por activación del oncogen. La oncoproteína Myc potencia la apoptosis a través de mecanismos dependientes e independientes de p53.

Finalmente, se produce la permeabilización de la membrana externa mitocondrial, desactivando el potencial de la membrana o la producción de especies reactivas de oxígeno (ROS). Liberando en el citoplasma proteínas mitocondriales que ayudan en la progresión de apoptosis, como SMAC/DIABLO y la serin-proteasa Omi/HtrA2 que contribuyen a la activación de caspasas, o AIF (Apoptosis Inductor Factor) y endonucleasa G (ENDOG) que inducen de forma indirecta a las caspasas, trasladándose al núcleo e induciendo la fragmentación del ADN (**Figura 15**) [77], [79].

Proteínas directamente relacionadas con la activación de esta ruta son p53 y JNK. El supresor tumoral 53 (p53) es una proteína multifuncional que regula el ciclo celular, la reparación del ADN, la apoptosis y las vías metabólicas sin embargo su mutación implica aproximadamente 50% de los cánceres humanos. La activación de gen supresor de tumores p53 regula ambas vías apoptóticas la extrínseca y la intrínseca. De modo que, mediante la vía apoptótica extrínseca, el p53 puede inducir transcripcionalmente los genes que codifican FAS (APO-1 y CD95) y posiblemente otros genes que codifican receptores de muerte relacionados. Mientras que en relación con la vía intrínseca induce la regulación de los genes proapoptóticos como Bax, el modulador de apoptosis Puma y p21, así como regula XIAP que promueve la liberación mitocondrial de SMAC y la inducción de la expresión de caspasa-3.[80] p53 es además un regulador transcripcional del inhibidor de quinasa dependiente de ciclina p21 (WAF1/CIP), induce la supresión del crecimiento tumoral mediante la detención del ciclo celular G1/S (**Figura 15**) [81].

La N-terminal quinasa Jun, JNK (*Jun N-terminal kinase*) pertenece a la superfamilia de MAP-quinasas involucradas en la regulación de la proliferación, diferenciación y apoptosis celular. Los análisis de las vías reguladas por JNK han demostrado que JNKs es indispensable tanto para la proliferación celular como para la apoptosis. Se ha observado que JNK desempeña un papel central en ambas vías apoptóticas la extrínseca y la intrínseca. La fosforilación de c-Jun por JNK, conduce a la formación del conjunto de factores transcripcionales AP-1, que participa en la transcripción de una amplia variedad de proteínas como las proteínas proapoptóticas. Además, se ha observado que la vía JNK-AP-1 está implicada en el aumento de la expresión de genes proapoptóticos como TNF- α , Fas-L y Bak. JNK también puede fosforilar varios otros factores de transcripción, incluidos p53 y c-Myc [82].

2.4.4. El ciclo celular

Para comprender mejor el mecanismo de acción de los agentes anticancerígenos y antiinflamatorios es necesario saber los procesos biológicos que regulan el ciclo celular. Varios eventos patológicos como la inflamación y el cáncer influyen en la regulación de la expresión de moléculas del ciclo celular y sobre su desarrollo. Normalmente, en un organismo hay un equilibrio entre la proliferación celular y la apoptosis. Sin embargo, en el caso del cáncer este equilibrio se rompe mediante mutaciones que pueden inducir, por un lado, la activación de los oncogenes que codifican proteínas del ciclo celular relacionadas con la proliferación y por otro lado, a la inactivación de genes supresores que codifican las proteínas que detienen el ciclo celular [83].

El ciclo celular es un mecanismo principal en todos los eucariotas. Mediante el cual, los diferentes componentes celulares se duplican y luego se segregan con precisión en células hijas, tanto en el desarrollo embrionario como para sustituir las células dañadas en un órgano adulto. En el ciclo celular se diferencian en varias fases: Fase G₀ o de reposo donde las células no se dividen, pero mantienen la capacidad de reiniciar el ciclo celular. Fase G₁ en que la célula contiene un número diploide de cromosomas, las células crean ARN y proteínas. Fase S en la que se sintetiza el ADN. Fase G₂ en la que el núcleo se organiza para la división celular. Fase M o de mitosis durante la cual la célula se divide (**Figura 16**) [83], [84].

Durante el desarrollo del ciclo celular hay varios puntos de control o “checkpoints” que controlan el orden y la integridad de los eventos más importantes del ciclo celular. Teniendo en cuenta, por ejemplo, el crecimiento celular apropiado, la replicación e integridad de los cromosomas y la segregación precisa en mitosis (**Figura 16**). Mediante estos puntos de control participan complejos de proteínas que actúan en cada una de las etapas y permiten, o no, el avance del ciclo [84]. El progreso del ciclo celular se regula negativamente por la familia de inhibidores de CDKs (CDKI). Estas proteínas se denominan ciclinas y cinasas dependientes de ciclinas (Cdk). Estas son proteínas quinasas serina/treonina que fosforilan sustratos clave para promover la síntesis de ADN y la progresión mitótica. Según la gravedad del defecto del ciclo celular, la disfunción del punto de control puede tener resultados que van desde la muerte celular hasta la reprogramación del ciclo celular, lo que puede provocar cáncer. Por ejemplo, durante la apoptosis la proteína p53 activa a la proteína p21^{CIP1}, CDKI (proteína inhibidora de la quinasa dependiente de ciclina) desactiva la fosforilación de la proteína supresora de tumor pRb, inhibiendo la liberación del factor de transcripción E2F, induciendo la parada del ciclo en G1 e induciendo apoptosis. En el caso de la pérdida de p53, posiblemente el defecto genético más común en el cáncer se ven afectadas varias decisiones sobre el destino de las células. Entre estas se encuentran la falta de control de CDK por parte de p21 y, por lo tanto, la pérdida del punto de control G1 [83].

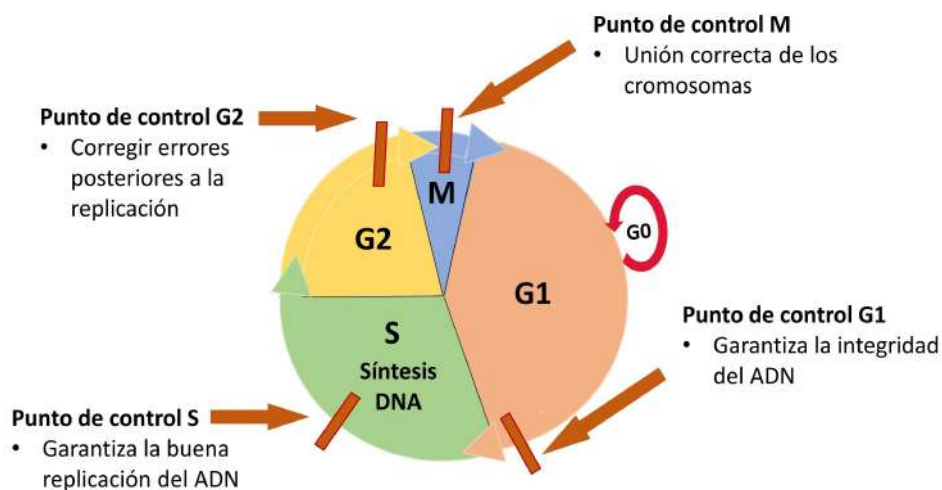


Figura 16: Representación esquemática de las diferentes fases del ciclo celular con sus correspondientes puntos de control (Figura adaptada de [84]).

2.5. La inflamación

La inflamación es un mecanismo de defensa esencial en el organismo, contribuye en la restauración de la homeostasis tisular. Sin embargo, la inflamación aguda no controlada puede volverse crónica, contribuyendo a una variedad de enfermedades inflamatorias crónicas, incluidas entre otras enfermedades cardiovasculares e intestinales, diabetes, artritis, asma, párkinson y cáncer. Esta respuesta biológica del sistema inmunológico puede desencadenarse por una variedad de factores, incluidos patógenos, células dañadas y compuestos tóxicos. Estos factores pueden inducir respuestas inflamatorias agudas y/o crónicas mediante las cuales se induce una sobreproducción de especies reactivas de oxígeno, de óxido nítrico, y citoquinas que inducen y median la respuesta inflamatoria [85], [86].

A nivel tisular, la inflamación se caracteriza por enrojecimiento, hinchazón, calor, dolor y pérdida de la función tisular, que resultan de las respuestas de las células inmunitarias, vasculares e inflamatorias locales a la infección o lesión. Los eventos importantes que ocurren durante el proceso inflamatorio incluyen cambios en la permeabilidad vascular, reclutamiento y acumulación de leucocitos y liberación de mediadores inflamatorios (**Figura 17**) [87].

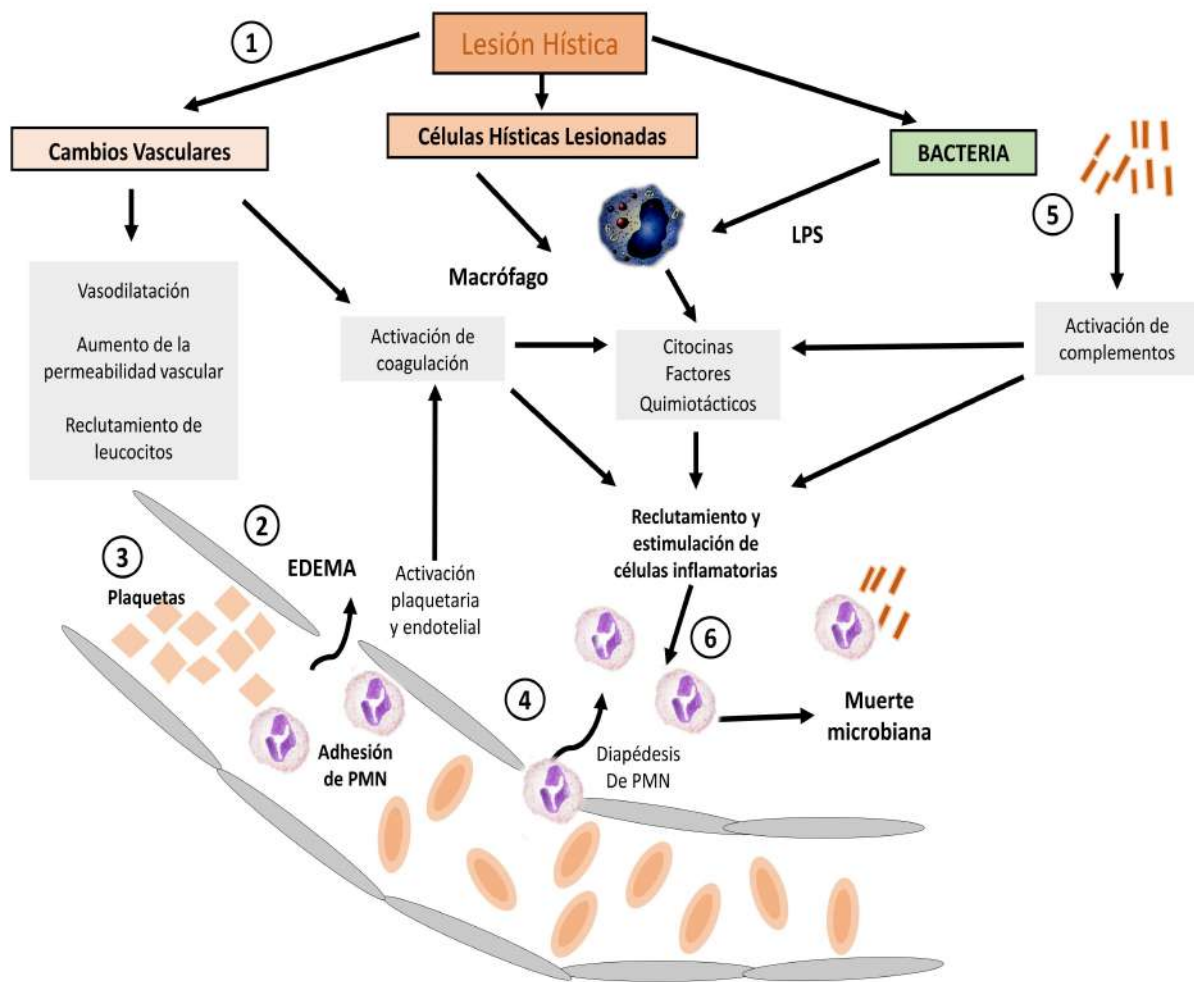


Figura 17: Inflamación en la situación en respuesta a una lesión. (1) La lesión de un tejido provoca una alteración vascular inmediata y prolongada. La vasodilatación y la lesión vascular son activadas por mediadores químicos y células de los tejidos dañados, lo que produce (2) el edema, entrada de líquidos hacia el tejido. (3) La activación de las plaquetas inicia la hemostasis, la formación de coágulos e incrementa la permeabilidad vascular por medio de la liberación de histamina. (4) Las células endoteliales vasculares inducen la formación de coágulos, anclando los neutrófilos circulantes por medio de sus moléculas de adhesión sobrepresadas, facilitando la permeabilidad vascular del plasma y de las células inflamatorias. Además, (5) microbios (barras rojas) activan la cascada de complementos con mediadores solubles de los macrófagos, (6) recluta los neutrófilos al sitio de la lesión. Los neutrófilos y macrófagos se deshacen de los microbios y retiran el tejido dañado para que la reparación comience. LPS, lipopolisacárido; PMN, neutrófilo polimorfonuclear (Figura adaptada de [88]).

Uno de los objetivos de nuestro estudio es evaluar el efecto antiinflamatorio de nuevas moléculas orgánicas de origen natural y sintéticas, capaces de detener el proceso inflamatorio. Para alcanzar este objetivo nuestro estudio consistió en evaluar el efecto antiinflamatorio del OADP y de N-derivados del DCF *in vitro* sobre células de macrófagos/monocitos de ratón RAW 264.7 estimuladas con el lipopolisacárido bacteriano e *in vivo* en el caso del OADP en modelo de inflamación aguda inducido por TPA sobre oreja de ratón.

2.5.1. Modelos de inflamación

Los monocitos y los macrófagos desempeñan funciones críticas en las respuestas inflamatorias durante la cual los macrófagos detectan, fagocitan y destruyen bacterias y otros microorganismos dañinos, por lo tanto, la modulación de sus funciones es una estrategia útil para las terapias antiinflamatorias [88], [89].

El lipopolisacárido (LPS) es ampliamente reconocido como un potente activador en monocitos/macrófagos, y se sabe que los macrófagos y monocitos que han sido activados por LPS producen mediadores clave de inflamación como el óxido nítrico (NO) y otros radicales libres, además de numerosas citoquinas, como el factor de necrosis tumoral (TNF- α), interleuquinas IL-1 β e IL-6. Los patógenos bacterianos, como el LPS, activan redes de citoquinas al inducir un gran número de genes proinflamatorios. Además, estas inducciones están mediadas por la activación de factores de transcripción inducibles. Durante el proceso inflamatorio, las isoformas inducibles de NO sintasa (NOS) y ciclooxigenasa (COX- 1, COX-2) generan grandes cantidades de mediadores proinflamatorios como el NO y la prostaglandina E2 (PGE2) [88], [90].

Los macrófagos se originan a partir de monocitos y son las principales células diana del LPS. Después del reconocimiento del LPS mediante el receptor tipo Toll (TLR), los macrófagos se activan para producir citoquinas proinflamatorias mediante la vía de señalización de TLR4 que incluye proteínas extracelulares, incluidas la proteína de unión a LPS, LBP, y la glicoproteína de membrana CD14, que desempeñan un papel en la transferencia de LPS a un complejo de señalización compuesto por la proteína de diferenciación mieloide 2 (MD2) y el factor de diferenciación MyD88 [88], [89]. Mediante este proceso, se activan las vías de transmisión de señales y los factores de transcripción que inducen la expresión de genes esenciales para las respuestas inflamatorias. Asimismo, se induce la activación de numerosas proteínas quinasas y varios factores de transcripción como el factor nuclear NF- κ B, el conjunto de factores de transcripción (AP-1), el factor de respuesta al interferón de tipo I, etc. NF- κ B y AP-1 estimulan la expresión de genes que codifican muchas de las moléculas requeridas para las respuestas inflamatorias, como citoquinas inflamatorias (TNF e IL-1) las quimiocinas (CCI2 y CXCL8) y las moléculas de adhesión endoteliales (selectina E) [88], [90].

El LPS, es una macromolécula anfipática que se localiza en la membrana exterior de aproximadamente todas las bacterias Gram negativas, responsables de la inducción de procesos inflamatorios. Su estructura está constituida por tres partes, de las que dos son hidrofílicas. Su parte central está formada por motivos repetidos de monosacáridos (oligosacárido central). La parte superior denominada antígeno O, está formada por la unión de distintos azúcares, y un dominio hidrofóbico (parte inferior) formada por seis cadenas de ácidos grasos, denominado lípido A y que es el elemento biológicamente activo del LPS (**Figura 17, A**) [90], [91].

Durante el proceso de inducción inflamatoria, en primer lugar, el LPS entra en contacto con varias proteínas presentes en el líquido extracelular, como la proteína LBP y los receptores CD14, TLR4 y MD-2. La proteína LBP se une al LPS y forma el complejo LPS-LBP de modo que esta asociación facilita la unión del LPS al receptor CD14, que transfiere el LPS al complejo encargado de su reconocimiento (TLR4/MD-2). Lo que permite que la proteína extracelular MD2 (proteína de diferenciación mieloide 2) se una al elemento lipídico A del LPS, constituyendo de esta forma un complejo que facilita la activación de TLR4 y la biosíntesis de varios mediadores inflamatorios [88], [92].

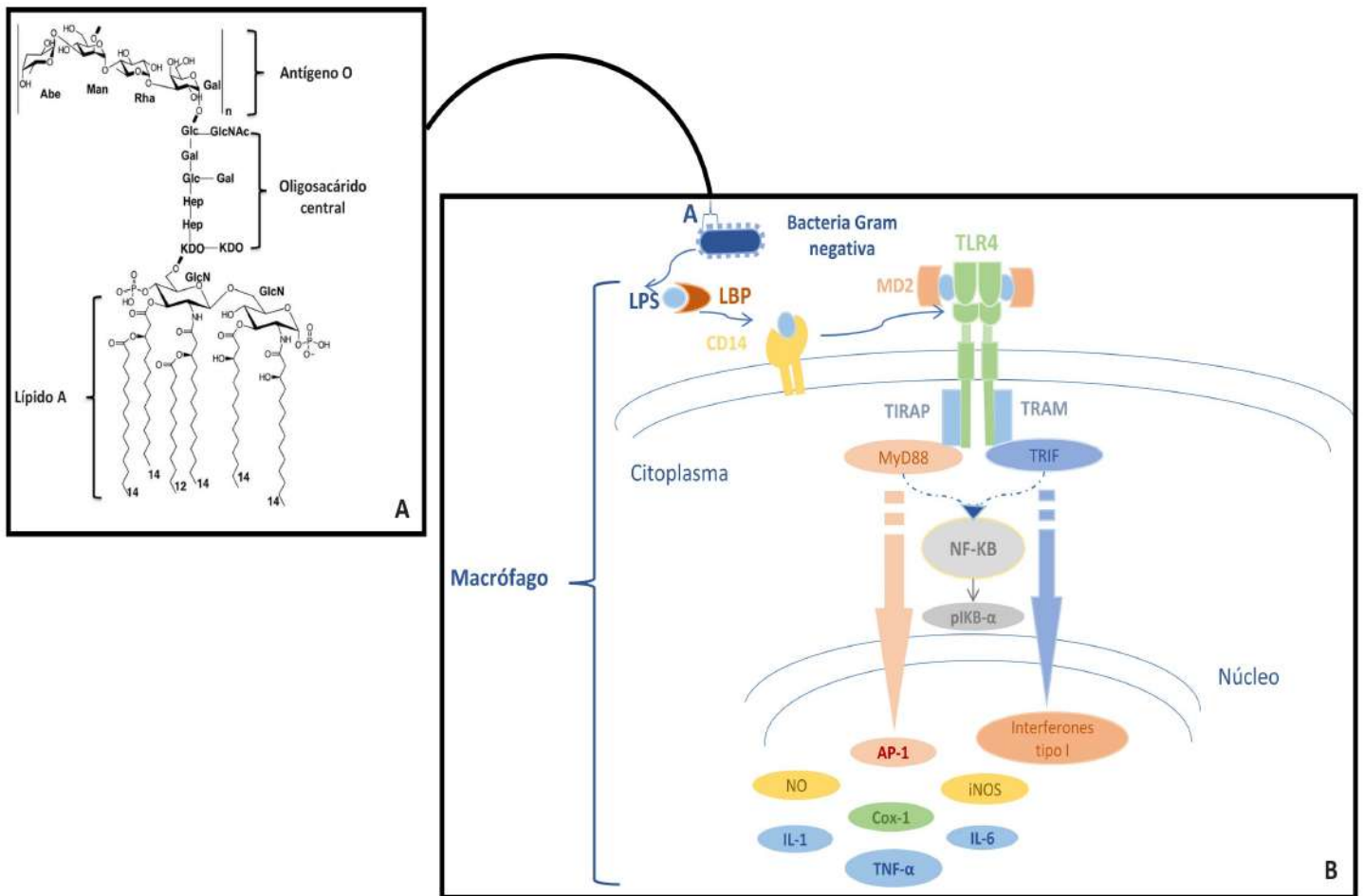


Figura 17: Activación de TLR4 por LPS. A: Estructura de LPS, B: Mecanismo molecular encadenado por LPS en macrófago. LBP facilita la transferencia de monómeros de LPS a CD14 y, posteriormente, CD14 cambia la endotoxina al complejo TLR4/MD-2. La dimerización del complejo receptor induce el ensamblaje de las quinasas TIRAP y MyD88 en el dominio TIR de TLR4, lo que induce una vía de señalización que conduce a la producción de citoquinas proinflamatorias. TRAM y TRIF se asocian con TLR4 desencadenando una vía de señalización que controla la producción de interferones tipo I (Figura adaptada de [91]).

Una vez formado el complejo LPS-TLR4/MD-2, el TLR4 se oligomeriza e interacciona con proteínas celulares que poseen dominios TIR (Receptores Toll de Interleuquina 1), que determinan la relación entre el TLR4 y las proteínas celulares de transducción del LPS. Estas proteínas son *MyD88*, *TIRAP*: proteína adaptadora del dominio TIR, *TRIF*: proteína adaptadora asociada al dominio TIR inductora de interferon, *TRAM*: molécula adaptadora relacionada con el TRIF [88], [92].

La señal de transducción del LPS a través del TLR4 se divide en dos vías, la vía dependiente a la proteína MyD88 y la vía dependiente de la proteína TRIF. Mediante las cuales se generan reacciones diferentes que se unen en el punto donde activan el factor de transcripción nuclear NF-κB. En condiciones normales (ausencia del LPS) este factor está inactivo en el citoplasma unido al inhibidor del factor κB (IκB), sin embargo, la señal enviada por las proteínas MyD88 o TRIF induce la activación de quinasas de IκB, fosforilándose, pasando a pIκB, separándose del NF-κB y por tanto activándolo. En caso de una activación por vía de la proteína MyD88 se genera las citoquinas proinflamatorias como (IL-1, IL6 y TNF-α). Mientras en el caso de la activación por vía del TRIF se genera como respuesta interferón tipo I (Figura 17, B) [88], [92].

En cuanto al modelo de inflamación aguda inducido por TPA sobre oreja de ratón. El tratamiento con ésteres de forbol produce que la célula adopte una morfología transformada, alterando su fenotipo, pero no el genotipo [93]. La aplicación 12-O-tetradecanoilforbol-13-acetato (TPA) sobre la oreja de ratón "epidermis" induce una reacción inflamatoria aguda que consiste en edema con infiltración de leucocitos polimorfonucleares (PMN) así como la hipertrofia de la dermis y epidermis. Otras acciones que tienen lugar consisten en alteración de la morfología de algunas células cutáneas. El TPA, también activa la inducción de un nuevo tipo celular, llamado "dark cells" en la piel de ratones adultos. Así mismo, induce el incremento de la síntesis proteica, de ARN y a largo plazo de ADN, eleva la síntesis de fosfolípidos, incrementa la liberación de ácido araquidónico y prostaglandinas implicados en el proceso de inflamación, aumenta la actividad ornitina decarboxilasa, enzima que participa en la regulación del crecimiento celular, estimula la actividad transglutaminasa, marcador de la diferenciación terminal, incrementa la activación de IL-1, inmunomoduladora y por último disminuye la actividad del AMPc y la actividad histidasa [93].

La epidermis es una barrera física que protege los organismos. Está constituida por múltiples capas de epitelio escamoso estratificado, compuesta casi por completo de células epiteliales especializadas llamadas queratinocitos que responden activamente a las lesiones. Las citoquinas producidas por los queratinocitos son el TNF, TSLP (*Thymic stromal lymphopoietin*), IL-1, IL-6, IL-18, IL-25 e IL-33, que promueven la inflamación. Los neutrófilos son los leucocitos más dominantes en esta fase, ya que se recluta de la sangre al foco de la lesión en la inflamación aguda. Además de los neutrófilos, encontramos monocitos sanguíneos que se diferencian a macrófagos en el tejido. Todas estas alteraciones son producidas mediante citoquinas y moléculas mediadoras [94]. Según nuestros resultados, al tratar esta inflamación con OADP y diclofenaco, se indujo la reparación del daño tisular mediante la migración y el reclutamiento de los leucocitos al foco de la lesión induciendo la reducción de edema.

2.5.2. Citoquinas y moléculas mediadoras de inflamación

La secreción de citoquinas es esencial para la respuesta inflamatoria, se clasifican dependiendo de sus propiedades estructurales y funcionales. En cuanto a su función podemos dividir las en dos tipos, las proinflamatorias y las antiinflamatorias. El primer tipo está constituido principalmente por: la interleuquina-1 (IL-1), el factor de necrosis tumoral (TNF α), la interleuquina-8, y la interleuquina-6 (IL-6), aunque esta última también tiene un importante papel induciendo la expresión de citoquinas antiinflamatorias. Al segundo grupo pertenecen la interleuquina-10, el antagonista del receptor IL-1Ra (receptor antagonista de IL-1), y los receptores solubles de IL-1 (p68) y de TNF (p55 y p75). Todas estas proteínas son mediadoras de la respuesta inflamatoria [90], [95].

2.5.2.1 Citoquinas Proinflamatorias

El TNF α es un mediador de la respuesta inflamatoria aguda, es producido principalmente por macrófagos activados. La pro-TNF α es una proteína de 26 kDa, se expresa en la membrana plasmática, donde es escindida en el dominio extracelular por las metaloproteinasas de la matriz, lo que resulta la liberación de una forma soluble de 17 kDa. La producción del TNF α por los macrófagos es estimulada los patrones moleculares asociados a los patógenos PAMP y por los patrones moleculares asociados a la lesión DAMP. Todas las respuestas conocidas a TNF α se desencadenan al unirse a uno de dos receptores, denominados TNFR1 y TNFR2, que se regulan de manera diferencial en varios tipos de células en tejidos sanos y enfermos. Los TLR pueden activar la expresión del gen TNF α , mediante la activación del factor de transcripción NF- κ B. Además, ejerce un efecto antitumoral a través de un doble mecanismo que incluye la inhibición de la angiogénesis, produciendo la necrosis hemorrágica del tumor, y el aumento de la respuesta inmunitaria antitumoral, acción en la que actúa sinérgicamente con el IFN- γ [88], [90].

La interleuquina 1 (IL-1) es otro mediador de la respuesta inflamatoria aguda, produce sus efectos biológicos a través del receptor de membrana para la IL-1 del tipo I. Además, posee varias acciones muy semejantes al TNF α . La principal fuente tanto de IL-1, como la de TNF α , son los macrófagos activados. La interleuquina 1 tiene dos formas, IL-1 α e IL-1 β , siendo la más secretada la IL-1 β se crea a partir del precursor inactivo (pro-IL-1 β) de 33 kDa que tras ser procesado enzimáticamente da lugar a la proteína bioactiva de 17 kDa. La caspasa-1 intracelular, es una de las principales enzimas responsables de este procesamiento, además, este proceso se regula por los "inflamomas", plataforma proteica multimérica a la que se une la caspasa-1 [88], [95].

La interleuquina 6 (IL-6) es otra citoquina esencial en la respuesta inflamatoria aguda, posee efectos locales y sistémicos, esta interleuquina se sintetiza por los fagocitos mononucleares y otras células en respuesta a PAMP, a IL-1 y a TNF α . El sistema de señalización del receptor de IL-6 está formado por dos tipos de receptores y moléculas de señalización. El receptor de IL-6 (IL-6R), se presenta en dos formas, transmembrana de 80 kDa e IL-6R soluble de 50–55 kDa (sIL-6R). La proteína gp130 de 130 kDa constituye la cadena transductora de señales, siendo además el elemento transmisor de señales para varias citoquinas [88], [90].

2.5.2.2 Mediadores lipídicos

Diversas respuestas fisiológicas a la inflamación son mediadas por los prostanoides: prostaglandinas (PGs), prostacilinas y tromboxanos. Estos eicosanoides son obtenidos mediante el metabolismo oxidativo de ácidos grasos, específicamente del ácido araquidónico (AA) [87]. La biosíntesis de los eicosanoides comienza con la hidrólisis del ácido araquidónico por medio de la acción de las fosfolipasas A₂ (PLA₂). El ácido araquidónico libre actúa como sustrato para tres grupos de enzimas: las lipoxigenasas, epoxigenasas y ciclooxigenasas (COX), también llamadas prostaglandina sintasas, que catalizan la formación de prostanoides (**Figura 18**) [87]. Los prostanoides actúan en el medio cercano a la célula o sobre ella misma mediante la activación de receptores acoplados generalmente a proteínas G. Estos receptores pertenecen a distintas vías de señalización acopladas, como la del AMPc y varían según su localización tisular [87].

Los niveles de producción de prostaglandinas están relacionados con la expresión y la actividad de las enzimas COX. Donde encontramos dos isoformas que generan las mismas reacciones, pero con distintos patrones de expresión: COX-1 y COX-2. Dado que las isoenzimas son proteínas genéticamente independientes, los genes humanos para las dos enzimas están ubicados en cromosomas diferentes y muestran propiedades diferentes. COX-1 se expresa en muchos tejidos y las PGs producidas por la COX-1 median las funciones de "mantenimiento" como la citoprotección de la mucosa gástrica, la regulación del flujo sanguíneo renal y la agregación plaquetaria. En cambio, COX-2 no se detecta en la mayoría de los tejidos normales, su expresión es rápidamente inducida por estímulos como las citoquinas proinflamatorias (IL-1 β , TNF- α), lipopolisacáridos, mitógenos (ésteres de forbol) y oncogenes [87], [96].

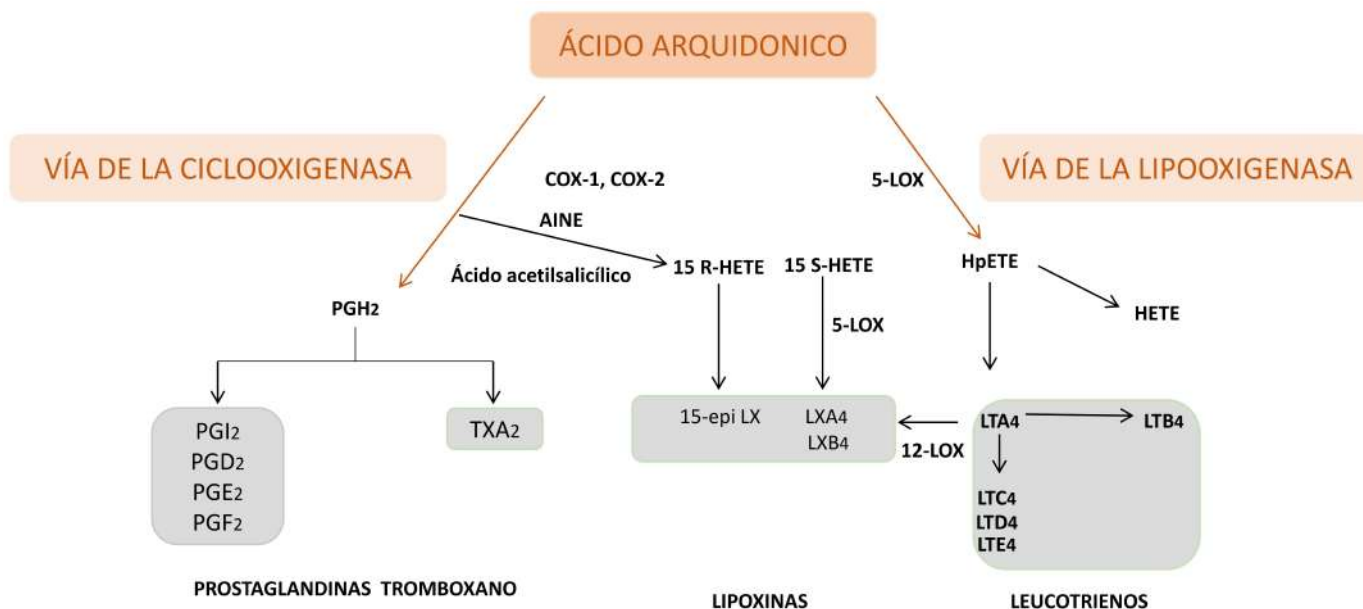


Figura 18. Metabolitos del ácido araquidónico. Mediante la vía de la ciclooxigenasa (COX) el metabolismo del ácido araquidónico da lugar a prostaglandinas (PG) y al tromboxano (TXA₂). Por medio de la vía de la lipooxigenasa (LOX) se origina lipoxinas (LX) y leucotrienos (LT). El ácido acetilsalicílico dificulta la formación de 5-HETE (ácido hidroxicoicosatetraenoico). Los fármacos antiinflamatorios no esteroideos (AINE) inhiben COX-1 y COX2. HpETE, ácido 5-hidroxiperoxiicoicosatetraenoico (Figura adaptada de [88]).

2.5.2.3 Factor de transcripción NF-κB

El factor de transcripción nuclear kappa B (NF-κB), interviene en la homeostasis de las células del sistema inmune al expresar genes de supervivencia y apoptosis, en la respuesta inmune, así como en la regulación de la inflamación [88], [90]. En los mamíferos, el NF-κB se activa por diversos estímulos como el lipopolisacárido bacteriano, ésteres de forbol, etc. Su activación se realiza por varias vías de señalización, como las mediadas por: TLR, TNFR1 y IL-1R1. La forma activa de NF-κB se presenta como un homo o heterodímero con miembros de la familia NF-κB/Rel. El dímero que se encuentra más habitualmente se compone de las subunidades p50 y p65. NF-κB está presente en el citoplasma en forma inactiva unido a la proteína inhibidora, IκB, la cual es fosforilada y degradada por el proteosoma, implicando así la liberación de NF-κB que migra al núcleo donde regula la transcripción de sus genes diana. La proteína IκB oculta la secuencia de localización nuclear (NLS) de la proteína NF-κB y manteniéndola retenida en un estado de inactivación en el citoplasma. Hay varias IκBs, pero la principal es la IκBα [88], [90].

No obstante, La activación de NF-κB puede provocarse mediante una gran variedad de estímulos tanto fisiológicos como patológicos. La ruta de activación comienza a partir de la señal creada por las proteínas IκBs. Esto ocurre por fosforilación de IκB por la quinasa de IκB (IKK). La IKK está constituida por un heterodímero con dos subunidades catalíticas IKKα e IKKβ y por una proteína reguladora IKKγ. Cuando se activa, la IKK fosforila dos residuos de serina situados en un dominio regulador de IκB. Tan pronto se fosforilan estas serinas, las moléculas del inhibidor IκB son transformadas por ubiquitinación, y posteriormente son degradadas en el proteosoma. Otro factor de transcripción que a menudo se une a NF-κB es la proteína activadora 1 (AP-1) [88], [90].

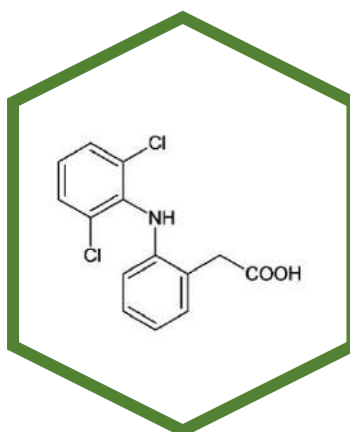
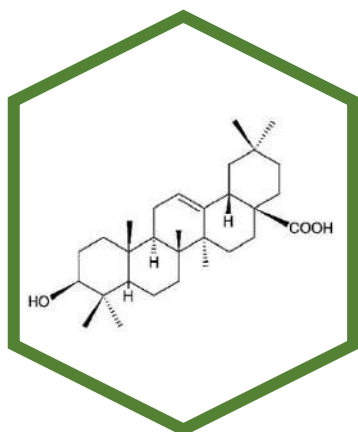
2.5.2.4 MAP quinasas (MAPKs)

Las proteínas MAP quinasas, quinasas activadas por mitógenos regulan el crecimiento celular, la diferenciación, la supervivencia, la respuesta inmune y el estrés. Su activación se produce a través de fosforilaciones consecutivas, reguladas por diferentes quinasas. Estos eventos fosforilativos pueden ser inactivados por fosfatasas específicas. Hay tres vías mediadas por MAPKs: ERK1/2, c-JUN N-terminal quinasa 1, 2 y 3, (JNK1/2/3) y p38 MAPK. Estas vías son desencadenadas por citoquinas, factores de crecimiento, hormonas y estrés osmótico. Una vez activadas tanto JNK, así como ERK1/2 y p38 regulan la expresión de los genes implicados en el crecimiento y la proliferación, como c-Myc y c-Jun [88], [90].

2.5.2.5 Óxido nítrico (NO)

El óxido nítrico (NO) es una molécula de señalización que juega un papel crucial durante la inflamación. El NO se considera un mediador proinflamatorio que induce inflamación por sobreproducción en situaciones anormales. Diferentes tipos de células producen óxido nítrico como los macrófagos por medio de la acción de la enzima óxido nítrico sintetasa (iNOS), a partir del aminoácido L-arginina que genera el óxido nítrico (NO) y L-citrulina, con la ayuda de NADPH en presencia de oxígeno. La iNOS es una enzima citosólica que está ausente en macrófagos en reposo, pero se induce en respuesta a moléculas microbianas que activan TLR [88], [90].

OBJETIVOS



3. OBJETIVOS

Como objetivo principal en esta tesis nos proponemos investigar las propiedades anticancerígenas y antiinflamatorias del derivado amino pegilado del ácido oleanólico OADP y de varios N-derivados del diclofenaco.

3.1. Objetivos específicos

1. Obtener las materias primas y sintetizar el derivado amino pegilado del ácido oleanólico OADP.

- Aislar los triterpenos naturales ácidos oleanólico (OA) y maslínico (MA) a partir de los residuos de molturación de la aceituna "alperujo".
- Sintetizar el derivado del OA el OADP mediante reacción de PEGilación.

2. Caracterizar la actividad anticancerígena del derivado OADP:

- Cuantificar del efecto citotóxico del OADP en las líneas celulares de hepatoma humano (HepG2), carcinoma de colon (HT29) y melanoma (B16-F10) y en macrófagos/monocitos de ratón RAW 264.7.
- Determinar la extensión de los fenómenos apoptóticos desencadenados por el OADP, mediante la determinación del porcentaje de células apoptóticas, el análisis del ciclo celular y el estudio del potencial de membrana mitocondrial
- Evaluar el mecanismo molecular anticancerígeno desencadenado por la acción del OADP, mediante el estudio de la expresión de las proteínas implicadas en los procesos anticancerígenos y de apoptosis.

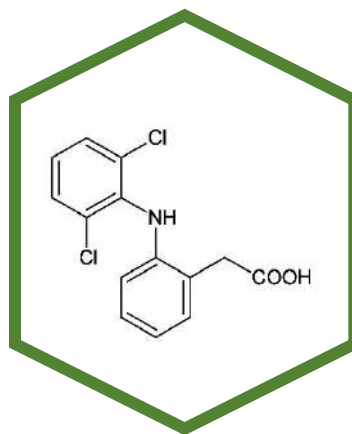
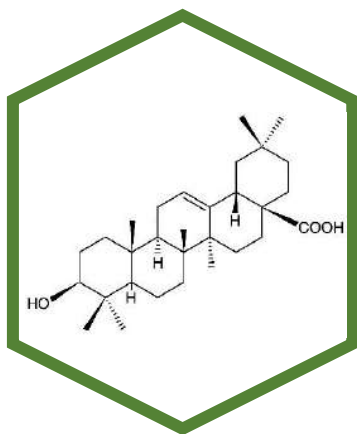
3. Caracterizar de la actividad antiinflamatoria del derivado OADP:

- Determinar cuáles son las concentraciones subcitotóxicas del OADP, en línea celular de macrófagos/monocitos de ratón RAW 264.7.
- Determinar del potencial antiinflamatorio del OADP en ausencia y presencia del agente proinflamatorio (LPS) mediante la determinación de los niveles de óxido nítrico en línea celular de macrófagos/monocitos de ratón RAW 264.7.
- Evaluar del mecanismo molecular antiinflamatorio desencadenado por la acción del OADP, mediante el estudio de la expresión de las proteínas responsables en los procesos antiinflamatorios encadenados.
- Evaluar el efecto antiinflamatorio del OADP, *in vivo*, en un modelo de inflamación aguda por edema inducido sobre oreja de ratón. Mediante la cuantificación de los cambios morfológicos, expresión de IL-6 y análisis de cortes histológicos producidos entre controles y tratados.

4. Caracterizar la actividad anticancerígena y antiinflamatoria de varios N-derivados del diclofenaco.

- Cuantificar del efecto citotóxico de los N-Derivados del diclofenaco en las líneas celulares de hepatoma humano (HepG2), carcinoma de colon (HT29) y melanoma (B16-F10) y en macrófagos/monocitos de ratón RAW 264.7.
- Determinar la extensión de los fenómenos apoptóticos desencadenados por los N-Derivados del diclofenaco, mediante la determinación del porcentaje de células apoptóticas, el análisis del ciclo celular y el estudio del potencial de membrana mitocondrial.
- Evaluar los fenómenos antiinflamatorios desencadenados de los N-Derivados del diclofenaco en línea celular de macrófagos/monocitos de ratón RAW 264.7 en ausencia y presencia del agente proinflamatorio (LPS) mediante la determinación de los niveles de óxido nítrico.

PUBLICACIONES



4.1. Publicación 1

A Diamine-PEGylated Oleanolic Acid Derivative Induced Efficient Apoptosis through a Death Receptor and Mitochondrial Apoptotic Pathway in HepG2 Human Hepatoma Cells

Autores: **Jannus, F.**; Medina-O'Donnell, M.; Rivas, F.*; Díaz-Ruiz, L.; Rufino-Palomares, E.E.; Lupiáñez, J.A.; Parra, A.; Reyes-Zurita, F.J.*

Revista: Biomolecules

Año: 2020

Volumen: 10 (10)

DOI: [10.3390/biom10101375](https://doi.org/10.3390/biom10101375)






Índice de impacto: 6,064
(JCR 2022)

Cuartil: *Biochemistry & Molecular Biology*: T1 (75/296)

Citas: 9 (25 July 2022)
(Semantic Scholar)

Article

A Diamine-PEGylated Oleanolic Acid Derivative Induced Efficient Apoptosis through a Death Receptor and Mitochondrial Apoptotic Pathway in HepG2 Human Hepatoma Cells

Fatin Jannus ^{1,†} , Marta Medina-O'Donnell ^{2,†}, Francisco Rivas ^{2,*} , Luis Díaz-Ruiz ¹,
Eva E. Rufino-Palomares ¹ , José A. Lupiáñez ¹ , Andrés Parra ² and
Fernando J. Reyes-Zurita ^{1,*} 

¹ Department of Biochemistry and Molecular Biology I, Faculty of Sciences, University of Granada, Av. Fuentenueva 1, 18071 Granada, Spain; fatin@correo.ugr.es (F.J.); luisdiazruiz96@gmail.com (L.D.-R.); evaevae@ugr.es (E.E.R.-P.); jlcara@ugr.es (J.A.L.)

² Department of Organic Chemistry, Faculty of Sciences, University of Granada, Av. Fuentenueva 1, 18071 Granada, Spain; mmodonnell@ugr.es (M.M.-O.); aparra@ugr.es (A.P.)

* Correspondence: frivas@ugr.es (F.R.); ferjes@ugr.es (F.J.R.-Z.); Tel.: +34-958-243-252 (F.J.R.-Z.)

† These authors contributed equally to this work.

Received: 31 August 2020; Accepted: 23 September 2020; Published: 28 September 2020



Abstract: Hepatocellular carcinoma (HCC) is the most common type of liver cancer. Our recent studies have shown that the diamine-(PEG)ylated oleanolic acid (OADP) has strong anti-tumor effects in HCCs. In this study, we evaluated the anti-tumor mechanisms of OADP in the HepG2 HCC cell line. The cytotoxicity results showed that HepG2 cell viability was markedly reduced, with a very low 50% of cell growth inhibitory concentration (IC₅₀, 0.14 µg/mL). We then investigated the anti-tumor mechanisms of OADP in HepG2 cells. The flow-cytometry analysis was used to evaluate cell apoptosis, indicating that 74–95% of cells were apoptotic. OADP caused cell cycle arrest in the G₀/G₁ phase and the loss of the mitochondrial membrane potential (MMP). Western blot analysis was performed to assess the expression levels of key proteins associated with the underlying molecular mechanism. The results showed the clear upregulation of caspase-8, caspase-9, caspase-3, Bak, p21, and p53, accompanied by the downregulation of Bcl-2. Similar results were obtained by the cotreatment with OADP and the c-Jun N-terminal kinase (JNK) inhibitor SP600125. Agents such as OADP, which are capable of activating extrinsic and intrinsic apoptotic pathways, may represent potential HCC cancer therapies.

Keywords: triterpenes; oleanolic acid; (PEG)ylated oleanolic acid; extrinsic apoptotic pathway; anti-tumor mechanisms; hepatocellular carcinoma

1. Introduction

According to the World Health Organization (WHO), in 2018, cancer was the second-leading cause of death worldwide, responsible for 9.6 million deaths. The most common form of primary liver cancer is hepatocellular carcinoma (HCC), which represents approximately 75–85% of all liver cancer cases and is considered the second leading cause of cancer-associated death in East Asia and sub-Saharan Africa and the sixth most frequent cause of cancer-associated death in western countries [1].

HCC is generally only observed in patients with cirrhosis-damaged livers [2]. The primary risk factors for HCC include chronic infections, such as hepatitis C virus (HCV) and hepatitis B virus (HBV). Other risk factors include alcohol abuse, smoking, and obesity [3]. The primary therapeutic approaches for HCC

patients include surgical resection, radiation therapy, liver transplantation, and chemotherapy [4]. However, several drugs have been developed in recent years to treat HCC, such as the tyrosine kinase inhibitors (TKIs) sorafenib, regorafenib, lenvatinib, and cabozantinib, which provide the efficient targeted therapy of HCC. Unfortunately, these drugs are also associated with adverse effects, including abdominal pain, hypertension, and hand-foot skin reactions [5].

Despite progress in the therapeutic approaches for HCC, the side effects caused by current treatment options necessitate the continued development of safe and efficient chemotherapy strategies. The use of natural products that are derived from plants represents a potential therapeutic approach to cancer treatment that could decrease the adverse effects of drugs. Therefore, many studies have focused on the identification of new anticancer drug treatments with natural origins [6]. Triterpenoids are the most abundant natural products, demonstrating anticancer and anti-tumor activities, and are often sources of anticancer agents, including oleanolic acid (OA).

Studies have shown that OA and its derivatives can exert anticancer activities in several cancer cell lines, including osteosarcoma, melanoma, breast cancer, and prostate cancer cells. OA also presents other pharmacological activities, such as anti-inflammatory, antidiabetic, hepatoprotective, and neuroprotective activities [7]. Our research group has applied polyethylene glycol (PEG)ylation techniques to OA, obtaining several OA derivatives [8–10]. PEGylation, which consists of the covalent bonding of a PEG polymer to an active biological agent, represents one of the most promising techniques for improving the therapeutic effects of drugs [11]. OADP is a diamine-PEGylated derivative of OA, obtained by performing a PEGylation reaction on the C-28 carboxyl group, using an amine-type PEG reagent (4,7,10-trioxatridecane-1,13-diamine, H₂N-PEG-NH₂) [8].

OA and its derivatives have been widely reported to induce apoptosis. OA and azaheterocyclic induce apoptosis through the alteration of Bax/Bcl2, resulting in the release of cytochrome-c and the activation of caspase-9 and caspase-3 in SMMC-7721 and BEL-7404 human HCC cells [12,13]. Another study showed that OA and ursolic acid induced apoptosis in four human liver cancer lines, including HepG2, Hep3B, Huh7, and HA22T, by enhancing caspase-8 and caspase-3 [14]. However, the effects of PEGylated oleanolic acid derivatives, such as OADP, on protein expression level in HCC cells and the underlying mechanisms of action have not yet been investigated. To study the anti-tumor effects of OADP on HCC cells, we used the HepG2 human carcinoma cell line because this cell line expresses the specific characteristics of hepatocytes, which are pathologically important to the progression of HCC.

Apoptosis, or programmed cell death, is defined as the active, physiological process of cell self-destruction. Two primary pathways have been described during apoptotic activation. The intrinsic pathway involves the release of pro-apoptotic factors, such as cytochrome-c, from the mitochondria, which activates the apoptotic mechanism through interaction with Apaf-1 and the stimulation of the initiator caspase-9. Caspase-9, in turn, proteolytically induces the activity of the executor caspase-3, one of the main proteases that participate in the apoptosis execution phase. In the extrinsic pathway, the activation of the death receptor stimulates the activation of the caspase-8 initiator, triggering downstream events by either directly activating caspase-3 or cleaving the Bid factor, which in turn, initiates the mitochondrial pathway. However, Bid activation has also been described as being mediated by c-Jun N-terminal kinase (JNK) [15,16]. Activated Bid targets the mitochondria, modulating other Bcl-2-like factors, such as Bax [17]. Furthermore, p53 has been identified as a key participant in the molecular mechanism associated with apoptosis induction, which involves both the transcriptional and non-transcriptional regulation of downstream effectors. For example, p53 induces apoptosis through the transcriptional upregulation of pro-apoptotic genes, such as Bax, and the transcriptional repression of the anti-apoptotic Bcl-2 [18]. p53 also translocates to the mitochondria prior to cytochrome-c release and pro-caspase-3 activation [19].

In our previous studies, our group described the anticancer properties of different triterpenoids, such as maslinic acid (MA) [20–26] and the OA derivative, 3-O-succinyl-28-O-benzyl oleanolate [27]. We also determined the underlying molecular mechanism associated with the anticancer effects of MA in Caco-2 and HT29 colon cancer cells. In Caco-2 colon cancer cells, MA treatment activated

the extrinsic apoptotic pathway by inducing the cleavage of caspase-8 and caspase-3, increasing the levels of t-Bid, and decreasing the level of Bcl-2 [20,23]. Furthermore, we demonstrated that MA treatment induced apoptosis in human HT29 colon cancer cells by activating the intrinsic apoptotic pathway, induced by the expression of JNK, which also increased p53 levels and upregulated the expression of Bid and Bax, whereas Bcl-2 expression decreased. Finally, MA treatment also induced cytochrome-c release, due to mitochondrial disturbances, and increased the levels of cleaved caspase-9, -3, and -7 [23–25].

In this study, OADP was found to exhibit the marked inhibition of cell viability, inducing apoptosis and causing G0/G1 cell-cycle arrest, in a concentration- and time-dependent manner. We also investigated the *in vitro* effects of OADP on the HepG2 cell line and determined the underlying molecular mechanisms associated with OADP treatment. We determined that in HepG2 cells, OADP activated the proapoptotic response of the Bcl-2 protein family, such as Bak, and inhibited Bcl-2. OADP also activated transcription factors, such as p53 and p21. Finally, this compound induced the activation of initiator caspase-8 and caspase-9 and the effector caspase-3.

2. Materials and Methods

2.1. Materials

Dulbecco2019s modified Eagle medium (DMEM), foetal bovine serum (FBS), penicillin/streptomycin (Biowest, Nuaille, France), dimethylsulfoxide (DMSO, Merck Life Science S.L., Madrid, Spain), and 3-(4,5-dimethylthiazol-2-yl)-2,5-diphenyltetrazolium bromide (MTT) were purchased from Thermo Fisher Scientific Inc. (Ward Hill, MA, USA). Caspase-3, Caspase-8, Caspase-9, Bcl-2, p53, Bak, and p21 antibodies were purchased from Santa Cruz Biotechnology (Santa Cruz, CA, USA). JNK inhibitor (SP600125) was purchased from Cell Signaling Technology, Inc. (Danvers, MA, USA). Caspase-8 inhibitor (IETD-CHO) and caspase-9 inhibitor (Ac-LEHD-CMK) were purchased from Merck Chemicals Ltd. (Padge Road, Beeston, UK). Secondary anti-rabbit, anti-mouse, and anti-goat antibodies and actin antibody were purchased from Santa Cruz Biotechnology (Santa Cruz, CA, USA). Culture flasks and well plates were obtained from VWR International, Ltd. (Radnor, PA, USA).

2.2. General Experimental Chemical Procedures

Measurements of nuclear magnetic resonance (NMR) spectra were made using VARIAN Inova unity (300 MHz ¹H NMR), and VARIAN direct drive (400 and 500 MHz ¹H NMR) spectrometers. The ¹³C chemical shifts were assigned with the aid of distortionless enhancement by polarization transfer (DEPT), using a flip angle of 135°. Infrared (IR) spectra were recorded on a MATTSON SATELLITE FTIR spectrometer. Optical rotations were measured with a Perkin-Elmer 241 polarimeter, at 25 °C. The purities of new compounds were determined by a WATERS ACQUITY UPLC system (ultra-performance liquid chromatography), coupled with a WATERS SYNAPT G2 HRMS spectrometer (high-resolution mass spectra) with electrospray ionization (ESI). The purities of all compounds were confirmed to be ≥95%. All reaction solvents and chromatography solvents were distilled prior to use. Commercially available reagents were used without further purification. Merck silica-gel 60 aluminium sheets (ref. 1.16835) were used for thin-layer chromatography (TLC), and spots were rendered visible by spraying with H₂SO₄–AcOH, followed by heating to 120 °C and visualized under ultraviolet (UV) light at 254 nm. Merck silica-gel 60 (0.040–0.063 mm, ref. 1.09385) was used for flash chromatography. CH₂Cl₂ (Fisher, ref. D/1852/17) or n-hexane (Merck, ref. 1.04374), with increasing amounts of acetone (Fisher, ref. A/0600/17) or EtOAc (Fisher, ref. E/0900/17), were used as eluents (all solvents were of analytical reagent grade purity). The PEG reagent 4,7,10-trioxatridecane-1,13-diamine (H₂N-PEG-NH₂, CAS Number 4246-51-9) was purchased from Sigma–Aldrich. Boc₂O (CAS Number 24424-99-5) was also purchased from Sigma–Aldrich.

The plant material, a specimen of the plant of *Olea europaea* L. (order Lamiales, family Oleaceae), was collected in Almegijar, Granada, Spain, in May 2001. Laura Baena, from the herbarium of the

University of Granada, identified this plant. A voucher specimen (53489-1-1) was deposited at the University of Granada Herbarium, Granada, Spain.

2.3. Isolation of OA

OA was isolated from solid olive oil production wastes, which were extracted successively in a Soxhlet, with hexane and EtOAc. OA was purified from hexane extracts, using column chromatography over silica gel and eluting with CH_2Cl_2 /acetone mixtures of increasing polarity [28].

2.4. PEGylation Reaction of OA

A solution of di-tert-butyl dicarbonate (Boc_2O , 2.75 mmol) in dried CH_2Cl_2 (2 mL) was added slowly, dropwise, to a solution of 4,7,10-trioxatridecane-1,13-diamine ($\text{H}_2\text{N-PEG-NH}_2$, 6.8 mmol) in CH_2Cl_2 (20 mL). The reaction mixture was maintained at room temperature (rt) for 12 h, and then diluted with water and extracted three times with CH_2Cl_2 . The organic layer was dried with anhydrous Na_2SO_4 , and the solvent was removed under reduced pressure, producing the diamine-Boc-PEGylated derivative ($\text{H}_2\text{N-PEG-NH-Boc}$, 85%), blocked in an amino group [8].

In a flask (20 mL), the reagent $\text{H}_2\text{N-PEG-NH-Boc}$ (0.45 mmol) was dissolved in dimethylformamide (5 mL) and afterwards, OA (2 mmol), 1-hydroxy-7-azabenzotriazole (HOAt, 3 mmol), (7-Azabenzotriazol-1-yloxy)tripyrrolidinophosphonium hexafluorophosphate (PyAOP, 2 mmol), and *N,N*-diisopropylethylamine (DIPEA, 8 mmol), were added. The reaction mixture was heated to 100 °C for 12 h, diluted with water, and extracted three times with CH_2Cl_2 . The organic layer was dried with anhydrous Na_2SO_4 , and the solvent was removed under reduced pressure. Finally, the residue was purified by column chromatography, using *n*-hexane/ethyl acetate as the solvents, to yield the OA-diamine-Boc-PEGylated derivative (94%) [8].

This OA-diamine-Boc-PEGylated derivative (0.3 mmol) was dissolved in tetrahydrofuran (THF, 20 mL), and then concentrated HCl (37%, 2 mL) was added. The reaction mixture was maintained at rt for 24 h, then diluted with water and extracted three times with CH_2Cl_2 . The organic layer was dried with anhydrous Na_2SO_4 , and the solvent was removed under reduced pressure. Finally, the residue was purified by column chromatography, using *n*-hexane/ethyl acetate as solvents, and to yield OADP (95%) (Figure 1) [8].

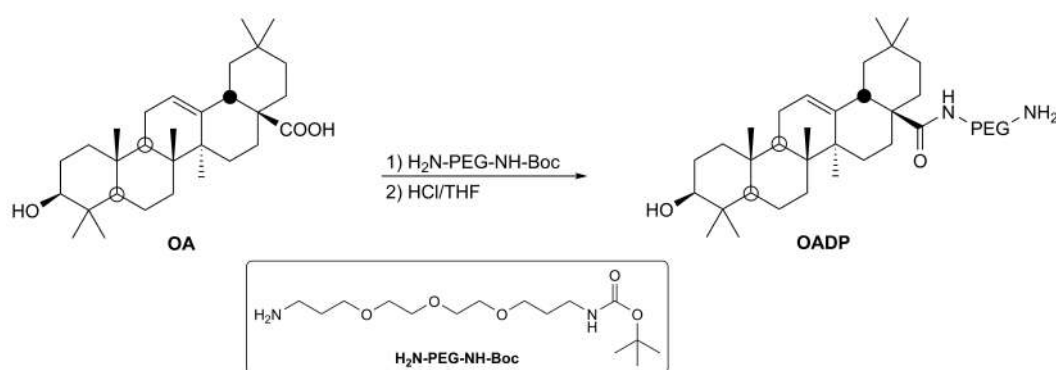


Figure 1. Semi-synthesis of a diamine-PEGylated derivative of oleanolic acid (OADP).

2.5. Drugs

OADP was dissolved, at 5 mg/mL, in DMSO. A stock solution was stored at -20 °C. Before the experiments, this solution was diluted in the cell culture medium, to the desired concentration. Cytometric analyses were performed at the OADP the 20%, 50%, and 80% cell growth inhibitory concentrations (IC_{20} , $\text{IC}_{50} \pm$ and IC_{80} , respectively) for 24, 48, and 72 h. Western blot analyses were performed after 72 h of treatment at the OADP IC_{50} and IC_{80} values.

2.6. Cell Culture

The HepG2 human HCC cell line (ECACC cell line no. 85011430) and the WRL68 non-tumor human embryo liver cells (EACC no. 89121403) were supplied by the cell bank of the University of Granada, Granada, Spain. Cell lines were cultured in DMEM, supplemented with 2 mM glutamine, 10,000 units/mL penicillin, and 10 mg/mL streptomycin, containing 10% decompemented FBS, at 37 °C, in an atmosphere of 5% CO₂ and 95% of humidity. Cells were grown in the absence of OADP, for 24 h before treatment. In all experiments, we used sub-confluent monolayer cells.

2.7. Cytotoxicity Assay

OADP treatment effects on the proliferation of HepG2 cells were assessed using the mitochondrial membrane potential (MTT) assay. Cell viability was determined by measuring the absorbance of the MTT dye in living cells. MTT cleaves the tetrazolium ring to produce formazan, which absorbs at 570 nm.

For this assay, 1.5×10^3 HepG2 cells and 8.0×10^3 WRL68 cells, were grown in each well of a 96-well plate and incubated with increasing concentrations (0–20 µg/mL) of OADP, for 24 and 48 h for HepG2 cells, and 72 h for HepG2 and WRL68 cells. After incubation, the media was removed, and 100 µL of MTT solution (0.5 mg/mL), in a mixture of 50% phosphate-buffered saline (PBS) and 50% medium, was added to each well. After 2 h of incubation, formazan was dissolved in 100 µL DMSO. Relative cell viability, with respect to the untreated control cells, was measured according to absorbance at 570 nm, using a plate reader (Tecan Sunrise MR20-301, TECAN, Salzburg, Austria). OADP showed high levels of cytotoxicity at the very lowest tested concentrations. Therefore, we examined the mechanisms through which this cytotoxicity occurred. Therefore, apoptosis, cell cycle, and mitochondrial membrane potential (MMP) analyses were performed, and we also investigated the activated molecular mechanisms associated with cell death in HepG2 cells.

2.8. Flow Cytometric Assay

2.8.1. Apoptosis Analysis

Apoptosis was quantified by flow cytometry, using a FACScan (fluorescence-activated cell sorter) flow-cytometer (Coulter Corporation, Hialeah, FL, USA), analyzing between 5000 and 10,000 events. HepG2 cells were plated at 1.5×10^5 cells per well on a 24-well plate, in 2 mL of medium, and treated with OADP for 24, 48, and 72 h, at the IC₂₀, IC₅₀, and IC₈₀ values. Cells were collected and resuspended in binding buffer (10 mM HEPES/NaOH, pH 7.4, 140 mM NaCl, 2.5 mM CaCl₂). Annexin V-fluorescein isothiocyanate (FITC) conjugate (1 µg/mL) was then added and incubated for 30 min at rt in the dark. Just before the FACS analysis, we stained the cells with 20 µL of 1 mg/mL propidium iodide (PI) solution. All experiments were performed two times, in triplicate, including the control.

2.8.2. Cell Cycle Analysis

To determine the main alterations in the cell cycle profiles, particularly DNA ploidy, we used FACS. We measured those alterations at 488 nm on an Epics XL flow cytometer (Coulter Corporation, Hialeah, FL, USA), analyzing between 2500 and 10,000 events. Cell subpopulations with differing DNA contents (cells in G₀/G₁, S or G₂/M phase) were visualized. In addition, we were able to distinguish the population size and the nucleus fractions in each phase of the cell cycle, and calculated the DNA ratios for each identified nuclear subpopulation. According to the previous protocol, the percentages of cells in different phases of the cell cycle were detected by PI staining. HepG2 cells, seeded at a density of 1.5×10^5 cells/well, were plated into 24-well plates with 2 mL of medium. For 24, 48 and 72 h, the cells were treated with OADP at the IC₂₀, IC₅₀ and IC₈₀ concentrations, previously obtained during the cell proliferation activity test. Cells were washed twice with cold PBS, trypsinised, centrifuged at 1500 rpm for 5 min, and then washed twice with cold PBS. After the second centrifugation, the cells were resuspended in 1 × TBS staining buffer (10 mM Tris, 150 mM NaCl), followed by the addition of Vindelov buffer (100 mM Tris, 100 mM NaCl, 10 mg/mL RNase, 1 mg/mL propidium iodide (PI),

pH 8). Just before the measurements, the total DNA content was stained with 1 mg/mL of PI. We used Multicycle software to determine the percentages of cells in different phases of the cell cycle (G0/G1, S, and G2/M). All experiments were performed two times, in triplicate, including the control.

2.8.3. Mitochondrial Membrane Potential Analysis

We studied mitochondrial damage using a FACScan flow cytometer. We used dihydrorhodamine (DHR), which becomes oxidized to the highly fluorescent rhodamine (Rh123), to measure the MMP. Fluorescence spectroscopy, using excitation and emission wavelengths of 500 and 536 nm, respectively, was used to monitor rhodamine formation. Intracellular measurements of MMP were determined by the cytometry of Rh123. HepG2 cells were plated at 1.5×10^5 cells per well in 24-well plates, in 1.5 mL of medium, and treated with the OADP for 24, 48, and 72 h at the previously calculated IC_{20} , IC_{50} , and IC_{80} concentrations. After treatment, the medium was removed, and fresh medium containing DHR was added, at a final concentration of 5 μ g/mL. The medium was removed, and the cells were washed and resuspended in PBS containing 5 μ g/mL of PI, after 30 min incubation. Finally, the fluorescence intensities of Rh123 and PI were determined using a FACScan flow cytometer (Coulter Corporation, Hialeah, FL, USA), analyzing between 4000 and 10,000 events. All experiments were performed two times, in triplicate, including the control.

2.9. Western Blotting Analysis

HepG2 cells (1.5×10^4) were treated with OADP at the previously calculated IC_{50} and IC_{80} concentrations for 72 h. Cells were also co-incubated for 72 h with the IC_{50} concentrations of OADP, a caspase-8 inhibitor (IETD-CHO, 18 nM), a caspase-9 inhibitor (Ac-LEHD-CMK, 70 nM), and JNK inhibitor (SP600125, 25 μ M). After the treatments, cells were washed twice with PBS and resuspended in lysis buffer (20 mM Tris/acetate, pH 7.5, 1 mM EDTA, 1 mM EGTA, 1% Triton X-100, 1 mM orthovanadate, 270 mM sucrose, 1 mM sodium glycerophosphate, 5 mM sodium fluoride, 1 mM sodium pyrophosphate, 5 mM β -mercaptoethanol, 1 mM benzamidine, 35 μ g/mL PMSF, and 5 μ g/mL leupeptin). Samples were homogenized, ultrasonicated, and incubated on ice for 20 min before centrifuging at $12,000 \times g$ for 15 min. Supernatants were assayed to determine the protein concentration. The protein concentration was determined by the Bradford method. For Western blot analyses, a 25–50 μ g sample of total proteins was used. Proteins were separated on 15% sodium dodecyl sulfate (SDS)-polyacrylamide gel and transferred to a polyvinylidene difluoride membrane. The membranes were blocked by incubation in TBS buffer containing 0.1% Tween and 5% milk powder, for 1 h at rt, and washed with TBS buffer containing 0.1% Tween. Membranes were blotted overnight, at 4 °C, with primary antibodies (Mouse monoclonal anti-caspase-8 (1/200 dilution), goat polyclonal anti-caspase-3 (1/600 dilution), mouse monoclonal anti-Bcl-2 (1/200 dilution), rabbit polyclonal anti-caspase9 (1/500 dilution), rabbit polyclonal anti-p53 (1/4000 dilution), rabbit polyclonal anti-Bak (1/800 dilution), and rabbit polyclonal anti-p21 (1/500 dilution)). The blots were then washed 3 times with TBS-0.1% Tween and developed with peroxidase-linked secondary antibodies for 1 h at rt, with the following dilutions (1/3000, 1/3000, 1/3000, 1/13,000, 1/13,000, 1/13,000, 1/12,000). All antibodies were obtained from Santa Cruz Biotechnology (Santa Cruz, Inc., CA, USA). Blots were then washed 3 times with TBS-0.1% Tween and once with TBS. Consequently, all blots were revealed using the ChemiDoc XRS Image System (Bio-Rad Laboratories, Hercules, CA, USA). Finally, the quantification of protein bands was performed using Multi-Gauge program (Fuji Film Europe, TK Tiburg, Holland).

2.10. Hoechst-Stained Fluorescence Microscopy

Morphological changes were analyzed by Hoechst-stained fluorescent microscopy. Therefore, 15×10^4 HepG2 cells were plated on coverslip in 24-well plates. After 24 h, OADP was added and cells were incubated for 72 h at their respective IC_{50} and IC_{80} concentrations. The cells were then washed twice with PBS, treated in cold MeOH for 3 min, washed in PBS, and incubated in 500 μ L

Hoechst solution (50 ng/mL) in PBS for 15 min in the dark. The samples were visualized by fluorescent microscopy (DMRB, Leica Microsystems, Wetzlar, Germany) with a DAPI filter.

2.11. Statistical Analysis

Data are represented as the mean \pm standard deviation (SD). For each experiment, the Student's *t*-test 2019 was used for statistical comparisons against untreated control cells. A limit of $p \leq 0.05$ was used to determine significant differences. Key: $p < 0.05$ (*), $p < 0.01$ (**), and $p < 0.001$ (***). All data shown here are representative of at least two independent experiments, performed in triplicate.

3. Results

3.1. Effects of a Diamine-PEGylated Derivative of Oleanolic Acid (OADP) on HepG2 Proliferation

To evaluate the cytotoxic effects of OADP (Figure 1) on the HepG2 cell line, we incubated these cells at increasing concentrations (0–20 $\mu\text{g/mL}$) of OADP for 24, 48, and 72 h. Cell viability was analyzed by MTT assay, based on formazan dye concentrations.

The percentage of growth inhibition in the presence of various concentrations of OADP for HepG2 cells was determined as the percentage of viable treated cells relative to viable, untreated control cells. As shown in Figure 2, OADP induced significant cell death, in a concentration- and time-dependent manner. The OADP concentrations required for 20% growth inhibition (IC_{20}), 50% growth inhibition (IC_{50}), and 80% growth inhibition (IC_{80}) were determined for all incubation times. The IC_{20} and IC_{50} concentrations were less than 3 $\mu\text{g/mL}$ for all three analyzed times. The IC_{80} concentration was less than 5 $\mu\text{g/mL}$ for all three times. The IC_{50} concentrations obtained for the 24 and 48 h time points were 45–62 times lower than those for OA. These concentrations were especially low after 72 h of OADP treatment, with values lower than 1 $\mu\text{g/mL}$ ($\text{IC}_{20} = 0.12 \pm 0.01 \mu\text{g/mL}$; $\text{IC}_{50} = 0.14 \pm 0.03 \mu\text{g/mL}$; $\text{IC}_{80} = 0.17 \pm 0.05 \mu\text{g/mL}$). The IC_{50} concentration for this compound (OADP), at 72 h, was 677 times lower than its precursor (OA), and 718 times lower at the IC_{80} concentration. This cytotoxicity appears to be selective for the HepG2 hepatic tumor cell line. Thus, in the WRL68 non-tumor liver cells of human embryos, the IC_{50} value at 72 h of incubation with OADP was $5.47 \pm 0.12 \mu\text{g/mL}$, which implies a cytotoxicity 39 times lower in this line than in the HepG2 tumor cell line.

The extremely low concentrations obtained in these tests led us to determine whether cytotoxicity was due to the activation of apoptosis and whether any cytostatic effects were associated with the cytotoxic response. Therefore, the following cytometric assays were performed, including the determination of apoptosis through annexin-V-FITC staining, cell cycle analysis using PI staining, and the evaluation of changes in MMP. These concentrations and times were selected for the rest of the assays: cell cycle analysis, characterization of apoptosis, and changes in mitochondrial membrane potential. IC_{50} and IC_{80} concentrations obtained for the 72 h treatment time point, were selected for the analysis of protein expression level by Western blot analysis because these concentrations resulted in the strongest effects.

3.2. Characterisation of the Apoptotic Effects of OADP by Flow Cytometry

The main objective of developing new drugs capable of blocking cell proliferation and inducing apoptosis is to obtain anticancer agents that can inhibit the growth of tumor cells and arrest the cell cycle. The loss of cytoplasmic membrane asymmetry occurs early during apoptosis, caused by the translocation of phosphatidylserine (PS) from the leaflet of the internal membrane to the external membrane, exposing PS to the external environment, where it can be recognized by macrophage cells [29]. The exposed PS is recognized by annexin V phospholipid-binding protein, which binds to and fluorescently labels apoptotic cells.

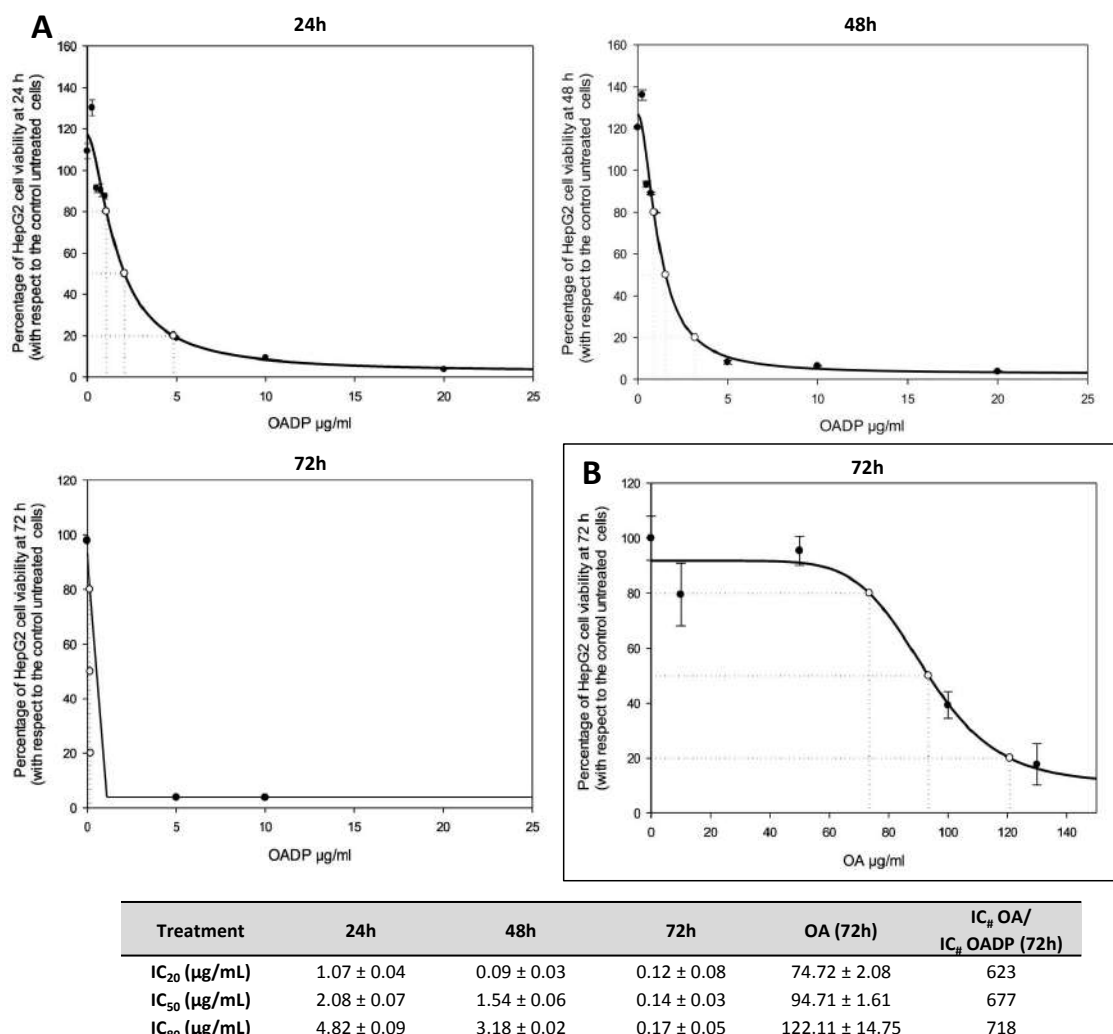


Figure 2. (A) Effects of OADP on the viability of the HepG2 human hepatocarcinoma cells. OADP treatment was applied for 24, 48, and 72 h, in the range of 0 to 20 µg/mL, and each point represents the mean ± S.D. of at least two independent experiments, performed in triplicate. (B) Effects of OA on the viability of HepG2 cells, after treatment for 72 h. IC₂₀, IC₅₀, and IC₈₀ represent the concentrations required for 20%, 50%, and 80% growth inhibition, respectively. OA, oleanolic acid; OADP, diamine-PEGylated OA.

We performed apoptosis cytometric studies in the HepG2 cell line, treated with OADP at the IC₂₀, IC₅₀, and IC₈₀ concentrations, for 24, 48, and 72 h. Apoptotic tests were performed by double staining with Annexin V, and conjugated to FITC and PI. Apoptosis percentages were determined for Annexin V-FITC/PI stained cells using FACS analysis (Figure 3). This double-staining method differentiated four cell populations: normal cells (Annexin V⁻ and PI⁻), early apoptotic cells (Annexin V⁺ and PI⁻), late apoptotic cells (Annexin V⁺ and PI⁺), and necrotic cells (Annexin V⁻ and PI⁺).

Treatment of HepG2 cells with OADP was shown to induce apoptosis, in a time- and concentration-dependent manner. The lowest percentage of total apoptosis was observed at the IC₂₀ concentration, with similar values for all three time points, (close to 25%, consisting of 1% early apoptosis and 24% late apoptosis). At the IC₅₀ concentration, the total percentage of apoptosis obtained was close to 30% (3% early apoptosis plus 27% late apoptosis), at the 24 and 48 h time points, whereas 60% of apoptosis was observed after 72 h of treatment. The highest percentage of apoptosis was obtained at the IC₈₀ concentration, after 48 h, which was 74% (34% early apoptosis plus 40% late apoptosis), and 72 h, which was 94% (77% early apoptosis plus 17% late apoptosis). In addition, the percentages of the necrotic populations were not remarkable.

The low IC₂₀, IC₅₀, and IC₈₀ values, and the good percentages of apoptosis observed indicated that OADP could represent a promising anticancer drug; therefore, we decided to explore the apoptotic trigger mechanisms. The effects of this product on the cell cycle were studied, below. The distribution of cells in different cell cycle phases was analyzed after 24, 48, and 72 h of incubation at the mentioned concentrations, based on the incorporation of PI.

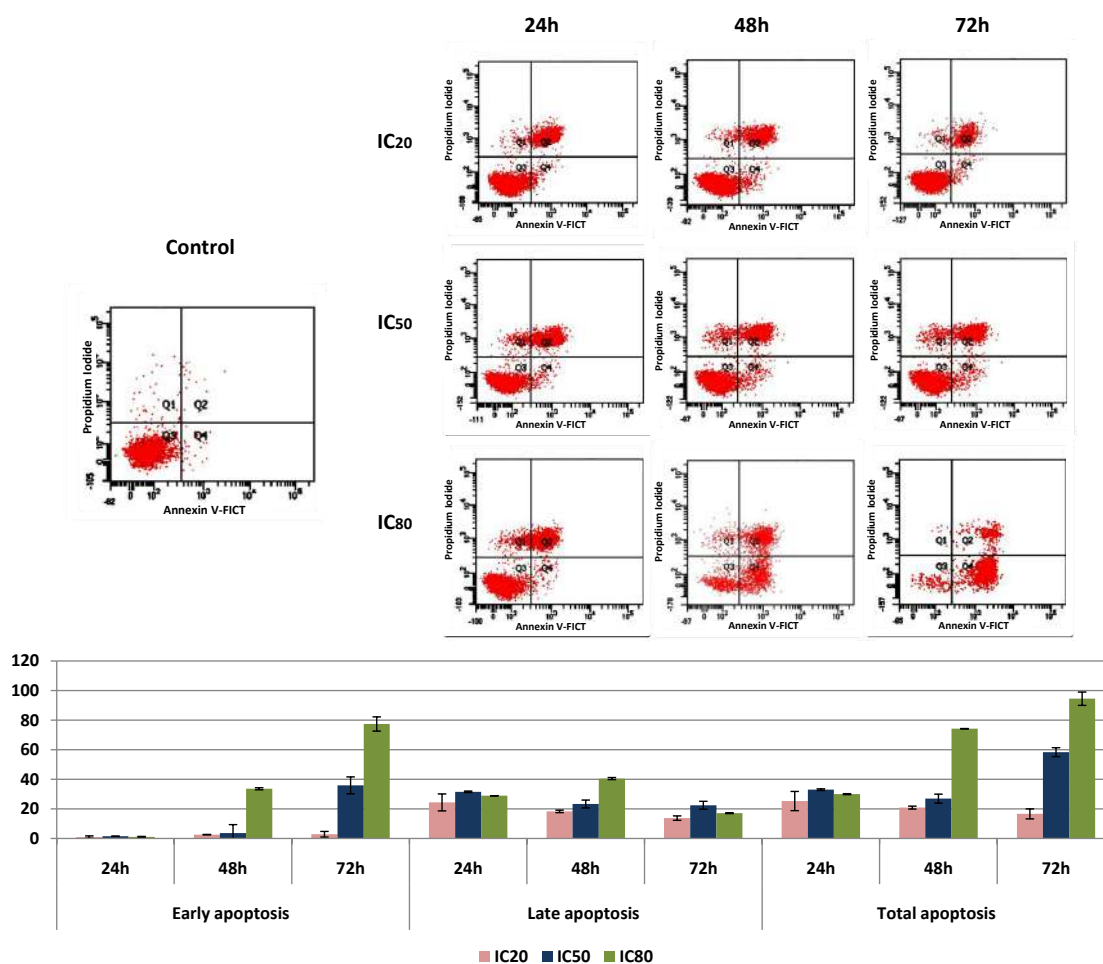


Figure 3. Flow cytometric analysis of Annexin V-FITC staining and propidium iodide (PI) accumulation after the exposure of HepG2 cells to OADP for 24, 48, and 72 h. The cell line was treated at concentrations equal to the IC₂₀, IC₅₀, and IC₈₀ values. Top: Diagrams of annexin V/PI flow cytometry. The right quadrants of each diagram represent apoptotic cells (Q2, late apoptosis; Q4, early apoptosis). Bottom: Flow cytometry analysis of Annexin V-FITC staining and PI accumulation. Values represent the mean \pm S.E.M of duplicate independent experiments, performed in triplicate.

3.3. OADP Induces Cell Cycle Arrest in the G₀/G₁ Phase

In response to treatment with the triterpene derivative OADP, cell proliferation is suppressed through cytotoxic and cytostatic effects. To determine the potential cytostatic effects associated with the cytotoxic response, we analyzed the cell cycle distribution and cell cycle arrest. Flow cytometry was used to sort PI-stained cells and to measure DNA ploidy and alterations in cell cycle profiles in HepG2 cells treated with the IC₂₀, IC₅₀, and IC₈₀ OADP values for 24, 48 and 72 h. The DNAs content are directly proportional to PI fluorescence, which allows the determination of the percentage of cells in each cell cycle phase. This method allows the cell subpopulations presenting different DNA contents to be visualized. Changes in DNA concentrations are characteristic of apoptosis and cell cycle arrest.

Alterations in the HepG2 cell cycle, induced by OADP treatment, are shown in Figure 4. After 24 h of incubation, the important growth arrest at the G₀/G₁ phase was observed (57.5% in the control,

86.5% at IC₂₀, 87.6% at IC₅₀, and 84.9% at IC₈₀). These percentages represented a 47% increase in the proportions of cells in this phase of the cycle compared with untreated control cells. These increased proportions of cells in the G₀/G₁ phase were accompanied by a concomitant decrease in the proportions of cells in S phase. The proportions of cells in S phase were markedly reduced, from 40% in control cells to 10.9%, 9.9%, and 7.0% following OADP treatments at IC₂₀, IC₅₀, and IC₈₀ concentrations, respectively.

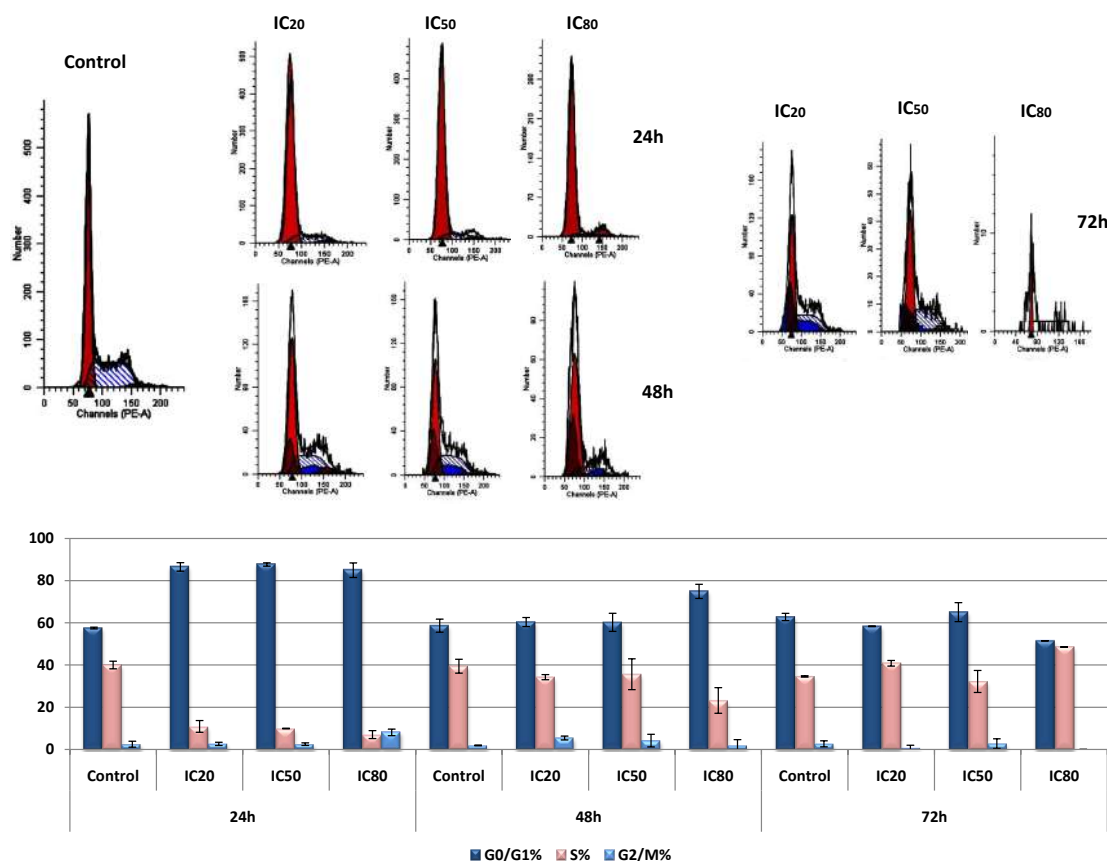


Figure 4. Changes occurred in the percentages of cells in each of the cell cycle phases, compared with untreated control cells. HepG2 cells were treated with OADP at the IC₂₀, IC₅₀, and IC₈₀ concentrations. Cell cycle analysis was performed after PI staining. Cells in the G₀/G₁ phase (dark blue bar), S phase (pink bar), and G₂/M phase (light blue bar) were counted. Values represent the mean \pm SEM of at least two independent experiments, performed in duplicate.

However, treatment at 48 h and 72 h, using the same concentrations, produced a slight arrest in the growth of the G₀/G₁ cell cycle. After 48 h of treatment, only a 15% increase in cells was observed in this cell cycle at the IC₈₀ concentration, whereas after 72 h of incubation, only a 5% increase was found in this phase at the IC₅₀ concentration. However, a 15% increase in the cell population was detected in the S phase at the IC₈₀ concentration.

These changes in the percentages of cells arrested at different stages suggested that the G₀/G₁ phase may be associated with an OADP-induced cytostatic process at the beginning of the treatment process, which disappears after 48 h of treatment. Future trials will be necessary to verify this possibility. The arrest in S phase, which was observed after 72 h of treatment, may be a consequence of apoptosis induction.

3.4. OADP Treatment Causes Changes in the Mitochondrial Membrane Potential

The two primary apoptotic pathways are the intrinsic mitochondrial apoptotic pathway and the extrinsic apoptotic pathway. The first pathway causes mitochondrial disruption and involves the loss of MMP. In contrast, the second pathway induces apoptosis without initial MMP changes.

To determine the apoptosis mechanism involved in the apoptotic response of HepG2 cells, we analyzed MMP using Rh123 staining. This compound is a membrane-permeable, fluorescent cationic dye that is selectively taken up by the mitochondria and its fluorescence is proportional to MMP.

To determine the possible mechanisms involved in the apoptotic response of HepG2 cells induced by OADP, we analyzed the MMP of these cells after incubation with OADP, at IC_{20} , IC_{50} , and IC_{80} concentrations, for 24, 48, and 72 h of incubation time (Figure 5).

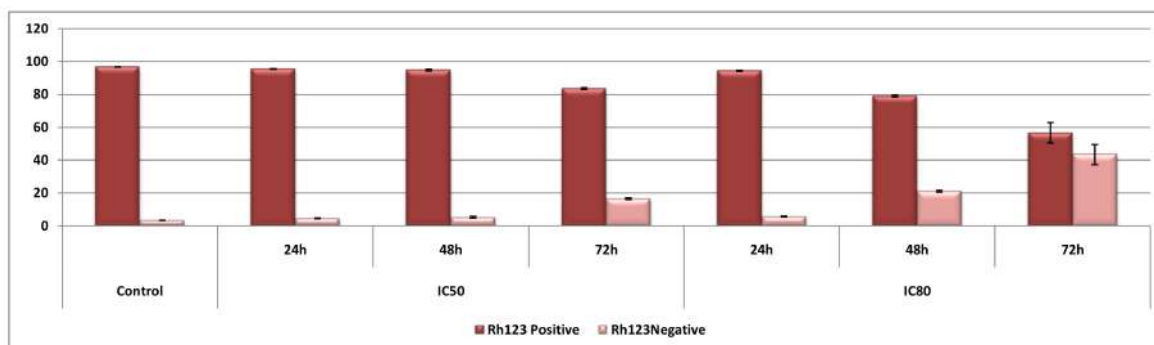


Figure 5. Percentage of HepG2 Rh123-positive cells, relative to untreated control cells (control), after treatment with OADP for 24, 48, and 72 h, at the IC_{50} and IC_{80} concentrations. Values are expressed as the mean \pm SD of two independent experiments, performed in triplicate.

The results obtained showed that 24 h after OADP treatment, no changes in MMP were observed. However, after 48 h of incubation at the IC_{80} concentration, the percentage of Rh123-negative cells increased by 18% compared with the untreated control cells. No changes were detected for the other tested concentrations. After 72 h of incubation at the IC_{50} concentration, the percentage of Rh123-negative cells increased by 15% compared with untreated controls cells, whereas this percentage increased by 40% at the IC_{80} concentration.

These results clearly showed that no changes in MMP occurred after the initial treatments with OADP. Subsequent changes in MMP occurred gradually, with the largest change observed after 48 h of treatment at the IC_{50} concentration, and visible changes at the IC_{80} concentration after 72 h of treatment. These results could be related to the initial activation of the extrinsic apoptotic pathway, followed by the subsequent, secondary activation after 72 h of incubation of the intrinsic apoptotic pathway in response to the initial extrinsic apoptotic signals, which likely intensifies the initial apoptotic signal produced by OADP treatment.

3.5. OADP Triggers the Activation of Caspases-8, -3 and -9 to Induce Apoptosis

Cancer occurs when the cells prevent the occurrence of apoptosis and begin to proliferate uncontrollably. However, during the discovery and development of anticancer drugs, new molecules have been identified that are capable of activating the cellular molecular mechanism of apoptosis induction. Apoptosis is regulated by a family of cysteine proteases named caspases.

The activation of the caspase cascade is one of the most important processes that occur during the induction of apoptotic cell death. Our cytometric results showed a significant increase in apoptotic cell death in the HepG2 cell line after 72 h of OADP treatment. Therefore, we examined the level of the initiator caspases, caspase-8 and caspase-9, and the executor caspase, caspase-3, at the 72-h time point. To determine whether OADP induced apoptosis in HepG2 cells using the extrinsic apoptotic pathway (caspase-8) or the intrinsic apoptotic pathway (caspase-9), HepG2 cells were treated at the IC_{50} and IC_{80} concentrations of OADP for 72 h. We also analyzed the level of the caspase-3 effector, which increases in response to the activation of the intrinsic and extrinsic apoptotic pathways.

To verify that the apoptotic pathway was activated and to determine the apoptotic implications of caspase-8, caspase-9, and JNK activation, we additionally used the caspase-8 inhibitor (IETD-CHO), caspase-9 inhibitor (Ac-LEHD-CMK), and JNK inhibitor (SP600125), to block their activated molecular

pathways. HepG2 cells were co-incubated with the caspase-8 inhibitor (18 nM), the caspase-9 inhibitor (70 nM), and JNK inhibitor (25 μ M), and the corresponding IC₅₀ OADP concentration, for 72 h. The protein expression levels of the apoptotic markers caspase-8, caspase-9, and caspase-3 were individually examined using western blot analysis.

Our results showed evidence that OADP significantly activates caspase-8 expression levels (1.2-fold increase at IC₅₀, 2.0-fold increase at IC₈₀, and 2.2-fold increase at IC₅₀ with the concomitant inhibition of JNK). However, no significant changes at the IC₅₀ OADP concentration were detected in conjunction with the caspase-9 or caspase-8 inhibitors. Increases in caspase-8 levels were accompanied by the cleavage of pro-caspase-8, under all conditions and concentrations tested.

These results indicated that OADP-induced apoptosis occurs initially through the activation of the extrinsic apoptotic pathway (level of active caspase-8), followed by the secondary activation of the intrinsic apoptotic pathway. JNK inhibition increased the level of caspase-8, likely because the inhibition of this part of the pathway increases the apoptotic signal through caspase-8 activation. (Figure 6A).

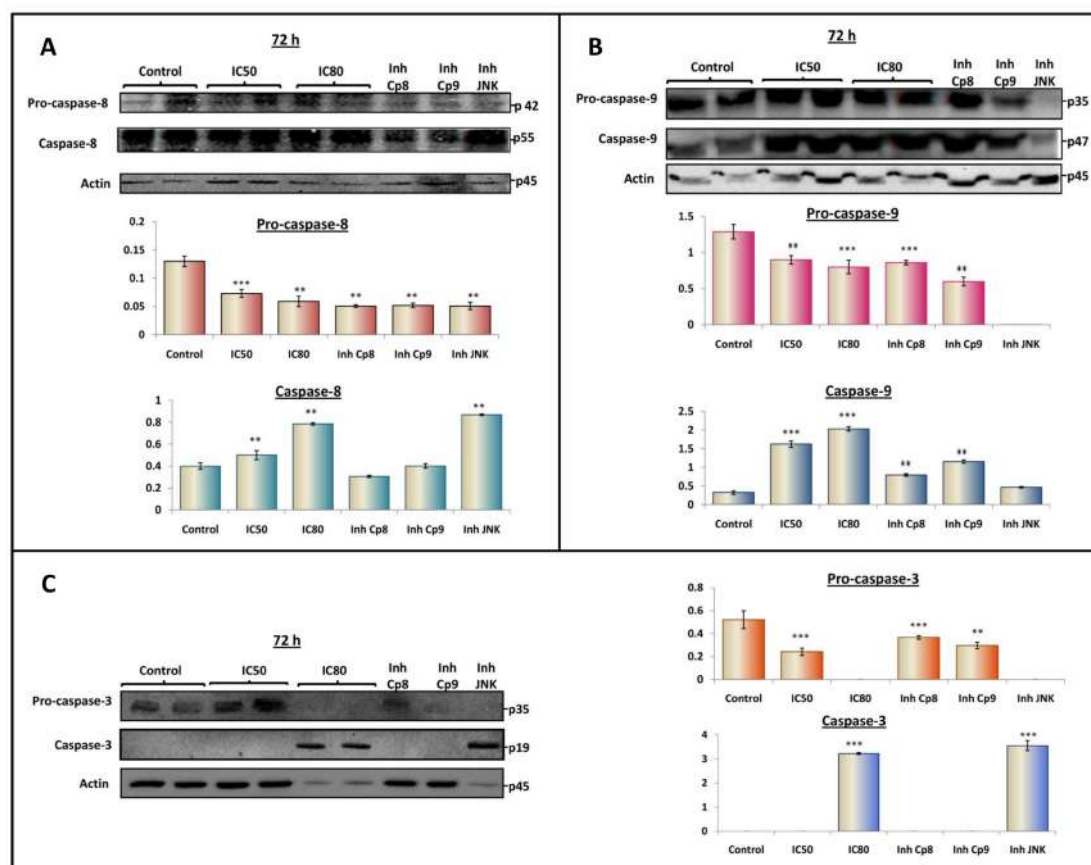


Figure 6. Western blotting analysis of the levels of pro-caspase-8, caspase-8 (A); pro-caspase-9, caspase-9 (B); and pro-caspase-3, caspase-3 (C). HepG2 cells were treated with OADP at IC₅₀ and IC₈₀ concentrations. ‘Inh Cp8’, ‘Inh Cp9’ and ‘Inh JNK’, correspond with the caspase-8 inhibitor, caspase-9 inhibitor, and JNK inhibitor, respectively. The levels of protein expression are expressed as the arbitrary intensity units for each band relative to the arbitrary intensity units of actin. The values represent the mean \pm SD of at least three separate experiments. Key: (***) $p < 0.001$ and (**) $p < 0.01$, with respect to the untreated control cells.

The level of active caspase-9 protein increased in HepG2 cells exposed to OADP (by 3.0-fold at IC₅₀ and by approximately 3.4-fold at IC₈₀). Although the expression level of active caspase-9 decreased significantly in the presence of caspase-8 and caspase-9 inhibitors, in the presence of the JNK

inhibitor, pro-caspase 9 was not detected and a lower level of active caspase-9 was detected, although these changes were not significant compared with the untreated control. These increases in the active caspase-9 were accompanied by the consequent decrease in pro-caspase-9 levels, under the conditions and concentrations analyzed (Figure 6B).

In this case, our results indicated that the JNK inhibition produced the lowest levels of pro-caspase-9 and active caspase-9. JNK inhibition likely completely inhibits the secondary activation of the intrinsic apoptotic pathway, which is mediated by caspase-9.

Finally, the expression level of active caspase-3 was remarkably improved in HepG2 cells in response to OADP combined with JNK inhibitor treatment (3.2-fold at the IC₈₀ concentration and 3.5-fold at the IC₅₀ concentration combined with the JNK inhibitor). However, no detectable levels of active caspase-3 were observed at the IC₅₀ concentration, either with or without caspase-8 or caspase-9 inhibitors. The undetectable levels of active caspase-3 under these conditions may be due to the reduced proportion of apoptotic cells compared with those obtained at the IC₈₀ concentration. These increases in caspase-3 levels were accompanied by the marked cleavage of pro-caspase-3. The decrease in pro-caspase-3 levels was visible under all concentrations and conditions assayed, although pro-caspase-3 was not detectable at the IC₈₀ concentration, nor in the treatment at the IC₅₀ concentration combined with the JNK inhibitor, likely because almost all pro-caspase-3 was activated under these conditions and concentrations (Figure 6C).

3.6. OADP Triggers the Activation of p53 and p21^{Cip1/Waf1} to Induce Apoptosis

The role of the p53 tumor-suppressor protein is well-known, regulating various phenomena, including cell growth, cell cycle arrest, and apoptosis induction. In contrast, JNK phosphorylates and regulates the activity of transcription factors, such as p53 [30,31].

Several mechanisms, both transcriptional and non-transcriptional, have been identified during the regulation of apoptosis induction by p53. For example, p53 induces apoptosis through the transcriptional upregulation of pro-apoptotic genes, such as Bax or Bak, and the transcriptional repression of the anti-apoptotic Bcl-2 [18]. Furthermore, p53 controls the gene expression of other regulators proteins, such as p21^{Cip1/Waf1}, which are involved in regulating the advance and arrest of the cell cycle [32]. This effect could be related to the G0/G1 cell-cycle arrest produced in response to OADP treatment.

We studied the effects of OADP on p53 expression level at the IC₅₀ and IC₈₀ concentrations, alone, and at the IC₅₀ concentration in combination with inhibitors of caspase-8, caspase-9, and JNK, to better understand the molecular mechanisms that underlie the activation of apoptosis in HepG2 cells, in response to OADP treatment. The results showed the clear induction of p53 level at the IC₈₀ concentration and during the co-treatment with the JNK inhibitor, at the IC₅₀ concentration. p53 induction resulted in protein expression levels 17–18 times that observed in the untreated control cells (Figure 7A). However, at the IC₅₀ concentration and in combination with the inhibition of caspase-8 or caspase-9, no significant changes were observed. These results are in agreement with the results that were previously found during the analysis of the cell cycle and apoptosis, in which the initial treatment resulted in stronger cell cycle arrest in the G0/G1 phase than was observed after 72 h of incubation. This result is likely due to the initial differentiation process induced by the activation of p53/p21 in response to OADP treatment, which was inhibited after long incubation times, activating the apoptosis process. However, p53 is also an important apoptosis inducer, which is reflected by the increased percentage of apoptosis induction observed for the IC₈₀ concentration compared with the IC₅₀ concentration. Finally, JNK inhibition resulted in the activation of p53 at the IC₅₀ concentration, likely due to the disappearance of p53 inhibition, which is mediated by JNK activation.

p21^{Cip1/Waf1} is a 21-kDa protein that acts as a cyclin-dependent kinase inhibitor and triggered in response to p53 protein activation. p53 activation tends to be described in response to stress stimuli, inhibiting the cyclin-cdk2 complex kinase activity required for the transition from the G1 to S phases of the cell cycle. At the initial time point, this protein is activated by p53, which blocks cell cycle progression, inducing cell arrest, cell differentiation, and DNA repair [33]. If the signal or stress

stimuli continue over time, the apoptotic signal overlaps with p21 function, and the cell eventually enters apoptosis.

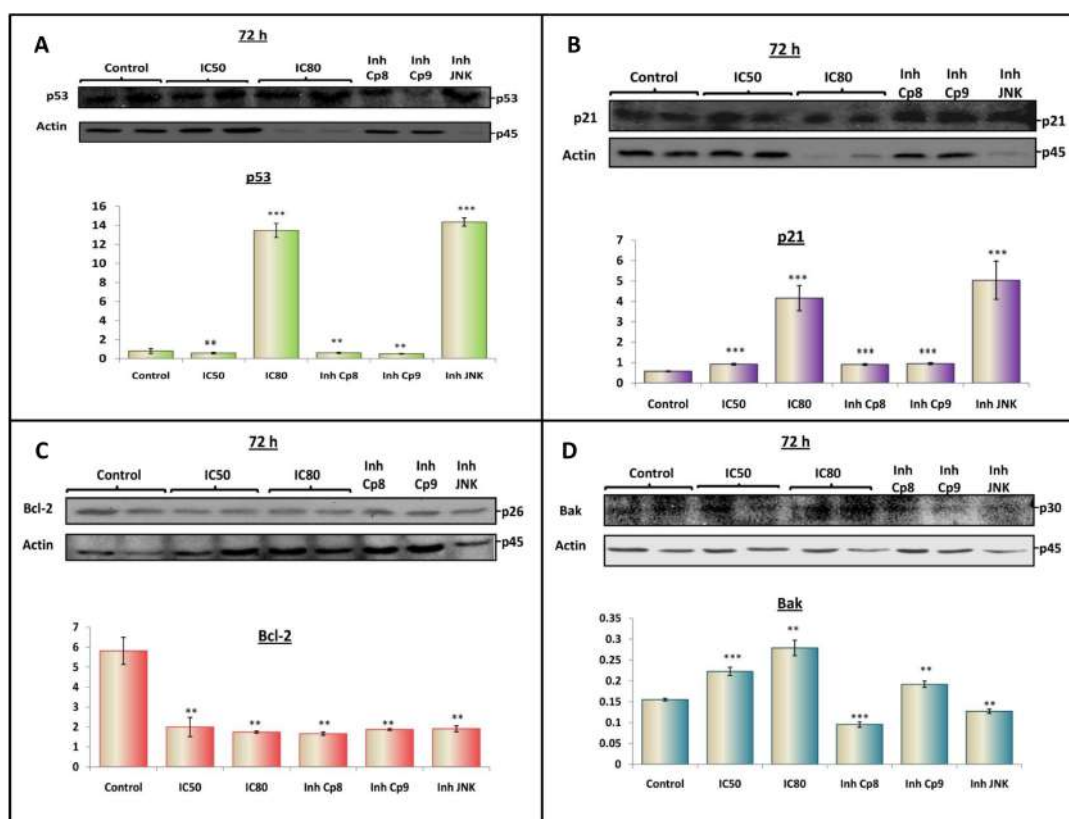


Figure 7. Western blot analysis of the protein levels of p53 (A), p21 (B), Bcl-2 (C), and Bak (D). HepG2 cells were treated with OADP at IC₅₀ and IC₈₀ concentrations. ‘Inh Cp8’, ‘Inh Cp9’ and ‘Inh JNK’ correspond to the combined treatment with caspase-8 inhibitor, the caspase-9 inhibitor, and the JNK inhibitor, respectively. Protein expression levels are expressed as units of arbitrary intensity for each band, compared to the units of arbitrary intensity for the actin band. Values represent the mean ± SD of at least three separate experiments. Key: (**) $p < 0.01$ and (***) $p < 0.001$, with respect to the untreated control cells.

To determine the effects of OADP treatment, we evaluated the expression level of p21 in HepG2 cells, at the concentrations and conditions mentioned above. The results showed that the p21 protein levels increased 1.6-fold at the IC₅₀ concentration and 7.2-fold at the IC₈₀ concentration, compared with the level in untreated control cells. Similar results were obtained between IC₅₀ concentrations and IC₅₀ concentrations combined with caspase-8 and caspase-9 inhibitors. However, when combined with JNK inhibition, the level of p21 increased by 9-fold compared with the level in control cells (Figure 7B). The activation of p21 is fully correlated with p53 activation, which is most likely due to the dependence of p21 levels on the transcriptional activity of p53. The activation of p21, in response to OADP treatment, could explain the cell cycle arrest observed in the presence of OADP, and the possible activation of differentiation processes. Future analysis will be necessary to verify this finding.

3.7. OADP Triggers the Activation of Bcl-2 and Bak to Induce Apoptosis

To gain a complete picture of the activated molecular mechanism associated with apoptosis induction by OADP, we determined the effects of this compound on the expression levels of the Bcl-2 protein family. The expression levels of the pro-apoptotic protein Bak and the anti-apoptotic protein Bcl-2 were analyzed after 72 h of incubation with OADP at the IC₅₀ and IC₈₀ concentrations, alone, and at the IC₅₀ concentration in combination with the caspase-8, caspase-9, and JNK inhibitors.

The secondary activation of the intrinsic apoptotic pathway, to strengthen the primary extrinsic apoptotic signal, has been extensively described in the apoptotic response to triterpenes compounds [34,35]. Caspase-8 and JNK can activate Bid protein (pro-apoptotic protein in the Bcl-2 protein family). Bid active, or t-Bid, targets the mitochondria to modulate other Bcl-2-like factors, such as Bcl-2 or Bak, which ultimately results in the loss of MMP and mitochondrial membrane permeability, releasing mitochondrial factors, such as cytochrome-c or Apaf-1 proteins, which activate caspase-9 through apoptosome formation.

Our results revealed a decrease in Bcl-2 protein levels, in a concentration-dependent manner, at IC_{50} and IC_{80} concentrations (OADP decreased Bcl-2 protein levels by 66% at IC_{50} , and by 70% at IC_{80}). Similar results were obtained at the IC_{50} concentration combined with caspase-8, caspase-9 or JNK inhibitors. These results may be associated with the inhibition of Bcl-2 protein expression, independent of JNK activity, likely due to p53 and/or caspase-8 activity (Figure 7C).

Bak protein levels increased in a concentration-dependent manner (1.44-fold at IC_{50} and approximately 2-fold at IC_{80}) following OADP treatment. In contrast, Bak protein levels decreased by 38% at the IC_{50} concentration combined with caspase-8 inhibitor, a slight decrease was observed at the IC_{50} concentration combined with the caspase-9 inhibitor, and decreased by 18% at the IC_{50} concentration combined with the JNK inhibitor. These results may be explained by the dependence of Bak activation on caspase-8 or JNK activities, whereas the inhibition of caspase-9 resulted in a lower decrease in this protein level, likely because caspase-9 is upregulated by this protein. Therefore, the inhibition of caspase-9 had a minor effect on its expression (Figure 7D).

3.8. OADP Induces Apoptotic Morphological Changes (Hoechst-Stained)

The Hoechst procedure stains nuclei containing nicked DNA, a characteristic that cells exhibit in apoptotic cell death. Morphological analysis of Hoechst-stained cells, in HepG2 cells, indicated that they had undergone remarkable morphological changes (Figure 8). At the IC_{50} concentration of OADP, cells showed typical apoptotic changes, including cell shrinkage, chromatin condensation, and loss of normal nuclear architecture. At the IC_{80} concentration, the disruption of the cell-membrane integrity was more prominent. Microscopic observation of fluorescence after Hoechst staining showed that a significant number of cells treated with OADP acquired apoptotic features, as evident by nuclear fragmentation.

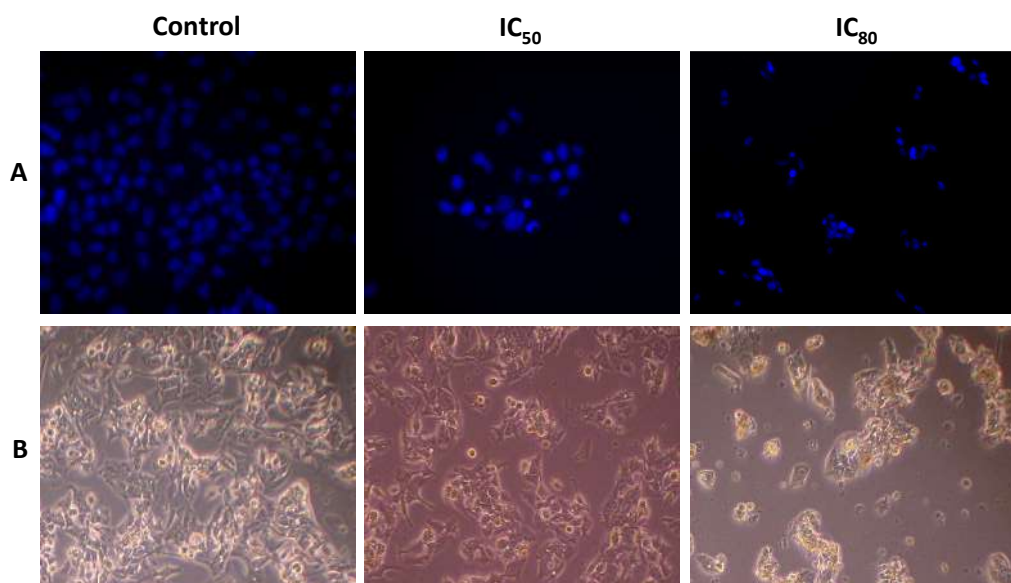


Figure 8. Morphological changes in HepG2 cells after exposure to OADP for 72h, at IC_{50} and IC_{80} concentrations. Cells were examined using fluorescence microscopy with a DAPI filter, following Hoechst-stained as described in the Section 2 (A). Phase-contrast light microscopy cell images (B).

4. Discussion

The lack or failure of apoptosis activation mechanisms and programmed cell death disrupts cell homeostasis, which is a primary cause of cancer induction. Therefore, many efforts and studies have focused on the identification of compounds capable of reactivating apoptosis mechanisms, to utilize this cell death process in the clinical treatment of cancer [36,37]. Our results showed that the triterpene derivative (OADP) is a promising compound that is capable of inducing apoptosis in a concentration- and time-dependent manner, at very low concentrations (Figure 3), producing the significant inhibition of cell viability. Compared with its natural precursor (OA), OADP is 718 times more effective in HepG2 cells, after 72 h of treatment [8]. Furthermore, OADP induces morphological changes that are characteristic of apoptosis [8,23,25–27,38], such as chromatin condensation and fragmentation, as evidenced by fluorescence microscopy. This effect appears to be selective for the tumor cell line, because the cytotoxicity found in the WRL68 non-tumor human embryonic liver cells was 39 times lower than in HepG2 cells.

Furthermore, the antiproliferative activity of OADP appears to be associated with its cytotoxicity, together with the activation of a cytostatic effect, as evidenced by the induction of cell-cycle arrest in the G0/G1 phase (Figure 4). We also discovered that during the initial treatment stage (24 and 48 h), no changes in the MMP were observed, which agrees with the activation of the extrinsic apoptotic mechanism. However, after 72 h of treatment, we observed the significant loss of MMP, which is likely associated with the secondary activation of the intrinsic apoptotic mechanism, to increase the initial apoptotic signal (Figure 5). Therefore, these results suggested that OADP activates the extrinsic apoptotic pathway first, followed by the intrinsic apoptotic pathway.

Because of the activation of the apoptosis mechanism, a family of cysteine proteases, known as caspases, was activated [39]. We can distinguish two groups or types of caspases, initiator caspases and effector caspases. Initiator caspases, such as caspase-8 and -9, are activated in response to apoptotic stimulation and cause the downstream activation of effector caspases, such as caspase-3 (main effector caspase), caspase-6, or caspase-7, which induce typical apoptotic changes, such as chromatin condensation and fragmentation, cell shrinkage, and loss of cell membrane asymmetry [40].

Two major apoptotic pathways are triggered during apoptotic cell death: the extrinsic apoptotic pathway, which is induced by external signals, and the intrinsic apoptotic pathway, which is induced by cellular stress stimuli [41]. To determine which apoptotic pathway was activated in response to OADP in HepG2 cells, we evaluated the expression level of key proteins involved in the apoptosis mechanisms of the extrinsic and intrinsic apoptotic pathways. First, we analyzed the expression level of the initiating caspases-8 and -9 and found that after 72 h of incubation with OADP, the expression levels of these caspases increased. However, no significant changes were observed in the expression level of caspase-8 at the IC₅₀ OADP concentration combined with the caspase inhibitors. Levels similar to those observed for the IC₈₀ OADP concentration were achieved by combining the IC₅₀ OADP concentration with the JNK inhibitor, likely because JNK may be involved in the potential secondary activation mechanism of the intrinsic apoptotic pathway. When JNK was inhibited, the apoptotic signal associated with caspase-8 activation increased (Figure 6B). Caspase-9 levels increased in response to IC₅₀ and IC₈₀ OADP concentrations in a similar manner as caspase-8 levels. Although no significant changes were observed at the IC₅₀ OADP concentration combined with caspase-8 or -9 inhibitors, the reduction of pro-caspase-9 and caspase-9 levels was observed when the IC₅₀ OADP concentration was combined with the JNK inhibitor. Finally, caspase-3 activation was observed at the IC₈₀ OADP concentration and the IC₅₀ OADP concentration combined with the JNK inhibitor, likely because these conditions promoted the activation of apoptosis pathways compared with the IC₅₀ OADP concentration, either alone or in combination with the caspases-8 and -9 inhibitors.

The co-treatment with inhibitors of caspase-8, -9, and JNK, combined with the IC₅₀ OADP concentration revealed that caspase-8 level was independent of these other factors, whereas caspase-9 increased when JNK was inhibited, indicating that caspase-9 level depends on caspase-8 and JNK expression level. Therefore, we suggest that the cleavage and activation of caspase-9 activation were

induced by caspase-8 and/or JNK. Based on these results, we suggest that the apoptotic mechanism activated in response to OADP involved the extrinsic apoptotic activation route, first, followed by the secondary intrinsic activation pathway, to enhance the initial apoptotic signal, as described in the apoptotic response to other triterpene compounds, such as MA and the oleanolic acid derivative CDDO [7].

In our previous study, we described the activation of the intrinsic and extrinsic apoptotic pathway following MA treatment in the HT-29 and Caco-2 cell lines. The activation of the extrinsic and intrinsic apoptotic pathways in response to many OA derivatives has been reported. 3-*O*-acetyloleanolic acid induced the increase of caspase-8 and caspase-3 levels in human colon carcinoma HCT-116 cells. Similarly, HIMOXOL (methyl 3-hydroxyimino-11-oxoolean-12-en-28-oate) also induced the activation of poly-ADP-ribose polymerase (PARP)-1 in MDA-MB-231 breast cancer cells [42,43]. Meanwhile, the OA derivative SZC015 induced a mitochondrial apoptotic pathway in human breast cancer cells by activating cleaved caspase-3, caspase-9, cytosolic Cyt C, and PARP and increasing the Bax/Bcl-2 ratio [44]. Additional studies demonstrate that OA methyl ester induced the intrinsic apoptotic pathway in PC-3 prostate cancer cells [45]. However, Koetjapic acid, a natural triterpenoid, induced apoptosis in HCT 116 colorectal carcinoma cells by activating both the extrinsic and intrinsic caspases, which increased the hypoxia-inducible factor (HIF)-1 α , mitogen-activated protein (MAP)/extracellular signal-related kinase (ERK)/JNK, and Myc/Max signaling pathways and decreased the nuclear factor (NF)- κ B signaling pathway [34].

This secondary activation of the intrinsic apoptotic route can be initiated by caspase-8 activation. Thus, caspase-8 targets the BH3-only protein Bid for cleavage, generating the activated t-Bid fragment, which activates pro-apoptotic Bcl-2 proteins, such as Bak or Bad, and ultimately results in the loss of the mitochondrial external membrane permeability and MMP and induces the activation of caspase-9 and caspase-3. Furthermore, Bid activation has been described as dependent on JNK and mediated by p53 [46], both of which may be involved in the proposed apoptosis mechanism.

JNK also activates molecular pathways during cellular proliferation or death [47], activating the downstream control of proteins related to cell cycle and apoptosis, such as p53, p21 or cyclin D. The main target of JNK (c-Jun) inhibits p-53-mediated cell cycle arrest, promoting p53-mediated apoptosis. c-Jun has also been reported to function as a direct repressor of p53-mediated gene transcription [48].

The involvement of p53 and p21^{Cip1/Waf1} has been reported to be important for apoptosis induction in many hepatoma cell lines triggered by triterpenoids, such as saikosaponin [49] or OA [50]. Several mechanisms have been identified for the induction of apoptosis by p53, involving both the transcriptional and/or non-transcriptional regulation of downstream effectors. In this study, we evaluated p53 expression levels in response to OADP after 72 h of incubation, which resulted in the significant increase of p53 level at the IC₈₀ concentration and the IC₅₀ concentration combined with the JNK inhibitor (Figure 7A). This effect may be due to JNK activation, which can suppress the transcription of the p53 gene [48]. When JNK expression is inhibited, p53 is transcribed, significantly increasing its cellular levels. Furthermore, the induction of p53 expression may explain the increasing levels of p21 because p21 is transcribed by p53, and the results obtained for these protein levels (Figure 7B) were very similar to those obtained for p53 protein levels. The expression of p53 and p21 proteins may be closely related to the significant cell cycle arrest observed during the initial treatment stage (24 h) with OADP. However, this cell cycle arrest effect disappears, due to the continued apoptotic stimulation, after 48 and 72 h of treatment. A similar mechanism has been described for other triterpenoids, such as Saikosaponin-d (SSd), which inhibited cell proliferation in the HepG2 and Hep3B HCC cell lines and DU145 prostate cancer cells, through the upregulation of p53 and p21, cell cycle arrest in the G₀/G₁ phase, and apoptosis induction [32,49].

JNK and p53 interact with the Bcl-2 family of anti-apoptotic and pro-apoptotic proteins, regulating the apoptotic process. JNK can act directly on the Bcl-2 family of proteins to induce the activation of the mitochondrial pathway. JNK phosphorylates members of the Bcl-2 family of proteins, such as Bcl-2, which inactivates their anti-apoptotic functions, and can induce proapoptotic Bcl-2 proteins containing

only the BH3 domain, such as Bid or Bim, which can mediate the activation of apoptosis by Bax or Bak [51]. In contrast, several p53 mechanisms of apoptosis induction have been identified that involve both the transcriptional and/or non-transcriptional regulation of downstream effectors. p53 induces the upregulation of Bax expression and the transcriptional repression of Bcl-2 [18]. In addition, the physical inhibition by p53 of the anti-apoptotic proteins Bcl-2 and Bcl-xL was described, and its participation in the formation of oligomers with Bax/Bak proteins results in the permeabilisation of the external mitochondrial membrane, causing the release of cytochrome-c into the cytosol [52]. Treatments with the JNK inhibitor have been reported to strongly induce CD95 expression, inducing apoptosis in six different tumor cell lines through p53- and p21-mediated G2/M cell cycle arrest, and caspase-8 and caspase-3 cleavage [53].

Next, we evaluated the expression levels of the Bcl-2 and Bak proteins, in response to treatment with OADP, to determine their participation in the molecular apoptosis mechanisms induced by this compound. Our results, after 72 h of treatment with OADP, showed the downregulation of the anti-apoptotic protein Bcl-2, accompanied by the upregulation of the pro-apoptotic protein Bak (Figure 7C,D). Co-treatment with the IC₅₀ OADP concentration and caspase-8, caspase-9, and JNK inhibitors, resulted in no changes in Bcl-2 levels, which remained lower in all conditions compared with untreated control cells, which may be caused by Bcl-2 levels being regulated by both JNK and p53. The inhibition of caspase-8 and JNK results in decreased Bak, whereas the inhibition of caspase-9 produced a smaller effect, so that Bak expression level depends on the activities of caspase-8 and JNK, and not on caspase-9, likely because caspase-9 is downregulated by Bak.

In summary, our results showed the clear activation of the initiating caspases-8 and -9 and the effector caspase-3, the increase in cell cycle and apoptosis regulating proteins p53 and p21, the upregulation of the proapoptotic protein Bak, and the downregulation of Bcl-2 anti-apoptotic protein. In the presence of the caspase-8 inhibitor, we found the downregulation of caspase-8, caspase-9, caspase-3, p53, p21, and Bak, indicating that the expression levels of these proteins were directly associated with caspase-8 activation. Therefore, we were able to demonstrate that apoptosis activation in HepG2 cells, in response to OADP treatment, occurs through the activation of the extrinsic apoptotic mechanism, mediated by caspase-8. In the presence of the caspase-9 inhibitor, we found the downregulation of caspase-9, caspase-8, caspase-3, p53, and p21, and the reduced inhibition in Bak, indicating that the intrinsic apoptosis mechanism was also activated, likely to enhance the initial extrinsic apoptotic signal. Finally, with JNK inhibition, we identified large increases in the levels of caspase-8, caspase-3, p53, and p21 proteins, whereas we observed decreased Bak and caspase-9 levels, indicating that JNK was likely involved in regulating the expression levels of these proteins, and is the likely link between the two apoptotic activation routes. The activation of the JNK-mediated intrinsic apoptotic pathway, in response to caspase-8 activation, has been previously described [54]. Bcl-2 level protein decreased in all treatment conditions assayed. These results are consistent with the different apoptosis mechanisms described in the literature [34,35].

5. Conclusions

The results reported here demonstrated that OADP triggered apoptosis and cell cycle arrest in the HepG2 cancer cell line, in a concentration- and time-dependent manner. These results showed that OADP is a powerful anticancer compound, capable of causing cell cycle arrest during the early stages of incubation, and the activation of the two main apoptotic pathways, the extrinsic and intrinsic apoptotic routes, in the HepG2 cell line, inducing the inhibition of cancer cell proliferation at very low concentrations (Figure 2). Finally, we observed that OADP treatment results in the loss of MMP after 72 h of treatment, indicating that the activation of the intrinsic apoptotic pathway is secondary to the activation of the extrinsic apoptotic pathway.

Based on these results, we propose the following mechanism for the apoptotic effect of OADP on HepG2 cells (Figure 9). First, OADP induces JNK and p53 protein level increase, causing cell cycle arrest and activating p21 during the early stages. Furthermore, we can assume that OADP initially

triggers the extrinsic apoptotic pathway, initiated by caspase-8, which activates the caspase-3 executor. The activation of caspase-8 and JNK causes the secondary activation of the intrinsic apoptotic pathway, through the upregulation of Bak and the downregulation of Bcl-2, triggering the mitochondrial apoptotic response, which subsequently activates caspase-9. Both the initial activation of caspase-8 and the secondary activation of caspase-9 lead to the cleavage of caspase-3. Finally, the complete process induces apoptosis in HepG2 cells, which is significant after 48 and 72 h of OADP treatment, as revealed by the FACS analysis. The apoptotic results of OADP suggest that this compound could serve as an effective compound during the treatment of HCC.

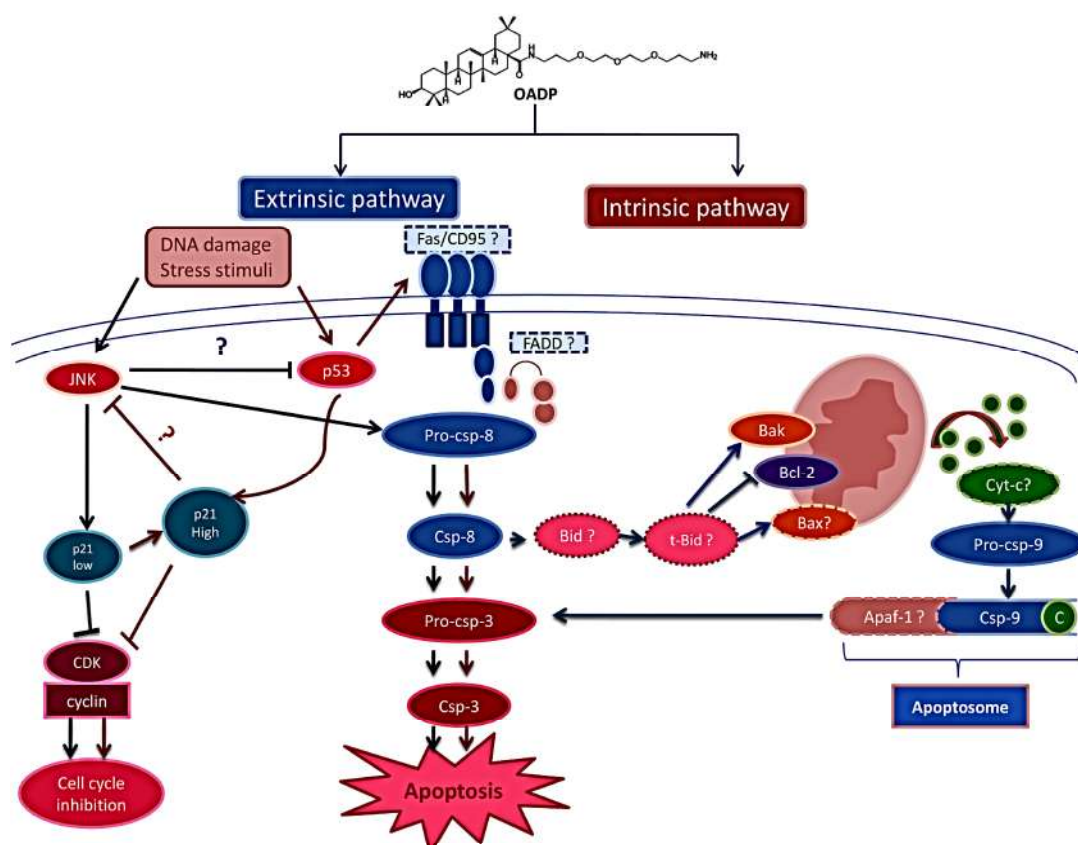


Figure 9. Mechanism of action underlying apoptosis induced by OADP in HepG2 cells after 72 h of treatment, at IC_{50} and IC_{80} concentrations, alone, and IC_{50} concentrations combined with the JNK inhibitor (SP600125). Dark blue arrows represent IC_{50} apoptotic pathway, and dark red arrows represent apoptotic pathways associated with the IC_{80} concentration and the IC_{50} concentration in combination with the JNK inhibitor (SP600125).

To our knowledge, this is the first time that the ability of OADP to induce efficient apoptosis through the extrinsic and intrinsic apoptotic pathways has been highlighted in the HepG2 human cell line, which is a particular type of HCC. Interestingly, our results indicated that OADP can act as an effective anticancer agent against the HepG2 human cell line, *in vitro*. The effects of OADP must be studied *in vivo* and in other HCC cell lines.

Author Contributions: Conceptualization, M.M.-O., F.R. and F.J.R.-Z.; Formal analysis, F.J., M.M.-O., L.D.-R., J.A.L., A.P. and F.J.R.-Z.; Funding acquisition, F.R., J.A.L., A.P. and F.J.R.-Z.; Investigation, F.J., M.M.-O., L.D.-R., E.E.R.-P. and F.J.R.-Z.; Methodology, M.M.-O., F.R., E.E.R.-P. and F.J.R.-Z.; Project administration, M.M.-O., F.R. and F.J.R.-Z.; Resources, M.M.-O., F.R., E.E.R.-P., J.A.L., A.P. and F.J.R.-Z.; Supervision, J.A.L. and A.P.; Validation, F.J., M.M.-O., L.D.-R., E.E.R.-P., J.A.L., A.P. and F.J.R.-Z.; Visualization, F.J., M.M.-O., F.R. and F.J.R.-Z.; Writing—original draft, F.J., M.M.-O., F.R. and F.J.R.-Z.; Writing—review & editing, F.R. and F.J.R.-Z. All authors have read and agreed to the published version of the manuscript.

Funding: This research was funded by the “Consejería de Economía, Conocimiento, Empresas y Universidad. Junta de Andalucía”, grant numbers B1-BIO-281-UGR18 and B1-FQM-217-UGR18.

Acknowledgments: We give special thanks to the BIO 157 and FQM 139 groups and the departments of Biochemistry and Molecular Biology I and Organic Chemistry, as well as the CIC of the University of Granada for their support.

Conflicts of Interest: The authors declare no conflict of interest. The funders had no role in the design of the study; in the collection, analyses, or interpretation of data; in the writing of the manuscript, or in the decision to publish the results.

References

1. Bray, F.; Ferlay, J.; Soerjomataram, I.; Siegel, R.L.; Torre, L.A.; Jemal, A. Global cancer statistics 2018: GLOBOCAN estimates of incidence and mortality worldwide for 36 cancers in 185 countries. *CA Cancer J. Clin.* **2018**, *68*, 394–424. [[CrossRef](#)]
2. Davis, G.L.; Dempster, J.; Meler, J.D.; Orr, D.W.; Walberg, M.W.; Brown, B.; Berger, B.D.; O'Connor, J.K.; Goldstein, R.M. Hepatocellular carcinoma: Management of an increasingly common problem. *Bayl. Univ. Med. Cent. Proc.* **2008**, *21*, 266–280. [[CrossRef](#)] [[PubMed](#)]
3. El-Serag, H.B.; Rudolph, K.L. Hepatocellular carcinoma: Epidemiology and molecular carcinogenesis. *Gastroenterology* **2007**, *132*, 2557–2576. [[CrossRef](#)] [[PubMed](#)]
4. Dageforde, L.A.; Fowler, K.J.; Chapman, W.C. Liver transplantation for hepatocellular carcinoma: Current update on treatment and allocation. *Curr. Opin Organ Transpl.* **2017**, *22*, 128–134. [[CrossRef](#)] [[PubMed](#)]
5. Kudo, M.; Finn, R.S.; Qin, S.; Han, K.H.; Ikeda, K.; Piscaglia, F.; Baron, A.; Park, J.W.; Han, G.; Jassem, J.; et al. Lenvatinib versus sorafenib in first-line treatment of patients with unresectable hepatocellular carcinoma: A randomised phase 3 non-inferiority trial. *Lancet* **2018**, *391*, 1163–1173. [[CrossRef](#)]
6. Chen, C.F.; Yang, J.S.; Chen, W.K.; Lu, C.C.; Chiang, J.H.; Chiu, H.Y.; Tsai, S.C.; Juan, Y.N.; Huang, H.J.; Way, T.D. Ursolic acid elicits intrinsic apoptotic machinery by downregulating the phosphorylation of AKT/BAD signaling in human cisplatinresistant oral cancer CAR cells. *Oncol. Rep.* **2018**, *40*, 1752–1760. [[CrossRef](#)]
7. Rufino-Palomares, E.E.; Perez-Jimenez, A.; Reyes-Zurita, F.J.; Garcia-Salguero, L.; Mokhtari, K.; Herrera-Merchan, A.; Medina, P.P.; Peragon, J.; Lupianez, J.A. Anti-cancer and Anti-angiogenic Properties of Various Natural Pentacyclic Tri-terpenoids and Some of their Chemical Derivatives. *Curr. Org. Chem.* **2015**, *19*, 919–947. [[CrossRef](#)]
8. Medina-O'Donnell, M.; Rivas, F.; Reyes-Zurita, F.J.; Martinez, A.; Martin-Fonseca, S.; Garcia-Granados, A.; Ferrer-Martin, R.M.; Lupianez, J.A.; Parra, A. Semi-synthesis and antiproliferative evaluation of PEGylated pentacyclic triterpenes. *Eur. J. Med. Chem.* **2016**, *118*, 64–78. [[CrossRef](#)]
9. Medina-O'Donnell, M.; Rivas, F.; Reyes-Zurita, F.J.; Martinez, A.; Galisteo-Gonzalez, F.; Lupianez, J.A.; Parra, A. Synthesis and in vitro antiproliferative evaluation of PEGylated triterpene acids. *Fitoterapia* **2017**, *120*, 25–40. [[CrossRef](#)]
10. Medina-O'Donnell, M.; Rivas, F.; Reyes-Zurita, F.J.; Martinez, A.; Lupianez, J.A.; Parra, A. Diamine and PEGylated-diamine conjugates of triterpenic acids as potential anticancer agents. *Eur. J. Med. Chem.* **2018**, *148*, 325–336. [[CrossRef](#)]
11. Belén, L.H.; Rangel-Yagui, C.d.O.; Beltrán Lissabet, J.F.; Effer, B.; Lee-Estevez, M.; Pessoa, A.; Castillo, R.L.; Fariás, J.G. From Synthesis to Characterization of Site-Selective PEGylated Proteins. *Front. Pharmacol.* **2019**, *10*. [[CrossRef](#)] [[PubMed](#)]
12. Fan, X.; Wang, P.; Sun, Y.; Jiang, J.; Du, H.; Wang, Z.; Duan, Z.; Lei, H.; Li, H. Induction of apoptosis by an oleanolic acid derivative in SMMC-7721 human hepatocellular carcinoma cells is associated with mitochondrial dysfunction. *Oncol. Lett.* **2018**, *15*, 2821–2828. [[CrossRef](#)] [[PubMed](#)]
13. Kang, X.; Hu, J.; Gao, Z.; Ju, Y.; Xu, C. Synthesis, anti-proliferative and proapoptotic activity of novel oleanolic acid azaheterocyclic derivatives. *MedChemComm* **2012**, *3*, 1245–1249. [[CrossRef](#)]
14. Yan, S.L.; Huang, C.Y.; Wu, S.T.; Yin, M.C. Oleanolic acid and ursolic acid induce apoptosis in four human liver cancer cell lines. *Toxicol. In Vitro* **2010**, *24*, 842–848. [[CrossRef](#)] [[PubMed](#)]
15. Deng, Y.; Ren, X.; Yang, L.; Lin, Y.; Wu, X. A JNK-dependent pathway is required for TNFalpha-induced apoptosis. *Cell* **2003**, *115*, 61–70. [[CrossRef](#)]

16. Tournier, C.; Hess, P.; Yang, D.D.; Xu, J.; Turner, T.K.; Nimmual, A.; Bar-Sagi, D.; Jones, S.N.; Flavell, R.A.; Davis, R.J. Requirement of JNK for stress-induced activation of the cytochrome c-mediated death pathway. *Science* **2000**, *288*, 870–874. [[CrossRef](#)]
17. Wajant, H.; Pfizenmaier, K.; Scheurich, P. Tumor necrosis factor signaling. *Cell Death Differ.* **2003**, *10*, 45–65. [[CrossRef](#)]
18. Yee, K.S.; Vousden, K.H. Complicating the complexity of p53. *Carcinogenesis* **2005**, *26*, 1317–1322. [[CrossRef](#)]
19. Marchenko, N.D.; Zaika, A.; Moll, U.M. Death signal-induced localization of p53 protein to mitochondria. A potential role in apoptotic signaling. *J. Biol. Chem.* **2000**, *275*, 16202–16212. [[CrossRef](#)]
20. Reyes-Zurita, F.J.; Rufino-Palomares, E.E.; Garcia-Salguero, L.; Peragon, J.; Medina, P.P.; Parra, A.; Cascante, M.; Lupianez, J.A. Maslinic Acid, a Natural Triterpene, Induces a Death Receptor-Mediated Apoptotic Mechanism in Caco-2 p53-Deficient Colon Adenocarcinoma Cells. *PLoS ONE* **2016**, *11*, e0146178. [[CrossRef](#)]
21. Sanchez-Tena, S.; Reyes-Zurita, F.J.; Diaz-Moralli, S.; Vinardell, M.P.; Reed, M.; Garcia-Garcia, F.; Dopazo, J.; Lupianez, J.A.; Gunther, U.; Cascante, M. Maslinic Acid-Enriched Diet Decreases Intestinal Tumorigenesis in Apc(Min/+) Mice through Transcriptomic and Metabolomic Reprogramming. *PLoS ONE* **2013**, *8*, e59392. [[CrossRef](#)] [[PubMed](#)]
22. Rufino-Palomares, E.E.; Reyes-Zurita, F.J.; Garcia-Salguero, L.; Mokhtari, K.; Medina, P.P.; Lupianez, J.A.; Peragon, J. Maslinic acid, a triterpenic anti-tumoural agent, interferes with cytoskeleton protein expression in HT29 human colon-cancer cells. *J. Proteom.* **2013**, *83*, 15–25. [[CrossRef](#)]
23. Reyes-Zurita, F.J.; Rufino-Palomares, E.E.; Medina, P.P.; Garcia-Salguero, E.L.; Peragon, J.; Cascante, M.; Lupianez, J.A. Antitumour activity on extrinsic apoptotic targets of the triterpenoid maslinic acid in p53-deficient Caco-2 adenocarcinoma cells. *Biochimie* **2013**, *95*, 2157–2167. [[CrossRef](#)] [[PubMed](#)]
24. Reyes-Zurita, F.J.; Pachon-Pena, G.; Lizarraga, D.; Rufino-Palomares, E.E.; Cascante, M.; Lupianez, J.A. The natural triterpene maslinic acid induces apoptosis in HT29 colon cancer cells by a JNK-p53-dependent mechanism. *BMC Cancer* **2011**, *11*, 154. [[CrossRef](#)] [[PubMed](#)]
25. Reyes-Zurita, F.J.; Rufino-Palomares, E.E.; Lupianez, J.A.; Cascante, M. Maslinic acid, a natural triterpene from *Olea europaea* L., induces apoptosis in HT29 human colon-cancer cells via the mitochondrial apoptotic pathway. *Cancer Lett.* **2009**, *273*, 44–54. [[CrossRef](#)] [[PubMed](#)]
26. Reyes, F.J.; Centelles, J.J.; Lupianez, J.A.; Cascante, M. (2 alpha,3 beta)-2,3-dihydroxyolean-12-en-28-oic acid, a new natural triterpene from *Olea europea*, induces caspase dependent apoptosis selectively in colon adenocarcinoma cells. *FEBS Lett.* **2006**, *580*, 6302–6310. [[CrossRef](#)] [[PubMed](#)]
27. Reyes-Zurita, F.J.; Medina-O'Donnell, M.; Ferrer-Martin, R.M.; Rufino-Palomares, E.E.; Martin-Fonseca, S.; Rivas, F.; Martinez, A.; Garcia-Granados, A.; Perez-Jimenez, A.; Garcia-Salguero, L.; et al. The oleanolic acid derivative, 3-O-succinyl-28-O-benzyl oleanolate, induces apoptosis in B16-F10 melanoma cells via the mitochondrial apoptotic pathway. *RSC Adv.* **2016**, *6*, 93590–93601. [[CrossRef](#)]
28. Martinez, A.; Perojil, A.; Rivas, F.; Parra, A.; Garcia-Granados, A.; Fernandez-Vivas, A. Biotransformation of oleanolic and maslinic methyl esters by *Rhizomucor miehei* CECT 2749. *Phytochemistry* **2015**, *117*, 500–508. [[CrossRef](#)] [[PubMed](#)]
29. Ravichandran, K.S. Find-me and eat-me signals in apoptotic cell clearance: Progress and conundrums. *J. Exp. Med.* **2010**, *207*, 1807–1817. [[CrossRef](#)]
30. Chang, L.; Karin, M. Mammalian MAP kinase signalling cascades. *Nature* **2001**, *410*, 37–40. [[CrossRef](#)]
31. Davis, R.J. Signal transduction by the JNK group of MAP kinases. *Cell* **2000**, *103*, 239–252. [[CrossRef](#)]
32. Yao, M.; Yang, J.; Cao, L.; Zhang, L.; Qu, S.; Gao, H. Saikosaponin inhibits proliferation of DU145 human prostate cancer cells by inducing apoptosis and arresting the cell cycle at G0/G1 phase. *Mol. Med. Rep.* **2014**, *10*, 365–372. [[CrossRef](#)] [[PubMed](#)]
33. Juntila, M.R.; Evan, G.I. p53—a Jack of all trades but master of none. *Nat. Rev. Cancer* **2009**, *9*, 821–829. [[CrossRef](#)] [[PubMed](#)]
34. Nassar, Z.D.; Aisha, A.F.; Idris, N.; Khadeer Ahamed, M.B.; Ismail, Z.; Abu-Salah, K.M.; Alrokayan, S.A.; Shah Abdul Majid, A.M. Koetjapic acid, a natural triterpenoid, induces apoptosis in colon cancer cells. *Oncol. Rep.* **2012**, *27*, 727–733. [[CrossRef](#)]
35. Lee, K.C.; Chen, Y.L.; Lin, P.Y.; Chuang, W.L. Ursolic Acid-Induced Apoptosis via Regulation of the PI3K/Akt and MAPK Signaling Pathways in Huh-7 Cells. *Molecules* **2018**, *23*, 2016. [[CrossRef](#)]

36. McComb, S.; Chan, P.K.; Guinot, A.; Hartmannsdottir, H.; Jenni, S.; Dobay, M.P.; Bourquin, J.P.; Bornhauser, B.C. Efficient apoptosis requires feedback amplification of upstream apoptotic signals by effector caspase-3 or-7. *Sci. Adv.* **2019**, *5*, eaau9433. [[CrossRef](#)]
37. Whitaker, R.H.; Placzek, W.J. Regulating the BCL2 Family to Improve Sensitivity to Microtubule Targeting Agents. *Cells* **2019**, *8*, 346. [[CrossRef](#)]
38. Bonesi, M.; Brindisi, M.; Armentano, B.; Curcio, R.; Sicari, V.; Loizzo, M.R.; Cappello, M.S.; Bedini, G.; Peruzzi, L.; Tundis, R. Exploring the anti-proliferative, pro-apoptotic, and antioxidant properties of Santolina corsica Jord. & Fourr. (Asteraceae). *Biomed. Pharmacother.* **2018**, *107*, 967–978.
39. Fan, T.J.; Han, L.H.; Cong, R.S.; Liang, J. Caspase family proteases and apoptosis. *Acta Biochim. Biophys. Sin.* **2005**, *37*, 719–727. [[CrossRef](#)]
40. Shalini, S.; Dorstyn, L.; Dawar, S.; Kumar, S. Old, new and emerging functions of caspases. *Cell Death Differ.* **2015**, *22*, 526–539. [[CrossRef](#)]
41. Pfeffer, C.M.; Singh, A.T.K. Apoptosis: A Target for Anticancer Therapy. *Int. J. Mol. Sci.* **2018**, *19*, 448. [[CrossRef](#)] [[PubMed](#)]
42. Yoo, K.H.; Park, J.H.; Cui, E.J.; Kim, K.I.; Kim, J.Y.; Kim, J.; Hong, S.G.; Baek, N.I.; Chung, I.S. 3-O-acetyloleanolic acid induces apoptosis in human colon carcinoma HCT-116 cells. *Phytother. Res.* **2012**, *26*, 1541–1546. [[CrossRef](#)] [[PubMed](#)]
43. Lisiak, N.; Paszel-Jaworska, A.; Bednarczyk-Cwynar, B.; Zaprutko, L.; Kaczmarek, M.; Rybczynska, M. Methyl 3-hydroxyimino-11-oxoolean-12-en-28-oate (HIMOXOL), a synthetic oleanolic acid derivative, induces both apoptosis and autophagy in MDA-MB-231 breast cancer cells. *Chem. Biol. Interact.* **2014**, *208*, 47–57. [[CrossRef](#)]
44. Wu, J.; Yang, C.; Guo, C.; Li, X.; Yang, N.; Zhao, L.; Hang, H.; Liu, S.; Chu, P.; Sun, Z.; et al. SZC015, a synthetic oleanolic acid derivative, induces both apoptosis and autophagy in MCF-7 breast cancer cells. *Chem. Biol. Interact.* **2016**, *244*, 94–104. [[CrossRef](#)] [[PubMed](#)]
45. Abdelmageed, N.; Morad, S.A.F.; Elghoneimy, A.A.; Syrovets, T.; Simmet, T.; El-Zorba, H.; El-Banna, H.A.; Cabot, M.; Abdel-Aziz, M.I. Oleanolic acid methyl ester, a novel cytotoxic mitocan, induces cell cycle arrest and ROS-Mediated cell death in castration-resistant prostate cancer PC-3 cells. *Biomed. Pharmacother.* **2017**, *96*, 417–425. [[CrossRef](#)] [[PubMed](#)]
46. Sax, J.K.; Fei, P.; Murphy, M.E.; Bernhard, E.; Korsmeyer, S.J.; El-Deiry, W.S. BID regulation by p53 contributes to chemosensitivity. *Nat. Cell Biol.* **2002**, *4*, 842–849. [[CrossRef](#)]
47. Ebelt, N.D.; Cantrell, M.A.; Van Den Berg, C.L. c-Jun N-Terminal Kinases Mediate a Wide Range of Targets in the Metastatic Cascade. *Genes Cancer* **2013**, *4*, 378–387. [[CrossRef](#)]
48. Liu, J.; Lin, A. Role of JNK activation in apoptosis: A double-edged sword. *Cell Res.* **2005**, *15*, 36–42. [[CrossRef](#)]
49. Hsu, Y.L.; Kuo, P.L.; Chiang, L.C.; Lin, C.C. Involvement of p53, nuclear factor kappaB and Fas/Fas ligand in induction of apoptosis and cell cycle arrest by saikosaponin d in human hepatoma cell lines. *Cancer Lett.* **2004**, *213*, 213–221. [[CrossRef](#)]
50. Wang, X.; Bai, H.; Zhang, X.; Liu, J.; Cao, P.; Liao, N.; Zhang, W.; Wang, Z.; Hai, C. Inhibitory effect of oleanolic acid on hepatocellular carcinoma via ERK-p53-mediated cell cycle arrest and mitochondrial-dependent apoptosis. *Carcinogenesis* **2013**, *34*, 1323–1330. [[CrossRef](#)]
51. Du, H.; Wolf, J.; Schafer, B.; Moldoveanu, T.; Chipuk, J.E.; Kuwana, T. BH3 domains other than Bim and Bid can directly activate Bax/Bak. *J. Biol. Chem.* **2011**, *286*, 491–501. [[CrossRef](#)] [[PubMed](#)]
52. Banjara, S.; Suraweera, C.D.; Hinds, M.G.; Kvensakul, M. The Bcl-2 Family: Ancient Origins, Conserved Structures, and Divergent Mechanisms. *Biomolecules* **2020**, *10*, 128. [[CrossRef](#)] [[PubMed](#)]
53. Kuntzen, C.; Sonuc, N.; De Toni, E.N.; Opelz, C.; Mucha, S.R.; Gerbes, A.L.; Eichhorst, S.T. Inhibition of c-Jun-N-terminal-kinase sensitizes tumor cells to CD95-induced apoptosis and induces G2/M cell cycle arrest. *Cancer Res.* **2005**, *65*, 6780–6788. [[CrossRef](#)] [[PubMed](#)]
54. Dhanasekaran, D.N.; Reddy, E.P. JNK signaling in apoptosis. *Oncogene* **2008**, *27*, 6245–6251. [[CrossRef](#)] [[PubMed](#)]



4.2. Publicación 2

Efficient In Vitro and In Vivo Anti-Inflammatory Activity of a Diamine-PEGylated Oleanolic Acid Derivative.

Autores: Jannus, F.; Medina-O'Donnell, M.; Neubrand, V.N.; Marín, M.; Sáez-Lara, M.J.; Sepúlveda, M.R.; Rufino-Palomares, E.E.; Martínez, A.; Lupiáñez, J.A.; Parra, A.; Rivas, F.*; Reyes-Zurita, F.J.*

Revista: International Journal of Molecular Sciences

Año: 2021

Volumen: 22 (15)

DOI: [10.3390/ijms22158158](https://doi.org/10.3390/ijms22158158)

Índice de impacto: 6,208
(JCR 2022)

Cuartil: *Biochemistry & Molecular Biology*: Q1 (69/296)

Citas: 3 (25 July 2022)
(Semantic Scholar)



Article

Efficient In Vitro and In Vivo Anti-Inflammatory Activity of a Diamine-PEGylated Oleanolic Acid Derivative

Fatin Jannus ¹, Marta Medina-O'Donnell ^{2,*}, Veronika E. Neubrand ³, Milagros Marín ¹,
Maria J. Saez-Lara ¹, M. Rosario Sepulveda ³, Eva E. Rufino-Palomares ¹, Antonio Martinez ²,
Jose A. Lupiañez ¹, Andres Parra ², Francisco Rivas ^{2,*} and Fernando J. Reyes-Zurita ^{1,*}

- ¹ Department of Biochemistry and Molecular Biology I, Faculty of Sciences, University of Granada, Av. Fuentenueva, 18071 Granada, Spain; fatin@correo.ugr.es (F.J.); mmarin@ugr.es (M.M.); mjsaez@ugr.es (M.J.S.-L.); evaevae@ugr.es (E.E.R.-P.); jlcara@ugr.es (J.A.L.)
- ² Department of Organic Chemistry, Faculty of Sciences, University of Granada, Av. Fuentenueva, 18071 Granada, Spain; aramon@ugr.es (A.M.); aparra@ugr.es (A.P.)
- ³ Department of Cell Biology, Faculty of Sciences, University of Granada, Av. Fuentenueva, 18071 Granada, Spain; neubrand@ugr.es (V.E.N.); mrsepulveda@ugr.es (M.R.S.)
- * Correspondence: mmodonnell@ugr.es (M.M.-O.); frivas@ugr.es (F.R.); ferjes@ugr.es (F.J.R.-Z.); Tel.: +34-958-243-252 (F.J.R.-Z.)



Citation: Jannus, F.; Medina-O'Donnell, M.; Neubrand, V.E.; Marín, M.; Saez-Lara, M.J.; Sepulveda, M.R.; Rufino-Palomares, E.E.; Martinez, A.; Lupiañez, J.A.; Parra, A.; et al. Efficient In Vitro and In Vivo Anti-Inflammatory Activity of a Diamine-PEGylated Oleanolic Acid Derivative. *Int. J. Mol. Sci.* **2021**, *22*, 8158. <https://doi.org/10.3390/ijms22158158>

Academic Editor: Codruta Soica

Received: 15 June 2021

Accepted: 20 July 2021

Published: 29 July 2021

Publisher's Note: MDPI stays neutral with regard to jurisdictional claims in published maps and institutional affiliations.



Copyright: © 2021 by the authors. Licensee MDPI, Basel, Switzerland. This article is an open access article distributed under the terms and conditions of the Creative Commons Attribution (CC BY) license (<https://creativecommons.org/licenses/by/4.0/>).

Abstract: Recent evidence has shown that inflammation can contribute to all tumorigenic states. We have investigated the anti-inflammatory effects of a diamine-PEGylated derivative of oleanolic acid (OADP), in vitro and in vivo with inflammation models. In addition, we have determined the sub-cytotoxic concentrations for anti-inflammatory assays of OADP in RAW 264.7 cells. The inflammatory process began with incubation with lipopolysaccharide (LPS). Nitric oxide production levels were also determined, exceeding 75% inhibition of NO for a concentration of 1 µg/mL of OADP. Cell-cycle analysis showed a reversal of the arrest in the G0/G1 phase in LPS-stimulated RAW 264.7 cells. Furthermore, through Western blot analysis, we have determined the probable molecular mechanism activated by OADP; the inhibition of the expression of cytokines such as TNF- α , IL-1 β , iNOS, and COX-2; and the blocking of p-I κ B α production in LPS-stimulated RAW 264.7 cells. Finally, we have analyzed the anti-inflammatory action of OADP in a mouse acute ear edema, in male BL/6J mice treated with OADP and tetradecanoyl phorbol acetate (TPA). Treatment with OADP induced greater suppression of edema and decreased the ear thickness 14% more than diclofenac. The development of new derivatives such as OADP with powerful anti-inflammatory effects could represent an effective therapeutic strategy against inflammation and tumorigenic processes.

Keywords: oleanolic acid; triterpenes derivatives; diamine-(PEG)ylated oleanolic acid; OADP; anti-inflammatory mechanism; RAW 264.7 cell line; TPA-induced acute ear edema

1. Introduction

Inflammation is an innate natural process of the immune system. When persisting for a long period, this process can trigger various chronic diseases such as autoimmune disorders, arthritis, cardiovascular diseases, diabetes, Parkinson's, and cancer. In recent years, new natural compounds with anti-inflammatory properties have been identified and studied, offering the potential to decrease excessive inflammation associated with many diseases [1]. Our research group has recently investigated the anti-inflammatory effect of various diclofenac derivatives [2].

Previous studies have reported the in vitro and in vivo anti-inflammatory effects of various triterpenoids. Several triterpenic saponins have significantly reduced NO production in LPS-stimulated RAW 264.7 cells, inhibiting the release of pro-inflammatory cytokines, such as the tumor necrosis factor (TNF- α), interleukine-1 β (IL-1 β), interleukine-6 (IL-6), and interleukine-8 (IL-8) [3]. In addition, SH479, a derivative of betulinic acid,

ameliorated experimental autoimmune encephalomyelitis in a mouse model by modulating the Th17/Treg balance, on inhibiting the signal transducer and activator of transcription 3 (STAT3) and the nuclear factor kappa-light-chain-enhancer of activated B-cell (NF- κ B) pathways and activating the STAT5 pathway [4]. Furthermore, oleanolic acid regulated the production of anti-inflammatory cytokines and decreased the production of pro-inflammatory cytokines in mice with experimental autoimmune myocarditis [5]. Similarly, in a mouse model of experimental autoimmune encephalomyelitis, oleanolic acid acetate suppressed the production of pro-inflammatory cytokines IL-1 β , IL-6, INF- γ , and TNF- α by regulating toll-like receptor 2 (TLR2) signaling [6]. A synthetic derivative of oleanolic acid (CDDO-Im) inhibited IL-6 and IL-17 expression and palliated dextran sulfate sodium (DSS) induced colitis in mice, as well as inhibited STAT3 activation [7]. Additional studies demonstrated that acetylated and methylated derivatives of oleanolic acid elicited a better anti-inflammatory response in male Wistar rat used as models of inflammation than did triterpenic acid [8,9].

Olives are a rich source of pentacyclic triterpenes such as oleanolic and maslinic acids. Oleanolic acid is present in high concentrations in olive pomace, which represents 37% of the total triterpenoids in this fruit [10]. The concentration of this compound in extra virgin olive oil is 57.3 mg/kg, whereas in pomace oil is 5592 mg/kg. The greatest increase in triterpenes as the quality of the oil decreases is because these compounds are found mainly in the outer waxy layer of the olive fruit so that successive pressing and extractions favor their elimination [11]. In this study, oleanolic acid was obtained from solid olive oil wastes, using the method described in [12].

PEGylation is a technique that enables ethylene glycol units to bond to drugs, forming linear or branched polymers with different molar masses, which improve their bio-distribution and bioavailability [13]. Our research group performed PEGylation reactions, covalently linking a polyethylene glycol (PEG) reagent to oleanolic acid (OA) and thereby producing a series of derivatives with greater solubility in aqueous media [14–16]. One of these PEGylated derivatives of oleanolic acid (OADP) has been studied due to its high cytotoxicity in Hep G2 cancer cells [17]. In the present study, we found that the cytotoxicity of OADP in human embryo WRL68 non-tumor liver cells was 39-fold lower than in the Hep G2 cancer cell line. Therefore, we studied the potential anti-inflammatory effect of OADP, since inflammation is related to cancer and plays a key role in tumorigenesis [18]. In this sense, an understanding of the molecular mechanisms involved in the inflammatory process can help to prevent certain chronic diseases and even some types of cancer.

In the inflammation process, different proteins such as protein kinases, PI3K/AKT, JAK, and MAPK are activated [19], so transcription factors such as STAT, AP-1 or NF- κ B are activated, inducing the expression of pro-inflammatory proteins such as COX-2, iNOS, TNF- α , IL-1 β , and IL-6 [20,21]. Of these, COX-2 and iNOS produce the intermediates of the inflammation process, PGE-2 and nitric oxide (NO), respectively. In addition, NO can regulate the acute and chronic inflammatory process. COX-2 is activated in immune cells such as macrophages, producing PGs that induce different inflammatory states [22,23]. Disruption of the activation of this process can lead to aberrant cell growth, cancer cell transformation, angiogenesis, and metastasis. To evaluate the *in vivo* topical anti-inflammatory effects of OADP, we used the animal model of induced ear edema in mice [24]. In this model, inflammation is provoked by topical treatment with 12-O-tetradecanoylphorbol 13-acetate (TPA), a phlogistic factor that causes the activation of MAP kinase proteins, activating the molecular pathway for the onset of the inflammatory process [25].

In this work, we examine the anti-inflammatory effect of OADP in LPS-stimulated RAW 264.7 cells and in mice having acute TPA-induced ear edema. Firstly, we conducted *in vitro* studies, determining NO release at different sub-cytotoxic concentrations of OADP after 72 h of incubation. The inhibition of NO production was accompanied by a reversal of G0/G1 phase arrest in LPS-stimulated RAW 264.7 cells. Secondly, we studied the underlying anti-inflammatory molecular mechanisms activated by OADP. Thus, OADP

inhibited the expression of the main inflammatory cytokines such as TNF- α , IL-1 β , iNOS, COX-2, and a regulated protein such as p-I κ B α . Furthermore, we evaluated the anti-inflammatory effect in mice with acute ear edema by using a series of morphological measurements, histopathological analyses, and IL-6 induction levels.

2. Results

2.1. Cytotoxicity of OADP in the Proliferation of RAW 264.7 Cells

To evaluate the cytotoxic effects of OADP and OA on RAW 264.7 murine macrophage cells, we incubated these cells at increasing concentrations (0–100 $\mu\text{g}/\text{mL}$) of OADP for 72 h (Figure 1). Cell viability was analyzed using the MTT assay, where the tetrazolium dye was transformed into formazan in the mitochondria of viable cells, its absorbance measured at 570 nm. The OADP concentration required for 50% cell growth inhibition (IC_{50}) after 72 h of incubation was less than 2 $\mu\text{g}/\text{mL}$ ($\text{IC}_{50} = 1.72 \pm 0.10 \mu\text{g}/\text{mL}$), and was 56 $\mu\text{g}/\text{mL}$ for OA. These cell viabilities with these compounds were determined to calculate the sub-cytotoxic concentrations at which to perform the anti-inflammatory tests. $\frac{3}{4} \text{IC}_{50} = 1.29 \mu\text{g}/\text{mL}$, $\frac{1}{2} \text{IC}_{50} = 0.86 \mu\text{g}/\text{mL}$, and $\frac{1}{4} \text{IC}_{50} = 0.43 \mu\text{g}/\text{mL}$ for OADP. $\frac{3}{4} \text{IC}_{50} = 41.78 \mu\text{g}/\text{mL}$, $\frac{1}{2} \text{IC}_{50} = 27.86 \mu\text{g}/\text{mL}$, and $\frac{1}{4} \text{IC}_{50} = 13.92 \mu\text{g}/\text{mL}$ for OA. These data for diclofenac were obtained from Galisteo et al. 2020 [2]. The use of these sub-cytotoxic concentrations ensures that the anti-inflammatory activity is due to an inflammatory process and not to its cytotoxicity.

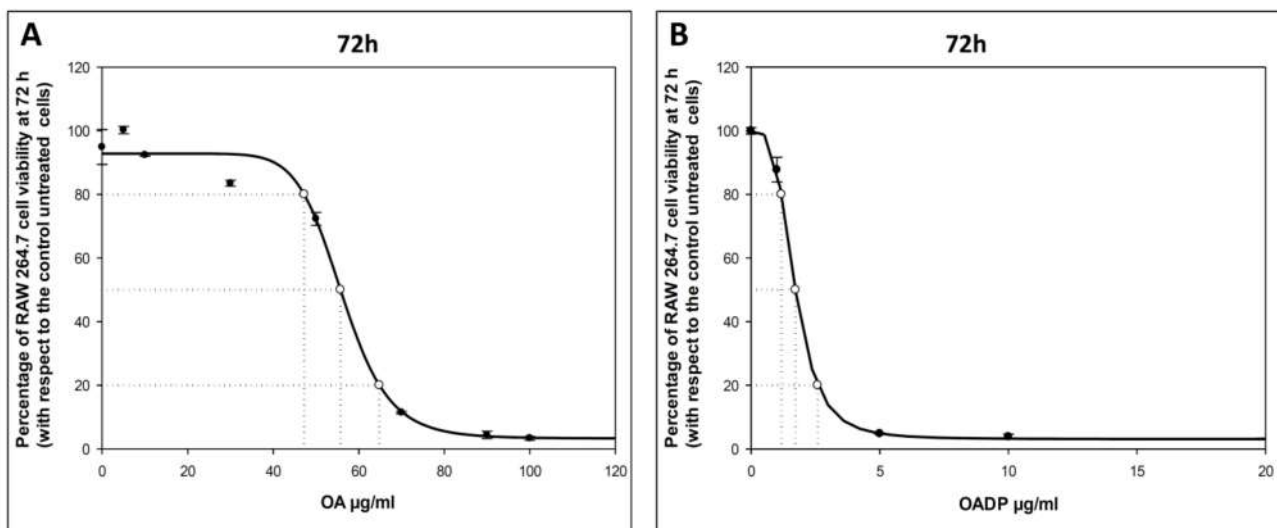


Figure 1. Effect of OA (A) and OADP (B) on cell proliferation of RAW 264.7 macrophage murine cells, after treatment with the compounds for 72 h. Each point represents the mean value \pm S.D. of at least two independent experiments performed in triplicate.

2.2. Nitric Oxide Production

In the inflammation process, NO is produced by inducible nitric oxide synthase (iNOS) and, as the main pro-inflammatory mediator, plays a key role in the immune system. Murine macrophage cells RAW 264.7 were used to study the anti-inflammatory effect of OADP, which induces a significant release of NO during the inflammatory process. Therefore, the anti-inflammatory activity of OADP was assessed with the Griess method by measuring the nitrite concentration, proportional to the NO released, in the cell culture medium. These macrophages (RAW 264.7) were activated with LPS for 24 h after the addition of OADP. The following sub-cytotoxic concentrations were used: $\frac{3}{4} \text{IC}_{50}$, $\frac{1}{2} \text{IC}_{50}$, and $\frac{1}{4} \text{IC}_{50}$.

NO production at 24, 48, and 72 h of incubation (Figure 2) was hardly detectable in the negative control (untreated cells), compared to the positive control (cells treated only

with LPS). After 24 h of incubation, OADP did not cause any anti-inflammatory effect. Meanwhile, at 48 h of incubation, a slight anti-inflammatory effect was noted at the $\frac{3}{4}$ IC₅₀ concentration, with a 33% inhibition of NO production. However, 72 h of incubation gave rise to a strong anti-inflammatory effect at the $\frac{3}{4}$ IC₅₀ concentration, with 75% inhibition of NO production. In addition, slight anti-inflammatory effects were detected at the $\frac{1}{2}$ IC₅₀ and $\frac{1}{4}$ IC₅₀ concentrations, with approximately 25% inhibition of NO production, with respect to the increase between the positive and negative control (Figure 2). At the concentrations tested, OA and diclofenac exerted no inhibitory effect on NO production in LPS-activated RAW 264.7 cells (Figure 3).

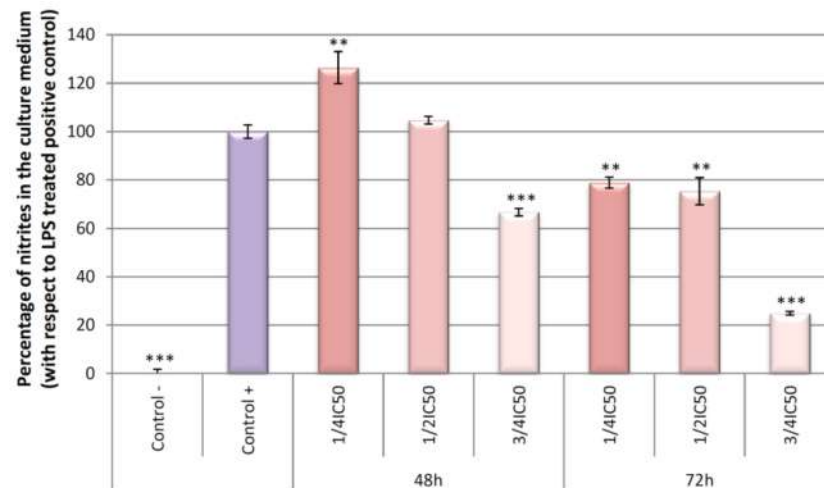


Figure 2. Effect of OADP on NO production in RAW 264.7 macrophage murine cells, after treatment with OADP for 48 h and 72 h at the $\frac{1}{2}$ IC₅₀ and $\frac{3}{4}$ IC₅₀ concentrations. Data represent the mean \pm S.D. of at least two independent experiments performed in triplicate. Key: (**) $p < 0.01$ and (***) $p < 0.001$, with respect to LPS-treated control cells (positive control).

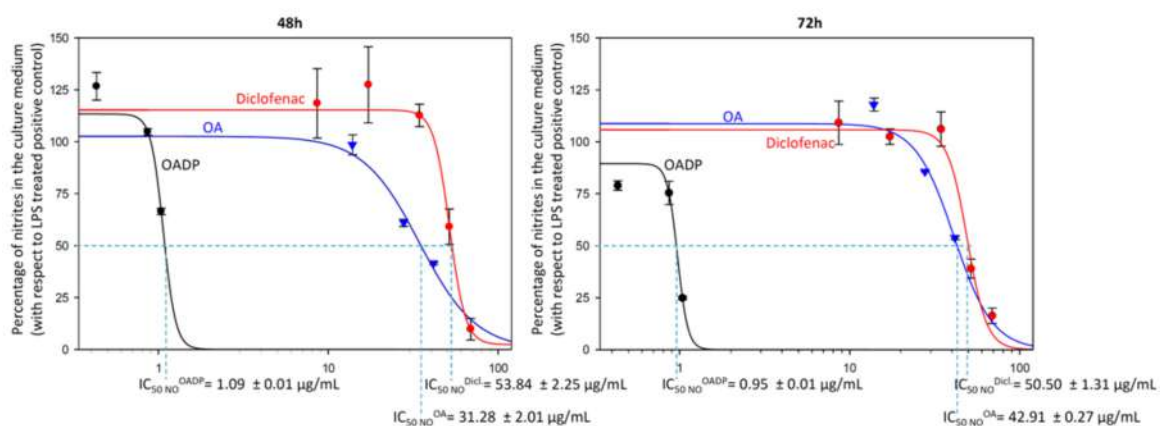


Figure 3. Sigmoidal curves of the effect of OADP (black), OA (blue) and diclofenac (red) on nitrite release in RAW 264.7 cells, after treatment with the compounds for 48 h and 72 h. Data represent the mean \pm S.D. of at least two independent experiments performed in triplicate.

To compile more data on the anti-inflammatory effect of OADP, we calculated the doses that result in 50% NO inhibition (IC₅₀ NO) for OADP and compared them with those of OA and diclofenac, in each case at both 48 h and 72 h of treatment. The IC₅₀ NO for OADP at 48 h (1.09 \pm 0.01 μ g/mL) and 72 h (0.95 \pm 0.01 μ g/mL) were significantly lower than for OA (31.28 \pm 2.01 μ g/mL for 48 h and 42.91 \pm 0.27 μ g/mL for 72 h) and diclofenac (53.84 \pm 2.25 μ g/mL for 48 h and 50.50 \pm 1.31 μ g/mL for 72 h) (Figure 3). Thus, OADP

proved to be some 30-fold more anti-inflammatory than OA and about 50-fold more than diclofenac.

2.3. Cell Cycle Arrest

Flow cytometry with propidium iodide (PI) staining was used to evaluate the DNA ploidy and alterations in the cell-cycle profiles since the DNA content is directly proportional to the PI fluorescence, which indicates the percentage of cells in each phase of the cycle (Figure 4). RAW 264.7 cells were treated with LPS for 24 h to induce the inflammatory process, after which the cells were treated with OADP for 72 h at the corresponding sub-cytotoxic concentrations. A significant growth arrest occurred during the G0/G1 phase in the positive control (100%) compared to the negative control (49.6%). A DNA histogram analysis revealed that OADP was capable of reversing LPS-induced cell-cycle arrest in the G0/G1 phase. When the cells were treated with OADP at the corresponding sub-cytotoxic concentrations ($\frac{1}{4}$ IC₅₀, $\frac{1}{2}$ IC₅₀, and $\frac{3}{4}$ IC₅₀), the percentage of cell-cycle arrest was significantly reduced in the G0/G1 phase by up to 40.4%, 43.6%, and 45.9%, respectively. This decrease in the percentage of cells in the G0/G1 phase was accompanied by a concomitant increase in the percentage of cells in the S phase (58.5% at $\frac{1}{4}$ IC₅₀, 50.7% at $\frac{1}{2}$ IC₅₀, and 54.2% at $\frac{3}{4}$ IC₅₀). This recovery in the cell cycle could be a result of the anti-inflammatory effects caused by OADP, which appears to have stimulated cell division. These results show no significant variations for the different sub-cytotoxic concentrations used, indicating that OADP has anti-inflammatory effects at all the concentrations tested. The changes were not significant in the G2/M phase of the cell cycle.

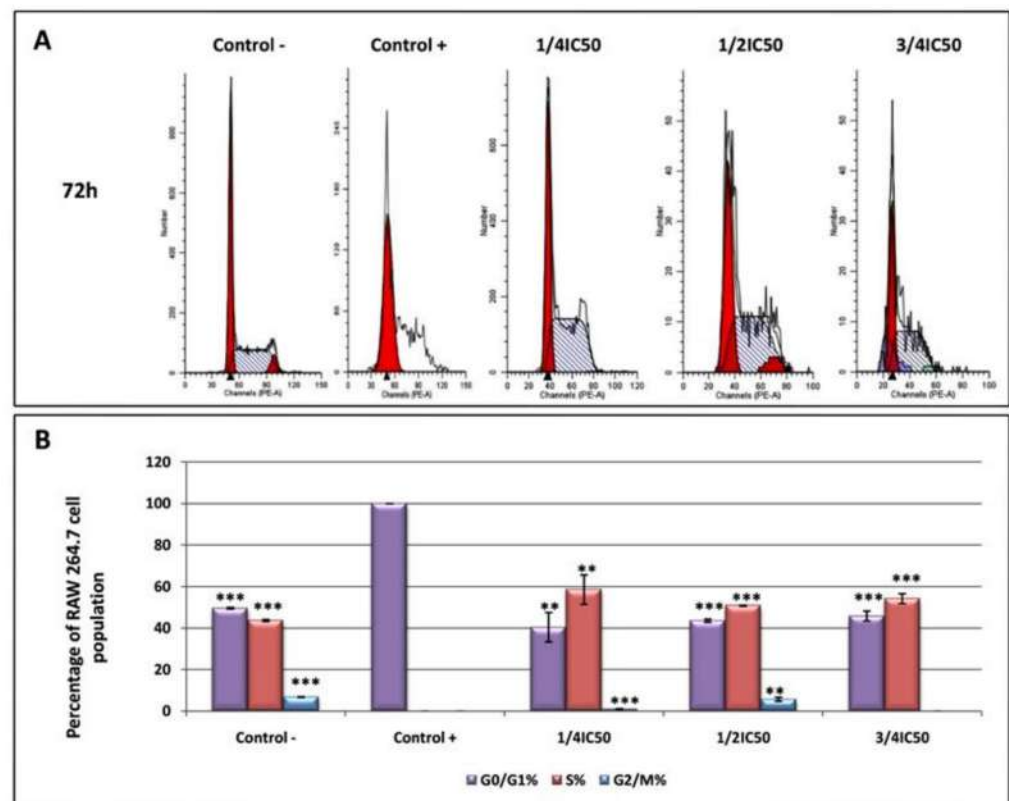


Figure 4. DNA histograms of cell cycle analysis of RAW 264.7 macrophage murine cell, after treatment with OADP for 72h at the $\frac{1}{2}$ IC₅₀ and $\frac{3}{4}$ IC₅₀ concentrations (A). Percentage of RAW 264.7 macrophage murine cell population in the different phases of the cell cycle (G0/G1, S and G2/M) (B). Data represent the mean \pm S.D. of at least two independent experiments performed in triplicate. Key: (**) $p < 0.01$ and (***) $p < 0.001$, with respect to LPS-treated control cells (positive control).

2.4. OADP-Induced Cell-Morphology Changes on LPS-Stimulated RAW 264.7 Cells

The cell morphology of RAW 264.7 cells was analyzed in the presence as well as the absence of LPS and OADP. Treatment of LPS-stimulated RAW 264.7 cells with OADP for 72 h at the sub-cytotoxic $\frac{1}{4}$ IC₅₀ and $\frac{3}{4}$ IC₅₀ concentrations led to morphological changes. In general, untreated cells were smooth and round, whereas LPS-stimulated RAW 264.7 cells had changed to an irregular and rough shape with dendritic formations. Dendritic morphology was characterized by multiple prominent cytoplasmic projections. Co-treatment of LPS with OADP decreased the level of dendritic formation, showing a shape more similar to that of untreated cells, in a dose-dependent manner. The cells were visualized under optical microscopy (Figure 5).

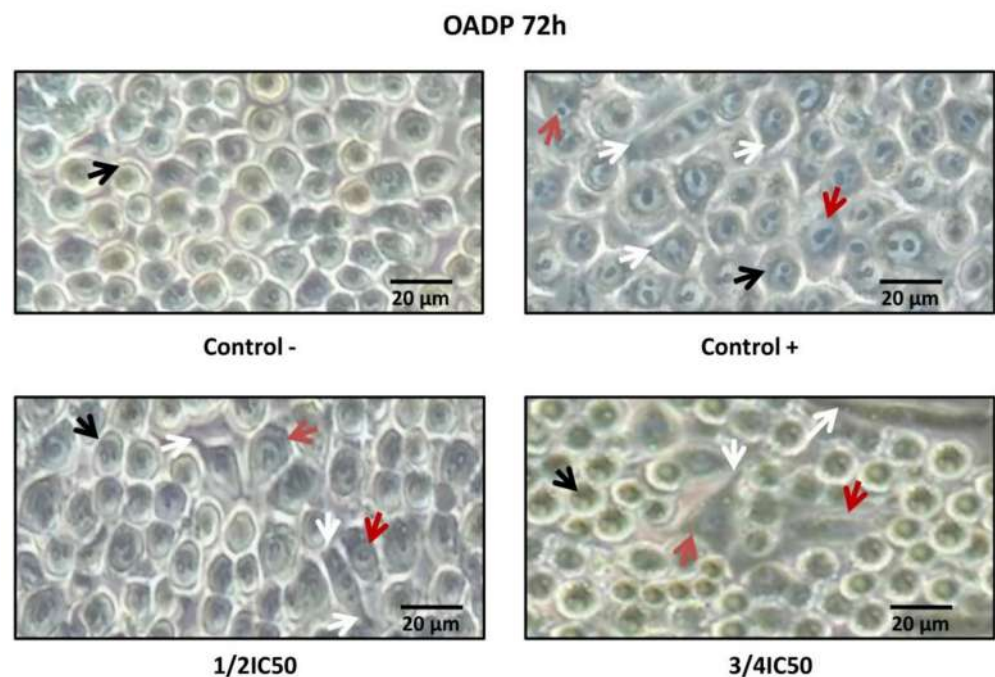


Figure 5. Morphological transformation in RAW 264.7 cells stimulated with LPS and OADP treatment for 72 h at the $\frac{1}{2}$ IC₅₀ and $\frac{3}{4}$ IC₅₀ concentrations. The black arrows indicate Raw 264.7 cells in monocyte state. The red arrows indicate Raw 264.7 cells in macrophage state. The white arrows indicate cytoplasmic projections.

2.5. OADP-Induced Inhibition of the Expression of Pro-Inflammatory Proteins TNF- α and IL-1 β on LPS-Stimulated RAW 264.7 Cells

The activation of pro-inflammatory cytokines is one of the central processes that occur during the induction of the inflammatory response. TNF- α and IL-1 β are potent pro-inflammatory cytokines capable of recruiting immune cells and triggering inflammation. TNF- α is a pro-inflammatory cytokine produced by various immunocompetent cells, including macrophages, neutrophils, Th1/Th2 cells, and dendritic cells. IL-1 β is a pro-inflammatory cytokine produced by B cells, endothelial cells, and fibroblast cells. However, its release is linked to an acute and chronic inflammatory process, inducing the acute-phase reaction and favoring prostaglandin synthesis. The results of the Griess test indicated that the strongest anti-inflammatory effect occurred after 72 h of incubation with OADP at the $\frac{3}{4}$ IC₅₀ concentration, accompanied by a weak anti-inflammatory effect at the $\frac{1}{2}$ IC₅₀ and $\frac{1}{4}$ IC₅₀ concentrations. Therefore, using Western blot analysis, we examined the expression of the pro-inflammatory cytokines TNF- α and IL-1 β after 72 h of incubation with OADP at $\frac{3}{4}$ IC₅₀ and $\frac{1}{2}$ IC₅₀ concentrations. In this case, we found that the expression of TNF- α and IL-1 β in RAW 264.7 cells increased significantly in the positive control (12-fold with respect to the TNF- α expression and 6-fold with respect to the IL-1 β expression, compared to the negative control). Treatment with OADP prompted a concentration-dependent decline

in the expression of these proteins. Thus, OADP significantly reduced the expression of TNF- α in RAW 264.7 cells (32% at $\frac{1}{2}$ IC₅₀ and 57% at $\frac{3}{4}$ IC₅₀) compared to the positive control (Figure 6A). Furthermore, the level of IL-1 β lowered in RAW 264.7 cells (29% at $\frac{1}{2}$ IC₅₀ and 96% at $\frac{3}{4}$ IC₅₀) compared to the positive control (Figure 6B). Therefore, OADP proved capable of suppressing the synthesis and release of these cytokines, becoming a possible candidate for the development of new anti-inflammatory drugs.

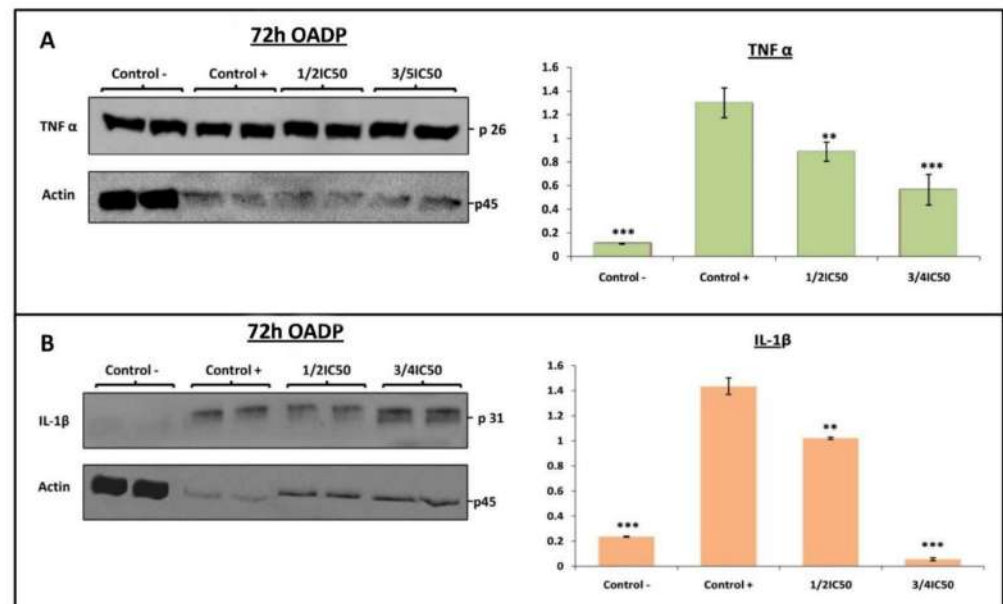


Figure 6. Western blot of the levels of TNF- α (A) (p26) and IL-1 β (B) (p31) proteins on LPS-stimulated Raw 264.7 cells, after treatment with OADP for 72h at the $\frac{1}{2}$ IC₅₀ and $\frac{3}{4}$ IC₅₀ concentrations. Protein expression levels are expressed as arbitrary intensity units for each band compared to arbitrary intensity units for actin (p45). Variations in the relative percentages of TNF- α and IL-1 β expression for each concentration are also shown. The values represent means \pm S.D. of at least two separate experiments. Key: (**) $p < 0.01$ and (***) $p < 0.001$, with respect to LPS-treated control cells (positive control).

2.6. OADP-Induced Inhibition of COX-2, iNOS, and p-I κ B α Protein Expression on LPS-Stimulated RAW 264.7 Cells

The uncontrolled inflammatory process can lead to tissue damage and various inflammatory diseases, such as autoimmune disorders, cardiovascular diseases or tumorigenesis. It is well known that stress and inflammatory cytokines induce phosphorylation and stimulation of active NF- κ B, protein involved in the activation of the cell-proliferation process. Furthermore, NF- κ B is the main transcription factor regulating the production of inflammatory proteins such as iNOS and COX-2, which are activated by cytokines TNF- α and IL-1 β during immune responses.

In this context, the levels of two main inflammatory mediators such as COX-2 and iNOS were examined by Western blot analysis at 72 h after treatment with OADP ($\frac{3}{4}$ IC₅₀ and $\frac{1}{2}$ IC₅₀ concentrations) in order to determine the anti-inflammatory effect caused in RAW 264.7 cells. The results indicate that in non-stimulated RAW 264.7 cells (negative control) iNOS and COX-2 expression was very low, whereas in LPS-stimulated cells (positive control) the protein levels rose markedly (14-fold with respect to iNOS expression and 10-fold with respect to COX-2 expression, compared to the negative control). As in the previous case, the treatment with OADP prompted a concentration-dependent decrease in the expression of these proteins. Therefore, OADP substantially reversed the high level of expression of COX-2 (56% at $\frac{1}{2}$ IC₅₀ and 85% at $\frac{3}{4}$ IC₅₀) and iNOS (67% at $\frac{1}{2}$ IC₅₀ and 81% at $\frac{3}{4}$ IC₅₀), induced by LPS treatment in a concentration-dependent manner, compared to the positive control (Figure 7A,B).

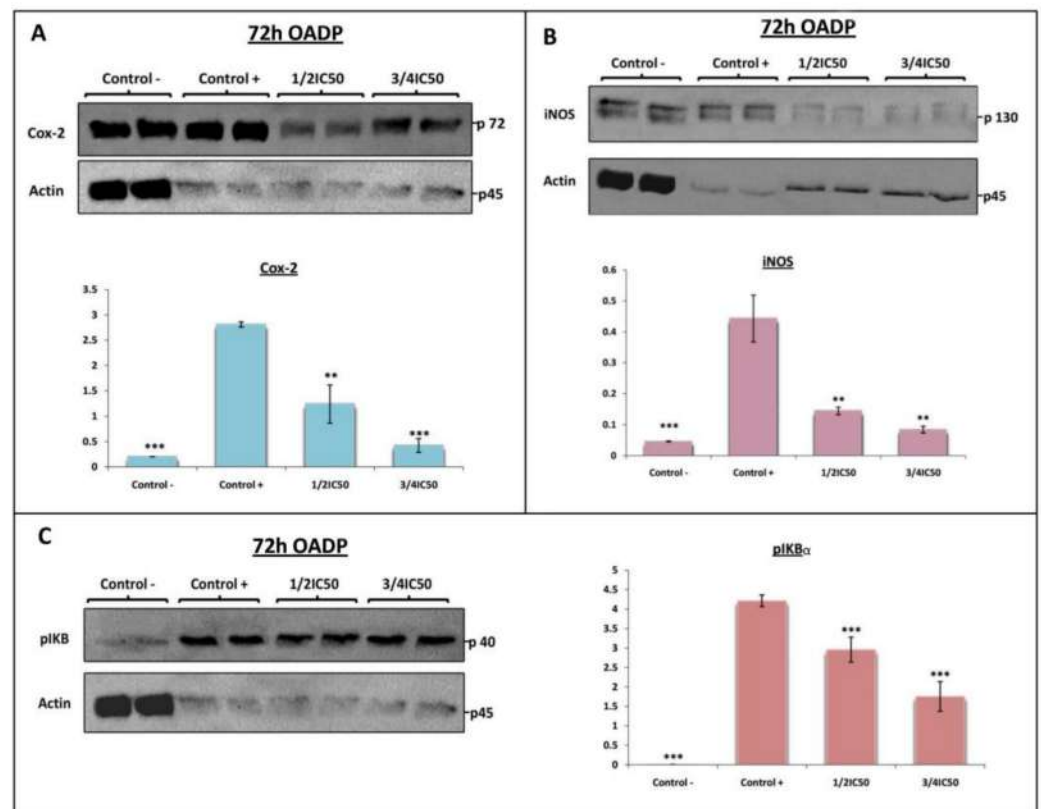


Figure 7. Western blot of the levels of proteins COX-2 (A) (p72), iNOS (B) (p130), and p-IκBα (p40) (C) on LPS-stimulated RAW 264.7 cells, after treatment with OADP for 72h at the $\frac{1}{2}$ IC₅₀ and $\frac{3}{4}$ IC₅₀ concentrations. Protein expression levels are expressed as arbitrary intensity units for each band compared to arbitrary intensity units for actin (p45). Variations in the relative percentages of TNF-α and IL-1β expression for each concentration are also shown. The values represent means ± S.D. of at least two separate experiments. Key: (**) $p < 0.01$ and (***) $p < 0.001$, with respect to LPS-treated control cells (positive control).

The IκBα protein (NF-κB inhibitory protein alpha) inhibited NF-κB, is inactivated and degraded by phosphorylation, resulting in p-IκBα. To further explore the anti-inflammatory role of OADP in LPS-stimulated Raw 264.7 cells, we used Western blot analysis to evaluate the expression level of the p-IκBα protein. This level rose some 480-fold more in LPS-stimulated Raw 264.7 cells than in the negative control (Figure 7C). In addition, OADP significantly reduced the expression level of the p-IκBα protein compared to the positive control. After treatment with LPS for 72 h, the expression levels of the protein p-IκBα clearly increased, but a co-treatment with LPS and OADP at sub-cytotoxic concentrations significantly attenuated this expression in a dose-dependent manner (30% at $\frac{1}{2}$ IC₅₀ and 58% at $\frac{3}{4}$ IC₅₀), compared to the positive control (Figure 7C). These results demonstrate that OADP clearly inhibited the expression of the p-IκBα protein in LPS-stimulated RAW 264.7 cells.

2.7. OADP Inhibition of TPA-Induced Inflammation in Mouse Ear

The results showed the clear induction of edema in response to treatment with TPA. Induction proved noticeable in all morphological measurements made, with an increase of approximately 25% to 40%, when comparing the right ears with the left, in each of the parameters measured (Figure 8). Thus, the width increased by 25% ($23.97 \pm 2.6\%$), the diameter of the external auditory canal by 30% ($27.81 \pm 5.8\%$), and the weight of the 6-mm disc (removed from the ear as a sample) by 40% ($37.42 \pm 5.6\%$). This effect was also appreciable in the phenotype presented by the right ear in the control mice (Figure 8D).

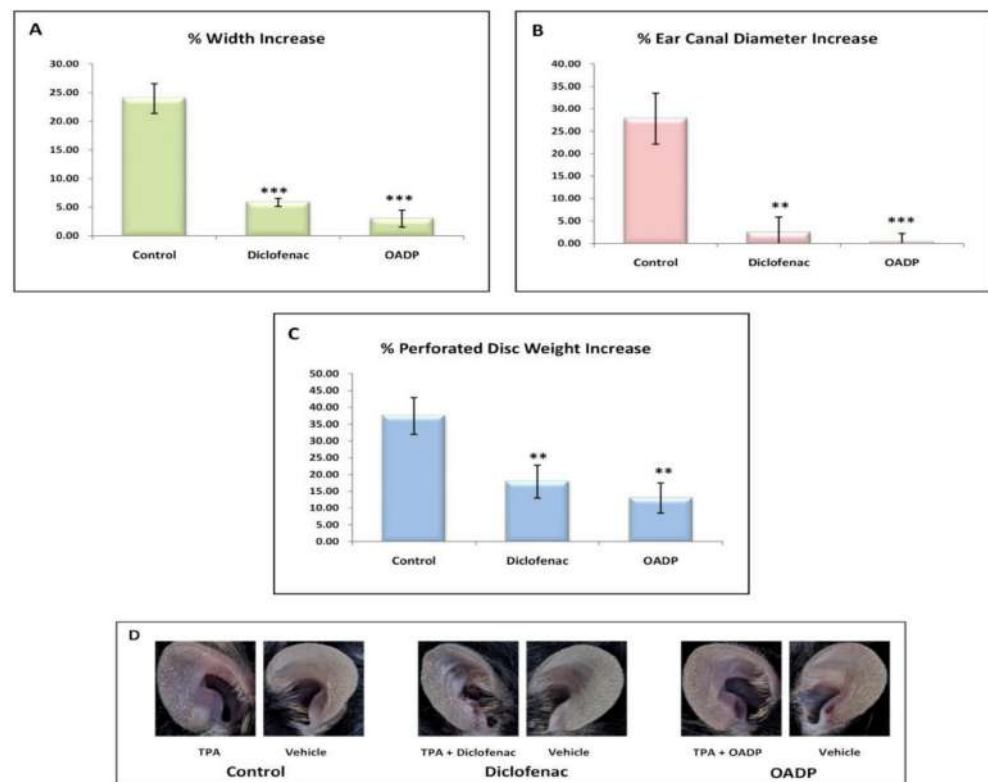


Figure 8. Increases in the percentage of the different morphological parameters: Width (A), diameter of the external auditory canal (B), and weight of the 6mm disc practiced (C). These increases have been calculated from the differences between the left and right ears in the different groups of mice (Control, Diclofenac, OADP) (D). The mean \pm S.E.M. is shown for each of these parameters ($n = 4$).

The TPA-induced edema was significantly inhibited in OADP-treated mice, with virtually no changes between the right and left ear. The width increase ($2.99 \pm 1.48\%$) was 22% less than in the control. No differences were detected in the diameter change of the external auditory canal on comparing the two ears ($0.18 \pm 6.10\%$), this being some 30% less than in the control. The weight of the 6-mm disc removed from the ear increase ($12.90 \pm 5.47\%$), being 24.5% less than in the control.

The results for the treatment with diclofenac were similar to those found with OADP, although higher values were registered for the increases in the different parameters evaluated: $5.83 \pm 0.71\%$ in the width, $2.34 \pm 3.5\%$ in the diameter of the external auditory canal, and $17.84 \pm 4.90\%$ in the weight of the 6-mm disc removed from the ear.

2.8. OADP-Induced Decreases in TPA-Induced Mouse Ear Injury

The main effect of OADP was studied in mouse edema biopsies in response to TPA treatment. In the control group, the right ear (treated with TPA) compared to the control left ear displayed intense tissue destruction and edema, with infiltrates of inflammatory polymorphonuclear leukocytes, mainly neutrophils, and hyperplasia as well as hypertrophy of the dermis and epidermis (vehicle, Figure 9A). However, pre-treatment with diclofenac and OADP significantly lowered the level of infiltration of edematous and inflammatory cells, compared to the control treated with TPA (Figure 9A). Furthermore, diclofenac and OADP reduced these impairments, markedly reducing ear thickness (by 21% and 35%, respectively) compared to the TPA-treated control (Figure 9B). Topical pre-treatment with OADP alleviated the lesion more effectively than did diclofenac, as it notably depressed the development of erythema (Figure 9A,B).

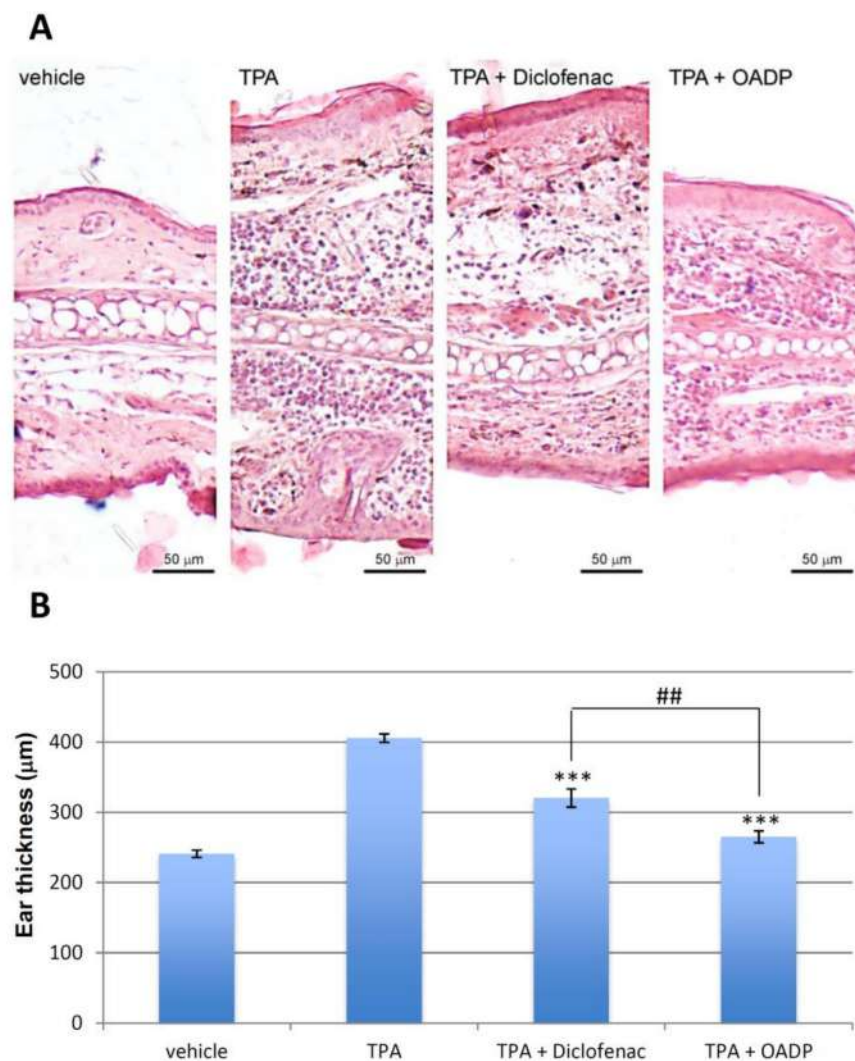


Figure 9. Representative photomicrographs. (A) The images show a cross section of the ears treated with vehicle (acetone), TPA alone, TPA + Diclofenac, TPA + OADP, at a 125x magnification. Scale bars = 50 μm. (B) The graph represents the mean thickness of the ear of each treatment, expressed as mean ± S.E.M. (***) $p < 0.001$ compared to TPA treated ears. (##) $p < 0.01$ compared to the ears treated with TPA + Diclofenac.

2.9. OADP-Induced Decreases in IL-6 Released by TPA in the Mouse Ear

Comparisons of the IL-6 concentrations between the right and left ear within each group of animals revealed a clear induction of inflammation in the control group, with an increase in IL-6 concentration of 91.84 ± 20.23 pg/mL in the right ear compared to the left (Figure 10A). In the rest of the groups treated with the different inhibitors, including diclofenac, no increase was detected in the right ear compared to the left, and the interleukin-6 concentration clearly decreased in this comparison (Figure 10B). Diclofenac lowered the IL-6 concentration by 180% ($186.41 \pm 8.37\%$), while OADP caused a fall of almost 250%, representing 60% stronger inhibition (Figure 10). Thus, regarding the production of IL-6, we conclude that OADP is clearly more efficient *in vivo* than is diclofenac.

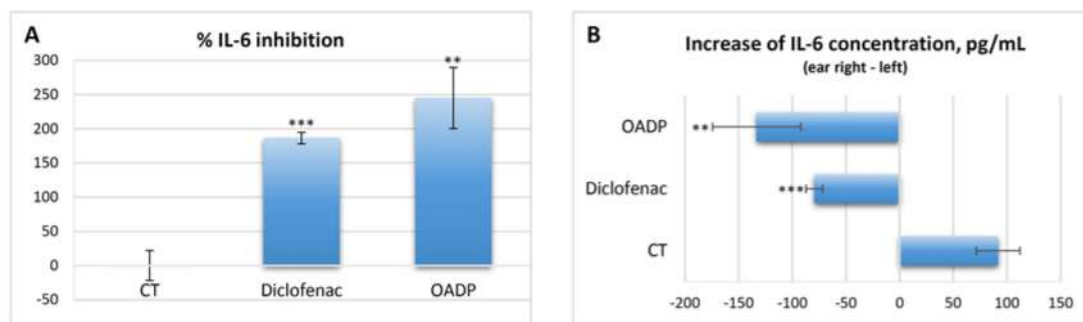


Figure 10. IL-6 inhibition percentage, calculated from the differences between the left and right ears in the different groups of mice (A). Increases in IL-6 concentration (pg/mL) calculated from the differences between the left and right ears in the different groups of mice (control, diclofenac and OADP) (B). The mean \pm S.E.M. is shown for each of these parameters ($n = 4$). Key: (**) $p < 0.01$ and (***) $p < 0.001$, with respect to the control group of mice.

3. Discussion

Inflammation is a common physiological response that when acute can be protective but when chronic can cause a wide variety of diseases, including cancer [26]. Therefore, inflammation becomes fundamental in tumor development, stirring intense interest in developing new anti-inflammatory agents that have significant anticancer properties [27]. Natural products, often used as an alternative to synthetic drugs in these types of afflictions, include oleanolic acid and its derivatives, which offer potential therapeutic effects in chronic diseases [28].

Previous results have shown that OADP can induce apoptosis at very low concentrations in different cancer cell lines [16,17]. In the present study, we examine the potential of OADP as an anti-inflammatory agent and investigate the underlying molecular mechanism for this effect in LPS-stimulated RAW 264.7 macrophage cells. Furthermore, we performed *in vivo* tests on a TPA-induced acute mouse ear edema model to evaluate the suppressive effect of OADP on pro-inflammatory mediators.

During the inflammation process, various types of leukocytes, lymphocytes, and other inflammatory cells are activated. Macrophages prove crucial in various inflammatory diseases by inducing the expression of pro-inflammatory mediators [29]. LPS is a strong inducer of monocytes to macrophages, stimulating the production of pro-inflammatory mediators [30]. Macrophage stimulation is represented by expanded cell size and extension of the cytoplasm. Other changes in stimulated macrophages serve to amplify the immune response [31]. OADP cytotoxicity was determined in murine monocyte/macrophage RAW 264.7 cells in order to establish sub-cytotoxic concentrations of this compound. The viability of these cells was tested at various OADP concentrations, using an MTT assay, which gave an IC_{50} concentration of 1.73 $\mu\text{g/mL}$.

The primary pro-inflammatory mediator for acute or chronic inflammation is NO. In general, NO inhibitors provide excellent opportunities to design new therapeutic methods for inflammatory diseases [32]. In the present work, the inhibitory activity of OADP against NO release in LPS-stimulated RAW 264.7 cells is studied. OADP improved the NO inhibitory activity compared to the positive control (Figure 2). At 72 h of incubation, OADP resulted in 75%, 25%, and 21% inhibition of NO, for concentrations of $\frac{3}{4} IC_{50}$, $\frac{1}{2} IC_{50}$ and $\frac{1}{4} IC_{50}$, respectively, with respect to the positive control. To compile more insight on this anti-inflammatory effect, we calculated the effective doses at 50% NO inhibition ($IC_{50\text{NO}}$) after 48 h and 72 h of treatment with OADP and found that the $IC_{50\text{NO}}$ for OADP at 48 h were significantly lower than for OA and diclofenac, being 30-fold more anti-inflammatory than OA and about 50-fold more than diclofenac (Figure 3). The flow-cytometry results revealed the anti-inflammatory effect of OADP in RAW 264.7 cells at the corresponding sub-cytotoxic concentrations tested. Furthermore, OADP exhibited anti-inflammatory activity at 72 h of treatment by reversing the cell-cycle arrest induced by LPS (Figure 4). Morphological changes of RAW 264.7 cells were viewed under a light

microscope ($\times 400$). Untreated cells (negative control) were circular but became irregular in shape with multiple prominent cytoplasmic projections and dendritic formations, after stimulation with LPS (positive control). After 72 h of treatment with OADP, at different sub-cytotoxic concentrations, the degree of cell propagation and dendritic formation diminished markedly, in a dose-dependent manner (Figure 5).

The NF- κ B and MAPK pathways are essential in regulating the production of inflammatory cytokines in activated macrophages such as TNF- α , IL-1 β , and IL-6. TNF- α participates in various processes such as cell survival, apoptosis, and necrosis, by stimulating TNF receptors and related pathways, such as NF- κ B and MAPKs [33]. The LPS-induced pattern of macrophage activation leads to high production of inflammatory mediators, such as TNF- α , IL-1 β , and IL-6. This model is widely used to detect anti-inflammatory drugs [34].

Triterpenoids and their derivatives have an effective inflammatory effect both in vitro and in vivo. Inhibition of MAPKs pathways in the anti-inflammatory actions of several triterpenoids has been observed. For example, ursolic acid (UA) inhibited mitogen-induced phosphorylation of ERK and JNK and prevented the activation of immunomodulatory transcription factors such as NF- κ B, NF-AT, and AP-1 in T and B lymphocytes [35]. OA decreased the levels of TLR4 and NF- κ B and MAPKs in the mouse model with salmonella-induced intestinal inflammation [36]. Indole OA derivatives, inhibited the expression of proteins of p-p38, p-JNK, p-ERK, p-NF- κ B p-Akt, iNOS and COX-2, and enhanced the expression of Nrf2 in LPS-activated BV2 cells [37].

Lupeol has been found to impede the expression of pro-inflammatory cytokines such as TNF α and IL- β in LPS-stimulated macrophages [38]. Additional studies have shown that maslinic acid exerts an anti-inflammatory effect by inhibiting the production of NO induced by oxygen and glucose deprivation, TNF- α suppressing the expression of COX-2 and iNOS at the levels of protein and mRNA [39]. Maslinic acid reportedly exerts its anticancer effects on HT29 colon-cancer cells through a JNK-p53 dependent mechanism [40]. In a chemoprevention of tumorigenesis in ApcMin/+ mice, maslinic acid has been found to inhibit molecular pathways of inflammation and cell survival [41]. On the other hand, OA reportedly prevented colitis by inhibiting Th17 cells and the down-regulation of the expression of interleukin IL-1 β , NF- κ B, MAPK, and ROR γ t in the colon [42]. CDDO-Me, a semi-synthetic derivative of OA has been found to induce downregulation of the expression of F4/80, CD11c, COX-2, IL-6, KI67, NF-B, and TNF- α [43].

In this context, to investigate whether the anti-inflammatory effects after 72 h of OADP treatment were associated with the activation of TNF α and IL-1 β , we performed a Western blot analysis and found that LPS markedly increased the production of TNF- α and IL-1 β in inflammatory responses in RAW 264.7 cells. Meanwhile, OADP reversed the LPS-induced production of TNF- α and IL-1 β after 72 h of treatment. In addition, a notable decrease in TNF- α expression was recorded in RAW 264.7 cells (32% at $\frac{1}{2}$ IC₅₀ and 57% at $\frac{3}{4}$ IC₅₀, Figure 6A), accompanied by a significant fall in the level of IL-1 β (29% at $\frac{1}{2}$ IC₅₀ and 96% to $\frac{3}{4}$ IC₅₀, Figure 6B). These results imply that OADP has a protective effect on LPS-induced inflammation in RAW 264.7 cells. Thus, OADP is capable of suppressing the release of TNF- α and appears to be an excellent choice for use as a model in developing efficient anti-inflammatory drugs.

The two major enzymes iNOS and COX-2 induce the production of two crucial inflammatory mediators, NO and PGE2, respectively [44]. Furthermore, increased iNOS expression prompts high levels of NO and has been associated with various chronic inflammatory disorders [45]. Prostaglandin E2 (PGE2), biosynthesized by COX-2 from arachidonic acid, is a major inflammatory mediator, increasing local blood flow, pain sensitization, and edema. The inhibition or down-regulation of COX-2 expression blocks PGE2 synthesis and inhibits inflammation [46].

In the present work, the expression of COX-2 and iNOS was evaluated by Western blot analysis after 72 h of OADP treatment in LPS-activated RAW 264.7 cells. OADP exerted a gradual anti-inflammatory effect in a concentration-dependent manner from $\frac{1}{2}$ IC₅₀ to $\frac{3}{4}$ IC₅₀, this effect being linked to the decline in the expression of COX-2 (56% at $\frac{1}{2}$ IC₅₀ and 85% at $\frac{3}{4}$ IC₅₀) and iNOS (67% at $\frac{1}{2}$ IC₅₀ and 81% at $\frac{3}{4}$ IC₅₀) (Figure 7A,B). Furthermore, the level of p-IκBα was studied at the corresponding sub-cytotoxic concentrations, revealing that phosphorylation of IκBα was significantly inhibited after treatment with OADP in a concentration-dependent manner (30% at $\frac{1}{2}$ IC₅₀ and 58% at $\frac{3}{4}$ IC₅₀), relative to only the LPS-treated RAW 264.7 cells (positive control, Figure 7C).

The TPA-induced mouse ear edema model is widely used to study the anti-inflammatory activity of new compounds [47]. Pentacyclic triterpene α-amyrin inhibited TPA-induced activation of PKCα, ERK, and p38 MAPK, thereby preventing IκBα degradation and p65/RelA phosphorylation [48].

The anti-inflammatory effect of diclofenac and OADP was evaluated in mice having acute ear edema induced by TPA, and the treatment was found to be remarkably effective after 6 h of treatment. This anti-inflammatory effect was analyzed as a percentage of edema suppression in the treated groups, in contrast to the control group (vehicle), determining a series of morphological measurements. TPA caused a strong inflammatory process, characterized by a significant increase in the percentage of length, width, thickness, diameter of the external auditory canal and weight (Figure 8). However, treatment with diclofenac and OADP showed a significant anti-inflammatory effect by reducing these morphological measurements. These results were confirmed by a histopathological analysis (Figure 9), where OADP reduced edema and leukocyte infiltration better than did diclofenac. The production of IL-6 was also evaluated. Treatment with OADP stemmed IL-6 production more effectively than did the diclofenac treatment, resulting in a 250% inhibition in cytokine production, this being 60% greater than with diclofenac (Figure 10).

In this sense, other triterpenoids such as Lupeol, have been effective against TPA-induced inflammation in acute ear edema mouse model, which also decreased myeloperoxidase levels causing a reduction in cellular infiltration in inflamed tissues, significantly inhibiting PGE₂ levels [38]. Lupeol reduced cellularity and eosinophil levels in bronchoalveolar fluid [49]. This compound has also been shown effective against inflammation in the arthritis mouse model [50]. Another pentacyclic triterpenoid such as ursolic acid (UA) has shown anti-inflammatory activity in activated T cells, B cells and macrophages, and against graft-versus-host disease in vivo mouse model, significantly reducing serum levels of pro-inflammatory cytokines IL-6 and IFN-γ [35]. Indole oleanolic acid derivatives inhibited the expression of pro-inflammatory cytokines (TNF-α, IL-6, IL-12 and IL-1β) and increased the expression of anti-inflammatory cytokine IL-10 [37].

With the results found and considering the bibliographic data on the anti-inflammatory action of triterpene compounds, the following molecular mechanism was proposed for the anti-inflammatory action of OADP (Figure 11). OADP could inhibit the activation of the TLR4 or TNFR2 receptors, preventing the activation of MAP kinases (ERK, JNK or p38) or inhibiting the phosphorylation of IκBα, which would lead to the inhibition of the activation of pro-inflammatory transcription factors such as NF-κB or the AP1 set (c-Jun, c-Fos, JunB, or JunD). Finally, all this could produce the inhibition of the expression of pro-inflammatory cytokines such as TNFα, IL-1β or IL-6, and the proteins that are expressed in pro-inflammatory processes such as COX-2 or iNOS.

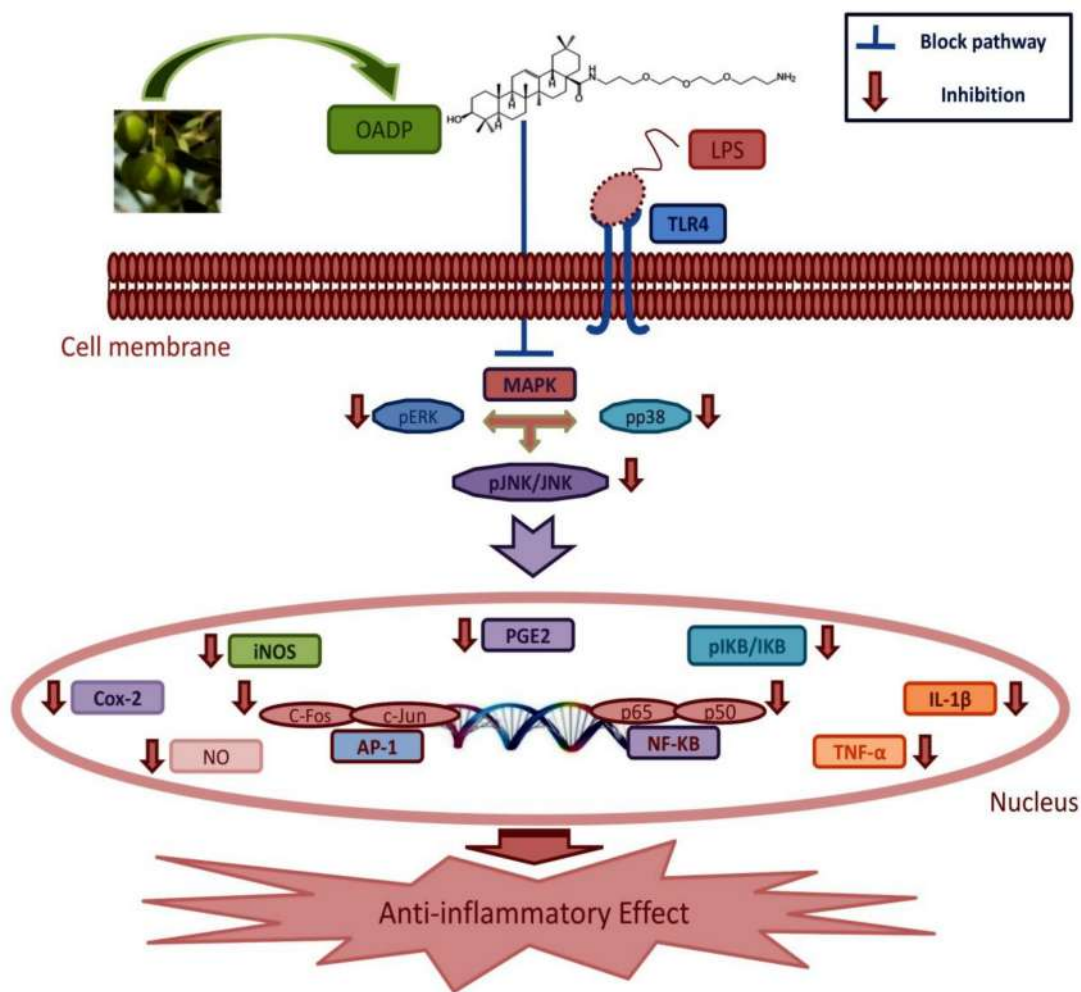


Figure 11. Mechanism of action underlying the anti-inflammatory effect induced by OADP in LPS-stimulated RAW264.7 cells, after 72 h of treatment, at the $\frac{1}{2}$ IC50 and $\frac{3}{4}$ IC50 concentrations. This process triggers the inhibition of phosphorylation of IκBα, the inhibition of the pro-inflammatory cytokines TNF-α and IL-1β. Inhibition of the inflammatory mediators COX-2 and iNOS, induced inhibition of NO production.

The mouse model with acute ear edema has been chosen due to the low rate of suffering exerted in animals, compared to other tumorigenic inflammation models, in which TPA is used as a tumor promoter. For example, induction of skin carcinoma, in a two stages carcinogenesis mouse model [51], where the tumorigenic process is initiated with 7,12-dimethylbenz[a]-anthracene (DMBA) and the animals are treated for weeks with TPA. Our main objective in this article is to demonstrate the effectiveness of OADP as an anti-inflammatory agent and to study its behavior against inflammation induced by tumor promoters as TPA. OADP has been shown to be a very effective agent against tumor cell proliferation in HepG2 human hepatoma cancer cell line [17], and against inflammatory processes. Due to these results, we defend that OADP can be a good agent against tumorigenic processes. However, it will be necessary to accomplish future trials in inflammation models derived from cancer growth or genetic defects or chronic tissue degeneration/infection, similar to those performed with maslinic acid in intestinal tumorigenesis in ApcMin/+ mice [41]. Further studies will be necessary to establish the anti-inflammatory potential of OADP against chronic inflammation diseases such as arthritis or Parkinson's. In this sense, it would be interesting to determine the role of OADP to counteract inflammation after neurodegeneration, in microglia murine cell line model stimulated by LPS [52]. Although the anti-tumor and anti-inflammatory potential

of OADP is clear, it will be necessary to perform all these studies before carrying out any clinical trials.

4. Materials and Methods

4.1. Materials

RPMI 1640 W/L-Glutamine, fetal bovine serum (FBS), gentamicin (Biowest, Nuaille, France), DMSO (Merck Life Science S.L., Madrid, Spain), and 3-(4,5-dimethylthiazol-2-yl)-2,5-diphenyltetrazolium bromide (MTT) (Thermo Fisher Scientific Inc., Ward Hill, MA, USA). IL-1 β , tumor necrosis factor alpha TNF- α , p-I κ B- α , iNOS, and COX-2 primary antibodies, and anti-rabbit, anti-goat, and actin secondary antibodies were purchased from Santa Cruz Biotechnology (Santa Cruz, CA, USA). Phorbol ester 12-O-tetradecanoylphorbol-13-acetate (TPA), culture flasks, and well plates were obtained from VWR International, Ltd. (Radnor, PA, USA).

4.2. Test Compounds

Oleanolic acid (OA) was isolated from solid olive oil production wastes, which were extracted successively in a Soxhlet extractor with hexane and EtOAc. Hexane extracts were a mixture from which OA was purified by column chromatography over silica gel followed by elution with CH₂Cl₂/acetone mixtures of increasing polarity [12].

A solution of di-tert-butyl dicarbonate (Boc₂O, 2.75 mmol) in dried CH₂Cl₂ (2 mL) was added slowly to a solution of 4,7,10-trioxatridecane-1,13-diamine (H₂N-PEG-NH₂, 6.8 mmol) in CH₂Cl₂ (20 mL). The reaction mixture was maintained at room temperature for 12 h, and then was diluted with water and extracted three times with CH₂Cl₂. After the organic layer was dried with anhydrous Na₂SO₄, the solvent was removed under reduced pressure, and thus the H₂N-PEG-NH-Boc (85%) was produced [16]. In a flask (20 mL), the compound H₂N-PEG-NH-Boc (0.45 mmol) was dissolved in DMF (5 mL) and afterwards OA (2 mmol), HOAt (3 mmol), PyAOP (2 mmol), and DIPEA (8 mmol), were added. The reaction mixture was heated at 100 °C for 12 h, diluted with water and extracted three times with CH₂Cl₂. The organic layer was dried with anhydrous Na₂SO₄ and the solvent was removed under reduced pressure. Finally, the residue was purified by column chromatography, yielding the OA-diamine-Boc-PEGylated derivative (94%) [16]. After this OA-diamine-Boc-PEGylated derivative (0.3 mmol) was dissolved in THF (20 mL), concentrated HCl (37%, 2 mL) was added. The reaction mixture was maintained at room temperature for 24 h, and then was diluted with water and extracted three times with CH₂Cl₂. The organic layer was dried with anhydrous Na₂SO₄, and the solvent was removed under reduced pressure. Finally, the residue was purified by column chromatography, yielding OADP (95%) [16].

Finally, OA and OADP (Figure 12) were dissolved in DMSO at 5 mg/mL and stored at −20 °C. Prior to treatment, the stock solution was diluted in cell culture medium to the appropriate concentration for each experiment.

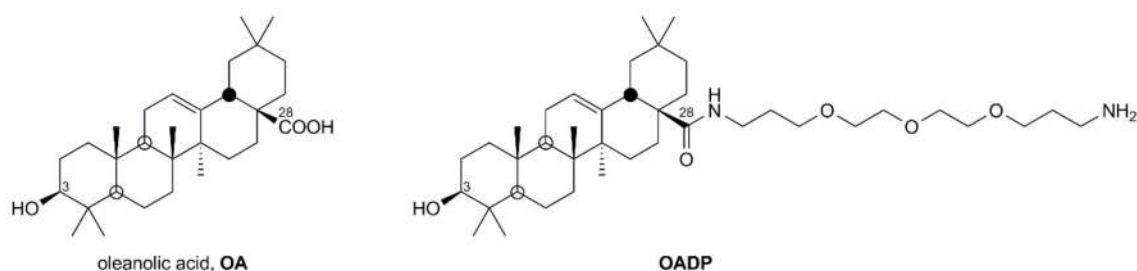


Figure 12. Structures of triterpene compounds OA and OADP.

4.3. Cell Culture

The RAW 264.7 monocyte/macrophage cell line (ATCC no. TIB-71) is a murine leukemia virus-induced tumor cell line from mouse *Mus musculus*. This cell line does not produce detectable retrovirus. The RAW 264.7 cell line was cultured in RPMI1640 medium, supplemented with 2 mM glutamine, 10% heat-inactivated FCS, 0.5 µg/mL of gentamicin, and incubated at 37 °C in a 5% atmosphere of CO₂ at 95% humidity. Cells were grown to 80–90% confluence in sterile cell-culture flasks. Sub-confluent monolayer cells were used in all experiments. The cell line was provided by the cell bank of the University of Granada, Spain.

4.4. Cell-Viability Assay

The OA and OADP assay on RAW 264.7 cells was evaluated using the MTT proliferation assay. Cell viability was evaluated by measuring the absorbance of MTT staining of live cells. For this test, 6×10^3 RAW 264.7 cells were grown in a 96-well plate and subsequently incubated with OA and OADP at different concentrations (0–100 µg/mL). After 72 h of incubation, 100 µL of MTT solution (0.5 mg/mL) in 50% of PBS with 50% of medium was placed in each well. After 1.5 h of incubation, the formazan was resuspended in 100 µL of DMSO. Finally, the relative cell viability, with respect to the untreated control cells, was evaluated by absorbance at 570 nm in an ELISA plate reader (Tecan Sunrise MR20–301, TECAN, Austria). The experimental data were fitted to a sigmoid function ($y = y_{\max}/(x/a)^{-b}$) by non-linear regression. IC₅₀ values were obtained by interpolation. Similar analyses were performed to determine the IC₅₀NO of NO production (vide infra). All these analyses were performed with the statistical software SigmaPlot (Version 12.5). The values of cell viability were expressed as means ± S.D. of at least two experiments performed in quadruplicate for each concentration.

4.5. Determination of the NO Concentration

The nitrite concentration was used as an indicator of NO production. The determination of the nitrite concentration in the culture medium was evaluated according to the Griess reaction. Cells were plated at 6×10^4 cells/well in 24-well cell culture plates and supplemented with 10 µg/mL of LPS. After 24h of plating, cells were incubated for 24, 48, and 72 h with OADP at $\frac{1}{4}$ IC₅₀, $\frac{1}{2}$ IC₅₀, and $\frac{3}{4}$ IC₅₀ concentrations. The supernatants were collected at 24 h, 48 h, and 72 h to determine their nitrite concentration and/or stored at –80 °C for later use. The Griess reaction was performed by taking 150 µL of supernatant test sample or the sodium nitrite standard (0–120 µM), mixing with 25 µL of Griess reagent A [0.1% N-(1-naphthyl)ethylenediamine dihydrochloride] and 25 µL of Griess reagent B (1% sulphanilamide in 5% of phosphoric acid) in a 96-well plate. After 15 min of incubation at room temperature, the absorbance at 540 nm was determined in an ELISA plate reader (Tecan Sunrise MR20–301, TECAN, Austria). The absorbance was referred to the nitrite standard curve to determine the nitrite concentration in the supernatant of each experimental sample. The percentage of NO production was determined, assigning 100% to the increase between the negative control (untreated cells) and the positive control (cells treated only with 10 µg/mL of LPS). The values of NO concentration were expressed as means ± S.D. of at least two experiments performed in triplicate for each concentration.

4.6. Cell-Cycle Analysis

PI staining flow cytometry constitutes a fast, efficient, and reproducible method for determining relative DNA content. Flow cytometry provides an estimate of alterations in cell-cycle profiles and characteristic changes in DNA levels of cell-cycle arrest and cell differentiation. The number of cells at each stage of the cell cycle is determined by fluorescence-associated cell sorting (FACS) at 488 nm on an Epics XL flow cytometer (Coulter Corporation, Hiialeah, FL, USA). For this test, 12×10^4 LPS-stimulated murine macrophage/monocyte RAW 264.7 cells were placed in 24-well plates with 1.5 mL of medium and incubated with OADP for 24 h at $\frac{1}{4}$ IC₅₀, $\frac{1}{2}$ IC₅₀, and $\frac{3}{4}$ IC₅₀ concentrations.

The positive control consisted of cells treated only by LPS stimulation, while the negative control comprised cells not treated with LPS. The treated cells were LPS-stimulated RAW 264.7 cells and cells treated with the compounds under study. Subsequently, the cells were washed twice with PBS, harvested by trypsinization, and then resuspended in TBS 1X (10 mM Tris, 150 mM NaCl), after which Vindelov Buffer (100 mM Tris, 100 mM NaCl, 10 mg/mL RNase, and 1 mg/mL PI) at pH 8.0 was added. The samples were placed on ice for 15 min. Immediately before FACS analysis, the cells were stained with 20 μ L of 1 mg/mL PI solution. The data were analyzed with the Multicycle software to determine the percentage of cells in each phase of the cell cycle (G0/G1, S, and G2/M). The values of cell percentage were expressed as means \pm S.D. of at least two experiments performed in triplicate for each concentration.

4.7. Western Blot Analysis

RAW 264.7 cells (12×10^4) were treated with OADP at the sub-cytotoxic concentrations cited above, for 72 h. The positive control consisted of cells treated only with LPS stimulation while the negative control was made up of untreated cells without LPS. After the treatments, cells were washed twice with PBS and resuspended in lysis buffer (20 mM Tris/acetate, pH 7.5, 1 mM EDTA, 1 mM EGTA, 1% Triton X-100, 1 mM orthovanadate, 270 mM sucrose, 1 mM sodium glycerophosphate, 5 mM sodium fluoride, 1 mM sodium pyrophosphate, 5 mM β -mercaptoethanol, 1 mM benzamidine, 35 μ g/mL PMSF, and 5 μ g/mL leupeptin). Samples were homogenized, ultra-sonicated, and incubated on ice for 20 min, before centrifuging at $12,000 \times g$, for 15 min. Supernatants were used to calculate the protein concentration, which was evaluated by the Bradford method. For Western blot analysis, a sample of 25 to 50 μ g of total protein was used. The proteins were separated on 15% sodium dodecyl sulfate (SDS)-polyacrylamide gel and transferred to polyvinylidene difluoride membranes. The membranes were blocked by incubation for 1 h in TBS buffer containing 0.1% Tween and 5% milk powder at room temperature and washed with TBS buffer containing 0.1% Tween. The membranes were blotted overnight at 4 $^{\circ}$ C, with primary antibodies: rabbit polyclonal interleukin IL-1 β (1/200 dilution), goat polyclonal TNF α (1/100 dilution), goat polyclonal p-I κ B α (1/200 dilution), rabbit polyclonal NOS2 (1/200 dilution), and goat polyclonal COX-2 (1/500 dilution). The blots were then washed 3 times with TBS-0.1% Tween, and developed with secondary antibodies bound to peroxidase, for 1 h at room temperature (1/3000 dilution). The blots were then washed 3 times with TBS-0.1% Tween and once with TBS. Afterwards, all blots were revealed using the ChemiDoc XRS Image System (Bio-Rad Laboratories, Hercules, CA, USA). The protein bands were quantified using the Multi-Gauge program (Fuji Film Europe, TK Tiburg, Holland). The data of protein expression were expressed as means \pm S.D. of at least three experiments performed in duplicate for each concentration.

4.8. Animals

Male BL/6J mice, 8 weeks old and weighing 21–28 g, were purchased from the Animal Experimentation Service of the Center for Scientific Instrumentation of the University of Granada (Spain). These mice were housed for 7 days at 22 $^{\circ}$ C with 70% humidity, a 12 h light/dark cycle and were fed a standard diet and water was provided ad libitum before experimentation. The experiment was conducted following the guidelines issued by the Animal Care Committee and accepted by the Institutional Ethics Committee of the University of Granada.

4.9. TPA-Induced Acute Ear Edema

Edema was induced by topical administration of TPA in acetone, specifically 2.5 μ g/ear. In groups of 8 individuals, the mice were treated on both surfaces of the right ear using a 20- μ L solution of acetone containing OADP (0.5 mg/ear), while the reference group was treated similarly using diclofenac (0.5 mg/ear) as a reference drug, the control group was not treated with any anti-inflammatory compound. Simultaneously, the TPA was placed

on both sides of the right ear at 0, 6, and 18 h. At 6 h after the end of the last treatment, the animals underwent cervical dislocation. The samples were then stored at -80°C . The left ear was treated with acetone only, as a control. A 6-mm diameter disc was removed from treated as well as untreated ears and weighed separately on an analytical balance. The degree of edema was determined by the weight increase of the right ear over the left. The anti-inflammatory effect was evaluated as a percentage of the suppression of edema in the treated groups in contrast to the control group. A series of morphological measurements were taken in these tissues, such as length, width, thickness, diameter of the external auditory canal, and weight, as detailed below. Length measurements were made with a precision digital caliper.

4.10. Histology Study of Acute Ear Edema

The ears of the mice were treated as described above. Subsequently, they were cut and fixed in 4% PFA for 24 h. After three washes in PBS, they were embedded in paraffin and cut into sections on a microtome (Zeiss). The sections were stained with hematoxylin and eosin. Images were taken using an Axiophot microscope (Zeiss) with a magnification of $125\times$. For its quantification, the thickness of the ear was measured using ImageJ imaging software (NIH) and expressed as mean \pm standard error of the mean (S.E.M.). Student's t-test was applied for the statistical analysis, and a value of $p < 0.05$ was considered statistically significant.

4.11. Interleukin-6 Release

After the activation of the inflammation process, key proteins that mediate this process are induced. These proteins are cytokines and proteins responsible for the arachidonic acid cascade. The concentration levels of IL-6 were analyzed as markers of inflammation in the aforementioned different groups of mice.

The tissue samples were washed with cold PBS and then homogenized at 10% tissue concentration in homogenization buffer (PBS, 0.1 M PMSF, 0.5% BSA, 10 mM EDTA, leupeptin $5\ \mu\text{g}/\text{mL}$). Two freeze-thaw cycles were performed to break down the cell membranes. The homogenates were centrifuged at $5000\times g$ for 5 min. Finally, the supernatants were removed and immediately analyzed for the cytokine concentration. The IL-6 concentration was determined by the ELISA technique, using a specific kit (E0079m, EIAab Science Co., Wuhan, China). The percentage of IL-6 inhibition was calculated according to:

$$\% \text{ IL}_6 \text{ inhibition} = \left\{ 1 - \frac{([IL_6]_{\text{ear}_{\text{right}}} - [IL_6]_{\text{ear}_{\text{left}}})_{\text{sample}}}{([IL_6]_{\text{ear}_{\text{right}}} - [IL_6]_{\text{ear}_{\text{left}}})_{\text{control}}} \right\} \times 100 \quad (1)$$

4.12. Statistical Analysis

The data are represented as the mean \pm standard deviation (S.D.). For each assay, the Student's t-test was used for statistical comparisons with control cells. A limit of $p \leq 0.05$ was used to assess significant differences: $p < 0.05$ (*), $p < 0.01$ (**) and $p < 0.001$ (***). The data shown are representative of at least two independent experiments performed in triplicate.

5. Conclusions

In the present study, we demonstrate that OADP has a powerful anti-inflammatory effect *in vitro* and *in vivo* in the models evaluated. Moreover, we deduced the underlying molecular mechanism for the anti-inflammatory effect of OADP on LPS-stimulated RAW 264.7 cells, after 72 h of treatment, at concentrations of $\frac{1}{2}$ IC_{50} and $\frac{3}{4}$ IC_{50} . That is, OADP weakened the expression of pro-inflammatory cytokines such as $\text{TNF}\alpha$ and $\text{IL-}\beta$ in LPS-stimulated macrophages. This in turn decreased inflammatory proteins such as iNOS and COX-2 and inhibited NO production, a crucial inflammatory mediator. Furthermore, $\text{I}\kappa\text{B}\alpha$ phosphorylation was significantly suppressed after 72 h of OADP treatment.

Among the most outstanding results of this study is the potent anti-inflammatory effect of OADP in LPS-stimulated RAW 264.7 cells and in mice with acute ear edema. The results demonstrate that OADP inhibits NO production and reverses the differentiation processes in LPS-stimulated RAW 264.7 cells. Furthermore, OADP impedes the expression of TNF- α , IL-1 β , iNOS, and COX-2, as well as blocking the production of p-I κ B α in these macrophage cells. Based on these results, the following mechanism is suggested for the anti-inflammatory effect of OADP in these macrophage cells. Firstly, OADP diminishes the expression of TNF- α and IL-1 β and decreases iNOS as well as COX-2, which in turn subsequently hinders p-I κ B α and NO production (Figure 11). Thus, these results suggest the possible pharmacological use of OADP as a potent and effective anti-inflammatory agent in acute and chronic inflammatory diseases.

Author Contributions: Conceptualization, M.M.-O., F.R. and F.J.R.-Z.; Formal analysis, F.J., M.M.-O., V.E.N., M.J.S.-L., M.R.S., J.A.L., A.P. and F.J.R.-Z.; Funding acquisition, F.R., J.A.L., A.P. and F.J.R.-Z.; Investigation, F.J., M.M.-O., V.E.N., M.M., M.J.S.-L., M.R.S., E.E.R.-P., A.M. and F.J.R.-Z.; Methodology, M.M.-O., A.M., F.R., M.J.S.-L., M.R.S., E.E.R.-P. and F.J.R.-Z.; Project administration, F.R. and F.J.R.-Z.; Resources, M.M.-O., F.R., E.E.R.-P., J.A.L., A.P. and F.J.R.-Z.; Supervision, J.A.L., A.P., F.R. and F.J.R.-Z.; Validation, F.J., M.M.-O., V.E.N., M.R.S., E.E.R.-P., J.A.L., A.P. and F.J.R.-Z.; Visualization, F.J., M.M.-O., V.E.N., M.R.S., F.R. and F.J.R.-Z.; Writing—original draft, F.J., M.M.-O., F.R. and F.J.R.-Z.; Writing—review & editing, F.R. and F.J.R.-Z. All authors have read and agreed to the published version of the manuscript.

Funding: This research was funded by the “Consejería de Economía, Conocimiento, Empresas y Universidad. Junta de Andalucía”, grant numbers B1-BIO-281-UGR18 and B1-FQM-217-UGR18.

Institutional Review Board Statement: The study was conducted and approved in accordance with the guidelines of the Ethics Committee for Animal Experimentation of the University of Granada (283-CEEA-OH-2019).

Informed Consent Statement: Not applicable.

Data Availability Statement: Not applicable.

Acknowledgments: We thank the CIC service of the University of Granada for their support and David Nesbitt for reviewing the English of the manuscript.

Conflicts of Interest: The authors declare no conflict of interest. The funders had no role in the design of the study; in the collection, analyses, or interpretation of data; in the writing of the manuscript, or in the decision to publish the results.

Abbreviations

AP-1	Activator protein 1
COX-2	Cyclooxygenase-2
IC ₅₀	Total concentration to obtain a 50% cell growth inhibition
IC ₅₀ NO	Doses that result in 50% NO inhibition
IL	Interleukin
INF- γ	Interferon- γ
iNOS	Inducible nitric oxide synthase
PI	Propidium iodide
I κ B α	NF- κ B inhibitory protein alpha
JAK	Janus-activated kinase
LPS	Bacterial lipopolysaccharide
MAPK	Mitogen-activated protein kinase
NF- κ B	Nuclear factor kappa B
NO	Nitric oxide
NSAID	Nonsteroidal anti-inflammatory drug
OADP	Diamine-PEGylated derivative of oleanolic acid
PI3K/AKT	Phosphatidylinositol-3-kinase

STAT	Signal transducer activator of transcription
TLR	Toll-like receptor
TNF α	Tumor necrosis factor α
TPA	12-O-tetra-decanoylphorbol-13-acetate

References

- Hankittichai, P.; Buacheen, P.; Pitchakarn, P.; Na Takuathung, M.; Wikan, N.; Smith, D.R.; Potikanond, S.; Nimlamool, W. Artocarpus lakoocha Extract Inhibits LPS-Induced Inflammatory Response in RAW 264.7 Macrophage Cells. *Int. J. Mol. Sci.* **2020**, *21*, 1355. [[CrossRef](#)]
- Galisteo, A.; Jannus, F.; García-García, A.; Aheget, H.; Rojas, S.; Lupiañez, J.; Rodríguez-Diéguez, A.; Reyes-Zurita, F.; del Moral, J.Q. Diclofenac N-Derivatives as Therapeutic Agents with Anti-Inflammatory and Anti-Cancer Effect. *Int. J. Mol. Sci.* **2021**, *22*, 5067. [[CrossRef](#)] [[PubMed](#)]
- Xiong, H.; Zheng, Y.; Yang, G.; Wang, H.; Mei, Z. Triterpene saponins with anti-inflammatory activity from the stems of *Entada phaseoloides*. *Fitoterapia* **2015**, *103*, 33–45. [[CrossRef](#)] [[PubMed](#)]
- Li, J.; Jing, J.; Bai, Y.; Li, Z.; Xing, R.; Tan, B.; Ma, X.; Qiu, W.-W.; Du, C.; Du, B.; et al. SH479, a Betulinic Acid Derivative, Ameliorates Experimental Autoimmune Encephalomyelitis by Regulating the T Helper 17/Regulatory T Cell Balance. *Mol. Pharmacol.* **2017**, *91*, 464–474. [[CrossRef](#)]
- Martín, R.; Cordova, C.; Román, J.S.; Gutierrez, B.; Cachofeiro, V.; Nieto, M. Oleanolic acid modulates the immune-inflammatory response in mice with experimental autoimmune myocarditis and protects from cardiac injury. Therapeutic implications for the human disease. *J. Mol. Cell. Cardiol.* **2014**, *72*, 250–262. [[CrossRef](#)] [[PubMed](#)]
- Kim, M.; Lee, S.; Lim, H.; Lee, J.; Park, J.-Y.; Kwon, H.-J.; Lee, I.-C.; Ryu, Y.-B.; Kim, J.; Shin, T.; et al. Oleanolic Acid Acetate Alleviates Symptoms of Experimental Autoimmune Encephalomyelitis in Mice by Regulating Toll-Like Receptor 2 Signaling. *Front. Pharmacol.* **2020**, *11*, 556391. [[CrossRef](#)] [[PubMed](#)]
- Fitzpatrick, L.R.; Stonesifer, E.; Small, J.S.; Liby, K.T. The synthetic triterpenoid (CDDO-Im) inhibits STAT3, as well as IL-17, and improves DSS-induced colitis in mice. *Inflammopharmacology* **2014**, *22*, 341–349. [[CrossRef](#)] [[PubMed](#)]
- Rali, S.; Oyedeji, O.O.; Aremu, O.O.; Oyedeji, A.; Nkeh-Chungag, B.N. Semisynthesis of Derivatives of Oleanolic Acid from *Syzygium aromaticum* and Their Antinociceptive and Anti-Inflammatory Properties. *Mediat. Inflamm.* **2016**, *2016*, 1–9. [[CrossRef](#)]
- Nkeh-Chungag, B.N.; Oyedeji, O.O.; Oyedeji, A.; Ndebia, E.J. Anti-Inflammatory and Membrane-Stabilizing Properties of Two Semisynthetic Derivatives of Oleanolic Acid. *Inflammation* **2015**, *38*, 61–69. [[CrossRef](#)] [[PubMed](#)]
- Stiti, N.; Triki, S.; Hartmann, M.-A. Formation of Triterpenoids throughout *Olea europaea* Fruit Ontogeny. *Lipids* **2007**, *42*, 55–67. [[CrossRef](#)]
- Pérez-Camino, M.C.; Cert, A. Quantitative determination of hydroxy pentacyclic triterpene acids in vegetable oils. *J. Agric. Food Chem.* **1999**, *47*, 1558–1562. [[CrossRef](#)]
- Martínez, A.; Perojil, A.; Rivas, F.; Parra, A.; Garcia-Granados, A.; Fernandez-Vivas, A. Biotransformation of oleanolic and maslinic methyl esters by *Rhizomucor miehei* CECT 2749. *Phytochemistry* **2015**, *117*, 500–508. [[CrossRef](#)]
- Zukancic, D.; Suys, E.J.A.; Pilkington, E.H.; Algarni, A.; Al-Wassiti, H.; Truong, N.P. The Importance of Poly(ethylene glycol) and Lipid Structure in Targeted Gene Delivery to Lymph Nodes by Lipid Nanoparticles. *Pharmaceutics* **2020**, *12*, 1068. [[CrossRef](#)] [[PubMed](#)]
- Medina-O'Donnell, M.; Rivas, F.; Reyes-Zurita, F.J.; Martínez, A.; Lupiañez, J.A.; Parra, A. Diamine and PEGylated-diamine conjugates of triterpenic acids as potential anticancer agents. *Eur. J. Med. Chem.* **2018**, *148*, 325–336. [[CrossRef](#)] [[PubMed](#)]
- Medina-O'Donnell, M.; Rivas, F.; Reyes-Zurita, F.J.; Martínez, A.; Galisteo-González, F.; Lupiañez, J.A.; Parra, A. Synthesis and in vitro antiproliferative evaluation of PEGylated triterpene acids. *Fitoterapia* **2017**, *120*, 25–40. [[CrossRef](#)] [[PubMed](#)]
- O'Donnell, M.M.; Rivas, F.; Reyes-Zurita, F.J.; Martínez, A.; Martín-Fonseca, S.; Garcia-Granados, A.; Ferrer-Martín, R.M.; Lupiañez, J.A.; Parra, A. Semi-synthesis and antiproliferative evaluation of PEGylated pentacyclic triterpenes. *Eur. J. Med. Chem.* **2016**, *118*, 64–78. [[CrossRef](#)]
- Jannus, F.; Medina-O'Donnell, M.; Rivas, F.; Díaz-Ruiz, L.; Rufino-Palomares, E.E.; Lupiañez, J.A.; Parra, A.; Reyes-Zurita, F.J. A Diamine-PEGylated Oleanolic Acid Derivative Induced Efficient Apoptosis through a Death Receptor and Mitochondrial Apoptotic Pathway in HepG2 Human Hepatoma Cells. *Biomolecules* **2020**, *10*, 1375. [[CrossRef](#)] [[PubMed](#)]
- Bondar, T.; Medzhitov, R. The Origins of Tumor-Promoting Inflammation. *Cancer Cell* **2013**, *24*, 143–144. [[CrossRef](#)] [[PubMed](#)]
- Steelman, L.S.; Pohnert, S.C.; Shelton, J.G.; Franklin, R.A.; Bertrand, F.E.; McCubrey, J.A. JAK/STAT, Raf/MEK/ERK, PI3K/Akt and BCR-ABL in cell cycle progression and leukemogenesis. *Leukemia* **2004**, *18*, 189–218. [[CrossRef](#)]
- Lee, S.; Shin, S.; Kim, H.; Han, S.; Kim, K.; Kwon, J.; Kwak, J.-H.; Lee, C.-K.; Ha, N.-J.; Yim, D.; et al. Anti-inflammatory function of arctiin by inhibiting COX-2 expression via NF- κ B pathways. *J. Inflamm.* **2011**, *8*, 16. [[CrossRef](#)]
- Wang, A.; Al-Kuhlani, M.; Johnston, S.C.; Ojcius, D.; Chou, J.; Dean, D. Transcription factor complex AP-1 mediates inflammation initiated by *Chlamydia pneumoniae* infection. *Cell. Microbiol.* **2013**, *15*, 779–794. [[CrossRef](#)] [[PubMed](#)]
- Kawahara, K.; Hohjoh, H.; Inazumi, T.; Tsuchiya, S.; Sugimoto, Y. Prostaglandin E2-induced inflammation: Relevance of prostaglandin E receptors. *Biochim. Biophys. Acta (BBA) Mol. Cell Biol. Lipids* **2015**, *1851*, 414–421. [[CrossRef](#)] [[PubMed](#)]
- Salvemini, D.; Kim, S.F.; Mollace, V. Reciprocal regulation of the nitric oxide and cyclooxygenase pathway in pathophysiology: Relevance and clinical implications. *Am. J. Physiol. Integr. Comp. Physiol.* **2013**, *304*, R473–R487. [[CrossRef](#)] [[PubMed](#)]

24. Gábor, M. Models of Acute Inflammation in the Ear. *Inflamm. Protoc.* **2003**, *225*, 129–138. [[CrossRef](#)]
25. Lee, S.H.; Kim, D.W.; Eom, S.A.; Jun, S.-Y.; Park, M.-Y.; Kim, D.-S.; Kwon, H.J.; Kwon, H.Y.; Han, K.H.; Park, J.-S.; et al. Suppression of 12-O-tetradecanoylphorbol-13-acetate (TPA)-induced skin inflammation in mice by transduced Tat-Annexin protein. *BMB Rep.* **2012**, *45*, 354–359. [[CrossRef](#)] [[PubMed](#)]
26. Furman, D.; Campisi, J.; Verdin, E.; Carrera-Bastos, P.; Targ, S.; Franceschi, C.; Ferrucci, L.; Gilroy, D.W.; Fasano, A.; Miller, G.W.; et al. Chronic inflammation in the etiology of disease across the life span. *Nat. Med.* **2019**, *25*, 1822–1832. [[CrossRef](#)] [[PubMed](#)]
27. Zappavigna, S.; Cossu, A.M.; Grimaldi, A.; Bocchetti, M.; Ferraro, G.A.; Nicoletti, G.F.; Filosa, R.; Caraglia, M. Anti-Inflammatory Drugs as Anticancer Agents. *Int. J. Mol. Sci.* **2020**, *21*, 2605. [[CrossRef](#)]
28. Ayeleso, T.B.; Matumba, M.G.; Mukwevho, E. Oleanolic Acid and Its Derivatives: Biological Activities and Therapeutic Potential in Chronic Diseases. *Molecules* **2017**, *22*, 1915. [[CrossRef](#)] [[PubMed](#)]
29. Laskin, D.L. Macrophages and Inflammatory Mediators in Chemical Toxicity: A Battle of Forces. *Chem. Res. Toxicol.* **2009**, *22*, 1376–1385. [[CrossRef](#)] [[PubMed](#)]
30. Kang, S.-R.; Han, D.-Y.; Park, K.-I.; Park, H.-S.; Cho, Y.-B.; Lee, H.-J.; Lee, W.-S.; Ryu, C.H.; Ha, Y.L.; Lee, D.H.; et al. Suppressive Effect on Lipopolysaccharide-Induced Proinflammatory Mediators by Citrus aurantium L. in Macrophage RAW 264.7 Cells via NF- κ B Signal Pathway. *Evid.-Based Complement. Altern. Med.* **2011**, *2011*, 1–12. [[CrossRef](#)]
31. McWhorter, F.; Wang, T.; Nguyen, P.; Chung, T.; Liu, W.F. Modulation of macrophage phenotype by cell shape. *Proc. Natl. Acad. Sci. USA* **2013**, *110*, 17253–17258. [[CrossRef](#)]
32. Tseng, H.-Y.; Wu, S.-H.; Huang, W.-H.; Wang, S.-F.; Yang, Y.-N.; Mahindroo, N.; Hsu, T.; Jiaang, W.-T.; Lee, S.-J. Benzothiazolium compounds: Novel classes of inhibitors that suppress the nitric oxide production in RAW264.7 cells stimulated by LPS/IFN γ . *Bioorg. Med. Chem. Lett.* **2005**, *15*, 2027–2032. [[CrossRef](#)] [[PubMed](#)]
33. Fang, L.; Wang, K.-K.; Huang, Q.; Cheng, F.; Huang, F.; Liu, W.-W. Nucleolin Mediates LPS-induced Expression of Inflammatory Mediators and Activation of Signaling Pathways. *Curr. Med. Sci.* **2020**, *40*, 646–653. [[CrossRef](#)]
34. Mori, T.; Miyamoto, T.; Yoshida, H.; Asakawa, M.; Kawasumi, M.; Kobayashi, T.; Morioka, H.; Chiba, K.; Toyama, Y.; Yoshimura, A. IL-1 and TNF-initiated IL-6-STAT3 pathway is critical in mediating inflammatory cytokines and RANKL expression in inflammatory arthritis. *Int. Immunol.* **2011**, *23*, 701–712. [[CrossRef](#)]
35. Checker, R.; Sandur, S.K.; Sharma, D.; Patwardhan, R.S.; Jayakumar, S.; Kohli, V.; Sethi, G.; Aggarwal, B.B.; Sainis, K.B. Potent Anti-Inflammatory Activity of Ursolic Acid, a Triterpenoid Antioxidant, Is Mediated through Suppression of NF- κ B, AP-1 and NF-AT. *PLoS ONE* **2012**, *7*, e31318. [[CrossRef](#)]
36. Dong, N.; Xue, C.; Zhang, L.; Zhang, T.; Wang, C.; Bi, C.; Shan, A. Oleanolic acid enhances tight junctions and ameliorates inflammation in Salmonella typhimurium-induced diarrhea in mice via the TLR4/NF- κ B and MAPK pathway. *Food Funct.* **2020**, *11*, 1122–1132. [[CrossRef](#)] [[PubMed](#)]
37. Jin, J.; He, H.; Zhang, X.; Wu, R.; Gan, L.; Li, D.; Lu, Y.; Wu, P.; Wong, W.-L.; Zhang, K. The in vitro and in vivo study of oleanolic acid indole derivatives as novel anti-inflammatory agents: Synthesis, biological evaluation, and mechanistic analysis. *Bioorganic Chem.* **2021**, *113*, 104981. [[CrossRef](#)]
38. Fernández, M.A.; Heras, B.D.L.; Garcia-Gimenez, M.D.; Sáenz, M.T.; Villar, A. New insights into the mechanism of action of the anti-inflammatory triterpene lupeol. *J. Pharm. Pharmacol.* **2001**, *53*, 1533–1539. [[CrossRef](#)]
39. Huang, L.; Guan, T.; Qian, Y.; Huang, M.; Tang, X.; Li, Y.; Sun, H. Anti-inflammatory effects of maslinic acid, a natural triterpene, in cultured cortical astrocytes via suppression of nuclear factor-kappa B. *Eur. J. Pharmacol.* **2011**, *672*, 169–174. [[CrossRef](#)] [[PubMed](#)]
40. Reyes-Zurita, F.J.; Pachón-Peña, G.; Lizárraga, D.; Rufino-Palomares, E.E.; Cascante, M.; Lupiáñez, J.A. The natural triterpene maslinic acid induces apoptosis in HT29 colon cancer cells by a JNK-p53-dependent mechanism. *BMC Cancer* **2011**, *11*, 154. [[CrossRef](#)] [[PubMed](#)]
41. Sánchez-Tena, S.; Reyes-Zurita, F.J.; Diaz-Moralli, S.; Vinardell, M.P.; Reed, M.; Garcia-Garcia, F.; Dopazo, J.; Lupiáñez, J.A.; Günther, U.; Cascante, M. Maslinic Acid-Enriched Diet Decreases Intestinal Tumorigenesis in ApcMin/+ Mice through Transcriptomic and Metabolomic Reprogramming. *PLoS ONE* **2013**, *8*, e59392. [[CrossRef](#)] [[PubMed](#)]
42. Kang, G.-D.; Lim, S.; Kim, D.-H. Oleanolic acid ameliorates dextran sodium sulfate-induced colitis in mice by restoring the balance of Th17/Treg cells and inhibiting NF- κ B signaling pathway. *Int. Immunopharmacol.* **2015**, *29*, 393–400. [[CrossRef](#)] [[PubMed](#)]
43. Dinh, C.H.L.; Yu, Y.; Szabo, A.; Zhang, Q.; Zhang, P.; Huang, X.-F. Bardoxolone Methyl Prevents High-Fat Diet-Induced Colon Inflammation in Mice. *J. Histochem. Cytochem.* **2016**, *64*, 237–255. [[CrossRef](#)]
44. Ahmad, S.F.; Ansari, M.A.; Zoheir, K.; Bakheet, S.A.; Korashy, H.M.; Nadeem, A.; Ashour, A.E.; Attia, S.M. Regulation of TNF- α and NF- κ B activation through the JAK/STAT signaling pathway downstream of histamine 4 receptor in a rat model of LPS-induced joint inflammation. *Immunobiol.* **2015**, *220*, 889–898. [[CrossRef](#)] [[PubMed](#)]
45. Kim, S.F.; Huri, D.A.; Snyder, S.H. Inducible Nitric Oxide Synthase Binds, S-Nitrosylates, and Activates Cyclooxygenase-2. *Science* **2005**, *310*, 1966–1970. [[CrossRef](#)] [[PubMed](#)]
46. Kao, E.-S.; Wang, C.-J.; Lin, W.-L.; Yin, Y.-F.; Wang, C.-P.; Tseng, T.-H. Anti-inflammatory Potential of Flavonoid Contents from Dried Fruit of Crataegus pinnatifida in Vitro and in Vivo. *J. Agric. Food Chem.* **2005**, *53*, 430–436. [[CrossRef](#)]
47. Li, H.-J.; Wu, N.-L.; Lee, G.-A.; Hung, C.-F. The Therapeutic Potential and Molecular Mechanism of Isoflavone Extract against Psoriasis. *Sci. Rep.* **2018**, *8*, 6335. [[CrossRef](#)]

48. Medeiros, R.; Otuki, M.; Avellar, M.C.W.; Calixto, J.B. Mechanisms underlying the inhibitory actions of the pentacyclic triterpene α -amyrin in the mouse skin inflammation induced by phorbol ester 12-O-tetradecanoylphorbol-13-acetate. *Eur. J. Pharmacol.* **2007**, *559*, 227–235. [[CrossRef](#)]
49. Vasconcelos, J.; Teixeira, M.; Filho, J.M.B.; Lúcio, A.; Almeida, J.; de Queiroz, L.P.; Ribeiro-Dos-Santos, R.; Soares, M. The triterpenoid lupeol attenuates allergic airway inflammation in a murine model. *Int. Immunopharmacol.* **2008**, *8*, 1216–1221. [[CrossRef](#)]
50. Geetha, T.; Varalakshmi, P. Anticomplement activity of triterpenes from *Crataeva nurvala* stem bark in adjuvant arthritis in rats. *Gen. Pharmacol. Vasc. Syst.* **1999**, *32*, 495–497. [[CrossRef](#)]
51. Abel, E.; Angel, J.M.; Kiguchi, K.; DiGiovanni, J. Multi-stage chemical carcinogenesis in mouse skin: Fundamentals and applications. *Nat. Protoc.* **2009**, *4*, 1350–1362. [[CrossRef](#)] [[PubMed](#)]
52. Chiocchio, I.; Prata, C.; Mandrone, M.; Ricciardiello, F.; Marrazzo, P.; Tomasi, P.; Angeloni, C.; Fiorentini, D.; Malaguti, M.; Poli, F.; et al. Leaves and Spiny Burs of *Castanea Sativa* from an Experimental Chestnut Grove: Metabolomic Analysis and Anti-Neuroinflammatory Activity. *Metabolites* **2020**, *10*, 408. [[CrossRef](#)] [[PubMed](#)]

4.3. Publicación 3

Diclofenac N-Derivatives as Therapeutic Agents with Anti-Inflammatory and Anti-Cancer Effect

Autores: Galisteo, A.; Jannus, F.; García-García, A.; Aheget, H.; Rojas, S.; Lupiañez, J.; Rodríguez-Diéguez, A.; Reyes-Zurita, F.J.*; del Moral, J.Q.*

Revista: International Journal of Molecular Sciences

Año: 2021

Volumen: 22 (10)

DOI: [10.3390/ijms22105067](https://doi.org/10.3390/ijms22105067)

Índice de impacto: 6,208
(JCR 2022)

Cuartil: *Biochemistry & Molecular Biology*: Q1 (69/296)

Citas: 5 (25 July 2022)
(Semantic Scholar)



Article

Diclofenac N-Derivatives as Therapeutic Agents with Anti-Inflammatory and Anti-Cancer Effect

Alberto Galisteo ¹, Fatin Jannus ², Amalia García-García ³, Houssam Aheget ⁴, Sara Rojas ³, José A. Lupiañez ², Antonio Rodríguez-Diéguez ³, Fernando J. Reyes-Zurita ^{2,*}, and José F. Quílez del Moral ^{1,*}

¹ Department of Organic Chemistry, Institute of Biotechnology, University of Granada, 18071 Granada, Spain; albertogapre@ugr.es

² Department of Biochemistry and Molecular Biology, University of Granada, C/Severo Ochoa s/n, 18071 Granada, Spain; fatin@correo.ugr.es (F.J.); jlcara@ugr.es (J.A.L.)

³ Department of Inorganic Chemistry, University of Granada, C/Severo Ochoa s/n, 18071 Granada, Spain; amaliagarcia@correo.ugr.es (A.G.-G.); srojas@ugr.es (S.R.); antonio5@ugr.es (A.R.-D.)

⁴ Centre for Genomics and Oncological Research, GENYO, C/Health Sciences Technology Park, Av. de la Ilustración 114, 18016 Granada, Spain; houssam.aheget@genyo.es

* Correspondence: ferjes@ugr.es (F.J.R.-Z.); jfquilez@ugr.es (J.F.Q.d.M.); Tel.: +34-958243252 (F.J.R.-Z.); +34-958243185 (J.F.Q.d.M.)



Citation: Galisteo, A.; Jannus, F.; García-García, A.; Aheget, H.; Rojas, S.; Lupiañez, J.A.; Rodríguez-Diéguez, A.; Reyes-Zurita, F.J.; Quílez del Moral, J.F. Diclofenac N-Derivatives as Therapeutic Agents with Anti-Inflammatory and Anti-Cancer Effect. *Int. J. Mol. Sci.* **2021**, *22*, 5067. <https://doi.org/10.3390/ijms22105067>

Academic Editor: Alexander Shtil

Received: 24 April 2021

Accepted: 8 May 2021

Published: 11 May 2021

Publisher's Note: MDPI stays neutral with regard to jurisdictional claims in published maps and institutional affiliations.



Copyright: © 2021 by the authors. Licensee MDPI, Basel, Switzerland. This article is an open access article distributed under the terms and conditions of the Creative Commons Attribution (CC BY) license (<https://creativecommons.org/licenses/by/4.0/>).

Abstract: A series of diclofenac N-derivatives (**2**, **4**, **6**, **8c**, **9c**, **10a-c**) were synthesized in order to test their anti-cancer and anti-inflammatory effects. The anticarcinogen activity has been assayed against three cancer cell lines: HT29, human colon cancer cells; Hep-G2, human hepatic cells; and B16-F10, murine melanoma cells. First, we determined the cytotoxicity of the different compounds, finding that the most effective compound was compound **8c** against all cell lines and both compounds **4** and **6** in human Hep-G2 and HT29 cell lines. Compounds **4** and **8c** were selected for the percentage of apoptosis determination, cell cycle distribution, and mitochondrial membrane potential measure because these products presented the lowest IC₅₀ values in two of the three cancer cell lines assayed (B16-F10 and HepG2), and were two of the three products with lowest IC₅₀ in HT29 cell line. Moreover, the percentages of apoptosis induction were determined for compounds **4** and **8c**, showing that the highest values were between 30 to 60%. Next, the effects of these two compounds were observed on the cellular cycle, resulting in an increase in the cell population in G2/M cell cycle phase after treatment with product **8c**, whereas compound **4** increased the cells in phase G0/G1, by possible differentiation process induction. Finally, to determine the possible apoptosis mechanism triggered by these compounds, mitochondrial potential was evaluated, indicating the possible activation of extrinsic apoptotic mechanism. On the other hand, we studied the anti-inflammatory effects of these diclofenac (DCF) derivatives on lipopolysaccharide (LPS) activated RAW 264.7 macrophages-murine cells by inhibition of nitric oxide (NO) production. As a first step, we determined the cytotoxicity of the synthesized compounds, as well as DCF, against these cells. Then, sub-cytotoxic concentrations were used to determine NO release at different incubation times. The greatest anti-inflammatory effect was observed for products **2**, **4**, **8c**, **10a**, **10b**, and **9c** at 20 µg·mL⁻¹ concentration after 48 h of treatment, with inhibition of produced NO between 60 to 75%, and a concentration that reduces to the 50% the production of NO (IC₅₀ NO) between 2.5 to 25 times lower than that of DCF. In this work, we synthesized and determined for the first time the anti-cancer and anti-inflammatory potential of eight diclofenac N-derivatives. In agreement with the recent evidences suggesting that inflammation may contribute to all states of tumorigenesis, the development of these new derivatives capable of inducing apoptosis and anti-inflammatory effects at very low concentrations represent new effective therapeutic strategies against these diseases.

Keywords: diclofenac; anticancer activity; anti-inflammatory activity; nitric oxide; drug development

1. Introduction

Non-steroidal anti-inflammatory drugs (NSAID) are compounds that produce anti-inflammatory effects, reducing pain, fever, and inflammation. The main mechanism of action of NSAID is the inhibition of cyclooxygenases (COX-1 and -2), enzymes related to the synthesis of key biological mediators (i.e., prostaglandins) involved in inflammation processes [1]. Particularly, diclofenac (DCF) is a well-known and common NSAID used to treat pain and inflammatory diseases, such as rheumatoid arthritis, post-operative traumatic pain, migraine, or fever. Like other NSAIDs, DCF is believed to work via inhibition of prostaglandin synthesis by blocking both COX-1 and -2. Other anti-inflammatory mechanisms proposed for the action of DCF are the inhibition of the thromboxane-prostanoid receptor, reduction of arachidonic acid release and uptake [2], protection on leukocyte-endothelium interactions, inhibition of lipoxygenase enzymes, and activation of nitric oxide-cGMP (3',5'-cyclic guanosine monophosphate) antinociceptive pathway [1,3]. One example of the activity of DCF is the inhibition of over 93% of the phospholipase A2 enzymes (PLA2) activity, enzyme promoting inflammation via eicosanoids production, and direct activation of pro-inflammatory cells in patients with acute pancreatitis [4].

Recent evidence suggests that inflammatory actions can contribute to all tumorigenesis states [5]. Inflammation is also involved in critical steps of metastasis due to the production of angiogenic factors and cell migration [6]. Particularly, DCF presents an important range of actions, which are of interest in an oncological context, displaying a range of effects on inflammation, immune system response, angiogenic cascade, chemo-sensitivity in tumoral cells, and tumor metabolism. Different molecular mechanisms have been proposed for the anti-cancer action of DCF, some of which are common with other NSAIDs drugs: inhibition of COX-2 and decrease of PGE2 levels. High levels of this PGE2 were found in different types of cancer associated with chronic inflammation, providing a pro-tumor microenvironment [7]. Particularly in processes related to reducing PGE2 synthesis, DCF has shown to delay tumor growth and angiogenesis in BALB/c injected with C-26 adenocarcinoma cells [8] and reduce tumor growth volumes in the murine model [9].

Several *in vitro* and *in vivo* studies have demonstrated the antitumor effect of DCF. DCF inhibited cell growth via apoptosis in different cell lines, such as neuroblastoma cells (half maximal inhibitory concentration, $IC_{50} = 30\text{--}178 \mu\text{g}\cdot\text{mL}^{-1}$) [10], ovarian cancer cells SKOV-3, CAOV-3, SW626 and 36M2 ($IC_{50} = 6\text{--}60 \mu\text{g}\cdot\text{mL}^{-1}$) [11], and HEY and OVACAR-5 ($IC_{50} = 15 \mu\text{g}\cdot\text{mL}^{-1}$) [12], glioblastoma cells HTZ-349, U87MG and A172 ($IC_{50} = 15\text{--}60 \mu\text{g}\cdot\text{mL}^{-1}$) [13], or Hep-G2 cells ($IC_{50} = 50 \mu\text{g}\cdot\text{mL}^{-1}$) [14]. *In vivo* studies have demonstrated that DCF promoted a significant growth inhibitory effect on different tumors, such as C57/BL6 mice inoculated with B16 melanoma cells [15], rats carrying neuroblastoma xenografts SH-SY5Y [16], mice SK-N-AS neuroblastoma cells injected [9], mice with implanted fibrosarcoma [17], or BALB/c and CB6F1 mice [18]. When administered combined with other drugs, such as the anti-angiogenic drug TL-118, DCF induces the partial or complete remission of tumors in mice injected with C-26 adenocarcinoma cells [19], or SK-N-AS neuroblastoma cells [20].

Some *in vitro* reported studies evidenced the pro-apoptotic role of DCF in cancer. For example, it has been demonstrated that DCF induces DNA fragmentation and apoptosis, with caspases activation and cytochrome *c* release, associated with reactive oxygen species (ROS) increase and inhibition of Akt phosphorylation via phosphoinositide-3-kinase (PI3K) in HL-60 leukemia cells [21]. DCF has been shown to promote DNA fragmentation and caspases activation in neuroblastoma cells [10], increase ROS, activation of caspases-9 and -3, and reduce Bcl-2/Bax ratio and cytochrome *c* release in A2058 and SAN melanoma cells [22]. In leukemia cells HL-60, THP-1, and samples of acute myeloid leukemia patients, DCF induced apoptosis through activator protein-1 (AP-1) transcription factors (c-Jun, JunB, and Fra-2), induction of growth arrest and DNA damage-45 α protein (GADD45 α), and activation of c-Jun N-terminal kinase (JNK) [23].

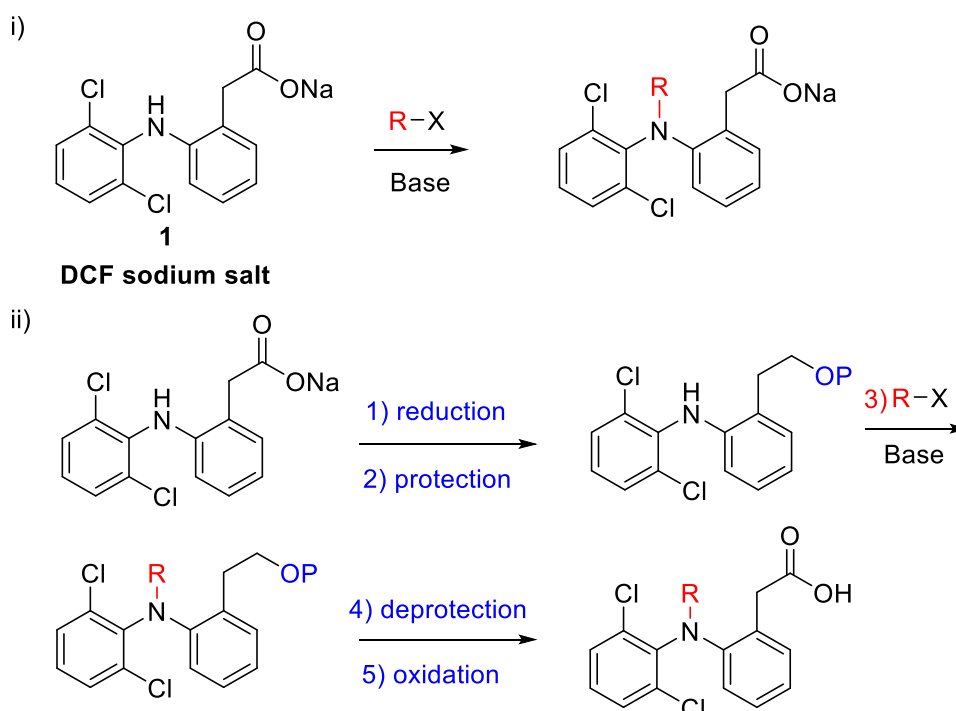
Although DCF has been proved to be an effective analgesic or anti-pyretic in the treatment of cancer-related pain, this drug exhibits limitations and adverse effects towards

gastrointestinal irritation, ulceration, platelet dysfunction, and hepatotoxicity [24]. In this context, we have synthesized a series of DCF N-derivatives with the final aim of improving the biological properties of DCF as an anti-cancer and anti-inflammatory drug. Cytotoxicity studies using three cancer cell lines, namely B16-F10 murine melanoma cells, Hep-G2 hepatoma cells, and HT29 colon cancer cells, demonstrated that six of the as-synthesized compounds (**2**, **4**, **6**, **8c**, **9c**, and **10c**) showed an important improvement in their cytotoxicity activity with regard to DCF, reaching IC_{50} values between 13 to 48 $\mu\text{g}\cdot\text{mL}^{-1}$. Compounds **4** and **8c** were selected, and their apoptosis properties were assayed in Hep-G2 cell line with the percentage of apoptosis between 15 to 60%. In order to determine the plausible apoptotic mechanism of these compounds, the mitochondrial membrane potential was measured. Finally, we investigated the anti-inflammatory properties of synthesized compounds by means of the inflammation process induced in RAW 264.7 macrophages murine cells by bacterial lipopolysaccharide (LPS).

2. Results and Discussion

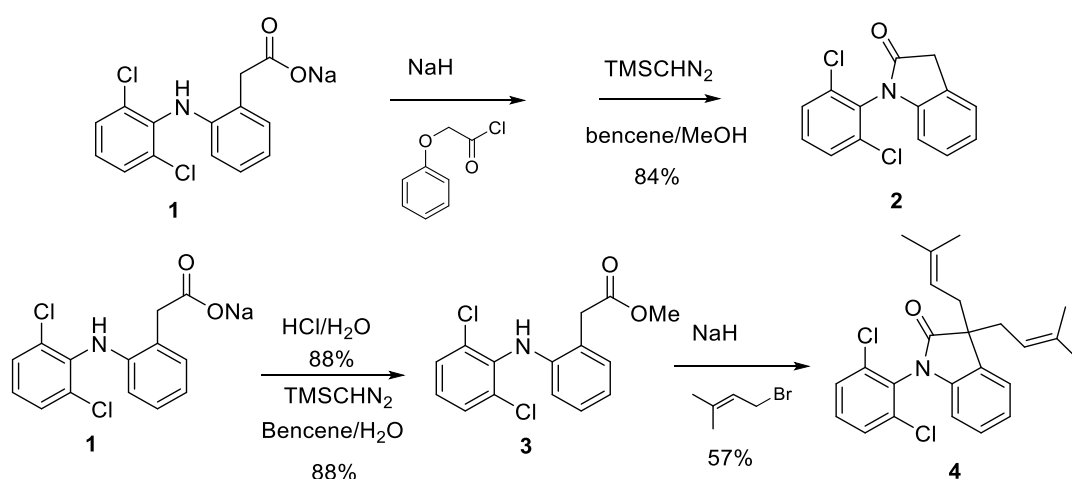
2.1. Synthesis of DCF Derivatives

Although the number of DCF analogs synthesized is overwhelming [25–28], the number of derivatives involving functionalization of the secondary amine of DCF is much more limited [29–37]. Scheme 1 shows the synthetic strategies employed for the synthesis of the DCF N-derivatives.



Scheme 1. Two approaches to DCF N-derivatives.

We first tried the direct functionalization of DCF by reacting its sodium salt (**1**) with different electrophiles in the presence of NaH or K_2CO_3 . Invariably the main reaction product was lactam **2** [38] (Scheme 2). When the corresponding methyl ester (**3**) was used as a starting material and isopentenyl bromide was used as electrophile, the dialkylated lactam **4** was obtained, again via lactam **2** (Scheme 2).



Scheme 2. Synthesis of lactam **2** and its diisopentenyl derivative **4**.

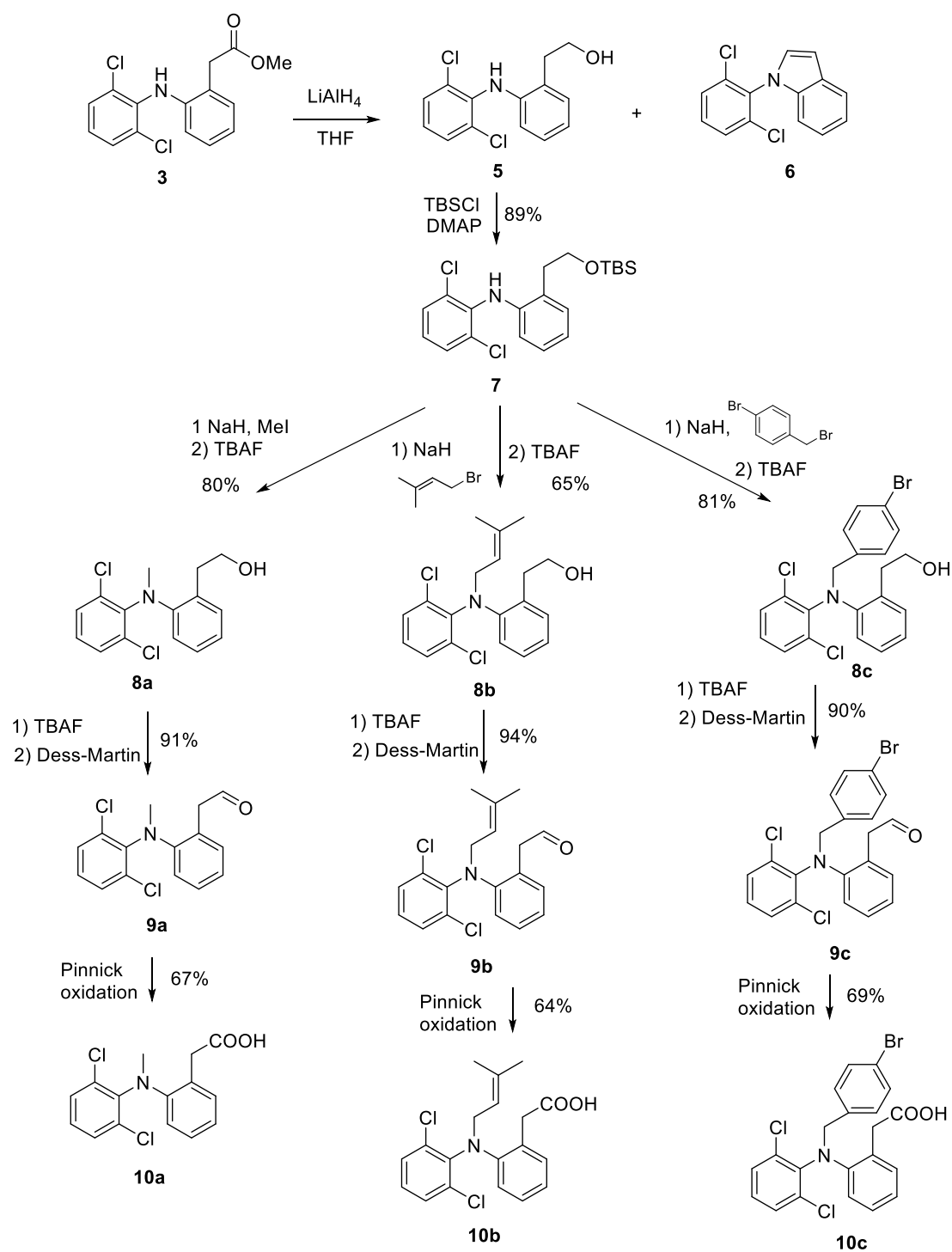
In our second approach, we envisaged that the reduction of the phenylacetic acid of DCF to the corresponding primary alcohol not only would avoid the lactamization side reaction but also would enable the generation of N-functionalized derivatives with different oxidation degree. Following this approach, LAH reduction of methyl ester **3** [39] to obtain alcohol **5** was achieved following the procedure described by Kelly et al. [40]. Together with **5**, variable minor amounts of the previously unreported indol derivative **6** were produced in this reduction (Scheme 3). Nucleophilic attack of the secondary amine to the aldehyde intermediate of the reduction process followed by a loss of water was proposed to rationalize the formation of **6**.

Continuing with our synthetic route, treatment of **5** with tert-butyldimethylsilyl chloride (TBSCl) in the presence of 4-dimethylaminopyridine (DMAP) led uneventfully to silyl derivative **7**. Gratifyingly the N-derivatization proceeds satisfactorily using NaH as a base and isopentenyl bromide, methyl iodide, and benzyl bromide to produce **8a-8c** after tetra-*n*-butylammonium fluoride (TBAF) deprotection of the silyl protecting group. Soft heating to 50 °C was necessary for the reaction to go to completion after approximately 6 h. Finally, the generation of the corresponding aldehyde derivatives was achieved using Dess-martin oxidations [41], whereas the generation of the targeted phenylacetic acids **10a** [37], **10b** and **10c** involved the oxidation the corresponding aldehydes via Pinnick oxidation [42] (Scheme 3).

2.2. Anti-Carcinogenic Activity

2.2.1. Cancer Cells Proliferation Studies

The eight DCF N-derivatives (**2**, **4**, **6**, **8c**, **9c**, **10a-c**) and their precursor (DCF) were assayed on B16-F10 murine melanoma cells, HT29 colon cancer cells, and Hep-G2 hepatoma cells, and IC₅₀ values were determined (Table 1). In addition, we estimated the concentration required for 20 and 80% growth inhibition (IC₂₀ and IC₈₀, respectively). These concentrations were used for the rest of the assays.



Scheme 3. Synthesis of DCF N-derivatives.

Table 1. Growth-inhibitory effects as IC₂₀, IC₅₀, and IC₈₀ (μg·mL⁻¹) values of compounds **2**, **4**, **6**, **8c**, **9c**, **10a-c**, and DCF on the three cancer cell lines B16-F10, Hep-G2, and HT29. The last column represents the ratio between IC₅₀ values of DCF and the corresponding N-derivative.

Cell Line	Compound #	IC ₂₀	IC ₅₀	IC ₈₀	IC ₅₀ of DCF/ IC ₅₀ of Compound
B16-F10	DCF	34.58 ± 8.46	52.45 ± 3.58	83.75 ± 0.54	1.0
	2	21.94 ± 3.44	40.77 ± 1.33	56.59 ± 1.29	1.3
	4	37.15 ± 0.07	37.79 ± 0.17	N/A	1.4
	6	28.22 ± 2.82	45.77 ± 6.46	N/A	1.1
	8c	14.83 ± 3.24	25.55 ± 1.19	42.01 ± 1.59	2.1
	9c	21.19 ± 2.00	27.35 ± 0.14	33.59 ± 1.06	1.9
	10a	26.79 ± 5.11	N/A	N/A	N/A
	10b	6.93 ± 5.48	35.45 ± 4.30	80.98 ± 0.33	1.5
	10c	27.42 ± 6.76	48.20 ± 3.05	63.56 ± 1.19	1.1
	Hep-G2	DCF	32.48 ± 2.51	46.87 ± 0.97	76.87 ± 1.60
2		18.45 ± 0.56	24.53 ± 1.11	35.28 ± 3.91	1.9
4		7.53 ± 3.02	14.56 ± 3.07	33.06 ± 2.07	3.2
6		12.30 ± 1.00	21.58 ± 1.77	52.70 ± 7.38	2.2
8c		12.83 ± 1.12	18.48 ± 1.25	29.74 ± 3.03	2.5
9c		17.62 ± 1.42	28.60 ± 1.75	49.21 ± 4.22	1.6
10a		23.15 ± 8.17	78.93 ± 10.67	146.47 ± 13.76	0.6
10b		40.63 ± 9.57	111.26 ± 16.58	184.08 ± 27.89	0.4
10c		17.41 ± 1.08	21.89 ± 0.90	32.33 ± 3.34	2.1
HT29		DCF	45.27 ± 0.52	52.63 ± 0.54	65.90 ± 2.12
	2	18.56 ± 1.26	28.66 ± 1.91	49.14 ± 6.00	1.8
	4	3.90 ± 4.74	19.80 ± 9.02	173.90 ± 25.19	2.7
	6	7.70 ± 4.60	13.23 ± 4.24	30.53 ± 11.87	4.0
	8c	14.10 ± 1.37	20.65 ± 0.76	30.48 ± 0.66	2.5
	9c	17.94 ± 1.06	24.93 ± 1.21	41.02 ± 3.24	2.1
	10a	62.79 ± 15.01	95.77 ± 7.88	113.61 ± 5.75	0.5
	10b	48.12 ± 2.33	69.52 ± 2.86	96.54 ± 1.50	0.8
	10c	31.10 ± 3.38	69.30 ± 2.36	103.99 ± 0.79	0.8

All tested products showed cytotoxic activity in the conditions assayed (Figure 1A), most of the compounds showed IC₅₀ values between 25 to 48 μg·mL⁻¹ in HT29 cells, 14 to 29 μg·mL⁻¹ in Hep-G2 and HT29 cells. Except for compounds **10a**, **10b**, and **10c**, all synthesized compounds displayed lower IC₅₀ values than DCF (IC₅₀ = 52.5, 46.9, and 52.6 μg·mL⁻¹ against B16-F10, Hep-G2, and HT29 cells, respectively). Particularly, derivatives **8c**, **9c**, **4** and **6** were between two to four times more cytotoxic than their precursor DCF, with IC₅₀ values of 25.6 and 27.4 μg·mL⁻¹ against B16-F10 cells for **8c** and **9c**, 18.5 and 14.6 μg·mL⁻¹ against Hep-G2 cells for **8c** and **4**, and 19.8 and 13.2 μg·mL⁻¹ against HT29 cells for **4** and **6**, respectively.

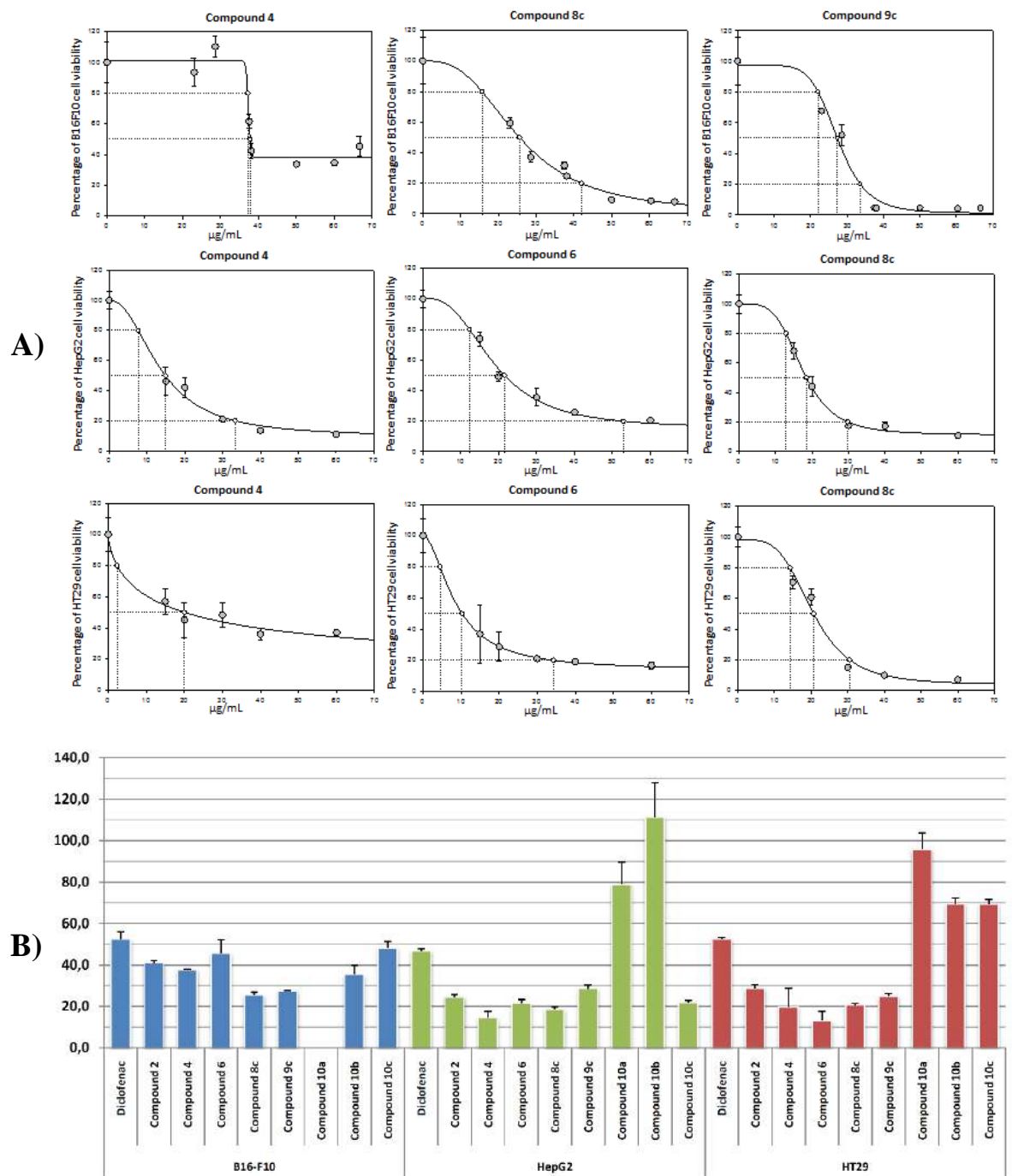


Figure 1. (A) Effects of compounds 4, 8c, and 9c, on the viability of cell B16-F10, and compounds 4, 6, and 8c on cells HT29 and Hep-G2, after treatment for 72 h in a range of 0 to 100 $\mu\text{g}/\text{mL}$. Each point represents the mean value \pm S.D. of at least two independent experiments performed in triplicate. (B) IC_{50} values ($\mu\text{g}\cdot\text{mL}^{-1}$) of compounds 2, 4, 6, 8c, 9c, 10a-c, and DCF on B16-F10, Hep-G2 and HT29 cancer cells.

In general terms, the most effective compound was compound 8c in all cell lines, and compounds 4 and 6 in Hep-G2 and HT29 cells lines, with IC_{20} values between 4 to 21 $\mu\text{g}\cdot\text{mL}^{-1}$, IC_{50} values between 13 to 27 $\mu\text{g}\cdot\text{mL}^{-1}$, and IC_{80} values between 30 to 42 $\mu\text{g}\cdot\text{mL}^{-1}$. These compounds were more effective than DCF in the three lines assayed, being between 1.4 to 2.1 times more cytotoxic than DCF in B16-F10 cells, between 2.2 to 3.2

times in Hep-G2 cells, and between 2.5 to 4.0 times in HT29 cells (Figure 1B). The lowest IC₅₀ values were reached by compound **8c** in B16-F10 cells, compound **4** in Hep-G2 cells, and compound **6** in HT29 colon cancer cells.

Compounds possessing a 2-(2-((4-bromobenzyl)(2,6-dichlorophenyl)amino)phenyl moiety, namely compounds **8c**, **9c** and **10c**, showed good results in the cytotoxicity induced in the three cell lines, except for compound **10c** in HT29 cells. Compound **10b** resulted in being the least cytotoxic compound in the three cell lines assayed. Compounds with indolin substituent, **2**, **4**, and **6**, also presented good results in all cell lines assayed. Finally, compound **10a** did not induce cytotoxicity in the lines assayed. These effects could be related to a rise of the polarity of the complete molecule, without increasing the molecular weight or molecular volume, since probably most of these products performed their biological activity through the cellular membrane, which is prevented by excessively large molecular volumes.

A limited number of articles have been found describing the anti-cancer potential of N derivatives of diclofenac. Thus, the cytotoxicity of the several oxadiazole DCF derivatives was analyzed in NIH 3T3 fibroblast cells. The oxadiazole derivative of diclofenac showed a value of IC₅₀ = 32,0 ± 0,6 µg/mL, whereas the phenacyl derivative of 1,3,4-oxadiazole diclofenac showed an IC₅₀ = 76,7 ± 6,0 µg/mL [43].

Compounds **4** and **8c** were selected since they showed the lowest IC₅₀ values in two out of the three cancer cell lines assayed (B16-F10 and HepG2), and were two of the three products with lowest IC₅₀ in HT29 cell line. Compound **6** was not chosen because it showed a low IC₅₀ value in HT29 cell line, and this value is very similar to that found for compound **4** in HepG2 cells. These products were selected for the percentage of apoptosis determination, cell cycle distribution, and mitochondrial membrane potential measure. All these assays were realized in HepG2 hepatoma cell line by flow cytometry analysis in a fluorescence-activated cell sorter.

2.2.2. Characterization of Apoptotic Effects

The two compounds assayed, **4** and **8c**, showed clearly apoptotic effects in treated cells, with total apoptosis between 30 and 57% at IC₅₀ concentrations and between 15 to 35% at IC₈₀ concentrations for products **8c** and **4**, respectively (Figure 2). The high percentage of necrosis (15%) for compound **8c** could be explained by a possible faster induction of apoptosis in response to product **8c**, and it could be related to the increase of the cell population in G2/M phase, as a consequence of apoptosis mechanism activation.

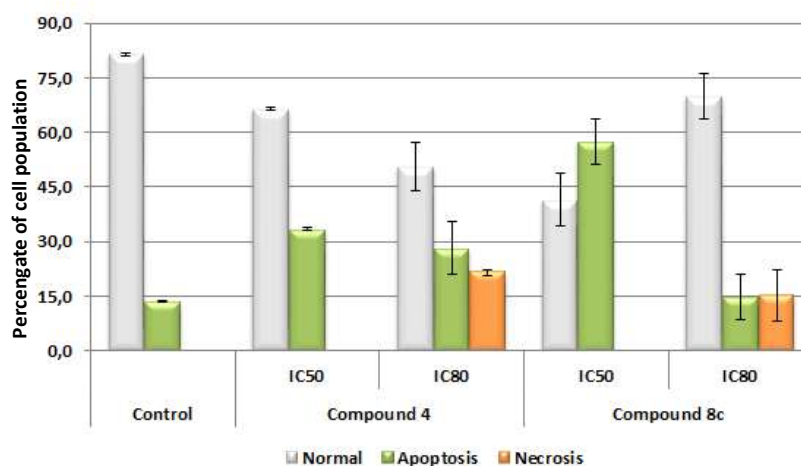


Figure 2. Flow cytometry results after exposure of Hep-G2 cells to DCF and the derivatives **4** and **8c** for 72 h at IC₅₀ and IC₈₀ concentrations. Apoptotic cells (green bars) were positive in annexin V, necrotic cells (orange bars) were positive in propidium iodide. Values are expressed as means ± S.E.M. of at least two experiments in duplicate.

2.2.3. Cell Cycle Arrest and Distribution

Further, we have investigated the effect of compounds **4** and **8c** on cell-cycle distribution in order to determine the possible cytostatic effects related to the cytotoxic response. Hep-G2 cells were treated with the selected products **4** and **8c** at both IC₅₀ and IC₈₀ concentrations. Flow cytometry was used to measure DNA ploidy as well as alterations in cell-cycle profiles (see the experimental section for further details). DNA histogram analysis (Figure 3) revealed that treatment with compound **8c** with both concentrations (IC₅₀ and IC₈₀) increase cell population at the G2/M phase compared with untreated control cells. This phenomenon might be a consequence of apoptosis induction, with an increase of 21% of cells in this cell cycle phase. On the other hand, treatment with product **4** produced an important increase in G0/G1 phase at IC₈₀ concentration, reaching 100% of cells in this cell cycle phase. In this case, this high value could be due to a possible differentiation process activated in response to product **4**. Future assays will be necessary to confirm this point.

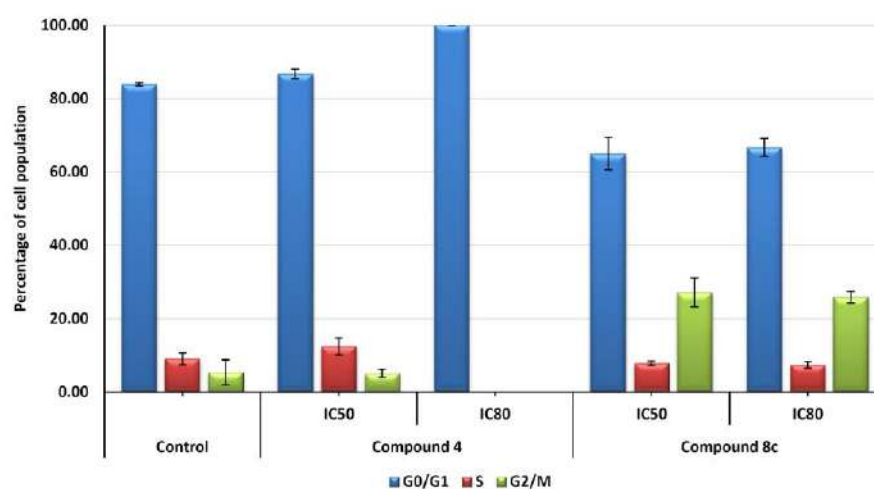


Figure 3. Cell-cycle phase representation (%) with respect to untreated control cells. Hep-G2 cells were treated with compounds **4** and **8c** for 72 h at IC₅₀ and IC₈₀ concentrations. Cells in the G0/G1 phase (blue bars), S phase (orange bars), and G2/M phase (green bars) were counted. Values represent means \pm S.E.M. of at least two independent experiments performed in triplicate.

2.3. Effects on Changes in Mitochondrial Membrane Potential

The treatment with both compounds **4** and **8c** produced changes in the mitochondrial membrane potential (MMP, Figure 4). For compound **8c** at concentrations IC₅₀ and IC₈₀, 35 and 75% of cells lost MMP (Rh123 negative). Regarding compound **4**, there were practically no changes with respect to untreated control cells at IC₅₀ concentration. However, at IC₈₀ concentration, the percentage of cells with loss of MMP was about 60%.

These results are in agreement with those found in the apoptosis and cell cycle analysis. In both cases, the treatment produced apoptosis without loss of MMP at IC₅₀ concentration, probably due to the activation of the extrinsic apoptosis mechanism. At IC₈₀ concentration, both products produced the loss of MMP, probably because of the secondary activation of the intrinsic apoptotic pathway. The loss of MMP was faster in response to compound **8c** than to compound **4**, as showed the percentage of cells with loss of MMP at IC₅₀ and IC₈₀ concentrations, which agreed with the results of apoptosis and cell cycle obtained previously.

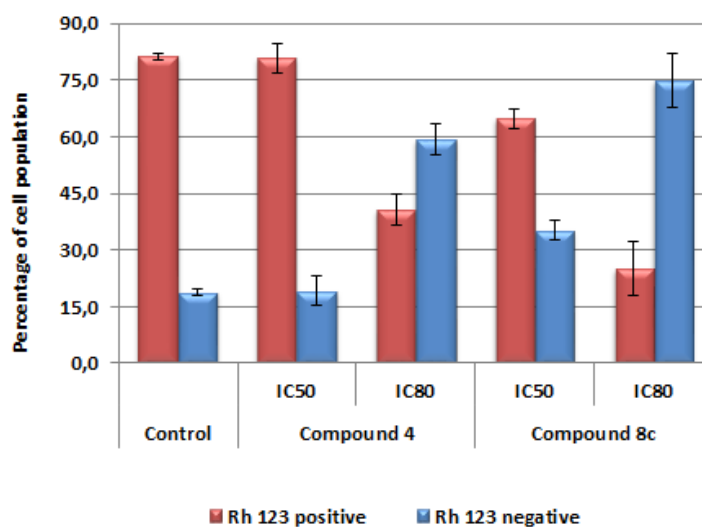


Figure 4. Flow-cytometry analysis of Rh123 staining after exposure of Hep-G2 cells to compounds 4 and 8c for 72 h at IC₅₀ and IC₈₀ concentrations. Rh123 positive cells (red bars) and Rh123 negative cells (blue bars) were counted. Values are expressed as means \pm S.E.M. of at least two experiments in duplicate.

2.4. Effects DCF N-Derivatives in the Inflammatory Process

Nitric oxide (NO), a molecule mediator in acute or chronic inflammation, is produced by constitutive or inducible nitric oxide synthases (iNOS). Its production is activated in response to pro-inflammatory signals as cytokines such as TNF α (tumor necrosis factor α) or INF- γ (interferon- γ), enterotoxin, or LPS (either bacterial lipopolysaccharide), in macrophages [44]. Here, the decrease of NO concentration has been used as an indirect marker of the inflammatory process [44,45]. In the inflammatory response process, NO is released as an intermediate or second messenger. RAW 264.7 murine macrophage cells are an especially indicated model in anti-inflammatory compounds screening studies since they produce the highest release of NO during the inflammatory response. In this study, the anti-inflammatory potential of DCF N-derivatives was analyzed by measuring nitrites in a cell culture medium since the nitrites concentration is proportional to the NO release. With this purpose, we measured the inhibition in NO production in activated LPS RAW 264.7 macrophage cells.

2.4.1. Raw 264.7 Cell Viability

First, RAW 264.7 cell viability was assayed with compounds 2 [46], 4, 6, 8c, 9c, 10a-c, and DCF to establish sub-cytotoxic concentrations and, thus, to assure that anti-inflammatory effects are a consequence of the anti-inflammatory activity of the compounds rather than their cytotoxicity. The concentration of products required for 50% growth inhibition was determined as previously described for B16-F10, Hep-G2, and HT29 cells (see the experimental section for further details). The results showed similar cytotoxicity for all compounds at the conditions assayed (Table 2). Based on these results, sub-cytotoxic concentrations used in the determination of anti-inflammatory response were set at 5, 10, and 20 $\mu\text{g}\cdot\text{mL}^{-1}$.

Table 2. Growth-inhibitory effects as IC₂₀, IC₅₀, and IC₈₀ (μg·mL⁻¹) values of compounds **2**, **4**, **6**, **8c**, **9c**, **10a-c**, and DCF against RAW 264.7 monocyte/macrophage murine cells. The last column represents the ratio between IC₅₀ of DCF and the IC₅₀ of the derivatives.

Cell line	Comp.	IC ₂₀	IC ₅₀	IC ₈₀	IC ₅₀ of DCF/ IC ₅₀ of Comp.
RAW 264.7	DCF	51.91 ± 0.89	69.00 ± 1.13	90.52 ± 1.85	1.0
	2	26.43 ± 3.68	30.99 ± 0.77	36.36 ± 3.44	2.2
	4	13.87 ± 0.89	17.90 ± 1.31	23.29 ± 2.41	3.9
	6	14.68 ± 1.30	19.08 ± 1.47	25.21 ± 2.27	3.6
	8c	14.01 ± 0.14	16.71 ± 0.47	20.07 ± 1.27	4.1
	9c	20.30 ± 0.83	22.70 ± 1.03	25.50 ± 1.51	3.0
	10a	41.42 ± 7.87	72.92 ± 3.57	95.37 ± 1.23	0.9
	10b	28.56 ± 1.10	35.64 ± 4.83	45.64 ± 12.53	1.9
	10c	35.29 ± 2.83	47.17 ± 3.66	64.92 ± 6.97	1.5

2.4.2. Nitric Oxide Production

Firstly, macrophages RAW 264.7 were activated with LPS for 24 h. After this stimulation period, cells were incubated with compounds **2**, **4**, **6**, **8c**, **9c**, **10a-c**, and DCF for 72 h. Aliquots at different incubation times were taken, and nitrite concentration was determined (see the experimental section for further details). Our results showed that at the concentrations assayed (5, 10, and 20 μg·mL⁻¹), all compounds produced inhibition of NO release higher than DCF with respect to the positive control (only LPS treated control cells, 100% release), except for compounds **6** and **10c** (Figure 5). After 24 h, NO release inhibition between 25 to 30% was achieved when using between 10 and 20 μg·mL⁻¹ of products **2**, **4**, **8c**, **9c**, **10a**, and **10b**, and 5 μg·mL⁻¹ of products **8c**, **9c**, and **10a**. The highest anti-inflammatory effect was reached with 20 μg·mL⁻¹ of compounds **8c** and **10b** at 48 h, with 75% of NO inhibition. Compound **9c** showed the highest NO inhibition (60%) at the lower concentration (5 μg·mL⁻¹). Products **2**, **4**, and **10a** showed an inhibition close to 50% at 10 and 20 μg·mL⁻¹ concentrations. The results obtained at 72 h of incubation were similar to those found at 48 h.

For a complete anti-inflammatory characterization of compounds, we calculated the concentration that reduces to 50% the production of NO (IC₅₀NO) at 48 h of cell incubation (Figure 6A). Our data showed that the IC₅₀NO concentration of compound **9c** (IC₅₀NO = 1.89 ± 0.11 μg·mL⁻¹) was lower than those found for the rest of the compounds. This value was 25 times less than that found for DCF (IC₅₀NO = 47.12 ± 4.85 μg·mL⁻¹). Products **2**, **4**, **8c**, **10a**, and **10b** showed IC₅₀NO values between 10 to 20 μg·mL⁻¹. These data were between 2.5 to 4.5 times more effective than DCF. The IC₅₀NO for compound **10c** was 24.57 ± 0.3 μg·mL⁻¹, the highest found. In summary, all products assayed, except **6**, inhibited the inflammation process produced by LPS in RAW 264.7 murine macrophage-monocyte cells. The greatest anti-inflammatory effects were observed at 48 h of incubation. At 20 μg·mL⁻¹, the products that showed greater inhibition of NO release were compounds **8c**, **9c**, and **10b**. However, according to IC₅₀NO values, the products with greater effectiveness were products **4**, **8c**, and **9c** (Figure 6B).

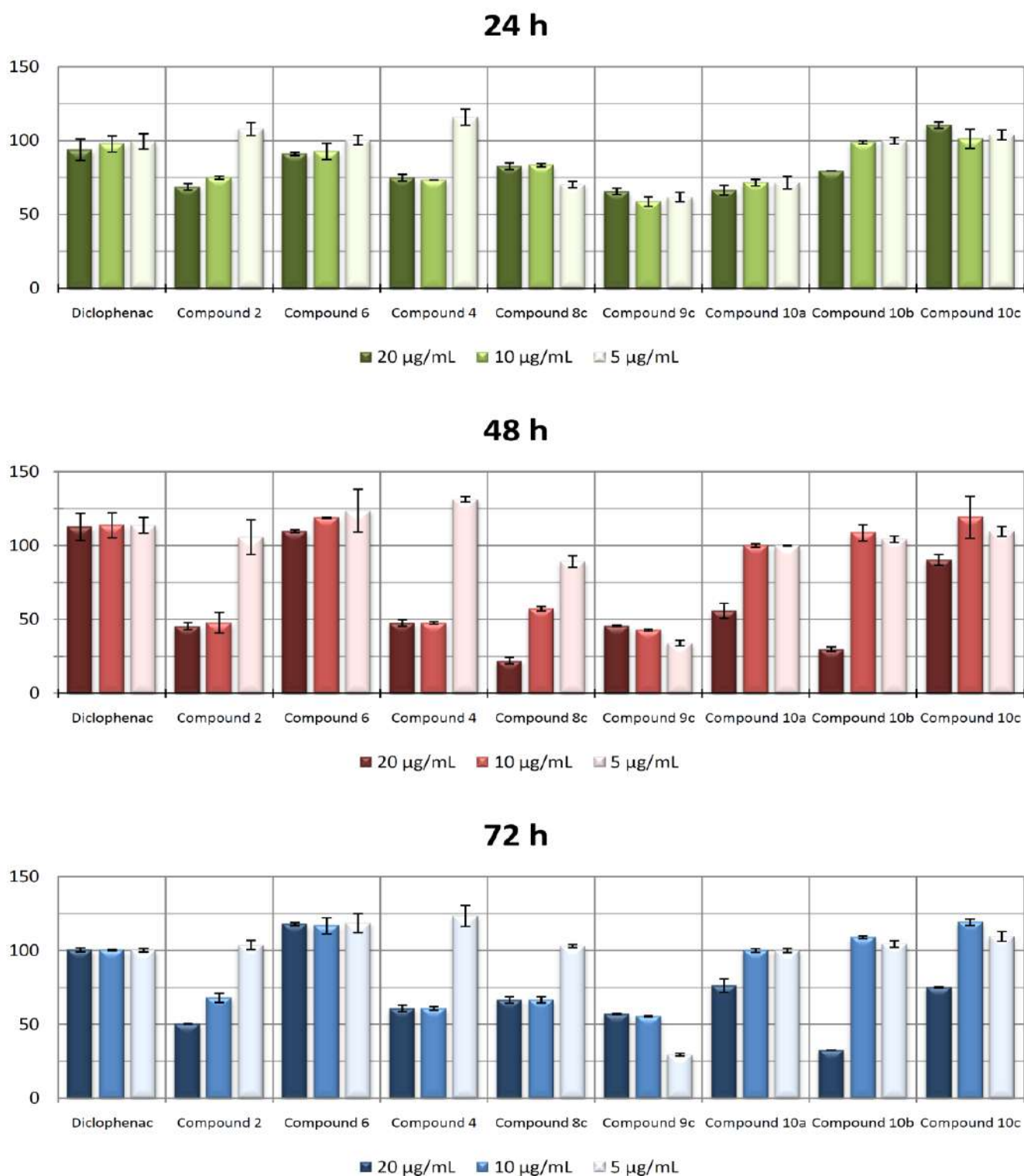


Figure 5. Effect of compounds 2, 4, 6, 8c, 9c, 10a-c, and DCF on the release of nitrites in RAW 264.7 macrophage murine cells. After activation of the inflammatory process, compounds were incubated for 24 h, 48 h, and 72 h at 5, 10, and 20 µg·mL⁻¹ concentrations. The data represent the mean ± S.D. of at least two independent experiments performed in triplicate.

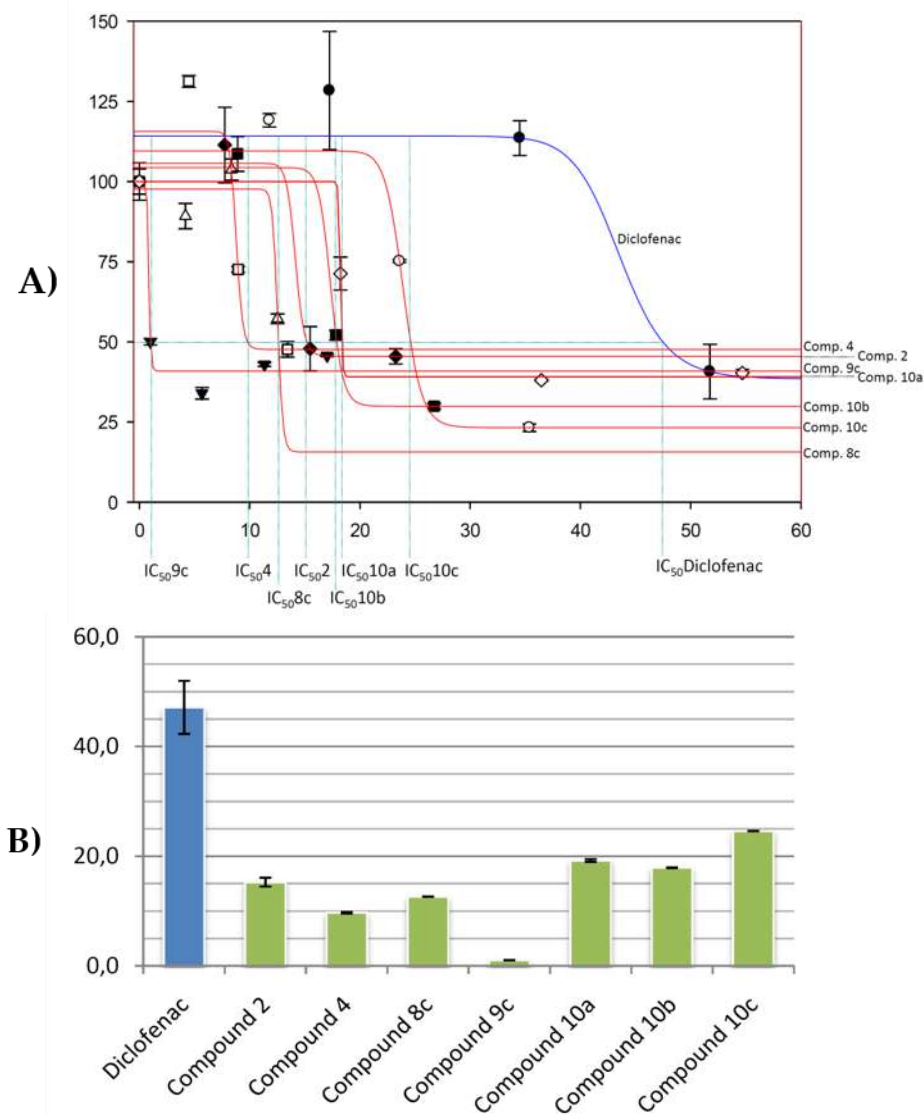


Figure 6. (A). Sigmoidal curves of the effect of compounds 2, 4, 6, 8c, 9c, 10a-c (red) and DCF (blue) on the release of nitrites in RAW 264.7 monocyte/macrophage murine cells activated with LPS. The values corresponding to IC₅₀ NO for each compound can be seen in the curves. The data represent the mean ± S.D. of at least two independent experiments performed in triplicate. (B). NO release-inhibitory effects. IC₅₀ NO µg·mL⁻¹ concentrations for compounds 2, 4, 6, 8c, 9c, 10a-c, and DCF in RAW 264.7 monocyte/macrophage murine cells activated with LPS.

Other DCF derivatives with potent inhibition of NO production have been synthesized, such as a number of oxadiazole derivatives, which presented IC₅₀ NO values ranging from $7,13 \pm 1,0$ µg/mL to $14,8 \pm 2,0$ µg/mL. These results were obtained in LPS stimulated mouse macrophage J774.2 cell line [43]. Additionally, different diclofenac-thiadiazole, diclofenac-triazole, and diclofenac oxadiazole hybrids proved to show moderate to strong anti-inflammatory activity in acute carrageenan-induced paw edema in male adult albino rats, in comparison with DCF [47]. Furthermore, a series S-substituted phenacyl 1,3,4-oxadiazoles and Schiff bases derived from diclofenac were tested in vivo for their anti-inflammatory activity [48]. Eight of these derivatives showed significant anti-inflammatory activity in the carrageenan-induced rat paw edema model.

2.5. Conclusions

The design of new drugs based on proven bioactive products, as DCF, is a new and promising strategy to find new compounds with high and enhanced biochemical prop-

erties. Particularly, the functionalization of the secondary amine in the development of new derivatives has demonstrated to be an efficient strategy to achieve several interesting bioactive compounds. N-derivatives **2**, **4**, **6**, **8c**, **9c**, and **10c** showed an improved cytotoxic effect against B16-F10, Hep-G2, and HT29 cancer cells than pristine DCF. Particularly, compounds **4** and **8c** were found to be the most effective against all cell lines, with IC₅₀ values between 13 to 27 µg·mL⁻¹. The selected compounds, **4** and **8c**, showed clearly apoptotic effects in treated cells, with a total apoptosis between 30 and 57% at IC₅₀ concentrations. DNA histogram analysis revealed that treatment with IC₅₀ concentration of compound **8c** produced an increase in the cell population at the G2/M phase compared with untreated control cells. On the contrary, when using IC₈₀ concentration of product **4**, an important increase of in G0/G1 phase. Further, **8c** was able to produce changes in MMP (35% at IC₅₀). Finally, the results obtained in the anti-inflammatory test showed that the anti-inflammatory response of **2**, **4**, **8c**, **10a**, and **10b** is from 2.5 to 4.5-fold better than DCF. Particularly, among all the tested compounds, after 48 h **4**, **8c** and **9c** (20 µg·mL⁻¹) showed the greater inhibition of NO release. In conclusion, **8c** shows the most encouraging results and could be further exploited for developing new, improved anti-inflammatory and anti-cancer agents.

3. Materials and Methods

3.1. Chemistry

Silica gel 60 (35-70 µm) was used for flash column chromatography. NMR spectra were obtained in a Varian Direct-Drive 600 (¹H 600 MHz/¹³C 150 MHz), Varian Direct-Drive 500 (¹H 500 MHz/¹³C 125 MHz), and Varian Direct-Drive 400 (¹H 400 MHz/¹³C 100 MHz). Accurate mass determinations were performed on a SYNAPT G2-Si Q-TOF mass spectrometer (Waters, Milford, MA, USA) equipped with high-efficiency T-Wave ion mobility and an orthogonal Z-sprayTM electrospray ionization (ESI) source. MassLynx v.4.1 software was used for HRMS instrument control, peak detection, and integration. Reactions were monitored by TLC on 0.25 mm E. Merck silica gel plates (60F-254) visualized under UV light and by applying a phosphomolybdic acid solution in EtOH followed by heat. High-quality reagents were purchased at the highest quality that was commercially available and was used without further purification.

3.2. Synthesis of DCF N-Derivatives

3.2.1. Preparation of DCF from Its Sodium Salt (**1**)

To a heated (50 °C) solution of DCF sodium salt (2 g, 6.76 mmol) in 500 mL of water, 2N HCl solution was added under stirring till pH = 6. The resulting precipitated was filtered to afford an 88% yield of DCF (1.75 g, 5.95 mmol).

3.2.2. Treatment of **1** with Phenoxyacetyl Chloride in the Presence of NaH

To a solution of **1** (200 mg, 0.63 mmol) in 17 mL THF, under an argon atmosphere, was added 50.3 mg of NaH (1.26 mmol). Then, 0.17 mL of phenoxyacetyl chloride (1.26 mmol) were added dropwise. The resulting solution was stirred for 18 h, and then 25 mL of EtOAc were added, followed by 5 mL of saturated NH₄Cl. The aqueous layer was diluted with water (15 mL) and extracted with MTBE (3 × 15 mL). The combined organic layers were washed with brine (3 × 25 mL) dried over anhydrous Na₂SO₄, and concentrated under reduced pressure. The crude product was purified by flash chromatography (H:MTBE, 1:1) to give a 84% yield of compound **2** (151 mg, 0.54 mmol) [38].

Compound 2. ¹H NMR (500 MHz, CDCl₃) δ 7.53 (d, *J* = 8.1 Hz, 2H), 7.39 (dd, *J* = 8.7, 7.6 Hz, 1H), 7.36 (bd, *J* = 7.4 Hz, 1H), 7.23 (td, *J* = 7.7, 1.2 Hz, 1H), 7.12 (td, *J* = 7.5, 1.1 Hz, 1H), 6.43 (dt, *J* = 8.0, 1.0 Hz, 1H), 3.80 (s, 2H) (Figure S1a). ¹³C NMR (125.1 MHz, CDCl₃) δ 173.65 (C), 143.34 (C), 135.52 (2C), 130.87 (CH), 130.48 (C), 129.08 (2CH), 127.97 (CH), 124.87 (CH), 124.32 (C), 123.11 (CH), 109.16 (CH), 35.77 (CH₂) (Figure S1b).

3.2.3. Treatment of DCF (5) with Diazomethane

To a stirred solution of DCF **5** (296 mg, 1.00 mmol) in 4.1 mL of benzene and 1 mL of MeOH, 0.6 mL (1.2 mmol) of a 2 M solution of TMSCH₂N₂ in hexanes were added dropwise. After consumption of the starting product (30 min), the mixture was concentrated under reduced pressure. Purification by flash chromatography (H:MTBE, 4:1) afforded 278 mg (88% yield) of ester **3** (278 mg, 0.9 mmol). The spectroscopic data of compound **3** coincide with those reported in the literature [39].

3.2.4. Treatment of Compound 3 with Isopentenyl Bromide in the Presence of NaH

To a stirred solution of ester **3** (165 mg, 0.53 mmol) in 5 mL THF, under an argon atmosphere, was added 21.2 mg of NaH (0.53 mmol). Then, 0.1 mL of isopentenyl bromide were added dropwise. The resulting solution was stirred for 30 min, and then 15 mL of MTBE were added, followed by 3 mL of saturated NH₄Cl. The aqueous layer was diluted with water (15 mL) and extracted with MTBE (3 × 15 mL). The combined organic layers were washed with brine (3 × 20 mL) dried over anhydrous Na₂SO₄, and concentrated under reduced pressure. The crude product was purified by flash chromatography (H:MTBE, 6:1) to afford 125 mg of compound **4** (0.30 mmol, 57%).

Compound 4. ¹H NMR (500 MHz, CDCl₃) δ 7.50 (d, *J* = 8.1 Hz, 2H), 7.36 (dd, *J* = 8.6, 7.6 Hz, 1H), 7.30 (dd, *J* = 7.4, 0.8 Hz, 1H), 7.19 (td, *J* = 7.7, 1.3 Hz, 1H), 7.10 (td, *J* = 7.5, 1.1 Hz, 1H), 6.37 (dt, *J* = 7.7, 0.8 Hz, 1H), 5.03 (thept, *J* = 7.6, 1.5 Hz, 2H), 2.72 (dd, *J* = 14.2, 8.0 Hz, 2H), 2.64 (dd, *J* = 14.1, 7.0 Hz, 2H), 1.57 (bs, 6H), 1.57 (bs, 6H) (Figure S1d). ¹³C NMR (125.1 MHz, CDCl₃) δ 178.35 (C), 142.01 (C), 135.59 (2C), 134.85 (2C), 131.93 (C), 130.73 (C), 130.41 (CH), 128.99 (2CH), 127.49 (CH), 123.88 (CH), 122.53 (CH), 118.53 (2CH), 108.58 (CH), 53.64 (C), 36.02 (2CH₂), 25.94 (2CH₃), 18.06 (2CH₃) (Figure S1e). HRMS TOF (ESI+) *m/z* calculated for C₂₄H₂₆ClNO [M + H]⁺ 414.1391, found 414.1399.

3.2.5. Reduction of DCF Methyl Ester 3 with Lithium Aluminum Hydride (LAH)

To a solution of DCF methyl ester (**3**) (1 g, 3.4 mmol) in 25 mL THF, cooled at 0 °C and under an argon atmosphere, was added 384 mg of LAH (10 mmol). The resulting solution was stirred for 1 h and then diluted with methyl *tert*-butyl ether (MTBE) (100 mL) and washed with saturated NH₄Cl (15 mL). The aqueous layer was extracted with MTBE (3 × 30 mL). The combined organic layers were washed with brine (3 × 25 mL), dried over anhydrous Na₂SO₄, and concentrated under reduced pressure. Purification by flash chromatography (H:MTBE, 1:1) afforded 190 mg (0.68 mmol, 20%) of compound **6** and 550 mg (1.97 mmol, 58%) of compound **5** [40].

Compound 5: ¹H NMR (600 MHz, CDCl₃) δ 7.36 (d, *J* = 8.1 Hz, 2H), 7.21 (dd, *J* = 7.4, 1.5 Hz, 1H), 7.10 (td, *J* = 7.7, 1.7 Hz, 1H), 7.00 (t, *J* = 8.1 Hz, 1H), 6.96 (td, *J* = 7.4, 1.1 Hz, 1H), 6.51 (dd, *J* = 8.0, 1.1 Hz, 1H), 4.04 (t, *J* = 5.9 Hz, 2H), 3.04 (t, *J* = 5.9 Hz, 2H) (Figure S1g). ¹³C NMR (151 MHz, CDCl₃) δ = 142.64 (C), 137.74 (C), 130.63 (CH), 129.84 (CH), 128.88 (CH), 128.71 (C), 126.99 (CH), 124.03 (CH), 121.62 (C), 116.88 (CH), 64.17 (CH₂), 34.85 (CH₂) (Figure S1h).

Compound 6: ¹H NMR (500 MHz, CDCl₃) δ 7.80 (m, 1H), 7.56 (d, *J* = 8.1 Hz, 2H), 7.40 (t, *J* = 8.1 Hz, 1H), 7.28 (m, 2H), 7.19 (d, *J* = 3.3 Hz, 1H), 7.06–7.01 (m, 1H), 6.84 (d, *J* = 3.4 Hz, 1H) (Figure S1j). ¹³C NMR (125.1 MHz, CDCl₃) δ 136.21 (C), 135.64 (2C), 134.86 (C), 130.09 (CH), 128.95 (2CH), 128.33 (C), 128.06 (CH), 122.60 (CH), 121.15 (CH), 120.58 (CH), 110.29 (CH), 103.87 (CH). HRMS TOF (ESI+) *m/z* calculated for C₁₄H₁₀Cl₂N [M + H]⁺ 262.0190, found 262.0177 (Figure S1k).

3.2.6. Treatment of Alcohol 6 with TBSCl

To a stirred solution of compound **6** (337 mg, 1.2 mmol) in 20 mL of dry dichloromethane (DCM) were added under argon atmosphere 500 mg (4.1 mmol) of 4-(dimethylamino)pyridine (DMAP) and *tert*-butyldimethylsilyl chloride (TBSCl) (328 mg, 2.2 mmol). After consumption of the starting product (45 min), the mixture was diluted with 150 mL of DCM and washed with 1 N HCl (3 × 20 mL), Na₂CO₃ (3 × 30 mL) and brine (3 × 30 mL). The

organic layer was dried over anhydrous Na_2SO_4 and concentrated under reduced pressure. The resulting reaction crude was flash chromatographed (H:MTBE, 5:1) to afford 423 mg (1.1 mmol) of compound **7** (89%).

Compound 7: ^1H NMR (500 MHz, CDCl_3) δ 7.36 (d, $J = 8.1$ Hz, 2H), 7.20 (dd, $J = 7.4$, 1.5 Hz, 1H), 7.07 (td, $J = 7.7$, 1.6 Hz, 1H), 7.01 (t, $J = 8.1$ Hz, 1H), 6.94 (td, $J = 7.4$, 1.2 Hz, 1H), 6.49 (dd, $J = 8.0$, 1.0 Hz, 1H), 3.99 (t, $J = 6.7$ Hz, 2H), 3.01 (t, $J = 6.7$ Hz, 2H), 0.88 (s, 9H), 0.06 (s, 6H) (Figure S1l). ^{13}C NMR (125.1 MHz, CDCl_3) δ 142.21 (C), 137.80 (C), 130.56 (CH), 130.09 (2C), 128.86 (2C), 128.59 (C), 126.78 (CH), 124.17 (CH), 121.60 (CH), 117.04 (CH), 63.91 (CH_2), 35.32 (CH_2), 26.04 (3CH_3), 18.60 (C), -5.22 (2CH_3). HRMS TOF (ESI+) m/z calculated for $\text{C}_{20}\text{H}_{28}\text{Cl}_2\text{NOSi}$ [$\text{M} + \text{H}$] $^+$ 397.1317, found 397.1308 (Figure S1m).

3.2.7. Treatment of Compound **7** with Methyl Iodide in the Presence of NaH: Synthesis of **8a**

To a stirred solution of compound **7** (395 mg, 1 mmol) in 18 mL THF, under an argon atmosphere, was added 75 mg of NaH (3.1 mmol). After stirring for 30 min, 0.15 mL (2.4 mmol) of methyl iodide was added dropwise, and the resulting solution was stirred for 1 h. The mixture was then cooled at 0 °C and diluted with 150 mL of MTBE. Then 5 mL of saturated NH_4Cl were added dropwise. The aqueous layer was diluted with water (15 mL) and extracted with MTBE (3×20 mL). The combined organic layers were washed with brine (3×40 mL) dried over anhydrous Na_2SO_4 , and concentrated under reduced pressure. The resulting crude product was dissolved in 8 mL of dry THF, and 700 mg of TBAF was added to the resulting solution at room temperature and under argon atmosphere. After stirring for 30 min, the reaction mixture was diluted with 150 mL of EtOAc, washed with brine (3×35 mL), dried over anhydrous Na_2SO_4 and concentrated in vacuo. The reaction crude was purified by flash chromatography (H:MTBE, 1:1) to afford 238 mg of compound **8a** (0.8 mmol, 80%).

Compound 8a. ^1H NMR (600 MHz, CDCl_3) δ 7.34 (d, $J = 8.0$ Hz, 2H), 7.25 (td, $J = 7.4$, 1.4 Hz, 1H), 7.21 (dd, $J = 8.2$, 1.4 Hz, 1H), 7.13 (dd, $J = 7.5$, 1.7 Hz, 1H), 7.10 (t, $J = 8.0$ Hz, 1H), 6.98 (td, $J = 7.4$, 1.4 Hz, 1H), 3.55 (t, $J = 6.9$ Hz, 2H), 3.32 (s, 3H), 2.45 (t, $J = 6.9$ Hz, 2H) (Figure S1o). ^{13}C NMR (151 MHz, CDCl_3) δ 147.95 (C), 147.95 (C), 135.14 (2C), 130.78 (C), 129.78 (2CH), 129.05 (CH), 127.05 (CH), 126.93 (CH), 121.83 (CH), 120.39 (CH), 62.33 (CH_2), 40.49 (CH), 35.06 (CH_2). HRMS TOF (ESI+) m/z calculated for $\text{C}_{15}\text{H}_{16}\text{NOCl}_2$ [$\text{M} + \text{H}$] $^+$ 296.0699, found 296.0691 (Figure S1p).

3.2.8. Dess-Martin Oxidation of **8a**

To a stirred solution of **8a** (100 mg, 0.34 mmol) in 15 mL of DCM under argon was added the Dess–Martin reagent (305 mg, 0.72 mmol). After stirring for 40 min at room temperature, the reaction was quenched with 10 mL of a saturated solution of $\text{Na}_2\text{S}_2\text{O}_3\text{--NaHCO}_3$ that was added slowly to the mixture. The organic layer was then washed with brine (3×20 mL), dried over anhydrous Na_2SO_4 and concentrated under reduced pressure. The crude product was purified by flash chromatography (H:MTBE, 2:1) to obtain 91 mg of **9a** (0.31 mmol, 91%).

Compound 9a. ^1H NMR (600 MHz, CDCl_3) δ 9.17 (t, $J = 1.9$ Hz, 1H), 7.36–7.33 (m, 1H), 7.33 (d, $J = 8.1$ Hz, 2H), 7.26 (d, $J = 8.1$ Hz, 1H), 7.10 (t, $J = 8.1$ Hz, 1H), 7.05–7.00 (m, 1.0 Hz, 2H), 3.31 (d, $J = 1.9$ Hz, 2H), 3.30 (s, 3H) (Figure S1y). ^{13}C NMR (151 MHz, CDCl_3) δ 199.56 (CHO), 148.57 (C), 143.59 (C), 135.35 (2C), 132.19 (CH), 129.93 (2CH), 128.20 (CH), 127.48 (CH), 123.41 (C), 121.98 (CH), 120.26 (CH), 46.65 (CH_2), 40.27 (CH) (Figure S1z). HRMS TOF (ESI+) m/z calculated for $\text{C}_{15}\text{H}_{14}\text{NOCl}_2$ [$\text{M} + \text{H}$] $^+$ 294.0452, found 294.0442.

3.2.9. Pinnick Oxidation of **9a**

Aldehyde **9a** (98 mg, 0.33 mmol) was dissolved in 7 mL of *tert*-butyl alcohol and 1.2 mL of 2-methyl-2-butene. A solution of sodium chlorite (85 mg, 0.94 mmol) and sodium dihydrogenphosphate dihydrate (95 mg, 0.61 mmol) in 1.5 mL of water was added dropwise over a 10 min period. The yellow reaction mixture was stirred at room temperature for 40 min. Volatile components were then removed under vacuum. The

residue was dissolved in 30 mL of water and extracted with two 25 mL portions of MTBE. The combined organic layers were washed with brine, dried, and concentrated under reduced pressure. Purification by flash chromatography (H:MTBE, 10:1) afforded 69 mg of compound **10a** [37] (0.22 mmol, 67%).

Compound 10a: ^1H NMR (600 MHz, CDCl_3) δ 7.31 (ta, $J = 8.1$ Hz, 1H), 7.29 (d, $J = 8.1$ Hz, 2H), 7.20 (d, $J = 8.1$ Hz, 1H), 7.13 (td, $J = 6.8$ Hz, 1H), 7.03 (t, $J = 8.1$ Hz, 1H), 7.01 (t, $J = 7.4$ Hz, 1H), 3.42 (s, 2H), 3.30 (s, 3H) (Figure S1h2). ^{13}C NMR (151 MHz, CDCl_3) δ 175.94 (COOH), 148.14 (C), 143.39 (C), 135.62 (2C), 132.09 (CH), 129.76 (2CH), 128.05 (CH), 127.28 (CH), 124.47 (C), 121.90 (CH), 120.47 (CH), 40.47 (CH), 36.85 (CH_2) (Figure S1i2). HRMS TOF (ES+) m/z calculated for $\text{C}_{15}\text{H}_{14}\text{NO}_2\text{Cl}_2$ $[\text{M} + \text{H}]^+$ 310.0402, found 310.0390.

3.2.10. Treatment of Compound 7 with Isopentenyl Bromide in the Presence of NaH: Synthesis of **8b**

To a stirred solution of compound **7** (675 mg, 1.65 mmol) in 25 mL THF, under argon atmosphere, was added 123 mg of NaH (5.1 mmol). After stirring for 30 min, 0.7 mL (0.95 mmol) of isopentenyl bromide were added dropwise, and the resulting solution was stirred for 6 h at 50 °C. The mixture was then cooled at 0 °C and diluted with 150 mL of MTBE. Then 15 mL of saturated NH_4Cl were added dropwise. The aqueous layer was extracted with MTBE (3 \times 30 mL). The combined organic layers were washed with brine (3 \times 40 mL) dried over anhydrous Na_2SO_4 and concentrated under reduced pressure. The resulting crude product was dissolved in 25 mL of dry THF, and 1.8 mL of 1M TBAF solution in THF was added to the resulting solution at room temperature and under argon atmosphere. After stirring for 3 h the reaction mixture was diluted with 200 mL of EtOAc, washed with brine (3 \times 50 mL), dried over anhydrous Na_2SO_4 and concentrated in vacuo. The reaction crude was purified by flash chromatography (H:MTBE, 9:1) to afford 384 mg of compound **8b** (1.1 mmol, 65%).

Compound 8b. ^1H NMR (500 MHz, CDCl_3) δ 7.31 (d, $J = 8.0$ Hz, 2H), 7.23–7.17 (m, 2H), 7.10 (dd, $J = 7.5, 1.5$ Hz, 1H), 7.05 (dd, $J = 8.3, 7.7$ Hz, 1H), 6.95 (ddd, $J = 7.6, 6.1, 2.3$ Hz, 1H), 5.39 (thept, $J = 6.13, 1.4$ Hz, 1H), 4.32 (d, $J = 6.2$ Hz, 2H), 3.52 (t, $J = 6.9$ Hz, 2H), 2.41 (t, $J = 6.9$ Hz, 2H), 1.67 (bd, $J = 1.4$ Hz, 3H), 1.63 (bd, $J = 1.4$ Hz, 3H) (Figure S1q). ^{13}C NMR (126 MHz, CDCl_3) δ 146.70 (C), 143.49 (C), 135.31 (2C), 134.25 (C), 130.70 (CH), 129.89 (C), 129.77 (2CH), 126.72 (CH), 126.55 (CH), 121.97 (CH), 121.94 (CH), 121.55 (CH), 62.39 (CH_2), 51.06 (CH_2), 35.03 (CH_2), 25.75 (CH_3), 17.90 (CH_3) (Figure S1r). HRMS TOF (ES+) m/z calculated for $\text{C}_{19}\text{H}_{22}\text{NOCl}_2$ $[\text{M} + \text{H}]^+$ 350.1078, found 350.1062.

3.2.11. Dess-Martin Oxidation of **8b**

To a stirred solution of **8b** (60 mg, 0.17 mmol) in 5 mL of DCM under argon was added the Dess–Martin reagent (144 mg, 0.34 mmol). After stirring for 20 min at room temperature, the reaction was diluted with DCM (20 mL) and quenched with 2 mL of a saturated solution of $\text{Na}_2\text{S}_2\text{O}_3$ – NaHCO_3 that was added slowly to the mixture. The organic layer was then washed with brine (3 \times 10 mL), dried over anhydrous Na_2SO_4 , and concentrated under reduced pressure. The crude product was purified by flash chromatography (H:MTBE, 2:1) to obtain 58 mg of **9b** (0.16 mmol, 94%).

Compound 9b. ^1H NMR (500 MHz, CDCl_3) δ 9.18 (t, $J = 2.0$ Hz, 1H), 7.34–7.28 (m, 3H), 7.24 (d, $J = 7.7$ Hz, 1H), 7.08 (t, $J = 8.1$ Hz, 1H), 7.05–6.98 (m, 2H), 5.41 (bt, $J = 6.3$ Hz, 1H), 4.32 (d, $J = 6.4$ Hz, 2H), 3.30 (d, $J = 2.1$ Hz, 2H), 1.70 (bs, 3H), 1.64 (bs, 3H) (Figure S1b2). ^{13}C NMR (126 MHz, CDCl_3) δ 199.67 (C), 147.44 (C), 142.94 (C), 135.58 (2C), 134.66 (C), 132.12 (CH), 129.94 (2CH), 127.90 (CH), 127.16 (CH), 124.26 (C), 122.10 (CH), 121.88 (CH), 121.21 (CH), 51.02 (CH_2), 46.64 (CH_2), 25.76 (CH_3), 17.91 (CH_3) (Figure S1c2). HRMS TOF (ES+) m/z calculated for $\text{C}_{19}\text{H}_{20}\text{NOCl}_2$ $[\text{M} + \text{H}]^+$ 348.0922, found 348.0901.

3.2.12. Pinnick Oxidation of **9b**

Aldehyde **9b** (243 mg, 0.71 mmol) was dissolved in 20 mL of *tert*-butyl alcohol and 3 mL of 2-methyl-2-butene. A solution of sodium chlorite (260 mg, 2.87 mmol) and sodium dihydrogenphosphate dihydrate (295 mg, 1.89 mmol) in 5 mL of water was added dropwise

over a 20 min period. The yellow reaction mixture was stirred at room temperature for 50 min. Volatile components were then removed under vacuum. The residue was dissolved in 30 mL of water and extracted with two 50 mL portions of MTBE. The combined organic layers were washed with brine, dried, and concentrated under reduced pressure. Purification by flash chromatography (H:MTBE, 10:1) afforded 164 mg of compound **10b** (0.45 mol, 64%).

Compound 10b: ^1H NMR (400 MHz, CDCl_3) δ 7.24 (d, $J = 8.0$ Hz, 1H), 7.27–7.24 (m, 1H), 7.19 (dd, $J = 8.3, 1.3$ Hz, 1H), 7.12 (dd, $J = 7.6, 1.7$ Hz, 1H), 7.02–6.96 (m, 2H), 5.40 (thep, $J = 6.4, 1.4$ Hz, 1H), 4.32 (dt, $J = 6.4, 1.3$ Hz, 2H), 3.40 (s, 2H), 1.68 (d, $J = 1.4$ Hz, 3H), 1.62 (d, $J = 1.4$ Hz, 3H) (Figure S1k2). ^{13}C NMR (101 MHz CDCl_3) δ 176.83 (C), 147.11 (C), 142.60 (C), 135.90 (2C), 134.47 (C), 131.97 (CH), 129.73 (2CH), 127.70 (CH), 126.95 (CH), 125.30 (C), 121.99 (CH), 121.98 (CH), 121.38 (CH), 51.15 (CH_2), 36.93 (CH_2), 25.74 (CH_3), 17.86 (CH_3) (Figure S1l2). HRMS TOF (ES+) m/z calculated for $\text{C}_{19}\text{H}_{20}\text{NO}_2\text{Cl}_2$ [$\text{M} + \text{H}$] $^+$ 364.0871, found 364.0862.

3.2.13. Treatment of Compound 7 with 4-Bromobenzyl Bromide in the Presence of NaH: Synthesis of **8c**

To a stirred solution of compound **7** (854 mg, 2.16 mmol) in 30 mL THF, under argon atmosphere, were added 500 mg of NaH (21 mmol). After stirring for 30 min, 1350 mg (5.4 mmol) of 4-bromobenzyl bromide were added portion wise, and the resulting solution was stirred for 8 h at 50 °C. The mixture was then cooled at 0 °C and diluted with 150 mL of MTBE. Then 15 mL of saturated NH_4Cl were added dropwise. The aqueous layer was extracted with MTBE (3 \times 30 mL). The combined organic layers were washed with brine (3 \times 40 mL) dried over anhydrous Na_2SO_4 , and concentrated under reduced pressure. The resulting crude product was dissolved in 50 mL of dry THF and 128 mL of 1M TBAF solution in THF was added to the resulting solution at room temperature and under argon atmosphere. After stirring for 4 h the reaction mixture was diluted with 200 mL of EtOAc, washed with brine (3 \times 50 mL), dried over anhydrous Na_2SO_4 and concentrated in vacuo. The reaction crude was purified by flash chromatography (H:MTBE, 9:1) to afford 786 mg of compound **8c** (1.75 mmol, 81%).

Compound 8c. ^1H NMR (600 MHz, CDCl_3) δ 7.37 (d, $J = 8.6$ Hz, 2H), 7.33 (d, $J = 8.6$ Hz, 2H), 7.33–7.29 (m, 1H), 7.31 (d, $J = 8.0$ Hz, 2H), 7.12 (d, $J = 7.3$ Hz, 1H), 7.08 (dd, $J = 8.4, 7.7$ Hz, 1H), 7.05–7.01 (m, 1H), 6.95–6.90 (m, 1H), 4.86 (s, 2H), 3.55 (t, $J = 7.0$ Hz, 2H), 2.58 (t, $J = 7.0$ Hz, 2H) (Figure S1t). ^{13}C NMR (151 MHz, CDCl_3) δ 145.16 (C), 143.87 (C), 136.74 (C), 135.21 (2C), 131.45 (2CH), 130.57 (C), 130.55 (CH), 130.01 (2CH), 129.35 (2CH), 127.04 (CH), 126.46 (C), 123.21 (CH), 122.68 (CH), 120.68 (C), 62.24 (CH_2), 55.46 (CH_2), 34.55 (CH_2) (Figure S1u). HRMS TOF (ES+) m/z calculated for $\text{C}_{21}\text{H}_{19}\text{NOCl}_2\text{Br}$ [$\text{M} + \text{H}$] $^+$ 450.0027, found 450.0021.

3.2.14. Dess-Martin Oxidation of **8c**

To a stirred solution of **8c** (375 mg, 0.80 mmol) in 25 mL of DCM under argon was added the Dess–Martin reagent (677 mg, 1.6 mmol). After stirring for 50 min at room temperature, the reaction was diluted with DCM (20 mL) and quenched with 10 mL of a saturated solution of $\text{Na}_2\text{S}_2\text{O}_3$ – NaHCO_3 that was added slowly to the mixture. The organic layer was then washed with brine (3 \times 20 mL), dried over anhydrous Na_2SO_4 , and concentrated under reduced pressure. The crude product was purified by flash chromatography (H:MTBE, 2:1) to obtain 325 mg of **9c** (0.72 mmol, 90%).

Compound 9c. ^1H NMR (600 MHz, CDCl_3) δ 9.15 (t, $J = 1.8$ Hz, 1H), 7.38 (d, $J = 8.4$ Hz, 2H), 7.31 (d, $J = 8.1$ Hz, 4H), 7.14–7.04 (m, 3H), 7.02 (dd, $J = 7.6, 1.7$ Hz, 1H), 6.96 (td, $J = 7.3, 1.3$ Hz, 1H), 4.82 (s, 2H), 3.44 (d, $J = 1.8$ Hz, 2H) (Figure S1e2). ^{13}C NMR (151 MHz, CDCl_3) δ 199.04 (CHO), 145.66 (C), 143.37 (C), 136.34 (C), 135.37 (2C), 132.22 (CH), 131.51 (2CH), 130.17 (2CH), 129.28 (2CH), 127.62 (CH), 127.60 (CH), 124.93 (C), 123.03 (CH), 122.77 (CH), 120.79 (C), 55.27 (CH_2), 46.50 (CH_2) (Figure S1f2). HRMS TOF (ESI+) m/z calculated for $\text{C}_{21}\text{H}_{17}\text{NOCl}_2\text{Br}$ [$\text{M} + \text{H}$] $^+$ 447.9871, found 447.9837.

3.2.15. Pinnick Oxidation of 9c

Aldehyde **9c** (335 mg, 0.72 mmol) was dissolved in 20 mL of *tert*-butyl alcohol and 3 mL of 2-methyl-2-butene. A solution of sodium chlorite (266 mg, 2.94 mmol) and sodium dihydrogenphosphate dihydrate (298 mg, 1.91 mmol) in 5 mL of water was added dropwise over a 20 min period. The yellow reaction mixture was stirred at room temperature for 50 min. Volatile components were then removed under vacuum. The residue was dissolved in 30 mL of water and extracted with 2 50 mL portions of MTBE. The combined organic layers were washed with brine, dried, and concentrated under reduced pressure. Purification by flash chromatography (H:MTBE, 10:1) afforded 131 mg of compound **10c** (0.5 mmol, 69%).

Compound 10c: ^1H NMR (600 MHz, CDCl_3) δ 7.37 (d, $J = 8.5$ Hz, 2H), 7.32 (d, $J = 8.4$ Hz, 1H), 7.27 (d, $J = 7.6$ Hz, 3H), 7.15–7.06 (m, 2H), 7.03 (d, $J = 8.1$ Hz, 1H), 7.01 (t, $J = 8.1$ Hz, 1H), 6.96 (td, $J = 7.1, 0.8$ Hz, 1H), 4.86 (s, 2H), 3.50 (d, $J = 4.3$ Hz, 2H) (Figure S112). ^{13}C NMR (101 MHz, CDCl_3) δ 174.54 (C), 145.26 (C), 143.04 (C), 136.46 (C), 135.53 (2C), 132.06 (CH), 131.46 (2CH), 130.03 (2CH), 129.30 (2CH), 127.56 (CH), 127.33 (CH), 126.03 (C), 123.15 (CH), 122.79 (CH), 120.73 (C), 55.49 (CH_2), 36.43 (CH_2) (Figure S1m2). HRMS TOF (ESI+) m/z calculated for $\text{C}_{21}\text{H}_{17}\text{NO}_2\text{Cl}_2\text{Br}$ $[\text{M} + \text{H}]^+$ 463.9820, found 463.9829.

3.3. Cell Viability Assays

All cell lines used in this article were provided by the cell bank of the University of Granada, Spain: HT29 human colorectal adenocarcinoma cell line (ECACC no. 9172201; ATCC no. HTB-38); Hep-G2 human hepatocarcinoma cell line (ECACC no. 85011430; B16-F10 mouse melanoma cell line (ATCC no. CRL-6475), and RAW 264.7 monocyte/macrophage murine cell line (ATCC no. TIB-71). All cell lines were cultured in DMEM supplemented with 2 mM glutamine, 10% heat-inactivated FCS, $50 \mu\text{g}\cdot\text{mL}^{-1}$ of gentamicin, being incubated at 37°C , in an atmosphere of 5% CO_2 and 95% humidity. Subconfluent monolayer cells were used in all experiments.

DCF and its 8 different derivatives were dissolved at $5 \text{ mg}\cdot\text{mL}^{-1}$ in DMSO, and stored at 4°C . Before use in cell treatment, these compounds were diluted in cell culture medium at adequate concentrations for each experiment. Apoptosis, mitochondrial-membrane potential and cell-cycle analysis were measured at IC_{50} and IC_{80} in HT29, Hep-G2 and B16-F10. For nitrite concentration, $\frac{3}{4}\cdot\text{IC}_{50}$, $\frac{1}{2}\cdot\text{IC}_{50}$ and $\frac{1}{4}\cdot\text{IC}_{50}$ concentrations were used to ensure sub-cytotoxic concentration against RAW 264.7 cells.

The effect of each treatment with compounds **2**, **4**, **6**, **8c**, **9c**, **10a-c**, and DCF on cell cytotoxicity were determined in all cell lines described before. The cells viability was determined by using MTT (3-(4,5-dimethylthiazol-2-yl)-2,5-diphenyltetrazolium bromide) proliferation assay (Sigma, St. Louis, MO, USA), which is based on the ability of live cells to cleave the tetrazolium ring, thus producing formazan, which absorbs at 570 nm.

For this assay, 6×10^3 HT29 cells, 15×10^3 Hep-G2 cells, 5×10^3 B16-F10 cells and 6×10^3 RAW 264 cells per well were grown on a 96-well plate and incubated with the different products ($0\text{--}200 \mu\text{g}\cdot\text{mL}^{-1}$). After 72 h, $100 \mu\text{L}$ of MTT solution ($0.5 \text{ mg}\cdot\text{mL}^{-1}$) in a mixture of 50% of PBS (Phosphate-Buffered Saline) and 50% of cell medium was added to each well. After 1.5 h of incubation, cells were washed twice with PBS, and formazan was resuspended in $100 \mu\text{L}$ DMSO. Relative cell viability, with respect to untreated control cells, was measured by absorbance at 570 nm on an ELISA plate reader (Tecan Sunrise MR20-301, Männedorf, Switzerland, Männedorf, Switzerland).

3.4. Annexin V-FITC/Propidium Iodide Flow-Cytometric Analysis

Apoptosis was analyzed with flow-cytometry by using a FACScan flow-cytometer (fluorescence-activated cell sorter) (Coulter Corporation, Hialeah, FL, USA). In brief, 15×10^4 Hep-G2 cells per well were plated in 24-well plates with 1.5 mL of medium, following treatment with the compounds for 72 h at the IC_{50} and IC_{80} concentrations, calculated previously. The cells were collected and resuspended in binding buffer (10 mM HEPES/NaOH, $\text{pH} = 7.4$, 140 mM NaCl, 2.5 mM CaCl_2). Annexin V-FITC conjugate

(1 mg·mL⁻¹) was added and incubated for 30 min at room temperature in darkness. Just before FACS analysis, cells were stained with 20 µL of 1 mg·mL⁻¹ propidium iodide (PI) solution. In each experiment, approximately 10 × 10³ cells were analyzed, and the experiment was duplicated 3 times. The percentages of apoptosis were determined with annexin V-FICT/PI by FACS (flow-activated cell sorter) cytometric analysis, differentiating early apoptotic cells (An-V⁺ and PI⁻) from late apoptotic (An-V⁺ and PI⁺), necrotic (An-V⁻ and PI⁺) or normal cells (An-V⁻ and PI⁻).

3.5. Cell-Cycle Analysis

The cell-cycle was analyzed again with flow cytometry by using a fluorescence-activated cell sorter (FACS) at 488 nm in an Epics XL flow cytometer (Coulter Corporation, Hialeah, FL, USA). For this assay, 15 × 10⁴ Hep-G2 cells per well were plated in 24-well plates with 1.5 mL of medium, following treatment with the compounds for 72 h at the IC₅₀ and IC₈₀ concentrations. After treatment, cells were washed twice with PBS and harvested by trypsinization, then were resuspended in 1X TBS (10 Mm Tris, 150 Mm NaCl), followed by the addition of Vindelov Buffer (100 mM Tris, 100 Mm NaCl, 10 mg/mL RNase, 1 mg/mL PI, pH 8). Samples were allowed to stand for 15 min on ice. Just before FACS analysis, cells were stained with 20 µL of 1 mg·mL⁻¹ PI solution. DNA content is directly proportional to the PI fluorescence, allowing to determine the percentage of cells in each cell-cycle phase. In this way, we are able to visualize cell subpopulations with differing DNA contents. Changes in DNA concentrations are characteristic of apoptosis and cell-cycle arrest. The data were analyzed to determine the percentage of cells at each phase of the cell cycle (G0/G1, S, and G2/M).

3.6. Flow-Cytometry Analysis of the Mitochondrial-Membrane Potential

The loss of mitochondrial membrane potential (MMP) during the apoptotic process has been related to the intrinsic mechanism of apoptosis activation. To approach the mechanism of apoptosis implicated in the apoptotic response of Hep-G2 cells, we analyzed the MMP with rhodamine 123 (Rh123) stained. This compound is a membrane-permeable fluorescent cationic dye selectively taken up by mitochondrial, and its fluorescence is proportional to the mitochondrial membrane potential. Oxidative damage was studied by flow-cytometry analysis of the mitochondrial membrane potential, using dihydrorhodamine 123 (DHR) oxidized to the highly fluorescent product rhodamine 123 (Rh123). The formation of Rh123 can be monitored by fluorescence spectroscopy using excitation and emission wavelengths at 500 and 536 nm, respectively. The intracellular measurement of the mitochondrial membrane potential was made by cytometry determination of Rh123. In the same way as in the apoptosis assays, 15 × 10⁴ Hep-G2 cells per well were plated in 24-well plates with 1.5 mL of medium, following treatment with the compounds for 72 h at the IC₅₀ and IC₈₀ concentrations. After treatment, the medium was removed and a fresh medium with DHR was added at a final concentration of 5 µg/mL. After 30 min of incubation, the medium was removed, and the cells were washed and resuspended in PBS with 5 µg·mL⁻¹ of PI. The intensity of fluorescence from Rh123 and PI was determined using a FACScan flow-cytometer (Coulter Corporation, Hialeah, FL, USA).

3.7. Determination of Nitrite Concentration

The concentration of nitrites was determined in assay based on the Griess reaction. This nitrite concentration was used as an indicator of NO production. RAW 264.7 cells were plated at 6 × 10⁴ cells/well in 24-well cell culture plates, supplemented with 10 µg/mL of LPS, except untreated negative control cells. After 24 h of plating, the cells were incubated for 24 h with the test compounds at $\frac{3}{4}$ ·IC₅₀, $\frac{1}{2}$ ·IC₅₀, and $\frac{1}{4}$ ·IC₅₀ concentrations determined by MTT proliferation assay. The supernatants were collected at 24, 48, and 72 h to determine nitrite concentration and/or stored at -80 °C for further use.

For the Griess reaction, 150 µL of supernatant test samples or sodium nitrite standard (0–120 µM) were taken and mixed with 25 µL of the Griess reagent A (0.1% N-N-

(1-naphthyl)-ethylenediamine dihydrochloride) and 25 μL of the Griess reagent B (1% sulfanilamide in 5% of phosphoric acid), in a 96-well plate. After 15 min of incubation at room temperature, the absorbance was measured at 540 nm on an ELISA plate reader (Tecan Sunrise MR20-301, Männedorf, Switzerland, Männedorf, Switzerland). The absorbance was referred to nitrite standard curve to determine the concentration of nitrite in the supernatant. The percentage of NO production was determined, assigning 100% at the increase between negative control (untreated cells) and positive control (cells only treated with 10 $\mu\text{g}\cdot\text{mL}^{-1}$ of LPS).

3.8. Statistics

Statistical and non-linear sigmoidal regression analyses were performed with the SigmaPlot 12.5 software (Systat Software Inc. San Jose, CA, USA). All quantitative data were summarized as the means \pm standard deviation (SD). All data shown here were representative of at least 2 independent experiments performed in triplicate.

Supplementary Materials: The following are available online at <https://www.mdpi.com/article/10.3390/ijms22105067/s1>, Figure S1. copies of NMR spectra of the synthesized compounds.

Author Contributions: Conceptualization, F.J.R.-Z., J.A.L., A.R.-D. and J.F.Q.d.M.; investigation, A.G., F.J., A.G.-G., H.A., S.R.; writing—original draft preparation, F.J.R.-Z., A.R.-D. and J.F.Q.d.M.; writing—review and editing, F.J.R.-Z., S.R. and J.F.Q.d.M.; funding acquisition, F.J.R.-Z. and J.F.Q.d.M. All authors have read and agreed to the published version of the manuscript.

Funding: This work has been supported by grant MINISTERIO DE ECONOMÍA Y COMPETITIVIDAD, PID2019-106222RB-C32/SRA (State Research Agency, 10.13039/501100011033) and by the “Consejería de Economía, Conocimiento, Empresas y Universidad. Junta de Andalucía”, grant number B1-BIO-281-UGR18.

Institutional Review Board Statement: Not applicable.

Informed Consent Statement: Not applicable.

Data Availability Statement: Data availability upon request.

Acknowledgments: José Luis Gómez Navas is thanked for his contribution in the early stages of this work.

Conflicts of Interest: The authors declare no conflict of interest.

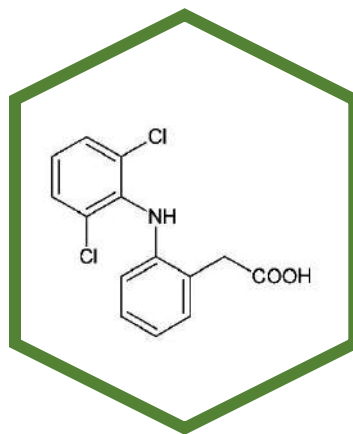
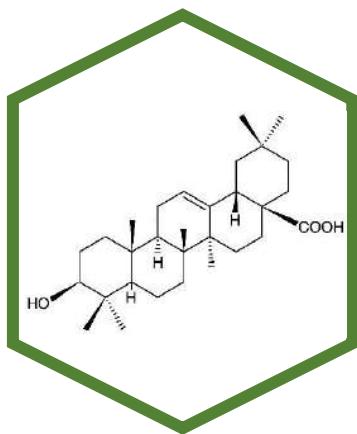
References

1. Gan, T.J. Diclofenac: An update on its mechanism of action and safety profile. *Curr. Med. Res. Opin.* **2010**, *26*, 1715–1731. [[CrossRef](#)] [[PubMed](#)]
2. Orido, T.; Fujino, H.; Hasegawa, Y.; Toyomura, K.; Kawashima, T.; Murayama, T. Indomethacin decreases arachidonic acid uptake in HCA-7 human colon cancer cells. *J. Pharmacol. Sci.* **2008**, *108*, 389–392. [[CrossRef](#)]
3. Triggiani, M.; Granata, F.; Frattini, A.; Marone, G. Activation of human inflammatory cells by secreted phospholipases A2. *Biochim. Biophys. Acta Mol. Cell Biol. Lipids* **2006**, *1761*, 1289–1300. [[CrossRef](#)] [[PubMed](#)]
4. Mäkelä, A.; Kuusi, T.; Schröder, T. Inhibition of serum phospholipase-A2 in acute pancreatitis by pharmacological agents in vitro. *Scand. J. Clin. Lab. Investig.* **1997**, *57*, 401–407. [[CrossRef](#)] [[PubMed](#)]
5. Bondar, T.; Medzhitov, R. The origins of tumor-promoting inflammation. *Cancer Cell* **2013**, *24*, 143–144. [[CrossRef](#)] [[PubMed](#)]
6. Grivennikov, S.I.; Greten, F.R.; Karin, M. Immunity, inflammation, and cancer. *Cell* **2010**, *140*, 883–899. [[CrossRef](#)]
7. Nakanishi, M.; Rosenberg, D.W. Multifaceted roles of PGE2 in inflammation and cancer. *Semin. Immunopathol.* **2013**, *35*, 123–137. [[CrossRef](#)] [[PubMed](#)]
8. Seed, M.P.; Brown, J.R.; Freemantle, C.N.; Papworth, J.L.; Colville-Nash, P.R.; Willis, D.; Somerville, K.W.; Asculai, S.; Willoughby, D.A. The inhibition of colon-26 adenocarcinoma development and angiogenesis by topical diclofenac in 2.5% hyaluronan. *Cancer Res.* **1997**, *57*, 1625–1629. [[PubMed](#)]
9. Larsson, K.; Kock, A.; Idborg, H.; Arsenian Henriksson, M.; Martinsson, T.; Johnsen, J.I.; Korotkova, M.; Kogner, P.; Jakobsson, P.-J. COX/mPGES-1/PGE₂ pathway depicts an inflammatory-dependent high-risk neuroblastoma subset. *Proc. Natl. Acad. Sci. USA* **2015**, *112*, 8070–8075. [[CrossRef](#)]
10. Johnsen, J.I.; Lindskog, M.; Ponthan, F.; Pettersen, I.; Elfman, L.; Orrego, A.; Sveinbjörnsson, B.; Kogner, P. Cyclooxygenase-2 is expressed in neuroblastoma, and nonsteroidal anti-inflammatory drugs induce apoptosis and inhibit tumor growth in vivo. *Cancer Res.* **2004**, *64*, 7210–7215. [[CrossRef](#)]

11. Zerbini, L.F.; Czibere, A.; Wang, Y.; Correa, R.G.; Otu, H.; Joseph, M.; Takayasu, Y.; Silver, M.; Gu, X.; Ruchusatsawat, K.; et al. A novel pathway involving melanoma differentiation associated gene-7/interleukin-24 mediates nonsteroidal anti-inflammatory drug-induced apoptosis and growth arrest of cancer cells. *Cancer Res.* **2006**, *66*, 11922–11931. [[CrossRef](#)]
12. Valle, B.L.; D'Souza, T.; Becker, K.G.; Wood III, W.H.; Zhang, Y.; Wersto, R.P.; Morin, P.J. Non-steroidal anti-inflammatory drugs decrease E2F1 expression and inhibit cell growth in ovarian cancer cells. *PLoS ONE* **2013**, *8*, e61836. [[CrossRef](#)]
13. Leidgens, V.; Seliger, C.; Jachnik, B.; Welz, T.; Leukel, P.; Vollmann-Zwerenz, A.; Bogdahn, U.; Kreutz, M.; Grauer, O.M.; Hau, P. Ibuprofen and diclofenac restrict migration and proliferation of human glioma cells by distinct molecular mechanisms. *PLoS ONE* **2015**, *10*, e0140613. [[CrossRef](#)] [[PubMed](#)]
14. Yagi, K.; Kawasaki, Y.; Nakamura, H.; Miura, T.; Takeda, T.; Esumi, S.; Matsunaga, H.; Kitamura, Y.; Sendo, T. Differential combined effect of COX inhibitors on cell survival suppressed by sorafenib in the HepG2 cell line. *Biol. Pharm. Bull.* **2014**, *37*, 1234–1240. [[CrossRef](#)]
15. Gottfried, E.; Lang, S.A.; Renner, K.; Bosserhoff, A.; Gronwald, W.; Rehli, M.; Einhell, S.; Gedig, I.; Singer, K.; Seilbeck, A.; et al. New Aspects of an Old Drug—Diclofenac targets MYC and glucose metabolism in tumor cells. *PLoS ONE* **2013**, *8*, e66987. [[CrossRef](#)]
16. Johnsen, J.I.; Lindskog, M.; Ponthan, F.; Pettersen, I.; Elfman, L.; Orrego, A.; Sveinbjörnsson, B.; Kogner, P. NSAIDs in neuroblastoma therapy. *Cancer Lett.* **2005**, *228*, 195–201. [[CrossRef](#)] [[PubMed](#)]
17. Hoferová, Z.; Fedorocko, P.; Hofmanová, J.; Hofer, M.; Znojil, V.; Minksová, K.; Soucek, K.; Egyed, A.; Kozubík, A. The effect of nonsteroidal anti-inflammatory drugs ibuprofen, flurbiprofen, and diclofenac on in vitro and in vivo growth of mouse fibrosarcoma. *Cancer Invest.* **2002**, *20*, 490–498. [[CrossRef](#)] [[PubMed](#)]
18. Falkowski, M.; Skogstad, S.; Shahzidi, S.; Smedsröd, B.; Sveinbjörnsson, B. The effect of cyclooxygenase inhibitor diclofenac on experimental murine colon carcinoma. *Anticancer Res.* **2003**, *23*, 2303–2308.
19. Edrei, Y.; Gross, E.; Corchia, N.; Abramovitch, R. Improved efficacy of a novel anti-angiogenic drug combination (TL-118) against colorectal-cancer liver metastases; MRI monitoring in mice. *Br. J. Cancer* **2012**, *107*, 658–666. [[CrossRef](#)]
20. Komar-Stossel, C.; Gross, E.; Dery, E.; Corchia, N.; Meir, K.; Fried, I.; Abramovitch, R. TL-118 and gemcitabine drug combination display therapeutic efficacy in a MYCN amplified orthotopic neuroblastoma murine model—Evaluation by MRI. *PLoS ONE* **2014**, *9*, e90224. [[CrossRef](#)]
21. Inoue, A.; Muranaka, S.; Fujita, H.; Kanno, T.; Tamai, H.; Utsumi, K. Molecular mechanism of diclofenac-induced apoptosis of promyelocytic leukemia: Dependency on reactive oxygen species, akt, bid, cytochrome and caspase pathway. *Free Radic. Biol. Med.* **2004**, *37*, 1290–1299. [[CrossRef](#)]
22. Albano, F.; Arcucci, A.; Granato, G.; Romano, S.; Montagnani, S.; De Vendittis, E.; Ruocco, M.R. Markers of mitochondrial dysfunction during the diclofenac-induced apoptosis in melanoma cell lines. *Biochimie* **2013**, *95*, 934–945. [[CrossRef](#)]
23. Okazaki, R.; Moon, Y.; Norimura, T.; Eling, T. Ionizing radiation enhances the expression of the nonsteroidal anti-inflammatory drug-activated gene (NAG1) by increasing the expression of TP53 in human colon cancer cells. *Radiat. Res.* **2006**, *165*, 125–130. [[CrossRef](#)]
24. Cooper, D.L.; Harirforoosh, S. Design and optimization of PLGA-based diclofenac loaded nanoparticles. *PLoS ONE* **2014**, *9*, e87326. [[CrossRef](#)] [[PubMed](#)]
25. Hafeez, F.; Zahoor, A.F.; Ahmad, S.; Ahmad, M.; Faiz, S. Recent progress in the synthesis of diclofenac based NSAIDs analogs/derivatives. *Synth. Commun.* **2019**, *49*, 325–350. [[CrossRef](#)]
26. Miyamoto, K.; Yasuda, Y.; Yoshioka, K. Glycosaminoglycan Derivative and Method for Producing Same. U.S. Patent US20190184023A1, 20 June 2019.
27. Laskin, J.D.; Heck, D.E.; Lacey, C.J.; Heindel, N.D.; Young, S.C. Augmenting moieties for anti-inflammatory compounds. U.S. Patent US10752582B2, 25 August 2020.
28. Akgul, O.; Di Cesare Mannelli, L.; Vullo, D.; Angeli, A.; Ghelardini, C.; Bartolucci, G.; Alfawaz Altamimi, A.S.; Scozzafava, A.; Supuran, C.T.; Carta, F. Discovery of novel nonsteroidal anti-inflammatory drugs and carbonic anhydrase inhibitors hybrids (NSAIDs–CAIs) for the management of rheumatoid arthritis. *J. Med. Chem.* **2018**, *61*, 4961–4977. [[CrossRef](#)] [[PubMed](#)]
29. Osman, H.A.; Nazeruddin, G.M. Design, synthesis, biological evaluation and docking studies of some new diclofenac analogues. *Br. J. Pharm. Res.* **2014**, *4*, 770–777. [[CrossRef](#)]
30. Ravichandran, V.; Mohan, S.; Kumar, K.S. Synthesis and antimicrobial activity of Mannich bases of isatin and its derivatives with 2-[(2,6-dichlorophenyl)amino]phenylacetic acid. *Arkivoc* **2007**, *14*, 51–57. [[CrossRef](#)]
31. Shah, B.; Patil, P.; Shah, H. Chemical modification of paracetamol and their antimicrobial and pharmacological evaluation. *Int. J. Pharm. Res. Bio-Sci.* **2014**, *3*, 12–31.
32. Blumberg, L.C.; Lowe, J.A.; Almarsson, O.; Alvarez, J.; Zeidan, T.A. Prodrugs of secondary amine compounds. U.S. Patent US8969337B2, 03 March 2015.
33. Chen, C.-H. Novel composition for treating metabolic syndrome and other conditions. U.S. Patent US20120183600A1, 19 July 2012.
34. Biere, H.; Rufer, C.; Boettcher, I. Diphosphonic acid derivatives and pharmaceutical preparations containing them. Germany Patent DE3225469A1, 05 January 1984.
35. Tsuchihashi, G.; Ogura, K.; Sakota, R.; Hashiba, I.; Fukushima, S. O-(N-Allyl-2,6-dichloroanilino)phenylacetic acid Derivative and a Process for Preparing the Same. U.S. Patent US4242522A, 30 December 1980.

36. Sakota, R.; Nagano, K.; Ando, Y.; Tsuchihashi, G.; Ogura, K. [N-Benzyl-O-(2,6-dichloroanilino)phenyl]acetic acid Derivatives. Canada Patent CA1113484A, 01 December 1981.
37. Sallmann, A.; Pfister, R. Substituted derivatives of 2-anilinophenylacetic acids and a process of preparation. U.S. Patent US3558690A, 26 January 1971.
38. Virsodia, V.; Manvar, A.; Upadhyay, K.; Loriya, R.; Karia, D.; Jaggi, M.; Singh, A.; Mukherjee, R.; Shaikh, M.S.; Coutinho, E.C.; et al. Synthesis of 1-(2,6-dichlorophenyl)-3-methylene-1,3-dihydro-indol-2-one derivatives and in vitro anticancer evaluation against SW620 colon cancer cell line. *Eur. J. Med. Chem.* **2009**, *44*, 1355–1362. [[CrossRef](#)]
39. Palkar, M.B.; Singhai, A.S.; Ronad, P.M.; Vishwanathswamy, A.H.M.; Boreddy, T.S.; Veerapur, V.P.; Shaikh, M.S.; Rane, R.A.; Karpoomath, R. Synthesis, pharmacological screening and in silico studies of new class of Diclofenac analogues as a promising anti-inflammatory agents. *Bioorg. Med. Chem.* **2014**, *22*, 2855–2866. [[CrossRef](#)]
40. Oza, V.B.; Smith, C.; Raman, P.; Koepf, E.K.; Lashuel, H.A.; Petrassi, H.M.; Chiang, K.P.; Powers, E.T.; Sachettinni, J.; Kelly, J.W. Synthesis, structure, and activity of diclofenac analogues as transthyretin amyloid fibril formation inhibitors. *J. Med. Chem.* **2002**, *45*, 321–332. [[CrossRef](#)]
41. Dess, D.B.; Martin, J.C. Readily accessible 12-I-5 oxidant for the conversion of primary and secondary alcohols to aldehydes and ketones. *J. Org. Chem.* **1983**, *48*, 4155–4156. [[CrossRef](#)]
42. Bal, B.S.; Childers, W.E.; Pinnick, H.W. Oxidation of α,β -unsaturated aldehydes. *Tetrahedron* **1981**, *37*, 2091–2096. [[CrossRef](#)]
43. Shah, S.; Arshia; Kazmi, N.S.; Jabeen, A.; Faheem, A.; Dastagir, N.; Ahmed, T.; Khan, K.M.; Ahmed, S.; Raza, A.; et al. Diclofenac 1,3,4-oxadiazole derivatives; biology-oriented drug synthesis (BIODS) in search of better non-steroidal, non-acid antiinflammatory agents. *Med. Chem.* **2018**, *14*, 674–687. [[CrossRef](#)] [[PubMed](#)]
44. Navas, A.; Jannus, F.; Fernandez, B.; Cepeda, J.; O'donnell, M.M.; Diaz-Ruiz, L.; Sanchez-Gonzalez, C.; Llopis, J.; Seco, J.M.; Rufino-Palomares, E.; et al. Designing single-molecule magnets as drugs with dual anti-inflammatory and anti-diabetic effects. *Int. J. Mol. Sci.* **2020**, *21*, 3146. [[CrossRef](#)] [[PubMed](#)]
45. García-Valdivia, A.A.; García-García, A.; Jannus, F.; Zabala-Lekuona, A.; Méndez-Arriaga, J.M.; Fernández, B.; Medina-O'donnell, M.; Ramírez-Rodríguez, G.B.; Delgado-López, J.M.; Pastrana-Martínez, L.M.; et al. Antiparasitic, anti-inflammatory and cytotoxic activities of 2D coordination polymers based on 1H-indazole-5-carboxylic acid. *J. Inorg. Biochem.* **2020**, *208*, 111098. [[CrossRef](#)]
46. Santos, J.L.; Moreira, V.; Campos, M.L.; Chelucci, R.C.; Barbieri, K.P.; Souto, P.C.; Matsubara, M.H.; Teixeira, C.; Bosquesi, P.L.; Peccinini, R.G.; et al. Pharmacological evaluation and preliminary pharmacokinetics studies of a new diclofenac prodrug without gastric ulceration effect. *Int. J. Mol. Sci.* **2012**, *13*, 15305–15320. [[CrossRef](#)]
47. Mahmoud, M.H.; El-Dean, A.M.K.; Abdel-Mohsen, S.A.; Tolba, M.S. New diclofenac derivatives as anti-microbial, anti-inflammatory agents: Design, synthesis, biological screening, and molecular docking study. *Russ. J. Bioorg. Chem.* **2021**, *47*, 208–220. [[CrossRef](#)]
48. Bhandari, S.V.; Bothara, K.G.; Raut, M.K.; Patil, A.A.; Sarkate, A.P.; Mokale, V.J. Design, synthesis and evaluation of antiinflammatory, analgesic and ulcerogenicity studies of novel S-substituted phenacyl-1,3,4-oxadiazole-2-thiol and Schiff bases of diclofenac acid as nonulcerogenic derivatives. *Bioorganic Med. Chem.* **2008**, *16*, 1822–1831. [[CrossRef](#)] [[PubMed](#)]

DISCUSIÓN



5. DISCUSIÓN

Según la Organización Mundial de la Salud (WHO), el cáncer es una de las principales causas de muerte en todo el mundo, provocando casi 10 millones de fallecidos en 2020. En el cáncer se produce la pérdida del balance homeostático entre la proliferación y muerte celular en el organismo. Uno de los principales mecanismos que controlan este balance es la apoptosis, proceso fisiológico de autoeliminación celular. Un segundo mecanismo que controla la homeostasis es la inflamación [85], [86]. Por tanto, apoptosis e inflamación son mecanismos relacionados de manera, que su desregulación puede producir inflamación crónica y tumorigénesis, ya que la inflamación juega un papel primordial en el desarrollo y la progresión del tumor [97].

En esta tesis doctoral se ha profundizado en el comportamiento de varios derivados como posibles agentes anticancerígenos y antiinflamatorios. Centrándonos en el derivado de ácido oleanólico amino pegilado (OADP) y diversos N-derivados del diclofenaco. La obtención de nuevos compuestos mediante modificaciones en su estructura por la unión de diferentes sustituyentes puede conducir a una mejora en sus actividades biológicas incluso disminuyendo los efectos secundarios del compuesto de partida [70], [71].

En el primer artículo presentado en esta tesis doctoral, se profundizó en el estudio de la actividad anticancerígena del compuesto OADP en la línea tumoral de hepatocarcinoma Hep-G2. Los resultados obtenidos mostraron que este compuesto es unas 718 veces más activo que su precursor (OA) tras 72 horas de tratamiento produciendo una clara y significativa inhibición en la proliferación celular ($IC_{50}=0.14 \pm 0.03 \mu\text{g/mL}$) siendo la IC_{50} , la concentración a la cual se produce el 50% de inhibición celular. Mientras que su efecto citotóxico sobre la línea normal o no transformada de células hepáticas WRL68, fue 39 veces menor. Los estudios de citometría de flujo demostraron que este compuesto presenta un potente efecto apoptótico alcanzando porcentajes de apoptosis en torno al 95% y deteniendo el ciclo celular en la fase G0/G1. Trabajos anteriores han demostrado que el OA y sus derivados presentan efectos anticancerígenos en diferentes líneas tumorales [32], [40] incluyendo la línea de carcinoma hepatocelular HCC, [31], [36], activando la vía apoptótica mitocondrial en células de carcinoma hepatocelular HuH7 [38]. Asimismo, resultados similares han sido encontrados para otros derivados del OA como el O^2 -(2,4-dinitrofenil) diazeniodiolato, este indujo la parada del ciclo celular en la fase G2/M y activo la vía apoptótica mitocondrial en las células HepG2 [31].

Como se ha comentado en la introducción la apoptosis es un proceso controlado por la familia de cisteinil proteasas, caspasas, y fundamentalmente transcurre a través de dos vías apoptóticas, la extrínseca y la intrínseca. La vía apoptótica extrínseca es activada por medio de señales extracelulares capaces de producir la respuesta en receptores de la membrana plasmática produciendo la activación de caspasas iniciadoras como la caspasa-8 la cual induce la activación de la caspasa efectora -3. Sin embargo, la vía apoptótica intrínseca es activada por numerosas señales intracelulares que a través de diferentes rutas moleculares regulan el comportamiento de la familia de proteínas Bcl-2, canales iónicos de membrana mitocondrial, que como Bax y Bak forman poros, produciendo la pérdida de permeabilidad, liberando factores mitocondriales como el citocromo-c y Apaf1 que mediante la formación del apoptosoma, activan a la caspasa iniciadora -9 que induce la activación de la caspasa-3 [76]–[78]. Estas vías de inducción de apoptosis están a su vez reguladas por proteínas tales como, el supresor tumoral p53 y las JNKs quinasas [81], [82]. A su vez p53, regula el ciclo celular a través del inhibidor de quinasa dependiente de ciclina, p21, el cual puede inducir la detención del ciclo celular en la fase G0/G1 y fase S [81].

En el primer artículo de los que componen esta tesis, mostramos que el OADP es capaz de activar claramente las caspasas iniciadoras -8 y caspasa-9, así como de la caspasa efectora -3. Produciendo la parada del ciclo celular a través de las proteínas p53 y p21. A su vez nuestros resultados muestran que esta inducción en la activación de la caspasa-9 está regulada por la inducción de la proteína proapoptótica Bak, y la inhibición de la proteína antiapoptótica Bcl-2. Así mismo nos preguntamos si el papel de la caspasa-8 y por tanto de la activación de la vía extrínseca de inducción de apoptosis era

determinante, para ello determinamos los niveles de expresión de las distintas proteínas mencionadas en presencia del inhibidor de la caspasa-8 (IETD-CHO), lo que nos reveló que la activación de esta caspasa es determinante para el incremento en la expresión de la caspasa-9, caspasa-3, p53, p21 y Bak. Por lo tanto, pudimos demostrar que la activación de la apoptosis en las células HepG2, en respuesta al tratamiento con OADP, se produce a través de la activación del mecanismo apoptótico extrínseco, mediado por la caspasa-8. Mientras, la presencia del inhibidor de la caspasa-9 (Ac-LEHD-CMK), reveló que la activación del mecanismo de apoptosis intrínseco es secundaria, y que probablemente se produce para mejorar la señal apoptótica extrínseca inicial. Finalmente, la inhibición de JNK por SP600125, nos reveló que, aunque esta proteína está involucrada en la regulación de las vías apoptóticas activadas por OADP, no es determinante en la producción de apoptosis inducida por este compuesto. Estudios previos han demostrado que otros triterpenos pentacíclicos son capaces de activar tanto la vía apoptótica extrínseca como intrínseca en diferentes líneas tumorales. Por ejemplo, nuestro grupo demostró que el ácido maslínico, MA, fue capaz de activar ambas vías apoptóticas extrínseca e intrínseca en las líneas de cáncer de colon Caco-2 y HT29 respectivamente [27] [43].

Una vez demostrada la actividad apoptótica inducida por el OADP nos preguntamos si este compuesto también produciría efectos antiinflamatorios. Compuestos capaces de tener ambos comportamientos bioactivos son muy interesantes en la lucha contra el cáncer ya que muchos de los procesos tumorigénicos involucran la activación de las rutas de inflamación y proliferación celular, por lo que, en nuestro segundo artículo, se evaluó la eficacia antiinflamatoria del OADP.

Los macrófagos son un sistema idóneo para llevar a cabo estudios de actividad antiinflamatoria. Por este motivo, se eligió la línea celular de monocitos/macrófagos de ratón, RAW 264.7 estimulados con LPS, potente activador del proceso de inflamación en este tipo celular [85], [86]. Para evaluar la eficacia antiinflamatoria del OADP tras 72 h de tratamiento, primero se investigó su efecto sobre la producción de NO (óxido nítrico), mediador inflamatorio que desempeña un papel fundamental en la activación del proceso de inflamación. La formación excesiva de NO durante este proceso es debida al aumento de la expresión y actividad de la enzima iNOS, que promueve la respuesta inflamatoria, aumenta el estrés oxidativo y el daño tisular [85], [86].

Los resultados obtenidos tras 48 y 72 horas de incubación con OADP a concentraciones subcitotóxicas, en células RAW 264.7 activadas con el LPS, muestran que este compuesto fue 30 veces más efectivo que su precursor OA y 50 veces más efectivo que el diclofenaco (compuesto tomado como referencia) con una IC_{50NO} de $0.95 \pm 0.01 \mu\text{g/mL}$. Durante la respuesta inflamatoria, los macrófagos secretan múltiples citoquinas proinflamatorias que están involucradas en varias vías de señalización y son esenciales para el inicio y la mejora de la respuesta inflamatoria [90], [95]. El nivel de expresión de estas citoquinas puede emplearse como indicador para evaluar la eficacia antiinflamatoria en macrófagos. Nuestros resultados muestran que el tratamiento con OADP redujo significativamente la producción de las citoquinas proinflamatorias TNF- α , IL-1 β en macrófagos RAW 264.7 activados con LPS. El factor de transcripción nuclear NF- κ B, implicado en la activación del proceso inflamatorio, es inducido por la acción del LPS. De forma constitutiva NF- κ B se encuentra inactivo en el citosol unido a una proteína inhibidora I κ B (I κ B α). Diferentes señales extracelulares pueden activar la enzima I κ B quinasa (IKK) a través de receptores de membrana. IKK, a su vez, fosforila la proteína I κ B α lo que conduce a su ubiquitinación y degradación por el proteosoma, produciendo la liberación de NF- κ B [88], [90]. Nuestros resultados muestran que el tratamiento con OADP en macrófagos LPS activados inhibe la fosforilación de I κ B α y por tanto cortando la activación de esta ruta. De acuerdo con nuestros resultados, trabajos anteriores con el OA y sus derivados han mostrado que este compuestos presentan efectos antiinflamatorios [47]–[50]. De igual manera varios triterpenos pentacíclicos presentaron una importante actividad antiinflamatoria en células RAW264.7 estimuladas con LPS, disminuyendo la producción de NO y la expresión de iNOS [51], [53].

Finalmente nos propusimos corroborar el potencial antiinflamatorio del OADP en un modelo *in vivo*, para lo cual utilizamos el modelo de inflamación aguda inducido por TPA sobre oreja de ratón. La administración tópica de TPA origina una inflamación cutánea del tejido asociada a la formación de edema auricular, hiperplasia epidérmica y sobreproducción de mediadores inflamatorios como TNF- α , IL-1, IL-6 y COX-2.

Nuestros resultados mostraron que el tratamiento con OADP inhibió eficientemente la formación del edema en los grupos de ratones BL/6J tratados con respecto al grupo control. Este efecto antiinflamatorio del OADP, se observó en la reducción del grosor de las orejas de ratón tratadas de un 35%, 14% mayor a la producida por el diclofenaco (compuesto de referencia). El peso del diámetro del disco de 6mm extraído de la oreja de ratón disminuyó en un 25% con respecto al control positivo, siendo un 5% mayor al producido por el diclofenaco. Asimismo, se observó una reducción significativa en la producción de IL-6 siendo de un 250% respecto al control positivo, un 60% mayor que en el caso del diclofenaco. Además, cortes histológicos mostraron que el OADP mantuvo la integridad del epitelio y disminuyó el edema del tejido conectivo, así como la infiltración de neutrófilos, reduciendo de esta forma la respuesta inflamatoria del tejido. Resultados similares se han obtenido en trabajos anteriores, donde encontramos derivados del OA, como el CDDO-Me que reprimió la expresión de IL-6, TNF- α en inflamación crónica en colon de roedores [48]. Otros derivados acetilados y metilados del OA como el 3-A,28-MOA y 3AOA presentaron una buena actividad antiinflamatoria en modelos de inflamación en ratas Wistar macho [50]. El desarrollo de nuevos derivados como el OADP, con un potente efecto antiinflamatorio y anticancerígeno podría representar una estrategia terapéutica efectiva contra la inflamación y los procesos tumorigénicos.

Finalmente, en el tercer artículo presentado en esta tesis hemos evaluado el efecto anticancerígeno y antiinflamatorio de los N-derivados del DCF, obtenidos mediante modificaciones estructurales al nivel del grupo funcional amina secundaria. Numerosos estudios *in vitro* e *in vivo* han demostrado el potente efecto anticancerígeno y antiinflamatorio de los agentes antiinflamatorios no esteroideos, NSAIDs, en concreto del DCF y de sus derivados en diferentes líneas cancerígenas y modelos de inflamación [60], [62], [63], [65], [66], [74]. Trabajos previos mostraron que el DFC presenta efecto anticancerígeno en la línea de cáncer de colon HCT 116, induciendo la inhibición de la ruta de supervivencia celular PTEN/PDK/Akt, produciendo MAP quinasas como p44/42, p38 y la ruta SAPK/JNK e inhibiendo la ruta de supervivencia celular PI3K/Akt [65].

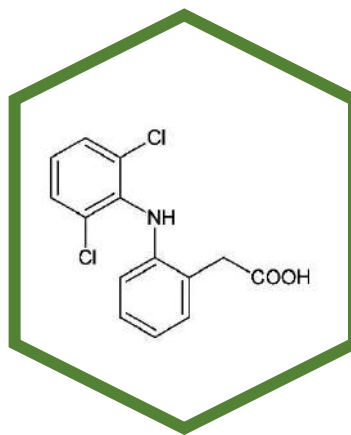
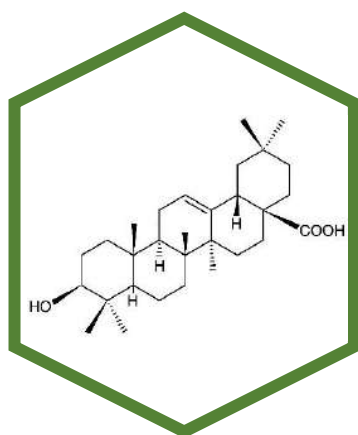
Se evaluó el efecto anticancerígeno de los N-Derivados del DCF, en las líneas de cáncer de colon humano (HT29), de hepatocarcinoma (HepG2) y de melanoma murino (B16-F10). Los resultados mostraron cierta correlación estructura-actividad, los compuestos 2, 4, 5, 8c y 9c fueron más citotóxicos que el DFC tras 72h de incubación, mientras que los compuestos 10a, 10b y 10c presentaron una citotoxicidad menor a la encontrada para el DFC, estos compuestos no presentan modificaciones el grupo ácido carboxílico (R_2), mientras que en los 5 primeros este grupo fue modificado disminuyendo su polaridad, incluso manteniendo el mismo sustituyente en R_1 . En el caso del compuesto 4 este mejoró su citotoxicidad con respecto al compuesto 2, al incluir dos cadenas alifáticas sobre el anillo lactama. Con respecto al compuesto 6, la transformación de esta lactama en un grupo indol mejoró su citotoxicidad. La presencia de este grupo indol ha sido descrita en otros agentes anticancerígenos como la vinblastina y la vincristina, inhibidores de la síntesis de tubulina que actualmente se encuentran en fase clínica [98].

El porcentaje de apoptosis encontrado para los compuestos con menor IC_{50} en las tres líneas tumorales ensayadas, 4 y 8c, fue de un 30% a un 60%, sin pérdida del potencial de membrana mitocondrial indicando la activación extrínseca del mecanismo de apoptosis a la concentración de IC_{50} , a la concentración de IC_{80} si se observó esta pérdida del PMM posiblemente como consecuencia de la activación secundaria del mecanismo de apoptosis intrínseca. Ambos compuestos produjeron arresto en el ciclo celular, el compuesto 4 en la fase G0/G1 y el compuesto 8c en la fase G2/M, en ambos casos posiblemente como consecuencia de la activación del fenómeno de apoptosis y de diferenciación para el compuesto 4. Otros estudios han mostrado el efecto anticancerígeno del DCF en la línea tumoral HepG2, induciendo apoptosis

a través de la activación de JNK, TNF- α e inhibición de NF- κ B [63]. El DCF produjo además la parada del ciclo celular en varias líneas tumorales [62]. Derivados conjugados del DCF, produjeron apoptosis a través de la activación de Bax y Caspasa-3 e inhibición del factor de transcripción Nrf2, y de las enzimas SOD-1 y NQO1 en la línea HepG2 [66].

En este artículo además se evaluó el efecto antiinflamatorio de estos N-derivados del DCF sobre monocitos/macrófagos de ratón RAW 264.7, activados con LPS. Nuestros resultados mostraron que a las concentraciones ensayadas (5, 10 y 20 μ g/mL) todos los compuestos, excepto 6 y 10c, mostraron un efecto inhibitorio en la producción de NO superior al diclofenaco. Tras 48h de incubación el compuesto 9c presentó la menor $IC_{50\text{ NO}}$ (1.89 ± 0.11 μ g/mL) siendo 25 veces menor que la encontrada para el diclofenaco ($IC_{50\text{ NO}} = 47.12 \pm 4.85$ μ g/mL). Los compuestos 2, 4, 8c, 10a y 10b mostraron valores de entre 10 a 20 μ g/mL para este parámetro. Como en el efecto antiinflamatorio el cambio del grupo ácido carboxílico en R₂, por grupos con menor polaridad pareció mejorar las bioactividades de los compuestos. Estos resultados correlacionan con los encontrados en la bibliografía donde la modificación del grupo ácido carboxílico en derivados del DFC mejora su actividad y minimiza sus efectos ulcerogénicos [70]. El efecto antiinflamatorio de diferentes derivados del DCF ha sido descrito previamente, así oxadiazol derivados del DCF inhibieron la inflamación inducida por carragenina en extremidad de rata, inhibiendo la expresión de COX-2 y sus efectos ulcerogénicos [70]. Otros oxidiazol derivados del DCF mostraron efecto inhibitorio en la producción de NO en macrófagos de ratón J774.2 activados por LPS [72]. Como ha sido mencionado anteriormente la obtención de nuevos derivados capaces de producir efectos apoptóticos y antiinflamatorios a muy bajas concentraciones puede ser una nueva estrategia terapéutica eficaz frente a este tipo de patologías y procesos tumorigénicos.

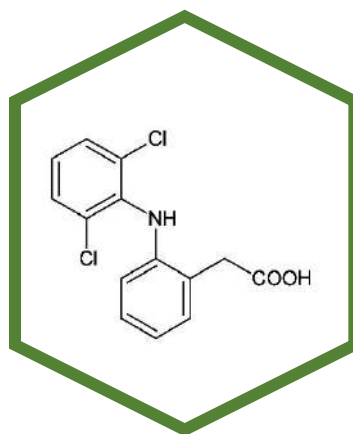
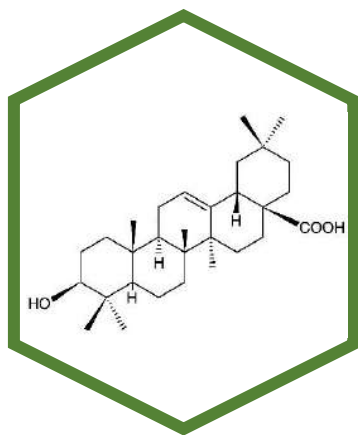
CONCLUSIONES



6. CONCLUSIONES

1. El OADP presentó un importante efecto anticancerígeno determinado mediante el ensayo de viabilidad celular MTT, mostrando ser más selectivo en línea tumoral de hepatoma HepG2 que en la línea de células normales WRL68. Efecto comprobado por microscopía de fluorescencia y citometría de flujo alcanzando un 95% de células apoptóticas, arresto del ciclo celular en la fase G0/G1 y pérdida final del potencial de membrana mitocondrial que sugirió la activación inicial de la vía extrínseca y secundaria de la vía apoptótica intrínseca, hechos confirmados por estudios de expresión.
 - Los estudios de expresión por *western blot* mostraron el siguiente mecanismo molecular: El OADP inicialmente desencadena la vía apoptótica extrínseca, iniciada por caspasa-8, que activa directamente a caspasa-3. Así mismo inicia la vía apoptótica encadenada por JNK y p53, induciendo la expresión de p21. Caspasa-8 y JNK provocan la activación secundaria de la vía apoptótica intrínseca, a través de la inhibición de Bcl-2 y activación de Bak, estimulando la respuesta apoptótica mitocondrial, formación del apoptosoma y activación de caspasa-9, reforzando la activación de la caspasa-3.
2. El OADP presentó además un importante efecto antiinflamatorio *in vitro* en línea celular de macrófagos/monocitos de ratón RAW 264.7 estimulados con LPS e *in vivo* en modelo de inflamación aguda por TPA en oreja de ratón. *In vitro*, se observó la inhibición de la producción de NO en la línea celular mencionada mediante el ensayo de Griess. Además, se comprobó por citometría de flujo, la recuperación de la parada en del ciclo celular en G0/G1, sufrida por estas células en respuesta a la acción del LPS.
 - Los estudios de expresión por *western blot* mostraron el siguiente mecanismo molecular: El OADP inhibiría la activación de receptores del tipo TLR4 o TNFR2, impidiendo la fosforilación de IκB, lo que inhibiría la activación de NF-κB. Finalmente, este proceso conduce a la inhibición de las citoquinas proinflamatorias: TNFα, IL-1β e IL-6, y proteínas mediadoras del proceso inflamatorio: COX-2 e iNOS. Los estudios *in vivo*, mostraron en respuesta al tratamiento con OADP la supresión del edema, descenso en la infiltración de leucocitos polimorfonucleares, disminución del grosor del tejido e inhibición en la producción de IL-6.
3. La mayoría de los N-derivados del diclofenaco analizados mostraron un importante efecto anticancerígeno y antiinflamatorio. Con una alta citotoxicidad en las tres líneas cancerígenas ensayadas (HT29, HepG2 y B16-F10). Los compuestos 4 y 8c, indujeron apoptosis, pérdida del PMM a la concentración de IC₈₀ y produjeron arresto en el ciclo celular en las fases G2/M y G0/G1 respectivamente.
 - Todos los compuestos presentaron una alta actividad antiinflamatoria, inhibiendo la producción de NO entre un 25% a un 75% en células RAW 264.7 estimuladas con LPS. Siendo el compuesto 9c el más efectivo con una IC_{50 NO}=1.89 ± 0.11 µg/mL, 25 veces menor que la del DCF.
4. Este tipo de compuestos con actividades proapoptóticas y antiinflamatorias podrían suponer una nueva estrategia terapéutica eficaz frente a patologías infamatorias crónicas, procesos tumorogénicos y cancerígenos.

BIBLIOGRAFÍA



7. BIBLIOGRAFÍA

- [1] W. G. D. Fernando, «Plants: An International Scientific Open Access Journal to Publish All Facets of Plants, Their Functions and Interactions with the Environment and Other Living Organisms», *Plants (Basel)*, vol. 1, n.º 1, pp. 1-5, feb. 2012, doi: 10.3390/plants1010001.
- [2] B. B. Petrovska, «Historical review of medicinal plants' usage», *Pharmacogn Rev*, vol. 6, n.º 11, pp. 1-5, ene. 2012, doi: 10.4103/0973-7847.95849.
- [3] K. Yazaki, «ABC transporters involved in the transport of plant secondary metabolites.», *FEBS Lett*, vol. 580, n.º 4, pp. 1183-1191, feb. 2006, doi: 10.1016/j.febslet.2005.12.009.
- [4] C. A. Seydler, *Analecta pharmacognostica*. Grunert, 1815. [En línea]. Disponible en: <https://books.google.es/books?id=zKZSngEACAAJ>
- [5] D. Tabajara de Oliveira Martins, E. Rodrigues, L. Casu, G. Benítez, y M. Leonti, «The historical development of pharmacopoeias and the inclusion of exotic herbal drugs with a focus on Europe and Brazil.», *J Ethnopharmacol*, vol. 240, p. 111891, ago. 2019, doi: 10.1016/j.jep.2019.111891.
- [6] S. D. Sarker, «Pharmacognosy in modern pharmacy curricula», *Pharmacogn Mag*, vol. 8, n.º 30, pp. 91-92, abr. 2012, doi: 10.4103/0973-1296.96545.
- [7] M. Assali *et al.*, «Self-assembly of diclofenac prodrug into nanomicelles for enhancing the anti-inflammatory activity», *RSC Adv.*, vol. 11, n.º 36, pp. 22433-22438, 2021, doi: 10.1039/D1RA03804D.
- [8] M. Medina-O'Donnell *et al.*, «Semi-synthesis and antiproliferative evaluation of PEGylated pentacyclic triterpenes.», *Eur J Med Chem*, vol. 118, pp. 64-78, ago. 2016, doi: 10.1016/j.ejmech.2016.04.016.
- [9] S.-L. Chen, H. Yu, H.-M. Luo, Q. Wu, C.-F. Li, y A. Steinmetz, «Conservation and sustainable use of medicinal plants: problems, progress, and prospects», *Chinese Medicine*, vol. 11, n.º 1, p. 37, jul. 2016, doi: 10.1186/s13020-016-0108-7.
- [10] H. I. A. Boy *et al.*, «Recommended Medicinal Plants as Source of Natural Products: A Review», *Digital Chinese Medicine*, vol. 1, n.º 2, pp. 131-142, jun. 2018, doi: 10.1016/S2589-3777(19)30018-7.
- [11] E. Salmerón-Manzano, J. A. Garrido-Cardenas, y F. Manzano-Agugliaro, «Worldwide Research Trends on Medicinal Plants.», *Int J Environ Res Public Health*, vol. 17, n.º 10, may 2020, doi: 10.3390/ijerph17103376.
- [12] D. J. Newman y G. M. Cragg, «Natural Products as Sources of New Drugs over the Nearly Four Decades from 01/1981 to 09/2019», *J. Nat. Prod.*, vol. 83, n.º 3, pp. 770-803, mar. 2020, doi: 10.1021/acs.jnatprod.9b01285.
- [13] M. Devilliers *et al.*, «Activation of TREK-1 by morphine results in analgesia without adverse side effects», *Nature Communications*, vol. 4, n.º 1, p. 2941, dic. 2013, doi: 10.1038/ncomms3941.
- [14] E. S. Seltzer, A. K. Watters, D. MacKenzie, L. M. Granat, y D. Zhang, «Cannabidiol (CBD) as a Promising Anti-Cancer Drug», *Cancers*, vol. 12, n.º 11, 2020, doi: 10.3390/cancers12113203.
- [15] G. A. Bonaterra, E. U. Heinrich, O. Kelber, D. Weiser, J. Metz, y R. Kinscherf, «Anti-inflammatory effects of the willow bark extract STW 33-I (Proaktiv®) in LPS-activated human monocytes and differentiated macrophages.», *Phytomedicine*, vol. 17, n.º 14, pp. 1106-1113, dic. 2010, doi: 10.1016/j.phymed.2010.03.022.
- [16] N. Vargas-Mendoza *et al.*, «Hepatoprotective effect of silymarin», *World J Hepatol*, vol. 6, n.º 3, pp. 144-149, mar. 2014, doi: 10.4254/wjh.v6.i3.144.
- [17] B. Salehi *et al.*, «The Therapeutic Potential of the Labdane Diterpenoid Forskolin», *Applied Sciences*, vol. 9, n.º 19, 2019, doi: 10.3390/app9194089.

- [18] B. A. Weaver, «How Taxol/paclitaxel kills cancer cells», *Mol Biol Cell*, vol. 25, n.º 18, pp. 2677-2681, sep. 2014, doi: 10.1091/mbc.E14-04-0916.
- [19] D. S. Hong *et al.*, «A phase I first-in-human trial of bardoxolone methyl in patients with advanced solid tumors and lymphomas.», *Clin Cancer Res*, vol. 18, n.º 12, pp. 3396-3406, jun. 2012, doi: 10.1158/1078-0432.CCR-11-2703.
- [20] A. G. Atanasov *et al.*, «Natural products in drug discovery: advances and opportunities», *Nature Reviews Drug Discovery*, vol. 20, n.º 3, pp. 200-216, mar. 2021, doi: 10.1038/s41573-020-00114-z.
- [21] V. Ninkuu, L. Zhang, J. Yan, Z. Fu, T. Yang, y H. Zeng, «Biochemistry of Terpenes and Recent Advances in Plant Protection», *International Journal of Molecular Sciences*, vol. 22, n.º 11, 2021, doi: 10.3390/ijms22115710.
- [22] Y. Fang y H. Xiao, «The transport of triterpenoids», *Biotechnology Notes*, vol. 2, pp. 11-17, ene. 2021, doi: 10.1016/j.biotno.2021.03.001.
- [23] C. M. Andre *et al.*, «Multifunctional oxidosqualene cyclases and cytochrome P450 involved in the biosynthesis of apple fruit triterpenic acids», *New Phytologist*, vol. 211, n.º 4, pp. 1279-1294, 2016.
- [24] N. Stiti y M.-A. Hartmann, «Nonsterol Triterpenoids as Major Constituents of *Olea europaea*.», *J Lipids*, vol. 2012, p. 476595, 2012, doi: 10.1155/2012/476595.
- [25] P. Xie *et al.*, «Phenolic Compounds and Triterpenes in Different Olive Tissues and Olive Oil By-Products, and Cytotoxicity on Human Colorectal Cancer Cells: The Case of Frantoio, Moraiolo and Leccino Cultivars (*Olea europaea* L.)», *Foods*, vol. 10, n.º 11, 2021, doi: 10.3390/foods10112823.
- [26] M. Medina-O'Donnell, F. Rivas, F. J. Reyes-Zurita, A. Martinez, J. A. Lupiañez, y A. Parra, «Diamine and PEGylated-diamine conjugates of triterpenic acids as potential anticancer agents.», *Eur J Med Chem*, vol. 148, pp. 325-336, mar. 2018, doi: 10.1016/j.ejmech.2018.02.044.
- [27] F. J. Reyes-Zurita *et al.*, «Maslinic Acid, a Natural Triterpene, Induces a Death Receptor-Mediated Apoptotic Mechanism in Caco-2 p53-Deficient Colon Adenocarcinoma Cells.», *PLoS One*, vol. 11, n.º 1, p. e0146178, 2016, doi: 10.1371/journal.pone.0146178.
- [28] R. Rodriguez-Rodriguez y V. Ruiz-Gutierrez, «Chapter 159 - Functional Properties of Pentacyclic Triterpenes Contained in Pomace Olive Oil», en *Olives and Olive Oil in Health and Disease Prevention*, V. R. Preedy y R. R. Watson, Eds. San Diego: Academic Press, 2010, pp. 1431-1438. doi: 10.1016/B978-0-12-374420-3.00159-5.
- [29] Sandeep y S. Ghosh, «Chapter 12 - Triterpenoids: Structural diversity, biosynthetic pathway, and bioactivity», en *Studies in Natural Products Chemistry*, vol. 67, Atta-ur-Rahman, Ed. Elsevier, 2020, pp. 411-461. doi: 10.1016/B978-0-12-819483-6.00012-6.
- [30] M. R. García-Risco *et al.*, «Supercritical fluid extraction of heather (*Calluna vulgaris*) and evaluation of anti-hepatitis C virus activity of the extracts.», *Virus Res*, vol. 198, pp. 9-14, feb. 2015, doi: 10.1016/j.virusres.2014.12.022.
- [31] J. Fu *et al.*, «Hybrid Molecule from O2-(2,4-Dinitrophenyl)diazeniumdiolate and Oleanolic Acid: A Glutathione S-Transferase π -Activated Nitric Oxide Prodrug with Selective Anti-Human Hepatocellular Carcinoma Activity and Improved Stability», *J. Med. Chem.*, vol. 56, n.º 11, pp. 4641-4655, jun. 2013, doi: 10.1021/jm400393u.
- [32] K. H. Yoo *et al.*, «3-O-Acetyloleanolic acid induces apoptosis in human colon carcinoma Hct-116 cells», *Phytotherapy Research*, vol. 26, n.º 10, pp. 1541-1546, 2012.
- [33] T. B. Ayeleso, M. G. Matumba, y E. Mukwevho, «Oleanolic Acid and Its Derivatives: Biological Activities and Therapeutic Potential in Chronic Diseases», *Molecules*, vol. 22, n.º 11, 2017, doi: 10.3390/molecules22111915.
- [34] M. H. Ghante y P. G. Jamkhande, «Role of Pentacyclic Triterpenoids in Chemoprevention and Anticancer Treatment: An Overview on Targets and Underling Mechanisms», *J Pharmacopuncture*, vol. 22, n.º 2, pp. 55-67, jun. 2019, doi: 10.3831/KPI.201.22.007.

- [35] E. E. Rufino-Palomares *et al.*, «Anti-cancer and Anti-angiogenic Properties of Various Natural Pentacyclic Tri-terpenoids and Some of their Chemical Derivatives», *Current Organic Chemistry*, vol. 19, n.º 10, pp. 919-947, 2015, doi: 10.2174/1385272819666150119225952.
- [36] X. Wang *et al.*, «Inhibitory effect of oleanolic acid on hepatocellular carcinoma via ERK-p53-mediated cell cycle arrest and mitochondrial-dependent apoptosis.», *Carcinogenesis*, vol. 34, n.º 6, pp. 1323-1330, jun. 2013, doi: 10.1093/carcin/bgt058.
- [37] S. Amara, M. Zheng, y V. Tiriveedhi, «Oleanolic Acid Inhibits High Salt-Induced Exaggeration of Warburg-like Metabolism in Breast Cancer Cells.», *Cell Biochem Biophys*, vol. 74, n.º 3, pp. 427-434, sep. 2016, doi: 10.1007/s12013-016-0736-7.
- [38] M.-H. Shyu, T.-C. Kao, y G.-C. Yen, «Oleanolic Acid and Ursolic Acid Induce Apoptosis in HuH7 Human Hepatocellular Carcinoma Cells through a Mitochondrial-Dependent Pathway and Downregulation of XIAP», *J. Agric. Food Chem.*, vol. 58, n.º 10, pp. 6110-6118, may 2010, doi: 10.1021/jf100574j.
- [39] P. Mishra, B. Nayak, y R. K. Dey, «PEGylation in anti-cancer therapy: An overview», *Asian Journal of Pharmaceutical Sciences*, vol. 11, n.º 3, pp. 337-348, jun. 2016, doi: 10.1016/j.ajps.2015.08.011.
- [40] M. Fukumura, H. Ando, Y. Hirai, K. Toriizuka, Y. Ida, y Y. Kuchino, «Achyranthoside H methyl ester, a novel oleanolic acid saponin derivative from *Achyranthes fauriei* roots, induces apoptosis in human breast cancer MCF-7 and MDA-MB-453 cells via a caspase activation pathway», *Journal of Natural Medicines*, vol. 63, n.º 2, pp. 181-188, 2009, doi: 10.1007/s11418-008-0311-7.
- [41] R. Ahmad, D. Raina, C. Meyer, y D. Kufe, «Triterpenoid CDDO-Methyl Ester Inhibits the Janus-Activated Kinase-1 (JAK1)→Signal Transducer and Activator of Transcription-3 (STAT3) Pathway by Direct Inhibition of JAK1 and STAT3», *Cancer Res*, vol. 68, n.º 8, p. 2920, abr. 2008, doi: 10.1158/0008-5472.CAN-07-3036.
- [42] X. Gao, D. Deeb, H. Jiang, Y. Liu, S. A. Dulchavsky, y S. C. Gautam, «Synthetic triterpenoids inhibit growth and induce apoptosis in human glioblastoma and neuroblastoma cells through inhibition of prosurvival Akt, NF-κB and Notch1 signaling», *Journal of Neuro-Oncology*, vol. 84, n.º 2, pp. 147-157, sep. 2007, doi: 10.1007/s11060-007-9364-9.
- [43] F. J. Reyes-Zurita, E. E. Rufino-Palomares, J. A. Lupiáñez, y M. Cascante, «Maslinic acid, a natural triterpene from *Olea europaea* L., induces apoptosis in HT29 human colon-cancer cells via the mitochondrial apoptotic pathway.», *Cancer Lett*, vol. 273, n.º 1, pp. 44-54, ene. 2009, doi: 10.1016/j.canlet.2008.07.033.
- [44] N. Yao *et al.*, «A piperazine derivative of 23-hydroxy betulinic acid induces a mitochondria-derived ROS burst to trigger apoptotic cell death in hepatocellular carcinoma cells», *Journal of Experimental & Clinical Cancer Research*, vol. 35, n.º 1, p. 192, dic. 2016, doi: 10.1186/s13046-016-0457-1.
- [45] Q. Huang *et al.*, «Anti-hepatocellular carcinoma activity and mechanism of chemopreventive compounds: ursolic acid derivatives», *null*, vol. 54, n.º 12, pp. 3189-3196, dic. 2016, doi: 10.1080/13880209.2016.1214742.
- [46] S. Zappavigna *et al.*, «Anti-Inflammatory Drugs as Anticancer Agents», *International Journal of Molecular Sciences*, vol. 21, n.º 7, 2020, doi: 10.3390/ijms21072605.
- [47] G.-D. Kang, S. Lim, y D.-H. Kim, «Oleanolic acid ameliorates dextran sodium sulfate-induced colitis in mice by restoring the balance of Th17/Treg cells and inhibiting NF-κB signaling pathway.», *Int Immunopharmacol*, vol. 29, n.º 2, pp. 393-400, dic. 2015, doi: 10.1016/j.intimp.2015.10.024.
- [48] C. H. L. Dinh, Y. Yu, A. Szabo, Q. Zhang, P. Zhang, y X.-F. Huang, «Bardoxolone Methyl Prevents High-Fat Diet-Induced Colon Inflammation in Mice.», *J Histochem Cytochem*, vol. 64, n.º 4, pp. 237-255, abr. 2016, doi: 10.1369/0022155416631803.

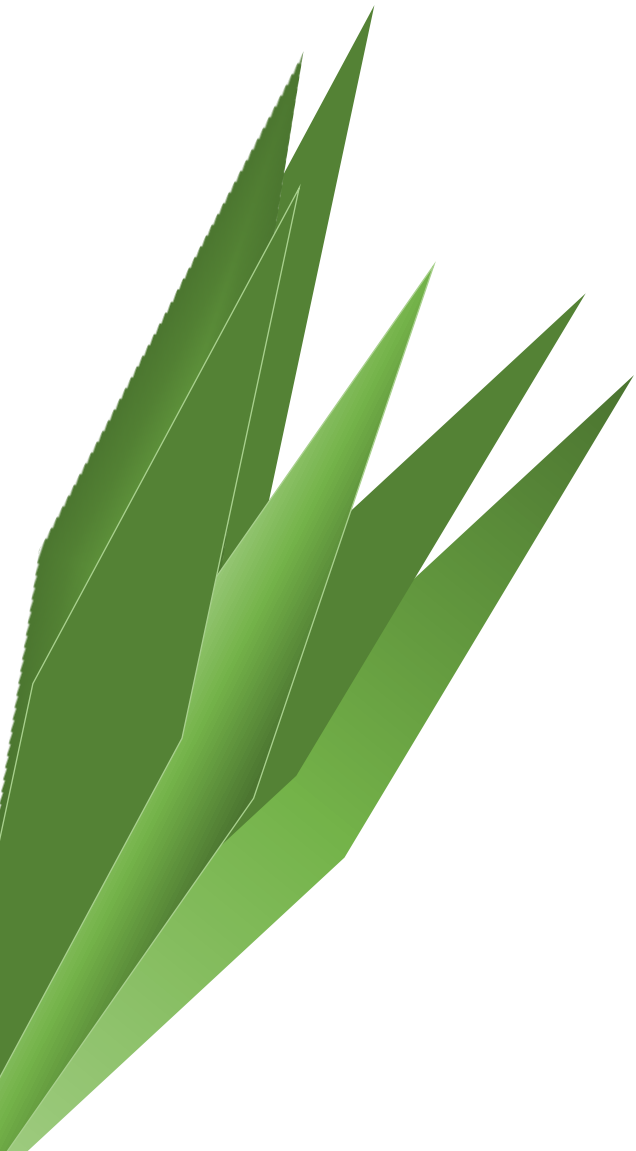
- [49] L. R. Fitzpatrick, E. Stonesifer, J. S. Small, y K. T. Liby, «The synthetic triterpenoid (CDDO-Im) inhibits STAT3, as well as IL-17, and improves DSS-induced colitis in mice.», *Inflammopharmacology*, vol. 22, n.º 6, pp. 341-349, dic. 2014, doi: 10.1007/s10787-014-0203-2.
- [50] B. N. Nkeh-Chungag, O. O. Oyedeji, A. O. Oyedeji, y E. J. Ndebia, «Anti-inflammatory and membrane-stabilizing properties of two semisynthetic derivatives of oleanolic acid.», *Inflammation*, vol. 38, n.º 1, pp. 61-69, feb. 2015, doi: 10.1007/s10753-014-0007-y.
- [51] Y. Han *et al.*, «Anti-Inflammatory Activity of Three Triterpene from *Hippophae rhamnoides* L. in Lipopolysaccharide-Stimulated RAW264.7 Cells», *International Journal of Molecular Sciences*, vol. 22, n.º 21, 2021, doi: 10.3390/ijms222112009.
- [52] J. F. Oliveira Costa *et al.*, «Potent anti-inflammatory activity of betulinic acid treatment in a model of lethal endotoxemia», *International Immunopharmacology*, vol. 23, n.º 2, pp. 469-474, dic. 2014, doi: 10.1016/j.intimp.2014.09.021.
- [53] T. Zerín, M. Lee, W. Jang Sik, K. Nam, y H. Song, «Anti-inflammatory potential of ursolic acid in *Mycobacterium tuberculosis*-sensitized and Concanavalin A-stimulated cells», *Mol Med Rep*, vol. 13, n.º 3, pp. 2736-2744, mar. 2016, doi: 10.3892/mmr.2016.4840.
- [54] M. J. R. Desborough y D. M. Keeling, «The aspirin story – from willow to wonder drug», *British Journal of Haematology*, vol. 177, n.º 5, pp. 674-683, jun. 2017, doi: 10.1111/bjh.14520.
- [55] I. Melnikova, «Pain market», *Nature Reviews Drug Discovery*, vol. 9, n.º 8, pp. 589-590, ago. 2010, doi: 10.1038/nrd3226.
- [56] Newman Osafo, «Mechanism of Action of Nonsteroidal Anti-Inflammatory Drugs», en *Nonsteroidal Anti-Inflammatory Drugs*, Christian Agyare, Ed. Rijeka: IntechOpen, 2017, p. Ch. 2. doi: 10.5772/68090.
- [57] D. T. Manallack, R. J. Prankerd, E. Yuriev, T. I. Oprea, y D. K. Chalmers, «The significance of acid/base properties in drug discovery», *Chem Soc Rev*, vol. 42, n.º 2, pp. 485-496, ene. 2013, doi: 10.1039/c2cs35348b.
- [58] R. Altman, B. Bosch, K. Brune, P. Patrignani, y C. Young, «Advances in NSAID development: evolution of diclofenac products using pharmaceutical technology», *Drugs*, vol. 75, n.º 8, pp. 859-877, may 2015, doi: 10.1007/s40265-015-0392-z.
- [59] K. M. Egan *et al.*, «Analgesic use and the risk of primary adult brain tumor», *Eur J Epidemiol*, vol. 31, n.º 9, pp. 917-925, sep. 2016, doi: 10.1007/s10654-016-0129-7.
- [60] R. S. Y. Wong, «Role of Nonsteroidal Anti-Inflammatory Drugs (NSAIDs) in Cancer Prevention and Cancer Promotion», *Adv Pharmacol Sci*, vol. 2019, pp. 3418975-3418975, ene. 2019, doi: 10.1155/2019/3418975.
- [61] L. Marinov, A. Georgieva, Y. Voynikov, R. Toshkova, I. Nikolova, y M. Malchev, «Cytotoxic and antiproliferative effects of the nonsteroidal anti-inflammatory drug diclofenac in human tumour cell lines», *null*, vol. 35, n.º 1, pp. 1118-1126, ene. 2021, doi: 10.1080/13102818.2021.1953401.
- [62] B. L. Valle *et al.*, «Non-Steroidal Anti-inflammatory Drugs Decrease E2F1 Expression and Inhibit Cell Growth in Ovarian Cancer Cells», *PLOS ONE*, vol. 8, n.º 4, p. e61836, abr. 2013, doi: 10.1371/journal.pone.0061836.
- [63] L. Fredriksson *et al.*, «Diclofenac inhibits tumor necrosis factor- α -induced nuclear factor- κ B activation causing synergistic hepatocyte apoptosis.», *Hepatology*, vol. 53, n.º 6, pp. 2027-2041, jun. 2011, doi: 10.1002/hep.24314.
- [64] R. Singh *et al.*, «The non-steroidal anti-inflammatory drugs Sulindac sulfide and Diclofenac induce apoptosis and differentiation in human acute myeloid leukemia cells through an AP-1 dependent pathway.», *Apoptosis*, vol. 16, n.º 9, pp. 889-901, sep. 2011, doi: 10.1007/s10495-011-0624-y.
- [65] E. D. Arisan *et al.*, «Diclofenac induced apoptosis via altering PI3K/Akt/MAPK signaling axis in HCT 116 more efficiently compared to SW480 colon cancer cells», *Molecular*

- Biology Reports*, vol. 45, n.º 6, pp. 2175-2184, dic. 2018, doi: 10.1007/s11033-018-4378-2.
- [66] M. Narożna *et al.*, «Conjugation of Diclofenac with Novel Oleanolic Acid Derivatives Modulate Nrf2 and NF-κB Activity in Hepatic Cancer Cells and Normal Hepatocytes Leading to Enhancement of Its Therapeutic and Chemopreventive Potential», *Pharmaceuticals*, vol. 14, n.º 7, 2021, doi: 10.3390/ph14070688.
- [67] Mahmoud M. Hamed, A. M. K. El-Dean, S. A. Abdel-Mohsen, y M. S. Tolba, «New Diclofenac Derivatives as Anti-Microbial, Anti-Inflammatory Agents: Design, Synthesis, Biological Screening, and Molecular Docking Study», *Russian Journal of Bioorganic Chemistry*, vol. 47, n.º 1, pp. 208-220, ene. 2021, doi: 10.1134/S1068162021010088.
- [68] F. M. Steckling *et al.*, «Diclofenac attenuates inflammation through TLR4 pathway and improves exercise performance after exhaustive swimming», *Scandinavian Journal of Medicine & Science in Sports*, vol. 30, n.º 2, pp. 264-271, feb. 2020, doi: 10.1111/sms.13579.
- [69] P. McGettigan y D. Henry, «Use of non-steroidal anti-inflammatory drugs that elevate cardiovascular risk: an examination of sales and essential medicines lists in low-, middle-, and high-income countries.», *PLoS Med*, vol. 10, n.º 2, p. e1001388, 2013, doi: 10.1371/journal.pmed.1001388.
- [70] M. B. Palkar *et al.*, «Synthesis, pharmacological screening and in silico studies of new class of Diclofenac analogues as a promising anti-inflammatory agents», *Bioorganic & medicinal chemistry*, vol. 22, n.º 10, pp. 2855-2866, 2014.
- [71] S. V. Bhandari, K. G. Bothara, M. K. Raut, A. A. Patil, A. P. Sarkate, y V. J. Mokale, «Design, synthesis and evaluation of antiinflammatory, analgesic and ulcerogenicity studies of novel S-substituted phenacyl-1, 3, 4-oxadiazole-2-thiol and Schiff bases of diclofenac acid as nonulcerogenic derivatives», *Bioorganic & medicinal chemistry*, vol. 16, n.º 4, pp. 1822-1831, 2008.
- [72] S. Shah *et al.*, «Diclofenac 1,3,4-Oxadiazole Derivatives; Biology-Oriented Drug Synthesis (BIODS) in Search of Better Non-Steroidal, Non-Acid Antiinflammatory Agents.», *Med Chem*, vol. 14, n.º 7, pp. 674-687, 2018, doi: 10.2174/1573406414666180321141555.
- [73] M. M. Ibrahim, T. Elsaman, y M. Y. Al-Nour, «Synthesis, Anti-Inflammatory Activity, and In Silico Study of Novel Diclofenac and Isatin Conjugates.», *Int J Med Chem*, vol. 2018, p. 9139786, 2018, doi: 10.1155/2018/9139786.
- [74] M. Narożna, V. Krajka-Kuźniak, R. Kleszcz, y W. Baer-Dubowska, «Indomethacin and Diclofenac Hybrids with Oleanolic Acid Oximes Modulate Key Signaling Pathways in Pancreatic Cancer Cells», *International Journal of Molecular Sciences*, vol. 23, n.º 3, 2022, doi: 10.3390/ijms23031230.
- [75] R. Singh, A. Letai, y K. Sarosiek, «Regulation of apoptosis in health and disease: the balancing act of BCL-2 family proteins», *Nat Rev Mol Cell Biol*, vol. 20, n.º 3, pp. 175-193, mar. 2019, doi: 10.1038/s41580-018-0089-8.
- [76] J. Li y J. Yuan, «Caspases in apoptosis and beyond», *Oncogene*, vol. 27, n.º 48, pp. 6194-6206, oct. 2008, doi: 10.1038/onc.2008.297.
- [77] S. Fulda y K.-M. Debatin, «Extrinsic versus intrinsic apoptosis pathways in anticancer chemotherapy», *Oncogene*, vol. 25, n.º 34, pp. 4798-4811, ago. 2006, doi: 10.1038/sj.onc.1209608.
- [78] M. Alam, S. Ali, T. Mohammad, G. M. Hasan, D. K. Yadav, y Md. I. Hassan, «B Cell Lymphoma 2: A Potential Therapeutic Target for Cancer Therapy», *International Journal of Molecular Sciences*, vol. 22, n.º 19, 2021, doi: 10.3390/ijms221910442.
- [79] S. Elmore, «Apoptosis: a review of programmed cell death», *Toxicol Pathol*, vol. 35, n.º 4, pp. 495-516, jun. 2007, doi: 10.1080/01926230701320337.
- [80] B. J. Aubrey, G. L. Kelly, A. Janic, M. J. Herold, y A. Strasser, «How does p53 induce apoptosis and how does this relate to p53-mediated tumour suppression?», *Cell Death & Differentiation*, vol. 25, n.º 1, pp. 104-113, ene. 2018, doi: 10.1038/cdd.2017.169.

- [81] B. Shamloo y S. Usluer, «p21 in Cancer Research», *Cancers*, vol. 11, n.º 8, 2019, doi: 10.3390/cancers11081178.
- [82] D. N. Dhanasekaran y E. P. Reddy, «JNK signaling in apoptosis», *Oncogene*, vol. 27, n.º 48, pp. 6245-6251, oct. 2008, doi: 10.1038/onc.2008.301.
- [83] K. J. Barnum y M. J. O'Connell, «Cell cycle regulation by checkpoints», *Methods Mol Biol*, vol. 1170, pp. 29-40, 2014, doi: 10.1007/978-1-4939-0888-2_2.
- [84] W. Ma, «Cell Cycle Checkpoint», en *Encyclopedia of Cancer*, M. Schwab, Ed. Berlin, Heidelberg: Springer Berlin Heidelberg, 2017, pp. 897-901. doi: 10.1007/978-3-662-46875-3_996.
- [85] L. Chen *et al.*, «Inflammatory responses and inflammation-associated diseases in organs», *Oncotarget*, vol. 9, n.º 6, pp. 7204-7218, dic. 2017, doi: 10.18632/oncotarget.23208.
- [86] I. Soufli, R. Toumi, H. Raza, y C. Touil-Boukoffa, «Overview of cytokines and nitric oxide involvement in immuno-pathogenesis of inflammatory bowel diseases», *World J Gastrointest Pharmacol Ther*, vol. 7, n.º 3, pp. 353-360, ago. 2016, doi: 10.4292/wjgpt.v7.i3.353.
- [87] E. Rubin y H. M. Reisner, *Rubin principios de patología / [autores principales] Emanuel Rubin, Howard M. Reisner*, 7ª ed. Philadelphia: Wolters Kluwer, 2019.
- [88] A. K. Abbas, A. H. Lichtman, y S. Pillai, *Inmunología celular y molecular / Abul K. Abbas, Andrew H. Lichtman, Shiv Pillai.*, 7ª ed. Barcelona: Elsevier, 2012.
- [89] M. M. Tucureanu *et al.*, «Lipopolysaccharide-induced inflammation in monocytes/macrophages is blocked by liposomal delivery of G(i)-protein inhibitor», *Int J Nanomedicine*, vol. 13, pp. 63-76, dic. 2017, doi: 10.2147/IJN.S150918.
- [90] J. A. Owen, J. Punt, S. A. Stranford, y P. P. Jones, *Kuby immunology / Judith A. Owen, Jenni Punt, Sharon A. Stranford ; with contributions by Patricia P. Jones*, 7th edition. New York: W.H. Freeman and Company, 2013.
- [91] X. Li, Y. Gu, H. Dong, W. Wang, y C. Dong, «Trapped lipopolysaccharide and LptD intermediates reveal lipopolysaccharide translocation steps across the Escherichia coli outer membrane», *Scientific Reports*, vol. 5, n.º 1, p. 11883, jul. 2015, doi: 10.1038/srep11883.
- [92] A. Płóciennikowska, A. Hromada-Judycka, K. Borzęcka, y K. Kwiatkowska, «Co-operation of TLR4 and raft proteins in LPS-induced pro-inflammatory signaling», *Cell Mol Life Sci*, vol. 72, n.º 3, pp. 557-581, feb. 2015, doi: 10.1007/s00018-014-1762-5.
- [93] A. Fournier y A. W. Murray, «Application of phorbol ester to mouse skin causes a rapid and sustained loss of protein kinase C», *Nature*, vol. 330, n.º 6150, pp. 767-769, dic. 1987, doi: 10.1038/330767a0.
- [94] S. Hannoodee y D. N. Nasuruddin, «Acute Inflammatory Response.» en *StatPearls*, Treasure Island (FL): StatPearls Publishing, 2021.
- [95] S. Kany, J. T. Vollrath, y B. Relja, «Cytokines in Inflammatory Disease», *International Journal of Molecular Sciences*, vol. 20, n.º 23, 2019, doi: 10.3390/ijms20236008.
- [96] A. Zarghi y S. Arfaei, «Selective COX-2 Inhibitors: A Review of Their Structure-Activity Relationships», *Iran J Pharm Res*, vol. 10, n.º 4, pp. 655-683, 2011, [En línea]. Disponible en: <https://pubmed.ncbi.nlm.nih.gov/24250402>
- [97] S. Zappavigna *et al.*, «Anti-Inflammatory Drugs as Anticancer Agents», *International Journal of Molecular Sciences*, vol. 21, n.º 7, 2020, doi: 10.3390/ijms21072605.
- [98] Y. Wan, Y. Li, C. Yan, M. Yan, y Z. Tang, «Indole: A privileged scaffold for the design of anti-cancer agents», *European Journal of Medicinal Chemistry*, vol. 183, p. 111691, dic. 2019, doi: 10.1016/j.ejmech.2019.111691.



**OTRAS
COLABORACIONES**



8. OTRAS COLABORACIONES

Durante la realización de esta tesis doctoral hemos colaborado con el grupo de Química Inorgánica "FQM-195: Química de la Coordinación y Análisis Estructural" y con el grupo de Química Orgánica "FQM-348 : Productos Naturales y Síntesis Orgánica Aplicada" que ha dado lugar a las siguientes publicaciones:
















International Journal of
Molecular Sciences



Article

Designing Single-Molecule Magnets as Drugs with Dual Anti-Inflammatory and Anti-Diabetic Effects

Arturo Navas ¹, Fatin Jannus ², Belén Fernández ^{3,*}, Javier Cepeda ⁴,
Marta Medina O'Donnell ⁵, Luis Díaz-Ruiz ², Cristina Sánchez-González ⁶, Juan Llopis ⁶,
José M. Seco ⁴, E. Rufino-Palomares ², José Antonio Lupiáñez ², Santiago Gómez-Ruiz ⁷,
José Luis Quiles ^{8,*}, Maurizio Battino ⁹, Duane Choquesillo-Lazarte ¹⁰,
Ana Belén Ruiz-Muelle ¹¹, Ignacio Fernández ¹¹, Fernando Reyes-Zurita ^{2,*} and
Antonio Rodríguez-Diéguez ^{1,*}

Abstract: We have designed and synthesized two novel cobalt coordination compounds using bumetanide (bum) and indomethacin (ind) therapeutic agents. The anti-inflammatory effects of cobalt metal complexes with ind and bum were assayed in lipopolysaccharide stimulated RAW 264.7 macrophages by inhibition of nitric oxide production. Firstly, we determined the cytotoxicity and the anti-inflammatory potential of the cobalt compounds and ind and bum ligands in RAW 264.7 cells. Indomethacin-based metal complex was able to inhibit the NO production up to 35% in a concentration-dependent manner without showing cytotoxicity, showing around 6–37 times more effective than indomethacin. Cell cycle analysis showed that the inhibition of NO production was accompanied by a reversion of the differentiation processes in LPS-stimulated RAW 264.7 cells, due to a decreased of cell percentage in G0/G1 phase, with the corresponding increase in the number of cells in S phase. These two materials have mononuclear structures and show slow relaxation of magnetization. Moreover, both compounds show anti-diabetic activity with low in vitro cell toxicities. The formation of metal complexes with bioactive ligands is a new and promising strategy to find new compounds with high and enhanced biochemical properties and promises to be a field of great interest.



Contents lists available at ScienceDirect

Journal of Inorganic Biochemistry

journal homepage: www.elsevier.com/locate/jinorgbio



5-Aminopyridine-2-carboxylic acid as appropriate ligand for constructing coordination polymers with luminescence, slow magnetic relaxation and anti-cancer properties[☆]

Antonio A. García-Valdivia^a, Javier Cepeda^b, Belén Fernández^{c,*}, Marta Medina-O'donnell^d, Itziar Oyarzabal^b, Jerónimo Parra^a, Fatin Jannus^e, Duane Choquesillo-Lazarte^g, José A. García^h, José Antonio Lupiáñez^e, Santiago Gómez-Ruiz^f, Fernando Reyes-Zurita^{e,*}, Antonio Rodríguez-Diéguez^{a,*}

ABSTRACT

Five new coordination polymers (CPs) constructed of aminopyridine-2-carboxylate (ampy) ligand have been synthesized and fully characterized. Three of them correspond to metal-organic chains built from the coordination of ampy to sodium and lanthanides with formulae $[MNa(ampy)_4]_n$ ($M = \text{terbium (2)}$, erbium (1) and ytterbium (3)) resembling a previously reported dysprosium material which shows anticancer activity. On another level, the reaction of Hampy with cobalt and copper ions ($\{[CoK(ampy)_3(H_2O)_3](H_2O)_3\}_n$ (4) and $[Cu(ampy)_2]_n$ (5)) lead to CPs with variable dimensionalities, which gives the opportunity of analyzing the structural properties of this new family. Lanthanide materials display solid state intense photoluminescent emissions in both the visible and near-infrared region and exhibit slow relaxation of magnetization with frequency dependence of the out-of-phase susceptibility. More interestingly, in our search for multifunctional materials, we have carried out antitumor measurements of these compounds. These multidisciplinary studies of metal complexes open up the possibility for further exploring the applications in the fields of metal-based drugs.



Contents lists available at ScienceDirect

Journal of Inorganic Biochemistry

journal homepage: www.elsevier.com/locate/jinorgbio



Antiparasitic, anti-inflammatory and cytotoxic activities of 2D coordination polymers based on 1H-indazole-5-carboxylic acid



Antonio A. García-Valdivia^a, Amalia García-García^a, Fatin Jannus^b, Andoni Zabala-Lekuona^c, José M. Méndez-Arriaga^d, Belén Fernández^{e,*}, Marta Medina-O'donnell^f, Gloria B. Ramírez-Rodríguez^a, José M. Delgado-López^a, Luisa M. Pastrana-Martínez^a, Javier Cepeda^c, José A. Lupiáñez^b, Fernando J. Reyes-Zurita^{b,*}, Antonio Rodríguez-Diéguez^{a,*}

ABSTRACT

We report on the formation of two novel multifunctional isomorphous (4,4) square-grid 2D coordination polymers based on 1H-indazole-5-carboxylic acid. To the best of our knowledge, these complexes are the first examples of 2D-coordination polymers constructed with this novel ligand. We have analysed in detail the structural, magnetic and anti-parasitic properties of the resulting materials. In addition, the capability of inhibiting nitric oxide production from macrophage cells has been measured and was used as an indirect measure of the anti-inflammatory response. Finally, the photocatalytic activity was measured with a model pollutant, *i.e.* vanillic acid (phenolic compound), with the aim of further increasing the functionalities and applicability of the compounds.



Contents lists available at [ScienceDirect](https://www.sciencedirect.com)

Journal of Inorganic Biochemistry

journal homepage: www.elsevier.com/locate/jinorgbio



Anti-cancer and anti-inflammatory activities of a new family of coordination compounds based on divalent transition metal ions and indazole-3-carboxylic acid







Antonio A. García-Valdivia^a, Fatin Jannus^b, Amalia García-García^a, Duane Choquesillo-Lazarte^c, Belén Fernández^d, Marta Medina-O'donnell^e, José A. Lupiáñez^b, Javier Cepeda^f, Fernando J. Reyes-Zurita^{b,*}, Antonio Rodríguez-Diéguez^{a,*}

ABSTRACT

A new family of mononuclear coordination compounds has been synthesized and characterized: $[M(3\text{-ind})_2(\text{H}_2\text{O})_2]$ ($M = \text{Co}$ (1), Ni (2), Zn (3), Fe (4), Mn (5); 3-ind = indazole-3-carboxylate). These materials are mononuclear coordination compounds that possess strong hydrogen bond interactions. The anti-inflammatory effects of these compounds were assayed in lipopolysaccharide activated RAW 264.7 macrophages by inhibition of NO production. Moreover, the cytotoxicity of the complexes and the ligand in RAW 264.7 cells were determined for the first time. The most significant results were obtained for the compounds 4 and 5 reaching values of NO inhibition close to 80% at 48 h, and above to 90% at 72 h of treatment. The highest inhibitory effects on NO production were showed at the range 7–23 $\mu\text{g}/\text{mL}$ for compounds 4 and 5. As a consequence, compounds 4 and 5 could be potential drugs due to the interesting anti-inflammatory properties showed. The anti-cancer potential of these compounds has been also tested against different tumor cell lines. The cytotoxicity of the ligand and of compounds 2 and 3 were assayed in three cell lines: HT29, colon cancer cells, Hep-G2, hepatoma cells and B16-F10 melanoma cells. The best results have been achieved with compound 2 in HepG2 and B16-F10 cell lines, being between 1.5 and 2 times more effective than the ligand in HepG2 cells, and B16-F10 cells. All in all, indazole-3-carboxylic acid is a promising ligand for the formation of coordination compounds with biochemical properties.

Article

Synthesis and Biological Evaluation of Cassane Diterpene (5 α)-Vuacapane-8(14), 9(11)-Diene and of Some Related Compounds

Houda Zentar ¹, Fatin Jannus ², Marta Medina-O'Donnell ¹, José A. Lupiáñez ², José Justicia ¹, Ramón Alvarez-Manzaneda ³, Fernando J. Reyes-Zurita ^{2,*}, Enrique Alvarez-Manzaneda ¹ and Rachid Chahboun ^{1,*}

Abstract: A set of thirteen cassane-type diterpenes was synthesized and an expedient synthetic route was used to evaluate 14-desmethyl analogs of the most active tested cassane. The anti-inflammatory activities of these 13 compounds were evaluated on a lipopolysaccharide (LPS)-activated RAW 264.7 cell line by inhibition of nitric oxide (NO) production, some of them reaching 100% NO inhibition after 72 h of treatment. The greatest anti-inflammatory effect was observed for compounds **16** and **20** with an $IC_{50\ NO}$ of $2.98 \pm 0.04 \mu\text{g/mL}$ and $5.71 \pm 0.14 \mu\text{g/mL}$, respectively. Flow-cytometry analysis was used to determine the cell cycle distribution and showed that the inhibition in NO release was accompanied by a reversion of the differentiation processes. Moreover, the anti-cancer potential of these 13 compounds were evaluated in three tumor cell lines (B16-F10, HT29, and Hep G2). The strongest cytotoxic effect was achieved by salicylaldehyde **20**, and pterolobirin G (**6**), with IC_{50} values around $3 \mu\text{g/mL}$ in HT29 cells, with total apoptosis rates 80% at IC_{80} concentrations, producing a significant cell-cycle arrest in the G0/G1 phase, and a possible activation of the extrinsic apoptotic pathway. Additionally, initial SAR data analysis showed that the methyl group at the C-14 positions of cassane diterpenoids is not always important for their cytotoxic and anti-inflammatory activities.